FRESH GROUNDWATER RESERVES IN MAJOR DELTAS

EVOLUTION AND CURRENT STATE OF DELTAIC GROUNDWATER RESOURCES

ZOETE GRONDWATERVOORRADEN IN BELANGRIJKE DELTA'S

EVOLUTIE EN HUIDIGE TOESTAND VAN DELTAGRONDWATERVOORRADEN

(MET EEN SAMENVATTING IN HET NEDERLANDS)

PROEFSCHRIFT

ter verkrijging van de graad van doctor aan de Universiteit Utrecht
op gezag van de rector magnificus, prof. dr. H.R.B.M. Kummeling,
ingevolge het besluit van het college voor promoties in het openbaar te
verdedigen op 23 november 2020 des middags te 2:30 uur

door

Joeri van Engelen

geboren op 25 januari 1992, te Delft

PROMOTOR:
Prof. dr. ir. M.F.P. Bierkens

CO-PROMOTOR:
Dr. ir. G.H.P. Oude Essink

This work was financially supported by the Netherlands Organisation for Scientific Research (NWO), under the New Delta programme (grant no. 869.15.013).

Utrecht Studies in Earth Sciences 224

FRESH GROUNDWATER RESERVES IN MAJOR DELTAS

EVOLUTION AND CURRENT STATE OF DELTAIC GROUNDWATER RESOURCES

JOERI VAN ENGELEN

Utrecht 2020

Department of Physical Geography
Faculty of Geosciences
Utrecht University

PROMOTOR:
Prof. dr. ir. M.F.P. Bierkens

CO-PROMOTOR:
Dr. ir. G.H.P. Oude Essink

EXAMINATION COMMITTEE:
Prof. dr. ir. M. Bakker
Delft University of Technology, The Netherlands
Dr. V.F. Bense
Wageningen University and Research, The Netherlands
Prof. dr. ir. M. Huysmans
Vrije Universiteit Brussel, Belgium
Prof. dr. G. Massman
Carl von Ossietzky Universität Oldenburg, Germany
Prof. dr. R.J. Schotting
Utrecht University, The Netherlands

ISBN 978-90-6266-587-7

Published by Faculty of Geosciences, Universiteit Utrecht, The Netherlands, in: Utrecht Studies in Earth Sciences (USES), ISSN 2211-4335

Printed by: ProefschriftMaken || www.proefschriftmaken.nl

Nam puteis fossis aquam dulcem reperiri posse adfirmabat:
omnia enim litora naturaliter aquae dulcis venas habere.
— Caesar - De Bello Alexandrino

CONTENTS

1

INTRODUCTION

1.1 BACKGROUND

Deltas are formed when rivers enter a body of water, often the open ocean. Here these rivers deposit thick layers of fine-grained sediments, resulting in flat and fertile lands. River deltas provide multiple services. First, the river mouths connect the open ocean with interior lands via rivers and are perfect locations for harbors; the economic opportunities in these harbors' cities are plentiful, resulting in heavily populated areas (Seto, 2011). Moreover, the fertile soils and naturally large supply of fresh surface water accommodated agriculture already at its' earliest stage (Pennington et al., 2016; Stanley, 1997). In addition, when the deltas remain largely untouched by mankind, they are unique ecological habitats (Loucks, 2019). Each delta therefore serves one or more important functions (Figure 1.1): a hub for socio-economic activity (e.g. the Rhine-Meuse and The Pearl), a food basket for a large region spanning multiple countries (e.g. the Nile and the Mekong), or a unique habitat (e.g. the Donana and the Saloum). Yet, the strong points of the deltas make them vulnerable as well. Firstly, the flat topography of these areas makes them prone to flooding (Tessler et al., 2015). Secondly, their fertile clays compact easily, leading to land subsidence under the influence of drainage, groundwater pumping or loading by infrastructure (Minderhoud et al., 2017; Higgins, 2016; Becker and Sultan, 2009). Thirdly, their downstream location makes deltas vulnerable to pollution, since pollutants disposed within the river basin accumulate here (Wolters and Kuenzer, 2015). Finally, their close connection to the sea in combination with the flat topography makes their fresh groundwater resources vulnerable to salt water intrusion, which is the landward movement of the salt water wedge in the groundwater system. **The fresh groundwater resources of deltas are the topic of this thesis.** Before discussing these resources, however, this chapter will continue with a historical side-step and provide some examples of problems with salinity in deltas to stress the importance of their fresh groundwater resources.

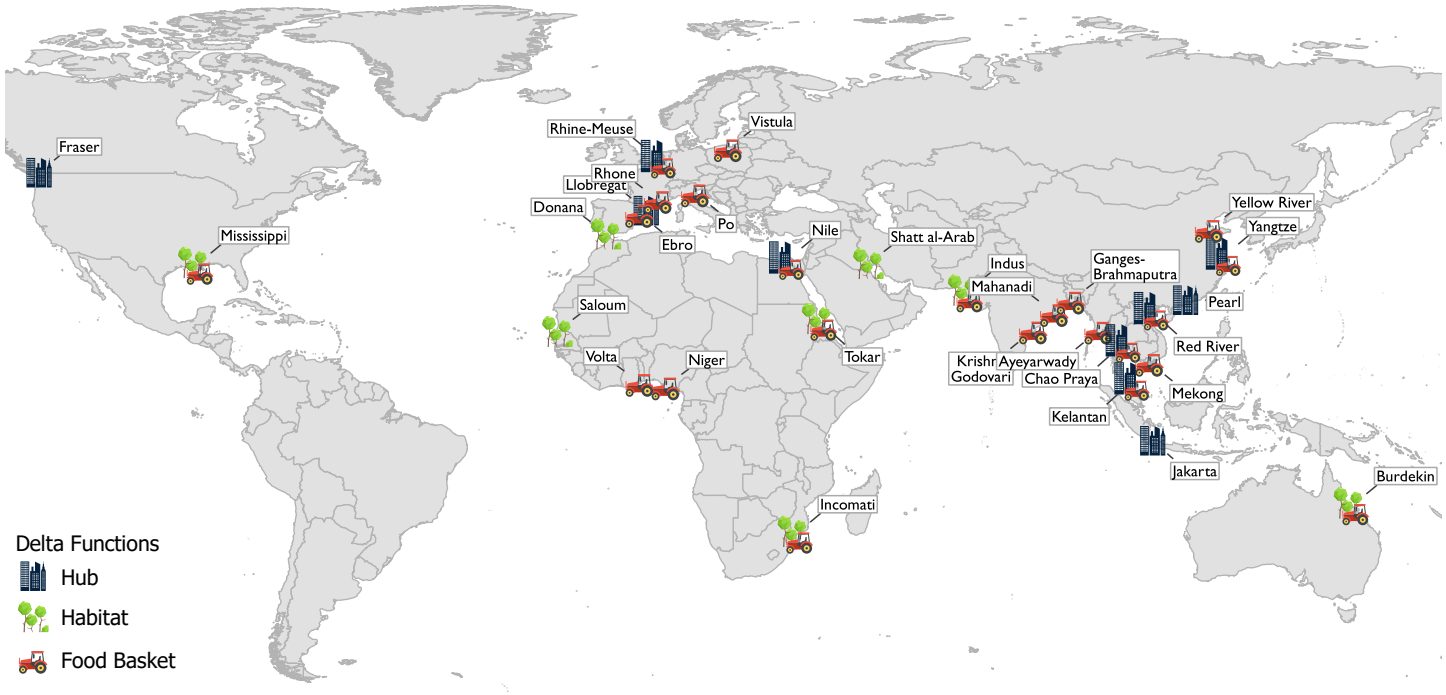

Figure 1.1: Delta functions for 31 major deltas. A combination of two symbols indicates that the delta serves two functions. Deltas were classified based on the Anthropogenic Biomes dataset (Ellis and Ramankutty, 2008). The script to reproduce delta classification can be found in the delta_aquifer Python package (van Engelen, 2020a).

HISTORICAL SIDE-STEP The first written account of the use of the word "Delta" is in Herodotus' Histories (440 BC), where he used it to refer to the Nile delta (Celoria, 1966), with its' iconic triangular shape. It is in this same delta for which we have the first written account on deltaic groundwater resources as far as I am aware of, namely in Caesar's De Bello Alexandrino (40 BC) (Post et al., 2018). Here the siege of Alexandria is described, which is a spectacular story to the hydrogeologist, because fresh groundwater resources helped winning the battle. After parts of Alexandria were occupied by the Romans (Figure 1.2), the Alexandrian commander Ganymedes ordered his men to divert seawater into the cities' canals to contaminate the drinking water source of the Romans, who occupied the quarters downstream. This caused panic amongst Caesar's men, after which the general bolstered his men as follows: *"By encouragement and reasoning Caesar allayed his men's alarm, declaring that fresh water could be found in wells and trenches, inasmuch all seashores naturally possessed veins of fresh water."* (paraphrased from Way 1955)

The story then continues with:

"*Whereupon, the business being once undertaken with unanimous enthusiasm for the task, in the course of that one night a great quantity of fresh water was discovered. Thus, the laborious machinations and supreme efforts of the Alexandrians were countered by a few hours' work.*" (paraphrased from Way 1955)

In the end, the Alexandrine War was won by the Romans in the Battle of the Nile (47 BC) after pharaoh Ptolemy XIII had drowned in the Nile during a chaotic retreat. De Bello Alexandrino serves as an interesting anecdote of how fresh groundwater resources are vital to endure periods of fresh surface water scarcity.

SALINITY Just as the Roman occupants of Alexandria in the past, the present-day inhabitants of the Nile delta are facing big problems with salinity. A large area of soils is already salinized, especially near the coast (Kubota et al., 2017),and once the surface water has passed through the delta, it enters the ocean already salinized and strongly polluted (Stanley and Clemente, 2017). These problems are not only constrained to the Nile delta, but to many other deltas as well (Rahman et al., 2019). For example, in the lower Indus delta, soil salinization has rendered agriculture impossible, causing its inhabitants to leave the area (Giosan et al., 2014). In the lower Ganges-Brahmaputra delta, many pregnant women suffer from complications due to high blood pressure, which is correlated to the high salinity content in tube wells (Khan et al., 2014). In the highly engineered Rhine-Meuse delta, saline seepage into the surface water of areas below sea-level ("polders") is creating problems for agriculture and aquatic ecosystems (De Louw et al., 2011).

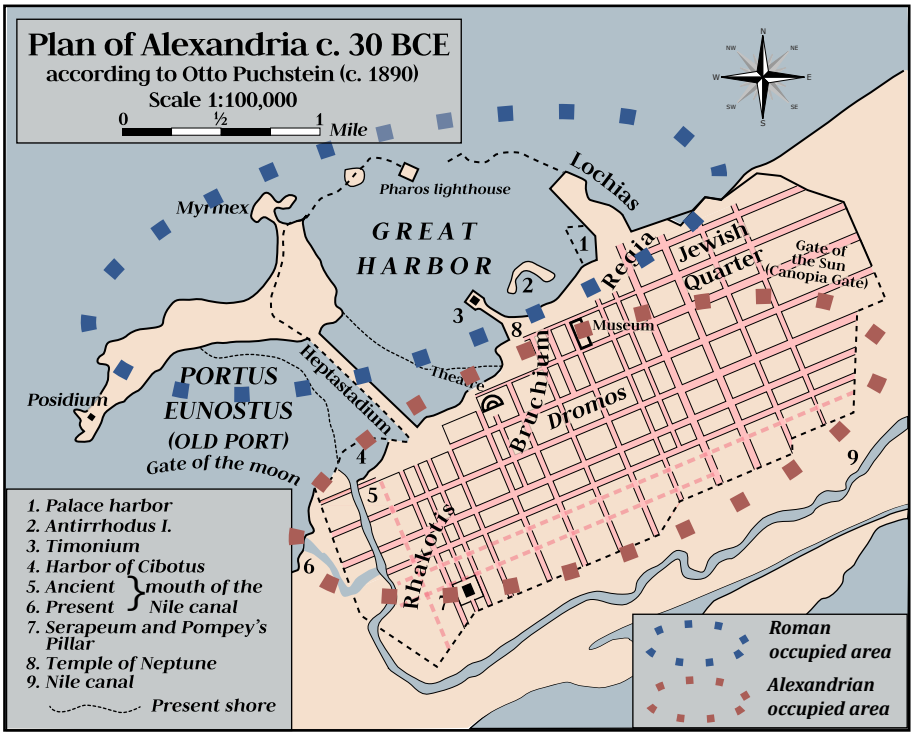

Figure 1.2: Plan of Alexandria 30 BC, denoting the approximate areas that were occupied by the Romans and Alexandrians during its' siege. This figure is modified from the figure created by user Philg88 published under CC BY-SA 3.0. The original can be found here: `https://en.wikipedia.org/wiki/History_of_Alexandria%23/media/File:Plan_of_Alexandria_c_30_BC_Otto_Puchstein_1890s_EN.svg`

FRESH GROUNDWATER The soil salinity and poor quality of the surface water in deltas cause people to resort to pumping the deltas' fresh groundwater resources, to support their drinking water, agricultural-, and industrial activities. This pumping leads to salt water intrusion and upconing (Michael et al., 2017; Werner et al., 2013), which reduces the total volume of fresh groundwater and causes wells to only extract saline groundwater, rendering these wells useless for their intended purpose. Because of the growing population in deltas (Neumann et al., 2015; Szabo et al., 2016), the increasing industrial activity (Seto, 2011), and intensifying agriculture (Tilman et al., 2011), the amount of groundwater extraction is projected to severely increase (Wada et al., 2012).

1.2 ESTIMATION OF CURRENT FRESH GROUNDWATER VOLUMES

Given the increasing pressure on water resources in deltas, it is important to have accurate knowledge about the current volume and location of their fresh groundwater resources for two reasons. First, it is vital input for informing on and designing of sustainable fresh groundwater management strategies. Second, given the large inertia of the fresh-brackish-saline groundwater system, any future model projection of the development of groundwater salinization under climate and socio-economic scenarios heavily depends on current salinities as initial condition. However, the volume of both onshore and offshore groundwater resources in many deltas are largely unknown (Faneca Sànchez et al., 2012; Post et al., 2013), especially at greater depth, as mapping these requires large (and expensive) datasets, which are often lacking. This can be partly resolved by conducting Airborne Electromagnetics (AEM) surveys, but at the time of writing their limited depth of investigation still hampers estimating complete volumes (King et al., 2018; Delsman et al., 2018; Meyer et al., 2019; Siemon et al., 2009). A complete view is important, since otherwise large quantities of groundwater can be overlooked. This is illustrated by the increased research efforts into the potential of groundwater in hard-to-reach locations, specifically offshore groundwater resources (Post et al., 2013; Thomas et al., 2019; Zamrsky et al., 2020) and groundwater at larger depths (Kang and Jackson, 2016). This makes three-dimensional numerical models, ideally contrained by as many in-situ observatyions of heads and salinity as possible, the only method of estimating total fresh groundwater volumes (Faneca Sànchez et al., 2012).

The drivers of coastal fresh groundwater resources are also often uncertain, but some trends are observed in literature. It becomes increasingly clear that long timescales (several thousands of years) are involved in the establishment of the current fresh-salt distribution in deltas. For example, the onshore groundwater in deltas often still shows saline/brackish remnants of the Holocene transgression (Delsman et al., 2014; Larsen et al., 2017). Offshore fresh groundwater is sometimes observed, of which the size is thought to be determined by the resistance of the confining layer and the speed with which the coastal shelf was inundated (Kooi et al., 2000). At large depths, however, it is often difficult to distinguish the drivers, since there are multiple potential processes and often little data as proof (Hanor, 1994). Adding to the complexity of deltaic groundwater systems, three-dimensional flow is prevalent in these areas (Abarca et al., 2007; Meyer et al., 2019; Oude Essink et al., 2010). Given the uncertainties in fresh groundwater volumes and the long timescales involved in their establishment, three-dimensional, paleohydrogeological numerical simulations are required to provide estimations of the fresh groundwater resources in deltas.

1.3 PREVIOUS WORK ON LARGE-SCALE AND PALEOHYDROLOGICAL SALINITY MODELLING

I will first provide an overview of relevant previous works and identify research gaps, before moving on to the research questions. This overview is confined to studies that investigated large-scale paleohydrogeology with numerical models which simulated groundwater salinity and/or simulated paleohydrogeology of deltas. These studies will be discussed in chronological order.

One of the first paleohydrogeologicial modelling investigations was the one conducted by Meisler et al. (1984), who used a steady-state sharp interface approach to show that the present-day fresh-salt distribution offshore of the Virginian coast (USA) was not in steady-state with present-day boundary conditions. Instead, they proposed that it was still affected by the past glacial lowstand, which causes the low salinity groundwater that is located offshore.

Ranganathan and Hanor (1988) conducted numerical simulations of both solute transport as well as heat transport around salt domes in low permeable sediments over millions of years. Their aim was to find whether thermal convection can transport large quantities of brine upwards around salt domes. They concluded that the velocities generated by gradients in salinity were 20 times higher than those generated by thermal gradients, concluding that likely thermal gradients were not involved in upward brine transport in this area. In contrast, they found that compaction could result in upward brine transport.

The first three-dimensional paleohydrogeological modelling study of a delta, as far as I am aware of, was conducted by Sanford and Buapeng (1996), who simulated groundwater ages in the Chao Praya delta, Thailand. In this area, groundwater ages were observed that exceeded 10 ka, indicating that the last glacial lowstand influenced the current groundwater age distribution. Therefore, simulations with Pleistocene and present-day boundary conditions were compared. They found that present-day boundary conditions created groundwater ages that were a lot older than the observed ages and that they required higher velocities, which could only be achieved with unrealistic porosities. Accounting for paleohydrogeological conditions generally improved their model's fit with the observed groundwater ages, since the steeper hydraulic gradient led to higher velocities.

A pioneering work into the influence of marine transgressions on the fresh-salt distribution was conducted by Kooi et al. (2000), who used two-dimensional transient variable-density groundwater models to explain offshore fresh groundwater resources. They found

that under the conditions of a shallow coastal shelf, that was exposed during the glacial lowstands, and a confining layer, vast quantities of fresh groundwater could persist offshore. The low permeable confining layer blocks most of the free-convective salt transport during, and after, the marine transgression. One year later the same authors showed that large quantities of fresh groundwater are favored by high onshore heads, a semi-confined aquifer with a high transmissivity and an confining layer with an optimal, not maximum, resistance (Kooi and Groen, 2001). This research later led to a study that showed that these offshore fresh groundwater resources are a global phenomenon Post et al. (2013).

The first three-dimensional variable-density groundwater model of (part of a) delta was created by Oude Essink (2001). The model results exposed that the century old land reclamation projects in the Rhine-Meuse delta have led to significant amounts of autonomous groundwater salinization, because their drainage level is below sea-level. The same author later used an improved three-dimensional model of the entire Rhine-Meuse delta to investigate the effects sea-level rise, land subsidence, autonomous salinization, and changes in recharge (Oude Essink et al., 2010). These simulations further confirmed the effect that the land reclamation projects had on groundwater salinity, but also showed that future land-subsidence and sea-level rise further increases this. They also demonstrated that the changes in recharge due to climate change had a relatively small effect on the Dutch fresh groundwater resources, compared to the autonomous salinization.

Post (2004) continued exploring the effects of marine transgressions studied by Kooi et al. (2000) to explain observed onshore salinities in the Rhine-Meuse delta, providing an important contribution to a long-lasting discussion in the Netherlands (Maas, 1987; Volker, 1961). In his PhD thesis he first explored this hypothesis with a hydrogeochemical analysis and further supported his findings with a physical underpinning based on 2D numerical experiments in chapters 5 and 6. With this interdisciplinary approach, he concluded that it is very likely that the Holocene transgression resulted in an extensive salinization of the Pleistocene aquifer, the effects of which are still observed today.

Gossel et al. (2010) created a large-scale 3D variable-density groundwater model of the Nubian Aquifer system, which spans Egypt, Libya, Sudan, and Chad. They investigated the effect of salt water intrusion into this system over the last 140 ka. They show that extensive autonomous salt water intrusion presumably occurred already during the glacial period towards the Qattara depression and Sirte basin, because these areas are 70 – 80 m below current mean sea-level. This resulted in a near-permanent hydraulic gradient from the Mediterranean sea towards these depressions throughout the glacial period.

Three years later, Voss and Soliman (2013) confirmed with a parsimonious 3D model of the same groundwater system that groundwater tables are naturally lowering in the Nubian aquifer during the Holocene, since they receive limited recharge and are drained in oases or sabkhas. Moreover, the authors used an inventive validation method by comparing the position of discharge areas in the model with a dataset on oases or sabkha locations.

Delsman et al. (2014) conducted a detailed paleo-reconstruction of the last 8500 ka over a cross-section in the Rhine-Meuse delta, which they validated with available classed hydrogeochemical data. They demonstated that the groundwater salinity distribution was never in a steady-state in this area during the simulated period . Moreover, the salt that entered the system during the Holocene transgression still dominates total salt mass in the groundwater system.

With a combination of geophysics, hydrogeochemistry, and simple 2D groundwater models, Larsen et al. (2017) proved that the saline groundwater in the Red River Delta (Vietnam), that reaches up to at least 100 km inland, was a result of the extensive Holocene transgression there. Furthermore, the authors conducted a literature review and found that traces of past marine transgression are found in a lot of coastal areas, especially in deltas.

Also in Vietnam, but this time in the Mekong Delta, Van Pham et al. (2019) showed with a two-dimensional, paleohydrogeological variable-density groundwater model that fresh groundwater volumes gradually freshened during the Pleistocene after which they rapidly declined at the onset of the Holocene. Furthermore they showed that the time lag of the Holocene sea-level rise and the decline in fresh water volume is several thousand years.

Finally, Meyer et al. (2019) conducted simulations with a detailed three-dimensional, paleohydrogeological variable-density groundwater model for a coastal lowland area in Denmark, and compared their results to a geophysical and hydrogeochemical observations. Their results showed that the salt water here originates from a combination of mostly laterally intruding sea water and, to a lesser extent, vertically infiltrated transgressive water. The infiltration with transgressive water was impeded here by an extensive shallow low-permeable aquitard. Despite the limited effect of the Holocene transgression, the groundwater system was not in equilibrium with present-day boundary conditions. In fact, the system is still facing autonomous salinization as an effect of the steep early-Holocene sea-level rise, which is further enhanced by anthropogenic drainage.

The literature overview shows that the present-day groundwater salinity distribution was formed over large timescales in many large-scale groundwater systems, especially in

deltaic groundwater systems. Numerical models proved to be an important tool in exploring the drivers and timescales of this distribution. However, a rigorous investigation of all drivers of the fresh-salt groundwater distribution across these timescales has never been conducted. In addition, only two studies quantified the fresh groundwater volume of the deltaic groundwater system (Oude Essink et al., 2010; Van Pham et al., 2019). Moreover, three-dimensional paleohydrogeological variable-density groundwater models have been only conducted very scarcely up to this day (Gossel et al., 2010; Meyer et al., 2019), presumably because of the computational burden these models bring.

1.4 RESEARCH QUESTIONS AND THESIS OUTLINE

The lack of sufficiently accurate estimates of the volumes of fresh groundwater resources in deltas, as well as their drivers is the main reason for this PhD research. Therefore, **the main objective of this thesis is to assess the status and drivers of the current fresh-salt groundwater distributions in major deltas of the world**. To this end and based on the knowledge gaps identified in the research efforts thus far, the following research questions were formulated:

What processes influence groundwater salinity in deltas at large depths?

In chapter 2, the origins of hypersaline groundwater that is found below 400 m depth in the Nile delta are investigated. Four hypotheses are tested with a set of analytical solutions and two-dimensional numerical models, some of which simulate the last 2.5 million years of variable-density groundwater flow. Consequently, links are made to other deltas where similar processes have or might have occurred.

How did the fresh water volumes evolve over time?

In chapter 3, as a first exercise in 3D paleogeographical modelling, the development over time of the fresh-salt groundwater distribution of the Nile delta is reconstruced. To this end, a three-dimensional delta-scale model is used that simulates groundwater salinity of the Nile delta over the last 32 ka, fed with boundary conditions based on paleogeographic maps. Several lithologies are tested as well. In chapter 5, results are generalized by simulating a full glacial cycle (120 ka) for 15 idealized representations of other deltas.

What are the driving factors of the natural fresh-salt distribution?

Chapter 4 presents a global sensitivity analysis of a numerical model of an idealized, synthetic delta, simulating groundwater salinity development over the last 40 ka. This delta is generated based on a set of 23 inputs, which are all varied in the sensitivity analysis as to represent every possible delta. A consistent analysis shows which input had the strongest influence on the total salt mass onshore and its time-derivative, the total fresh water volume offshore, and the amount of initial salt still present in the system.

What are the current fresh groundwater volumes in deltas and will they be depleted?

In chapter 5, idealized deltas are simulated that represent 15 major deltas around the world, based on inputs found in the literature. Some models are validated against available data of fresh groundwater volumes and known well depth distributions. Furthermore, the time is calculated until these fresh groundwater resources will be depleted, given the estimations of the current amount of groundwater extracted in these areas.

Finally, chapter 6 summarizes the results of this thesis, in particular the answers to the research questions and ends with recommendations for further research. Note that chapters 2 and 3 have been published as articles in peer-reviewed journals, and 4 and 5 are either submitted, or planned to submit, to a peer-reviewed journal. Therefore, there might be some overlap between chapters.

2

ON THE ORIGINS OF HYPERSALINE GROUNDWATER IN THE NILE DELTA AQUIFER

ABSTRACT

The Nile Delta is essential to Egypt's agro- and socio-economy. Although surface water is the traditional source for Egypt's irrigation, the shallow fresh groundwater resources underlying the delta are increasingly burdened by groundwater pumping, which increases interest in the status of the groundwater resources. Groundwater up to three times more saline than sea water was found at 600 m depth. The occurrence of this hypersaline groundwater raises doubts on the often-made assumption in the literature that seawater is the only source of salt in the Nile Delta aquifer and makes further investigation necessary. Knowledge on the origin of this hypersaline groundwater is key in assessing the possibility of deep fresh groundwater pockets. In this paper we conducted computational analyses to assess possible origins using both analytical solutions and numerical models. It is concluded that the hypersaline groundwater can either originate from Quaternary free convection systems, or from compaction-induced upward salt transport of hypersaline groundwater that formed during the Messinian salinity crisis. Our results also indicate that with groundwater dating it is possible to discriminate between these two hypotheses. Furthermore, it is deduced that the hydrological connection between aquifer and sea is crucial to the hydrogeological functioning of the Nile Delta Aquifer.

Based on: van Engelen, J., Oude Essink, G.H.P., Kooi, H., Bierkens, M.F.P. (2018) On the Origins of Hypersaline Groundwater in the Nile Delta Aquifer, *Journal of Hydrology 560*, 301–317

2.1 INTRODUCTION

The Nile Delta is essential to Egypt's agro- and socio-economy, as it constitutes most of the limited 3% of the country that is suitable for agriculture (WRI, 2008). Its wet and fertile lands have supported the Egyptian population for over 5000 years (Maczyńska, 2014), and currently host nearly 50 million inhabitants, making it the second most populated delta in the world, after the Bengal delta (Higgins, 2016). However, its fresh groundwater resources are suffering from agriculture increasingly relying on groundwater (Barrocu and Dahab, 2010) and a growing population (Bucx et al., 2010) that will further amplify extraction rates, making fresh water availability its most challenging issue for agriculture (FAO, 2005).

These stress factors have led to a continuous interest in available fresh groundwater resources and several studies on the topic. Kashef (1983) critically reviewed the available data, conducted water balance calculations, and estimated the extent of salt water intrusion with the Ghyben Herzberg relationship. He found several discrepancies in the available data, and concluded based on his water balance that at that time the aquifer was gaining fresh water. Despite this gain, he found that the salt water wedge reached far inland. Sherif et al. (1988) constructed the first numerical groundwater model for the area, which was a 2D finite element model for variable density flow, also accounting for dispersion. Next to the large extent of the salt water wedge, the model showed that the width of the hydrodynamic dispersion zone could be considerable. Sefelnasr and Sherif (2014) created a 3D model and showed the sensitivity of the Nile Delta aquifer to sea level rise, as the shallow relief of the area resulted in a large extent of land surface inundation. Geirnaert and Laeven (1992) used hydrogeochemistry to reconstruct the paleohydrogeology of the area, up to 20 ka (=20,000 years BP), providing the first conceptual model for this period. They furthermore found that that the shallow groundwater in the center of the Nile Delta was recharged 3.5 ka as river water and in the bordering desert over 5 ka. Barrocu and Dahab (2010) extended this conceptual model up to 180 ka, and further discussed the hydrogeochemistry. They concluded that the saline groundwater in the north is likely not in connection with the current sea, instead it is connate sea water, and further stress the fragility of the groundwater system. Despite that the previously discussed works increased our understanding of the system, we identify several research gaps: a) The numerical models made for this area do not take the paleohydrogeology in account, presumably due to computational limitations. b) Most studies implicitly assumed a completely open connection between aquifer and the sea, while this is uncertain. c) The studies mainly used data of the shallow groundwater system (roughly the upper 200 m of the upper aquifer), even though the upper aquifer is believed to extend up to 1000 m depth (Kashef, 1983; Sestini, 1989).

With increasing stress on the shallow groundwater system, interest in possible deeper fresh groundwater grows (Kang and Jackson, 2016). Therefore, the Egyptian Research Institute for Groundwater (RIGW) measured salinity at 200 m, 400 m and 600 m depth in 2013 and measured high values of Total Dissolved Solids (TDS) (Nofal et al., 2015) starting from 400 m depth at several locations (Figure 2.1a), strongly suggesting a widespread occurrence of "hypersaline" groundwater at larger depths. No hypersaline groundwater was observed at 200 m depth. Given the interest in finding deeper fresh groundwater resources in the Nile Delta Aquifer (NDA, see figure 2.1b), a better understanding of the possible origins and transport of this hypersaline groundwater is necessary to assess further possibilities. "Hypersaline" groundwater is defined as groundwater exceeding the salinity of sea water (35 g/l) in this paper. Apart from the findings shown in figure 2.1a, two other observations of hypersaline groundwater in the NDA have been published. Firstly, Diab and Saleh (1982) found hypersaline groundwater near the shore, but did not report the depths of their samples. Secondly, there is the incidental remark by Shata (1999): "hot brine is recorded in oil wells at a depth of 1000 m below ground surface". As far as we are aware of, no other observations, hydrogeophysical or hydrogeochemical, have been published that reach 600 m depth, despite the multiple petroleum exploration wells that have been drilled, and logged, in the area.

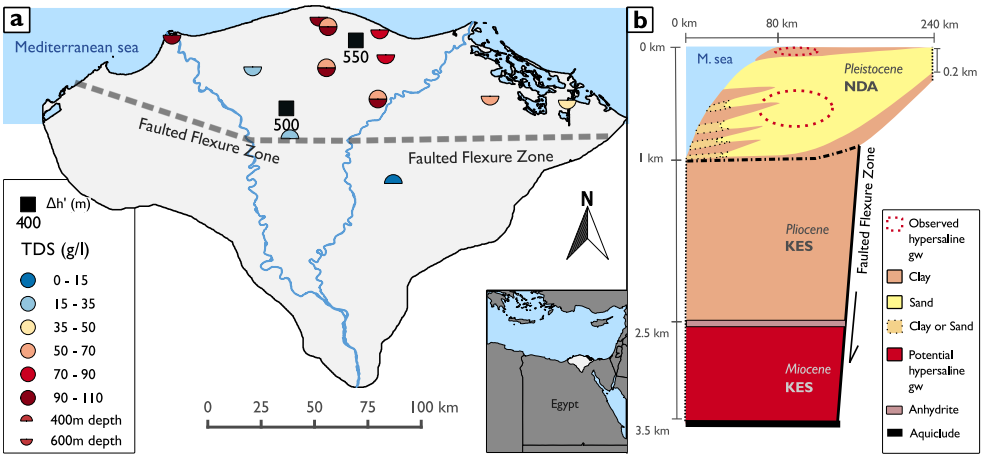

Figure 2.1: (a) Total Dissolved Solids (TDS) measurements at 400 and 600 m depth in the Nile Delta and head difference (Δ h') over the anhydrite layer, expressed in freshwater head. The dotted black line represents the location of geological cross section. The map in bottom right corner shows the location of the Nile Delta in Egypt. (b) Sketched conceptual geological cross-section of the Nile Delta. The dash-dotted line indicates the boundary between separate model domains Nile Delta Aquifer (NDA) and Kafr El Sheikh formation (KES).

Given the occurrence of this hypersaline groundwater, we question the often-made assumption that seawater is the only source of salt in NDA groundwater and deem further investigation necessary. Therefore, we test a number of plausible hypotheses on the origin of the NDA hypersaline groundwater using a combination of analytical solutions and numerical simulations. This analysis provides more insight into a) the timescales of salt transport involved in this large delta, b) which measurements should be collected to discern the origins of this hypersaline groundwater, and c) the possibility of deep fresh groundwater pockets. The goals of this study are to investigate the plausibility of a number of hypotheses (Listed in section 3), to find a method to discriminate them in the field, and, where possible, falsify hypotheses.

Given the lack of study on this topic in this area, a brief summary of findings in other deltaic areas is warranted. As far as we are aware of, four other cases have been published that are relevant to this research. Firstly, hypersaline groundwater is found in fluvio-deltaic sediments near the Louisiana Gulf coast (Mississippi delta), which is probably the most well-studied area for this topic. Here, it is thought to originate from dissolution of salt domes brought upwards by thermal convection (Hanor and Mercer, 2011). Secondly, in the Netherlands (the Rhine-Meuse delta), hypersaline groundwater is found below the hydrogeological base, presumably caused by rock salt dissolution (Griffioen et al., 2016). Largely varying salinities are observed on the national scale, which can be partly explained by the presence of evaporite deposits and diffusive transport. Thirdly, high salinities found in the Burdekin Delta are explained by transpiration of mangroves and subsequent downward free convection (Fass et al., 2007). Fourthly, it is thought that intruded evapoconcentrated seawater is the cause of hypersaline groundwater near the Yellow River Delta (Han et al., 2011). In summary, these cases can be seperated into two groups: 1) those where hypersaline groundwater is thought to have originated from rock salt dissolution and 2) those where it is thought to be caused by evapoconcentration.

We argue here that these four cases are relevant to the Nile Delta, since evaporites are found below the hydrogeological base (Rizzini et al., 1978) and its climate provides ample opportunity for evapoconcentration. These processes will be discussed in further detail in section 3. The methods and findings of this research can also be applied to other deltaic areas overlying thick unconsolidated formations, such as the four previously mentioned cases. Furthermore, they might be applied to cases where hypersaline groundwater might be found in the future, such as the Mekong Delta (Minderhoud et al., 2017), the Ganges-Brahmaputra Delta (Lindsay et al., 1991), and, in particular, the Niger Delta, which is geologically similar to the Nile Delta (Summerhayes et al., 1978).

2.2 HYDROGEOLOGICAL SETTING

A conceptual geological cross-section of the central NDA is shown in figure 2.1b. The NDA ranges in thickness from approximately 200 m near Cairo to 1000 m near the coast (Farid, 1980). It consists mainly of coarse Pleistocene sands and gravels, with some clay intercalations (Laeven, 1991). It is topped by a Holocene clay cap, ranging in thickness from 3 m at Cairo to a maximum of 100 m near the shore (Shata, 1999). In seismic studies, it is found that the bottom 750 m of the coastal boundary of the NDA is partially closed off by marine clays (Abdel Aal et al., 2000; Samuel et al., 2003; Abdel-Fattah, 2014), which is unaccounted for in previous groundwater research, though the existence of connections between the NDA and the sea is deemed possible in the form of conductive paleo-channels. There is an east-west trending fault system, "Fault Flexure zone", that presents a break in stratigraphy (Sestini, 1989) and causes an increase in thickness of the aquifer in northern direction. North of the fault flexure zone, the NDA is resting on top of a 1500 m thick formation consisting of mainly Pliocene marine clays (Sestini, 1989; Farouk et al., 2014) called the Kafr El Sheikh formation (KES). South of the fault flexure zone, the Nile Delta is underlain by limestones and shales ranging from Miocene to Oligocene age (Geirnaert and Laeven, 1992). Directly below KES, there is a 50 m thick layer of Messinian evaporites, consisting mainly of anhydrite (Rizzini et al., 1978). Below these evaporites, there is 1000 m of Miocene sands and conglomerates, underlain by compacted Miocene shales. Below these shales the pore pressures approach geostatic pressure (Nashaat, 1998), implying limited flow through the shales, therefore we assumed this serves as a hydrogeological base. Furthermore, we assumed the Fault Flexure zone is an impermeable boundary to flow, since 1) at larger depths there are several processes that can reduce fault horizontal permeability (Bense et al., 2013), such as clay smearing and particulate flow, and 2) offshore faults at similar depth clearly compartmentalize the subsurface, inferring from the high lateral differences in overpressure underneath the evaporate layer in Nashaat (1998).

2.3 HYPOTHESES

There are two possible origins of the hypersaline groundwater. Firstly, the hypersaline groundwater could originate from deeper deposits. We argue that it is certainly possible that hypersaline groundwater occurs in the 1 km thick Miocene layer, as evaporites are found up to the Fault Flexure Zone just underneath KES. These are correlated with the Messinian salinity crisis (Rizzini et al., 1978), during which the Mediterrenean sea reached high salinities and its water intruded bottom sediments. Some of this residual hypersaline water remained here (Vengosh et al., 1998). Furthermore, mud volcanos are found that seep

hot brines originating from Messinian salt formations offshore at 3,000 m water depth (Pierre et al., 2014). If hypersaline groundwater was transported upwards from deeper deposits onshore, it had to overcome resistance exerted by the high groundwater density and the low-permeable KES. There are three physical processes that can possibly overcome these resistances (Hanor, 1994; Person and Garven, 1994), namely 1) molecular diffusion (Domenico and Schwartz, 1990; Shackelford and Daniel, 1991b; Shackelford and Daniel, 1991a), 2) thermal driven free convection (Nield, 1968; Trevisan and Bejan, 1990; Nield and Bejan, 2013), as temperatures up to 90 °C have been observed underneath the KES (Riad et al., 1989) which may be associated with strong temperature gradients, and 3) upward solute transport driven by sediment compaction, since considerable overpressures have been measured onshore underneath the KES (Figure 2.1a). These overpressures were likely caused by sediment loading, since the sedimentation rates during the Pleistocene and Pliocene were extreme (Nashaat, 1998), roughly 2500 m of deposits in 5.3 million years.

Secondly, it could originate from the top as the effect of 4) Holocene or Pleistocene free convection systems, originating from the evapotranspiration of sea or river water (Schreiber and Hsu, 1980; Wooding et al., 1997); similar to the cases in the Burdekin Delta and near the Yellow River Delta that were mentioned in Section 1 (Fass et al., 2007; Han et al., 2011). The high evapotranspiration rates in the Nile Delta of the past 10 ka provide ample opportunity for the formation of hypersaline groundwater, deduced from the pockets of hypersaline groundwater found in the Holocene clay layer (Diab et al., 1997) and the hypersaline groundwater found underneath a sabkha neighbouring the Nile Delta (West et al., 1979). Stanley and Warne (1993) made a paleogeographical reconstruction of the past 30 ka, showing several possibilities for hypersaline groundwater formation in this relatively short geological period. For example, sabkha muds (salt muds) were deposited in seasonally dry depressions between former channels from 30 to 11.5 ka. Furthermore, the widespread wetlands of 6.5 to 2 ka also at times transpired enough to create hypersalinity, inferred from the previously mentioned pockets of hypersaline groundwater in the Holocene clay (Diab et al., 1997). Another option might be a coastal lagoon that received little river water for a long period of time, such as during the early Holocene arid phase (Geirnaert and Laeven, 1992), analogue to the coastal sabkhas in the Northern Sinai (Gat and Levy, 1978).

We want to stress that this list of hypotheses is not exhaustive, due to the limited amount of data available at the depth of interest.

2.4 METHODS

Computational analyses were conducted with either analytical solutions (hypotheses 1 and 2) or numerical models (hypotheses 3 and 4), to test the physical feasibility of mentioned four hypotheses. Since this is exploratory research, we tried to reduce the risk of incorrect hypothesis rejection as much as possible. Our ground rule was to set unconstrained parameters and boundary conditions in favor of the respective hypothesis under research, since constraining data was often scarce. If the hypothesis was then still falsified, we could then be quite certain that this process played no important role in bringing hypersaline groundwater to 600 m depth.

One assumption we made in this research affected our analyses for all hypotheses, namely we assumed NaCl as the sole source of salt, as this is the dominant salt in groundwater under natural conditions at TDS values up to 200 g/l (Hanor, 1994). At larger TDS values calcium becomes the more dominant cation, as groundwater gets saturated with respect to halite. This assumption affected both the molecular diffusion coefficient used, used for hypotheses 1 to 4, and the conversion from concentration to density, used for hypotheses 2 to 4. The effects of this assumption on our computational analyses are deemed unimportant, since the molecular diffusion coefficient of NaCl is higher than that of CaCl2 (Shackelford and Daniel, 1991b) thus not interfering with our ground rule, and the uncertainties introduced by a different linear equation of state are negligible compared to the other uncertainties in this research (Kohfahl et al., 2015).

2.4.1 *Hypothesis 1: Analytical solution*

Here we test whether molecular diffusion could have transported enough dissolved salts to explain the observed salinities upwards over the KES. Assuming no groundwater flow, solute transport is purely governed by Fick's second law of diffusion in 1D (adapted for porous media), which is written as follows:

$$\frac{\partial C}{\partial t} = -D_c^* n_e \frac{\partial^2 C}{\partial z^2} \tag{2.1}$$

Where C is the concentration of the solute (g/l), $n_e$the effective porosity (-), z the vertical distance (m), t is time (s), and D_c^* the effective diffusion coefficient (m2/s). There is no general consensus regarding the exact definition of D_c^* (Domenico and Schwartz, 1990;

Shackelford and Daniel, 1991b). In this study, we used values of Shackelford and Daniel (1991a), who defined:

$$D_c^* = D_0 \tau_a \tag{2.2}$$

Where D_0 is the molecular diffusion in free water at a certain temperature (m^2/s) and τ_a is an "apparent tortuosity" (-), which accounts for the combined effects of tortuosity, anion exclusion, and viscosity. The following analytical solution to equation 2.1 describes the concentration development through the compacted clay through time:

$$C(z,t) = C_{max} + (C_{min} - C_{max}) \operatorname{erf} \frac{z}{\sqrt{4 D_c^* t}} \tag{2.3}$$

Where C_{max} and C_{min} are the maximum and minimum concentrations respectively. We varied C_{max} in our analysis and set C_{min} to the TDS of seawater, which is 35 g/l. D_c^* was approximated by estimatingτ_a. We used the highest values of D_c^* that we could estimate from the literature, in order to reduce the risk of incorrect hypothesis rejection. (Shackelford and Daniel, 1991a) rigorously conducted multiple experiments (8 test series) in triplicate at 25 °C for multiple species, of which they calculated the mean D_c^* of each test series. The highest mean these authors found for Cl- at 25 °C is 10.6e-10 m^2/s. Since D_0 of Cl- at 25 °C is 20.3e-10 m^2/s (Shackelford and Daniel, 1991b), an upper limit for τ_a of 0.522 is inferred. In addition we corrected for temperature, as Riad et al. (1989) measured temperatures of 80 °C on average directly underneath the Kafr El-Sheikh layer at multiple points in the onshore Nile Delta. D_0 of NaCl at 80 °C is around 44e-10 m^2/s (Fell and Hutchison, 1971). Thus, assuming that for Cl- is isotherm and is representative for NaCl, a D_c^* = 22.9e-10 m^2/s was used for compacted clay at 80 °C.

This hypothesis is rejected if filling in equation 2.3 with the most favourable parameters does not result in a concentration of 100 g/l at 1000 m depth (the top of the KES formation). This is the concentration that was observed at 600 m depth in the NDA.

2.4.2 *Hypothesis 2: Rayleigh Number for Double Diffusive Convection*

Here we will test thermal convection could have had its onset over the KES, which could subsequently transport dissolved salts upwards. Assuming initially stagnant groundwater and a homogeneous, isotropic aquitard, the onset of free convection over the KES formation

was investigated by calculating the double-diffusive Rayleigh number (Nield, 1968; Trevisan and Bejan, 1990) and comparing it to its critical boundary:

$$Ra_t + Ra_c = Ra_t + Ra_t NLe > Ra_{crit} \tag{2.4}$$

With:

$$Ra_t = \frac{kgH\zeta_t \Delta T}{D_t \nu} \tag{2.5}$$

$$Ra_c = \frac{kgH\zeta_c \Delta C}{D_c^* \nu} \tag{2.6}$$

$$N = \frac{\zeta_c \Delta C}{\zeta_t \Delta T} \tag{2.7}$$

$$Le = \frac{D_t}{D_c^*} \tag{2.8}$$

$$\zeta_t = -\frac{1}{\rho}\frac{\partial \rho}{\partial T} \tag{2.9}$$

$$\zeta_c = -\frac{1}{\rho}\frac{\partial \rho}{\partial C} \tag{2.10}$$

Where Ra_t is the thermal Rayleigh number, Ra_c the compositional Rayleigh number, Ra_{crit} the critical Rayleigh number; the rest of the parameters is explained in table 2.1. These are extreme parameters, all chosen to maximize Ra_t and Ra_c, to minimize the risk of incorrect hypothesis rejection. It should be noted that Ra_t and Ra_c become negative when temperature or concentration gradients act stabilizing (Trevisan and Bejan, 1990); in this case Ra_c is negative. When $Ra_t + Ra_c > Ra_{crit}$, the groundwater system in the KES becomes unstable and free convection is possible. The value of Ra_{crit} depends on the chosen type of boundary conditions; in this case a fixed head, concentration, and temperature on top, and a no flux boundary and a fixed temperature and concentration at the bottom, gives$Ra_{crit} = 27.10$ (Nield, 1968; Trevisan and Bejan, 1990). The hypothesis is rejected if $Ra_t + Ra_c \ll Ra_{crit}$.

Table 2.1: Limits of parameters chosen to fill in double diffusive convection analysis.

Symbol	Description	Value	Unit	Source
k	Permeability	4.80e-16	m^2	Table 3.2 in Domenico and Schwartz 1990
g	Gravitational acceleration	9.81	m/s^2	
H	Thickness of clay layer	1500	m	Rizzini et al. 1978
ζ_t	Volumetric thermal expansion coefficient†	7.20e-4	1/°C	Beaton et al. 1987
ζ_c	Volumetric compositional expansion coefficient	-7.14e-4	l/g	Guo and Langevin 2002
ΔT	Temperature difference over clay layer	70	°C	Riad et al. 1989
ΔC	Assumed concentration difference over clay layer	65	g/l	Nofal et al. 2015
D_t	Thermal diffusivity of clay	8.53e-7	m^2/s	Eppelbaum et al. 2014
D_c^*	Effective molecular diffusion coefficient of clay	22.9e-10	m^2/s	See section 4.1
ν	Kinematic viscosity of water	2.899e-7	m/s^2	Beaton et al. 1987

† *at 100 °C and 250 bar at 2500m depth*

2.4.3 *Hypotheses 3 & 4: Numerical Models*

2.4.3.1 *General approach*

The variable-density solute transport code SEAWAT (Langevin et al., 2008) was used to simulate the development of TDS-fields, pore pressures, and groundwater age within a cross-sectional domain up to 1 km depth representing the NDA (Figure 2.1b). All of the models described in this paper were built with the Flopy package (Bakker et al., 2016). Groundwater ages were modeled directly, as first implemented by Voss and Wood (1993) and later extensively supported by Goode (1996), by adding "age" as an extra species with a constant production rate (Zheng, 2010). SEAWAT solves the following governing equation for flow:

$$-\nabla \cdot (\rho \vec{q}) + \bar{\rho} q_s = \rho S_p \frac{\partial P}{\partial t} + n_e \frac{\partial \rho}{\partial C} \frac{\partial C}{\partial t} \tag{2.11}$$

with:

$$S_p = (\beta_p(1 - n_e) + n_e\beta_w) \tag{2.12}$$

And for solute transport:

$$\frac{\partial C}{\partial t} = \nabla \cdot (D \cdot \nabla C) - \nabla \cdot \left(\frac{\vec{q}}{n_e}C\right) - \frac{q_s}{n_e}C_s + \sum_{i=1}^{N} R_i \tag{2.13}$$

Where ρ is the density of groundwater (kg/m^3), $\bar{\rho}$ is density of water entering through a source or leaving through a sink (kg/m3), $\vec{q}$ is the specific discharge vector (m/d), q_s is the source/sink term (d^{-1}), P is the pore pressure (N/m^2), t is time (d), S_p is the specific storage in terms of pressure (m^2/N), β_p and β_w are the compressibility of the pores and water (m^2/N), respectively, C is the salt concentration (g/l), C_s is the source concentration (g/l), D is the hydrodynamic dispersion coefficient (m^2/d) R_i is the rate of solute production or decay in reaction i of N different reactions, and n_e is the effective porosity (-). For an elaborate explanation of equations 2.11 to 2.13, the reader is referred to the SEAWAT manual (Guo and Langevin, 2002).

Boundary conditions were varied to either model salt input by compaction-driven inflow from below (NDA-c model) or free convection from the top (NDA-f model). These models evaluate hypotheses 3 and 4 based on their ability to approach the observed TDS at several points at 600 m. A separate model for the "KES" domain (1 – 3.5 km depth) was developed to produce the basal boundary condition of the NDA-c model. This sequential, "split-domain" approach (first KES, then NDA-c) was chosen to maintain practicable computation times, which ranged from half a day (KES model) up to a week (NDA-c model, with open coastal boundary). These large differences in computational times were caused mainly by the solute transport solver (MT3DMS), which based its time step internally on the maximum velocity in the model domain (Zheng and Wang, 1999). The NDA model had the highest velocities, while the KES model had a larger number of cells. Therefore, combining model domains would seriously burden simulation times, as this would result in three times the number of cells of the NDA model, with the same small time steps, causing maximum predicted model simulation times of three weeks per simulation. The sequential split-domain approach is reasonable since groundwater flows predominantly upwards from KES into NDA.

2.4.3.2 *Methodological aspects of the numerical models*

The NDA numerical models spanned 240 km by 1 km, the KES model 180 km by 3 km, and all models were discretized into cells of 1000 m (horizontal) by 10 m (vertical) (see also

figure A.3 for a grid convergence test). The time domain of the models ranged from 120 ka (NDA-f) up to 2.5 Ma (KES & NDA-c). The latter time domain implies we assume no overpressure build-up during the Pliocene in the KES formation.

KES MODEL To quantify volumetric flow and solute transport within the KES depositional strata during the Pleistocene and, in particular the outflow at the top of this formation, we used a modified version of the partial differential equation for mass conservation in a deformable porous medium with external loading of Bear (1972, his equation 6.3.26).

$$-\nabla \cdot (\rho \vec{q}) + \rho \beta_p \left(\frac{\partial \sigma}{\partial t} - \frac{\partial P}{\partial t} \right) = \rho n_e \beta_w \frac{\partial P}{\partial t} + n_e \frac{\partial \rho}{\partial C} \frac{\partial C}{\partial t} \tag{2.14}$$

Where $\sigma$is the total stress or confining pressure (m^2/N), which is a function of sediment loading, and β_p $(\partial\sigma/\partial t - \partial P/\partial t) = \partial\varepsilon/\partial t$ is the strain rate of the porous medium ($d^{-}1$).

The applied modifications to Bear's original equation, which allow the equations to be solved with SEAWAT without any modifications to the original code, were a) the addition of the last term which allows local groundwater mass change due to change in salt content and b) the use of Eulerian (fixed space coordinates) rather than Lagrangian (relative to moving solids) time derivatives. The latter modification reflects the fact that we solve for pore pressure, TDS, and flows on a rigid model domain (present-day compressed state) and neglect temporal changes of vertical grid spacing and domain height associated with the compaction. This is considered reasonable as it yields conservative, underestimated magnitudes of the compaction-driven flow.

To solve equation 2.14 in SEAWAT, three variables of equation 2.11 were altered: S_p, q_s, and $\bar{\rho}$. Firstly, whereas normally $S_p = (\beta_p(1 - n_e) + n_e\beta_w)$ (2.12), in the KES model $S_p = n_e\beta_w$ (2.14). This required no modifications to the original code, as SEAWAT takes S_p as an input parameter directly.

Secondly, the strain rate, which equals the volumetric source term in equation 2.11, was specified to be constant in the model, proportional to a constant Pleistocene sedimentation rate and constant pore compressibility.

$$q_s = \beta_p \left(\frac{\partial \sigma}{\partial t} - \frac{\partial P}{\partial t} \right) \approx \beta_p \left(\rho_b g \frac{\partial z_b}{\partial t} - \rho_w g \frac{\partial z_b}{\partial t} \right) = \beta_p (\rho_b - \rho_w) g \frac{\partial z_b}{\partial t} \tag{2.15}$$

Where ρ_b the bulk density of the sediment, ρ_w the density of fresh water (kg/m3), and $\frac{\partial z_b}{\partial t}$ the sedimentation rate (m/d). Equation 2.15 approximates the temporal change of

pore pressure to equal a hydrostatic pressure change ($\partial P = \partial P_h$) as the depth of the KES strata relative to the water table increases during burial. This overestimates the compression during early phases of Pleistocene sedimentation when excess pore pressures increase, but this overestimation becomes negligible after a short time as excess pore pressures stabilize. The validity of this approach is shown in appendix C. q_s is constrained by the fact that the total amount of expelled pore water cannot exceed the pore water volume at time of deposition, and the latter can be approximated a-priori by:

$$V_s = \int_{t_0}^{T} q_s \, \mathrm{d}t \leq n_{init} \tag{2.16}$$

Where V_s is the total volume of water expelled from the pores relative to the initial bulk volume (-), or total strain, t_0 and T are the beginning and the end of the time domain (d), respectively, and n_{init} is the initial porosity (-), just after sediment deposition. With the parameters chosen in this research (Table 2.2), V_s equaled 0.26 and 0.13 for the Pliocene clay and Miocene deposits, respectively. We consider this an upper limit of the total water expelled by the pores during the Pleistocene.

Thirdly $\bar{\rho}$, the density of the water injected in a cell by q_s, had to equal the current concentration of the cell. This was determined by SEAWAT internally by using the "recirculation well option" of MT3DMS (Zheng, 2010). To ensure convergence, the maximum number of outer iteration steps of the dispersion solver (GCG) was set at 10 (the default value is 1). In practice, no more than three outer iterations were required for convergence.

The upper boundary of the KES model was a Cauchy boundary condition, of which the fresh water head is set at zero. To incorporate the effects of deposition of NDA sediments on this upper boundary, namely that the distance to the fixed head boundary increases, the conductance of the top boundary of the KES model (m^2/d) was adapted. SEAWAT takes the conductance as input for its Cauchy boundary condition, together with a prescribed head. The conductance is defined as follows (Guo and Langevin, 2002):

$$Cond = \frac{KA}{l} \tag{2.17}$$

where K is the hydraulic conductivity, A is the cross-sectional area of the flow, l is the distance of the boundary to the model cell (m). We increased this conductance with time as sedimentation progresses:

$$Cond = \frac{K_{v,\,sand} A_{cell\ top}}{\frac{\partial z_b}{\partial t} t} \tag{2.18}$$

$K_{v,\,sand}$ is the vertical hydraulic conductivity of the NDA deposits (m/d), $A_{cell\ top}$ is the area of a model cell top interface (m2), t is the time (d), and $\frac{\partial z_b}{\partial t}$ is the sedimentation rate (m/d). All other boundaries were assumed to be no flow boundaries.

As for the initial conditions, we assumed completely stagnant conditions during the Pliocene, and therefore applied 3.4 Ma (duration of the Pliocene) of molecular diffusion over the KES clay layer. The initial TDS concentration at the Miocene deposits varied between 125, 200, 300, 400 g/l, (respectively scenarios M125, M200, M300, and M400), and the initial groundwater age of the Miocene deposits was set at 3.4 Ma. The upward salt fluxes of the KES scenario that showed the best fit to pressure observations were injected into the NDA-c model, as part of a "base case". In this base case, all parameters of the NDA-c model were set in favor of hypothesis 3, based on their expected behavior.

NDA MODELS The boundary conditions of both NDA models are shown in figure 2.2. The fresh water boundary had a fixed point water head, linearly increasing land inwards, roughly following the topography of the delta. The coastal boundary of the NDA models was modeled either open or closed off from 250 m to 1000 m depth (see also the next section on the sensitivity analysis), as the connectivity between the deeper parts of the NDA and the sea is still uncertain. The geometry of this boundary was determined with the General Bathymetric Chart for the Oceans' gridded dataset (GEBCO, 2014). This is a 30 arc-second grid, providing global bathymetric coverage. In addition, four horizontal clay layers were placed at different depths, spanning from the coastal boundary to the middle of the onshore model domain, following the conceptual cross-section by (Shata and Hefny, 1995).

At the bottom of the NDA-c model, the model receives its flow, dissolved salts and groundwater ages from the KES model as a fixed flux. The large time domain of the NDA-c model (2.5 Ma) matches the extent of the deposition of sediments that form the NDA. Therefore, the aquifer is initially thin at the start of the Pleistocene and grows in thickness with time; this implies that the distance between the bottom and top boundary increases with time. SEAWAT does not support a change of spatial domain size over time, therefore we ensured the "undeposited" part of the model did not contribute to the flow or solute transport system by making every "undeposited" cell a Cauchy boundary cell with zero salinity and a head matching the sea level at that timestep. After "deposition" of a cell, the boundary condition in that cell was deactivated, turning it into a regular active cell. This created stacked Cauchy boundaries (Figure 2.2), which were deactivated upwards as sedimentation progresses. The validity of this approach is shown in Appendix C. We used the most parsimonious sedimentation possible, namely assuming a constant sedimentation

Table 2.2: Parameters chosen for the KES model. We are purposely inconsistent with the units, as it allows for easier comparison with values found in the literature.

Parameter	Description	Value	Unit
$\beta_{p,\ Pliocene}$	Representative vertical compressibility Pliocene deposits	1e-8	m^2/N
$\beta_{p,\ Miocene}$	Representative vertical compressibility Miocene deposits	7.5e-9	m^2/N
$\beta_{p,\ Evaporites}$	Representative vertical compressibility evaporites	1e-10	m^2/N
$\rho_b - \rho_w$	Bulk density minus density fresh water	1100	kg/m^3
$\frac{\partial z_b}{\partial t}$	Sedimentation rate	3.9e-4 – 2.7e-4	m/year.
$n_{Pliocene}$	Representative effective porosity Pliocene deposits	0.10	-
$n_{Miocene}$	Representative effective porosity Miocene deposits	0.10	-
$n_{Evaporites}$	Representative effective porosity evaporites	0.01	-
$\frac{\partial \rho}{\partial C}$	Slope linear equation of state	0.71	$(kg/m^3)/(g/l)$
$K_{v,\ Pliocene}$	Vertical hydraulic conductivity Pliocene	1e-4	m/d
$K_{v,\ Miocene}$	Vertical hydraulic conductivity Miocene	1	m/d
$K_{v,\ Evaporites}$	Vertical hydraulic conductivity evaporites	1e-8	m/d
$\alpha_l, \alpha_t, \alpha_v$	Longitudinal, transversal and vertical dispersion length	10, 1, 0.1	m
D_c^*	Effective molecular diffusion	22.9e-10	m^2/s..

rate. With this we determined the location of the Cauchy boundary cells apriori for every input timestep (called "stress-period" in SEAWAT). We used a number of input timesteps (365) that exceeded the amount of model layers (100), to ensure the most gradual increase of the aquifer size that was possible.

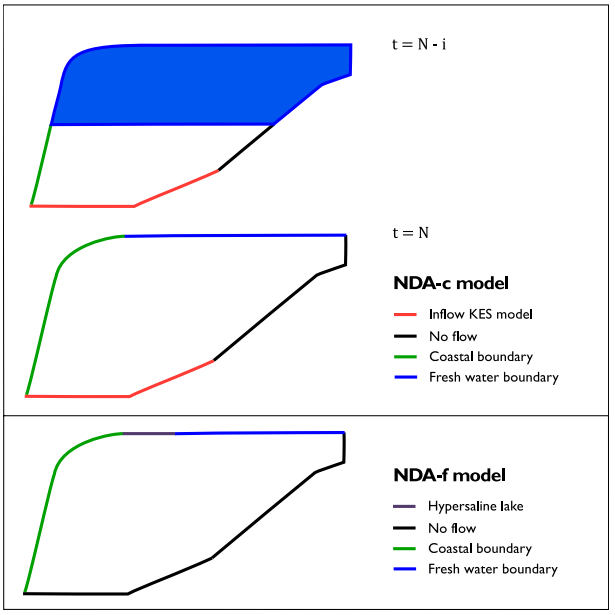

Figure 2.2: Boundary condition types for the NDA models. The NDA-c model figure shows 2 plots, the bottom plot is at the end of the time domain (t = N), the upper a moment in the time domain (t = N-i).

On top of the NDA-f model, a hypothetical 50 km long hypersaline inundation of 90 g/l was added for 8 ka, roughly the spatiotemporal extent of the Late Pleistocene Sabkha muds near the current coastline (Stanley and Warne, 1993), as these were the most favorable circumstances for free convection (appendix A.2). It is assumed that free convection was not limited by salt production or by water availability. The aim of the free convection model was not to accurately model chaotic fingering patterns nor their onset, as these are controlled by a) model discretization (for example, see Kooi et al., 2000; Prasad and Simmons, 2005; Zimmermann et al., 2006); b) heterogeneity (Simmons et al., 2001; Post and Simmons, 2010); c) dimensionality (Simmons et al., 2010); d) numerical solvers chosen (Zimmermann et al., 2006); e) dynamic boundary conditions, e.g. as reflected by the differences between the dimensionless numbers in Nield (1968) and Wooding et al. (1997) for flooded and dry circumstances respectively. This model was intended to obtain a sense of the time scale of free convection in a regional groundwater system of this size, for which this setup is sufficient (Figure A.4). For this model, a warm-up period of 120 ka was chosen to set the

Table 2.3: Parameters for the NDA-c model. In brackets the parameter value alterations for the NDA-f model. We are purposely inconsistent with units, as it allows for easier comparison with values found in the literature.

Parameter	Description	Value	Unit
$K_{h,\,sand}$	Horizontal hydraulic conductivity sand. Compaction case and free convection case	10 (75)	m/d
$K_{h,\,clay}$	Horizontal hydraulic conductivity horizontal clay layer.	5e-4	m/d
$\frac{K_h}{K_v}$	Anisotropy	10	-
$\alpha_l, \alpha_t, \alpha_v$	Longitudinal, transversal and vertical dispersion length	10, 1, 0.1	m
n_e	Effective porosity	0.10	-
$\frac{\partial z_b}{\partial t}$	Sedimentation rate	3.9e-4 (0)	m/year
$\frac{\Delta h_{riv}}{\Delta x}$	River gradient	3.125e-2 (9.375e-2)	m/km
S_f	Specific storage in terms of fresh water head	1e-5	1/m
$\frac{\partial \rho}{\partial C}$	Slope linear equation of state	0.71	$(kg/m^3)/(g/l)$.

initial conditions, roughly the extent of a glaciation cycle, but sea levels were kept constant to their relatively high current level, for the sake of parsimony. To ensure both vertical and horizontal propagation of hypersaline plumes, the clay layers were further extended land-inward with a conductivity of:

$$\log(K_{extension}) = \frac{\log(K_{sand}) + \log(K_{clay})}{2} \tag{2.19}$$

Without this extension, hypersaline plumes would only travel vertically downwards without intruding horizontally in-between clay layers. The conceptual idea behind this extension is a clay layer becoming thinner land-inwards (see also figure 2.1b), thus reducing in hydraulic conductivity.

SENSITIVITY ANALYSIS A sensitivity analysis was performed on the compaction models (KES + NDA-c), to study the influence of some of the underlying assumptions on the results. Inputs (parameters, boundary conditions and initial conditions) were altered one at a time from a base case, of which the values can be found in table 2.3. Firstly, the initial concentration in the Miocene deposits in KES was increased from 125 g/l to 200 g/l and the increased upward salt flux is injected into NDA-c model. Secondly, the horizontal clay layers in the NDA-c model were removed. Thirdly, the river stage at the apex was increased from 5 m to 15 m. Fourthly, the hydraulic conductivity of the NDA-c model was increased from 10 m/d to 25 m/d and 75 m/d, respectively. Finally, the bottom 750 m of the seaside boundary was either open or closed off, by setting the conductance (2.18) of the sea boundary to 1000 m^2/d or 2.5e-9 m^2/d. The first is seen as an extreme upper limit, and was calculated by assuming a 1 m thick layer of gravel of 100 m/d, and multiplying this by the area of a horizontal cell interface (10 m^2). The latter was calculated by multiplying an assumed horizontal hydraulic conductivity for unweathered marine clay (5e-6 m/d) by the area of a horizontal cell interface (10 m^2) and dividing this by the maximum observed horizontal extent of 20 km (Abdel Aal et al., 2000), and thus presents a lower limit. Scenarios were compared by looking at the depth difference between the 70 g/l isoconcentration line and 600 m at three observation locations, ε (m).

2.5 RESULTS

2.5.1 *Hypothesis 1: Molecular Diffusion*

Figure 2.3 shows that, even given a TDS concentration of 643 g/l, the highest ever measured as far as we are aware of (Hanor, 1994), the concentration at 1000 m depth is still below the observed concentration at 600 m depth. Even though all parameters are set in favor of this hypothesis, the observed TDS cannot be reproduced, which means that diffusion cannot be the sole cause of the observed hypersalinity at 600 m and there has to be at least a second process involved to cause enough upward salt transport through KES.

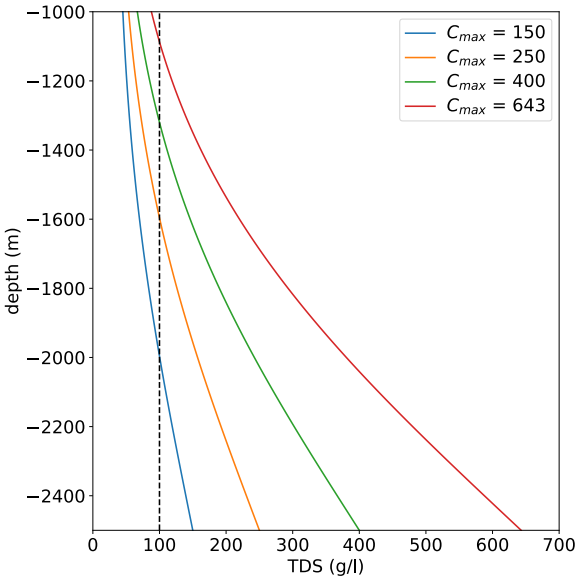

Figure 2.3: Modeled concentrations of pure molecular diffusion with depth for different maximum concentrations over the KES formation after 5.33 Ma (from the start of the Pliocene to present). The dashed line presents the maximum measured concentration that was measured at 600 m depth (100 g/l).

2.5.2 *Hypothesis 2: Double Diffusive Convection*

Filling in the most favorable limits for this hypothesis (see table 2.1 for their values) results in $Ra_t + Ra_c$ being strongly negative (-516), which is caused by the high Le (690). This entails that the buoyancy due to salinity works very stabilizing. Assuming there is enough mechanical dispersion (D_{mch}) so that the theoretical minimum of Le is approached:

$$\lim_{D_{mch}\to+\infty} Le = \lim_{D_{mch}\to+\infty} \frac{D_t + D_{mch}}{D_c^* + D_{mch}} = 1 \tag{2.20}$$

Then, given the parameters in table 2.1, still $N \approx -1$, meaning that:

$$Ra_t + Ra_c = Ra_t + Ra_t NLe \approx Ra_t - Ra_t \approx 0 \tag{2.21}$$

Furthermore, $Ra_t = 0.089 \ll Ra_{crit}$. So even with a constant salinity gradient, no free thermohaline convection is expected. Based on the high Le, $N \approx -1$, and low Ra_t, it is unlikely that there was any upward transport of solutes due to thermohaline induced free convection through KES. The thick, low-permeable KES formation's potential for dampening instabilities is too high for any large-scale instability to occur.

2.5.3 *Hypothesis 3: Sediment Compaction*

Figure 2.4a shows a comparison between modeled pressures and observations in a well near the city of Kafr El Sheikh (personal communication with dr. M. Tingay), per initial concentration scenario M125-M400. Both observations and our models follow a hydrostatic pressure distribution up to a depth of less than approximately 2.8 km, to which an initial concentration of 125 g/l seems to give the best fit. Around 2.8 km depth the observations show a sudden jump in pressure, indicating the presence of a low permeable seal, which consists of the Messinian evaporites (Rizzini et al., 1978; Nashaat, 1998). This seal is not completely impermeable; otherwise the observed pressure underneath the seal would approach lithostatic pressure. Our models also capture the pressure difference across this Messinian seal, which means that the upward groundwater flow encounters enough resistance. The resistance in our model might be overestimated as part of the pressure difference may already have been established during the Pliocene. In addition, the dissolved salts had more time to be transported through the seal. Thus our model represents a conservative estimate of upward salt transport. Figure 2.4b shows hypersaline groundwater with a concentration above the observed 100 g/l (Figure 2.1a) moving from the KES to the NDA due to compaction-induced upward salt transport and molecular diffusion. The increasing concentrations over time imply that salt transport has not yet reached steady-state. Therefore, if the hypersaline groundwater in the NDA is caused by compaction-induced salt transport, the mass flux of salt into the NDA is still present and presumably even increasing slowly on a geological time scale.

The results in figure 2.5a as obtained from the NDA-c model show that these upward salt mass fluxes from the KES to the NDA have the potential to cause salinities similar to those observed at 600 m depth in the NDA nowadays. Furthermore, if this has indeed occurred in reality, the hypersaline groundwater should be older than 2.5 Ma, and thus older than its surrounding sediment matrix. A subsequent sensitivity analysis shows that hypothesis 3 only holds if the bottom of the coastal boundary is closed as shown in figure 2.5b. If the boundary were open, the TDS at 600 m would decrease towards the coast (see also Figure A.1), which

is not observed in the field (Figure 2.1a). Moreover, with an open coastal boundary, the 70 g/l contour would not reach 600 m.

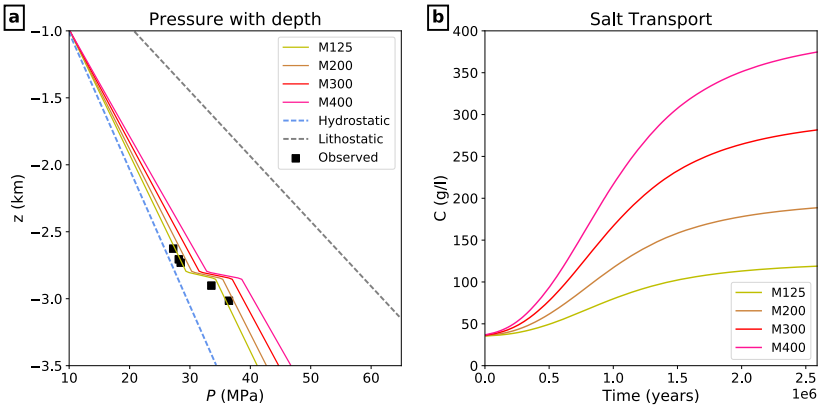

Figure 2.4: (a) Modeled pressure with depth, varied over different initial concentrations. M125 to M400 represent the KES model results, where the number indicates the initial concentration taken for the Miocene deposits. The hydrostatic pressure is calculated with a density of fresh water (1000 kg/m^3) and represents the minimum expected pressure. The lithostatic pressure is calculated with a ρ_b of 2100 kg/m^3 and represents the maximum possible pressure. The observations are from a well near the city of Kafr El Sheikh. (b) Concentrations (C) across the top boundary of the KES model.

2.5.4 *Hypothesis 4: Free Convection*

In the NDA-f model, a considerable volume of hypersaline groundwater is transported downwards in this model (Figure 2.6). After onset, the plume travels downwards for roughly 600 years until it reaches the bottom. This plume subsequently reaches the observation points in the case of an open boundary, but does not in the case of closed boundary. A closed coastal boundary in our model results in rejection of the NDA-f hypothesis: the hypersaline groundwater has difficulty to replace fresh groundwater that is trapped between clay layers and a closed coastal boundary.

We also make two observations that might be relevant to groundwater age measurement campaigns in the future. Firstly, free convective transport leads to an inversion in groundwater ages (Figure 2.6 left), though this inversion becomes negligible on longer timescales with an open coastal boundary (Figure 2.6 right).Secondly, it is observed that a closed boundary

results in groundwater ages exceeding the duration of glacial cycles (100 ka), despite the high hydraulic conductivity (75 m/d) and low porosity (0.10) of the aquifer in this model.

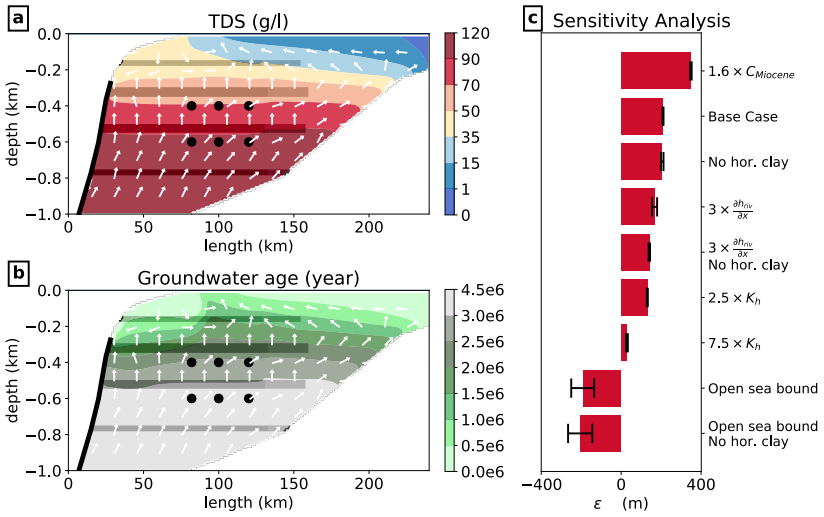

Figure 2.5: (a&b) Salinities (TDS) and groundwater ages after 2.5 Ma in the base case NDA-c model. The black dots represent the approximate location where observations are taken; the white arrows indicate the direction of the groundwater flow; the shaded areas represent the location of clay layers in the model. Note that the cross-section is stretched in the vertical direction by a factor 100. The left upper intrusion of young groundwater is caused by the sudden shift land inwards of the coastal boundary when the sea level rises over the top left rounded corner of the delta front. (c) Bar plot showing the results of a sensitivity analysis performed with the NDA-c model. ε is the depth difference between the observation locations (3 points at 600 m depth) and the 70 g/l isoconcentration contour at the observation locations. The error bars show the range of ε; a higher range means a stronger inclined isoconcentration line. For input values, see table 2.3.

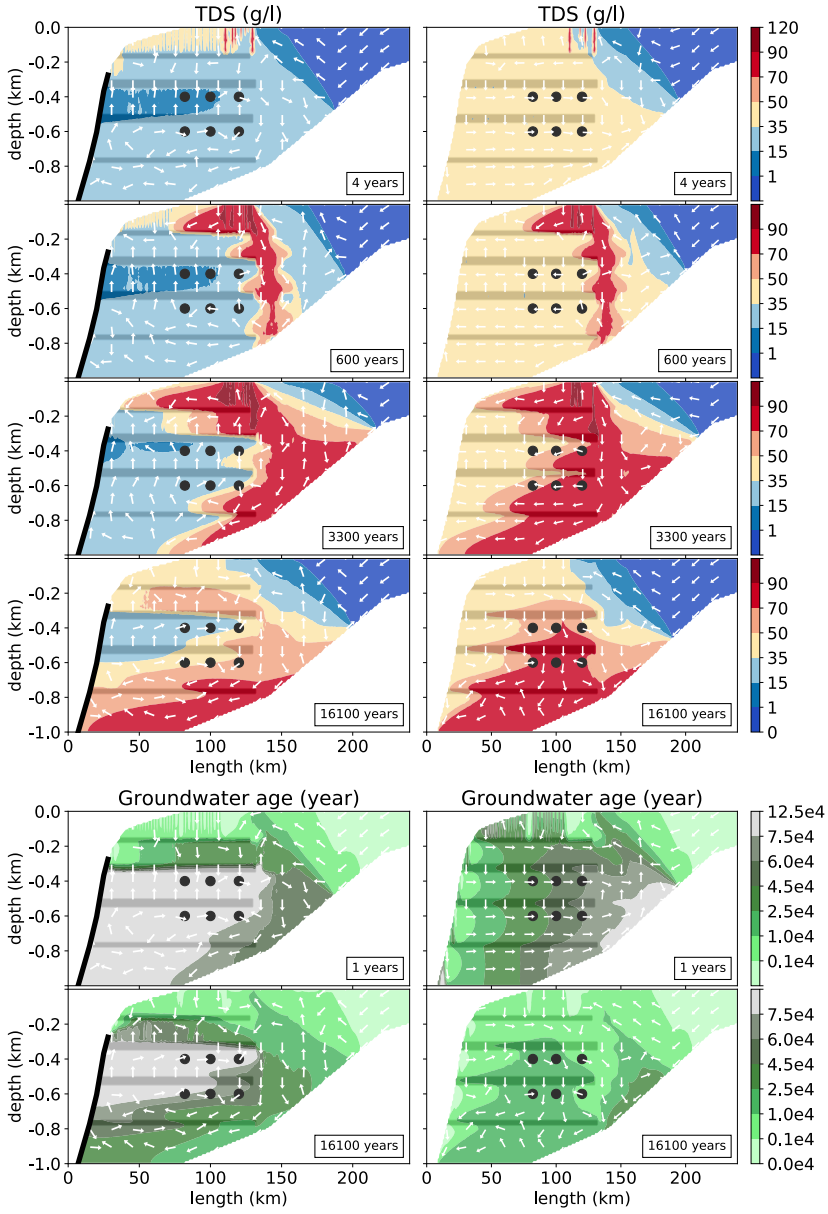

Figure 2.6: Salinities and groundwater ages after a hypersaline inundation (of c = 90 g/l, that lasted 8 ka) was formed. Note that the NDA-f model had 120 ka of spin-up time prior to the inundation (reflected in the groundwater ages) and that the groundwater ages legend scale differs from that in figure 2.5a. The left hand column presents the results with a closed off coastal boundary, the right with an open boundary. The ribbed shape of the downward moving plume at 600 years is due to the horizontal extensions of the clay layers, see equation 2.19.

2.6 DISCUSSION

Our computational investigation did not lead to a final conclusion as to the origins of the hypersaline groundwater. Consequently a brief discussion of measurements to discriminate hypothesis 3 from 4 is necessary. With groundwater dating it might be possible to discriminate these two hypotheses. Upward compaction-induced salt transport leads to groundwater ages older than the surrounding sediment matrix. Since overpressures are a common phenomenon in deltas (Sharp and Domenico, 1976; Neuzil, 2003), it is safe to assume that the same holds for upward transport of major volumes of connate groundwater into delta aquifers, e.g. as presumably occurred in The Netherlands (Verweij, 1999; Griffioen et al., 2016). Whether this groundwater is still present in these aquifers highly depends on the hydrogeological connection between aquifer and sea. This connection is critical to coastal hydrogeology (Yechieli et al., 2009), since it also influences potential offshore fresh water resources (Post et al., 2013) and submarine groundwater discharge (Taniguchi et al., 2002). Groundwater dating in combination with our current analysis could thus lead to important conclusions regarding both the origins of the hypersaline groundwater and the interaction between the deeper parts of the NDA and the Mediterranean Sea. If the groundwater is found to be older than 2 Ma (Figure 2.5), it originates from Messinian deposits and the hydrogeological connection with the sea is limited. In contrast, if it is found to be younger than 100 ka old, it presumably is the result of free convective systems and the coastal boundary is open. $^{81}Kr^{-}$ dating may be the most suitable method to discriminate these two hypotheses (Sturchio et al., 2004; Aeschbach-Hertig, 2014), as $^{36}Cl^{-}$ dating is not suited for saline fluids (Park et al., 2002).

Determining the chemical composition of the groundwater and comparing this to published cases will certainly lead to new insights. A start would be the Br^{-}/Cl^{-} ratio, which is useful in discriminating whether salinity is caused by evapoconcentration or rock salt dissolution (Hanor, 1994). This is not necessarily enough information to discriminate hypothesis 3 from 4, since the groundwater from underneath the KES could also have been evapoconcentrated during the Messinian, as thought to have happened in the East Mediterranean Sea (Vengosh et al., 1998). More suitable might be non-conservative environmental tracers that interact with clay, as hypersaline groundwater of hypothesis 3 had more time to interact with clay minerals, under higher temperatures, than groundwater of hypothesis 4. Examples of these are Na^{+}, Ca^{2+}, Sr^{2+}, B, K^{+}, and δ^{11} B (Vengosh et al., 1999). Useful cases for the comparison are the hypersaline water found in the deep eastern Mediterranean basin (Vengosh et al., 1998) and at the coastal sabkhas in the Northern Sinai (Levy, 1977; Gat and Levy, 1978), which might be suitable analogues for the hypersaline groundwater of respectively hypothesis 3 and 4.

There are limitations to this computational investigation. Regarding the free convection model (NDA-f), it is difficult to constrain a paleo-reconstruction of a process controlled so strongly by heterogeneity and that acted on such a relatively small timescale. This is in part reflected by the very limited number of field observations of free convection in groundwater; despite over a century of research, the first field observations started to be reported only in the last decade (Andersen et al., 2007; Van Dam et al., 2009). In addition, our assumption of free convection unrestricted by salt or fluid availability is applicable to a sabkha delta which continuously receives new saline water, but may be inappropriate for a floodplain. Furthermore, in both this model and NDA-c we did not take the sea level variation of a glacial cycle into account. The low sea-level stands during a glacial period would result in a wider fresh water zone (Post et al., 2013) and the sea level variations might also result in a wider mixing zone, e.g as happens on a larger spatiotemporal scale in carbonate platforms (Jones et al., 2002). The effect of a higher hydraulic gradient on the NDA-c model is shown in the sensitivity analysis, though not to the extent as the gradient reached during the Pleistocene. In short, our results intentionally present a hypothetical, extreme case.

Regarding the KES model, it is possible that the hydrogeological system in the pre-Miocene deposits is connected to the Miocene deposits in some compartimized areas through faults, which may imply that thermal processes become important in determining the salt concentration underneath the KES formation (Garven, 1995; Lopez and Smith, 1995). However, this is excluded from this research, because of the scarcity of published data of the deep hydrogeology underneath the Nile Delta. Furthermore, we assumed that the side boundaries are impermeable due to faulting. For the side boundary offshore (in the north) this is reasonable, given the high lateral differences in overpressure (Nashaat, 1998), but onshore this might be different. As far as we are aware off, no pressure measurements in the deeper strata underneath the Nile Valley have been published to assess the validity of this assumption.

Two processes are not covered in this research, which could serve as alternative hypotheses. Firstly, hypersaline groundwater may preferentially flow along faults, as faults are observed that propagate through the KES formation (Abd-Allah et al., 2012). These faults might act as a conduit for upward flow (Bense et al., 2013). Secondly, leaking abandoned petroleum exploration wells could act as an anthropogenic source of salt water. At least 90 wells had been drilled by 1989 (Sestini, 1989) because of the area's high oil and natural gas potential (Kirschbaum et al., 2010), which may potentially leak hypersaline groundwater upwards driven by the overpressures underneath KES. This would result in high salinities focused around exploration areas. Both these processes would result in a more heterogeneous distribution of salinities and also in temperature anomalies (Bense et al., 2013), thus testing these

two hypotheses requires more data than is currently available and is therefore a topic for further research.

The origins of the hypersaline groundwater have crucial implications for the expected occurrence of deeper fresh water pockets; our results show that the salinity distribution by free convection is largely affected by clay layers whereas the slow compaction-induced upward advection is quite insensitive to these layers. Our models with free convection show that lower salinity water might be trapped between clay layers, whereas no salinity inversions were simulated in models with sedimentation compaction as the driver.

2.7 CONCLUSIONS

Two of the four hypotheses of this research remain valid. The hypersaline groundwater in the NDA is either caused by compaction-induced salt transport (hypothesis 3) or free convective systems (hypothesis 4). Both the NDA-c model and the NDA-f model are able to reproduce the observed high TDS values, given the right coastal boundary condition. This condition has opposite effects on the plausibility of these models; an open boundary results in the rejection of the NDA-c model (the hypersaline groundwater does not reach 600 m depth), whereas in the NDA-f model a closed boundary hinders the hypersaline groundwater in replacing the fresh water between the clay layers, and in our conceptualization, reaching the observation point. The origins of this hypersaline groundwater affect the probability of the existence of deep fresh water pockets. This probability is reduced if the hypersaline groundwater originates from underneath the KES and was transported upwards following the assumptions made in this paper. Deep fresh water pockets are considered more probable if the hypersaline groundwater was brought downwards by free convection.

ACKNOWLEDGEMENTS

Firstly, we thank Hanneke Verweij and Andrea Forzoni for their helpful ideas and remarks on the hydrogeology. Secondly, we thank Mark Tingay for kindly providing us with overpressure data. Thirdly, we thank two anonymous reviewers for their critical, helpful comments and remarks, which greatly enhanced the quality of this paper. This research is financially supported by the Netherlands Organization for Scientific Research (NWO), and carried out within The New Delta program. The data used are listed in the references and supplements.

3

A THREE-DIMENSIONAL PALEOHYDROGEOLOGICAL RECONSTRUCTION OF THE GROUNDWATER SALINITY DISTRIBUTION IN THE NILE DELTA AQUIFER

ABSTRACT

The Holocene transgression is often put forward to explain observed groundwater salinities that extend far inland in deltas. This hypothesis was also proposed in the literature to explain the large landward extent of saline groundwater in the Nile Delta. The groundwater models previously built for the area used very large dispersivities to reconstruct this saline and brackish groundwater zone. However, this approach cannot explain the observed freshening of this zone. Here, we investigated physical plausibility of the Holocene-transgression hypothesis to explain observed salinities by conducting a paleohydrogeological reconstruction of groundwater salinity for the last 32 ka with a complex 3D variable-density groundwater flow model, using parallel computation. Several scenarios with different lithologies and hypersaline groundwater provenances were simulated, of which five were selected that showed the best match with observations. Amongst these selections, total freshwater volumes varied strongly, ranging from 1526 to 2659 km^3, mainly due to uncertainties in the lithology offshore and at larger depths. In all five selected scenarios the total volume of hypersaline groundwater exceeded that of sea water. We also show that during the last 32 ka, total freshwater volumes significantly declined, with a factor ranging from 2 to 5, due to the rising sea-level. Furthermore, the time period required to reach a steady state under current boundary conditions exceeded 5.5 ka for all scenarios. Finally, under highly permeable conditions the marine transgression simulated with the paleohydrogeological reconstruction led to a steeper fresh-salt interface compared to its steady-state equivalent, while low permeable clay layers allowed for the preservation of fresh groundwater volumes. This shows that long-term transient simulations are needed when estimating present-day fresh-salt groundwater distributions in large deltas. The insights of this study are also applicable to other major deltaic areas, since many also experienced a Holocene marine transgression.

Based on: van Engelen, J., Verkaik, J., King, J., Nofal, E.R., Bierkens, M.F.P. Oude Essink, G.H.P. (2019) A three-dimensional palaeohydrogeological reconstruction of the groundwater salinity distribution in the Nile Delta Aquifer, *Hydrology and Earth System Science 23*, 5175—5198

3.1 INTRODUCTION

Paleohydrogeological conditions have influenced groundwater quality in the majority of large-scale groundwater systems (Edmunds, 2001; Jasechko et al., 2017). These conditions can especially be found in deltaic areas, where the effects of marine transgressions are often still observed in groundwater salinities (Larsen et al., 2017). More specifically, their low elevation allowed for far reaching marine transgressions, leading to a large vertical influx of sea water, and hampered subsequent flushing with fresh water after the marine regression. This hypothesis is supported by hydrogeochemical research in several deltas (e. g. Colombani et al., 2017; Fass et al., 2007; Faye et al., 2005; Manzano et al., 2001; Wang and Jiao, 2012). The physical feasibility of this hypothesis, however, has not often been tested in the form of paleohydrogeological modelling, with a few notable exceptions (Delsman et al., 2014; Larsen et al., 2017; Van Pham et al., 2019). Delsman et al. (2014) conducted a detailed paleohydrogeological reconstruction of the last 8.5 ka over a cross-section in the Netherlands to show that the system has never reached a steady state. They showed that the Holocene transgression caused substantial groundwater salinization, from which the system is still recovering. Using a combination of geophysical data and 2D numerical models, Larsen et al. (2017) showed that during the Holocene transgression sea water preferentially intruded in former river branches in the Red River Delta, Vietnam. Van Pham et al. (2019) showed that most of the fresh groundwater in the Mekong Delta (Vietnam) was likely recharged during the Pleistocene and preserved by the Holocene clay cap. Despite being in a humid climate, recharge to the deeper Mekong Delta groundwater system is very limited and freshwater volumes are still declining naturally.

The Nile Delta is one of the deltas where the marine transgression hypothesis has not been tested by physical analysis yet, despite severe problems with groundwater salinity (section 3.2.1). This saline groundwater issue has led to a continuous line of research into fresh and saline groundwater occurrences in the Nile Delta Aquifer (NDA). These studies can be divided into hydrogeochemical and groundwater-mechanical studies. The latter subdivision covers all studies focused on groundwater flow, following Strack (1989). Starting with the hydrogeochemical studies, Geirnaert and Laeven (1992) provided the first conceptual paleohydrological model (dating back to 20 ka). They used groundwater dating to show that shallow groundwater was likely recharged as fresh river water around 3.5 ka. Barrocu and Dahab (2010) extended this conceptual model to up to 180 ka and concluded that the saline groundwater in the north is old connate groundwater trapped in the Early Holocene, because it is freshening. Geriesh et al. (2015) further supported this conceptual model with additional measurements. As an example of a study based on groundwater mechanics, Kashef (1983) used the Ghyben-Herzberg relationship to demonstrate that the

seawater wedge reached far inland. This was further confirmed by the 2D numerical model constructed by Sherif et al. (1988), who concluded that the width of the dispersion zone may be considerable. Sefelnasr and Sherif (2014) showed the sensitivity of the area to sea-level rise with a 3D numerical model, as the low topography of the Nile Delta allowed for a far reaching land surface inundation that can be detrimental to freshwater volumes (Ketabchi et al., 2016; Kooi et al., 2000). Mabrouk et al. (2018) showed that groundwater extraction is a larger threat to freshwater volumes than sea-level rise, under the assumption that land surface inundation with sea water is prevented. van Engelen et al. (2018) investigated the origins of hypersaline groundwater that is found starting from 400 m depth, which was overlooked in previous studies. They tested four hypotheses of which two remained valid: 1) free convection of hypersaline groundwater formed in the Late-Pleistocene coastal sabkha deposits and 2) upward compaction-induced flow of hypersaline groundwater, formed during the Messinian Salinity Crisis. Moreover, they showed the influence of uncertain lithology on the groundwater salinity distribution.

All the previously discussed groundwater-mechanical studies except van Engelen et al. (2018) neglected the influences of paleohydrogeological conditions that were inferred by hydrogeochemists. Instead, they used longitudinal dispersivities exceeding 70 m to simulate the large brackish zone in the groundwater system (Figure 3.1) (Sefelnasr and Sherif, 2014; Sherif et al., 1988). The hydrogeochemical studies, however, attribute this zone to a former, more landward extent of the seawater wedge during the Holocene transgression, since a large fraction of the brackish zone is presumably freshening (Geriesh et al., 2015; Laeven, 1991) and the extent of this brackish zone coincides with paleo-shorelines (Kooi and Groen, 2003; Stanley and Warne, 1993) (Figure 3.1). A variable-density groundwater flow model with present-day boundary conditions and a large amount of hydrodynamic dispersion cannot support the freshening of the brackish zone, since hydrodynamic dispersion would only lead to progressive salinization. In addition, currently no reliable field data exists that supports longitudinal dispersivities beyond 10 m (Zech et al., 2015). This discrepancy in conceptualization still exists, despite the large influence of paleohydrogeologcial conditions on salinities previously shown by applying variable-density groundwater flow models to other cases (e. g. Kooi et al., 2000; Meisler et al., 1984)

The lack of including paleohydrogeological development in variable-density groundwater flow and coupled salt transport models is understandable as it requires vast amounts of computational resources, especially when 3D reconstructions are considered. The availability of a newly developed model code that allows for high-performance computing (Verkaik et al., 2017), has now made it possible to create the first numerical paleohydrogeological reconstruction of the NDA in 3D. Therefore, in this study we have constructed a variable-

density groundwater flow and coupled salt transport model of the NDA and use it for a paleohydrogeological reconstruction of salinity over the last 32 ka. Specifically, we use the model to 1) investigate the physical plausibility of the Holocene transgression hypothesis for the Nile Delta; 2) investigate the influence of the uncertain geology (Enemark et al., 2019); 3) provide volume estimates of present-day fresh groundwater [FGW]; 4) assess the relative importance of using paleohydrogeological reconstructions against less expensive steady-state modelling.

3.2 AREA DESCRIPTION

3.2.1 *Area relevance and vulnerability*

The Nile Delta is vital for Egypt. It is an important bread basket, as it has been through history (Dermody et al., 2014), since it is the main area suitable for agriculture in an otherwise water-scarce region (WRI, 2008). Furthermore, the area is densely populated (Higgins, 2016), and the population is only expected to increase over the coming decades (World Bank, 2018). Although the area is traditionally irrigated with surface water, agriculture increasingly relies on groundwater (Barrocu and Dahab, 2010). For instance, a majority of interviewed farmers in the central delta indicated that they are pumping groundwater almost continuously during the summer (El-Agha et al., 2017). This groundwater pumping will increase in the future, as large dams are planned or built upstream, e.g. the Grand Ethiopian Renaissance Dam (GERD), which will reduce the discharge of the Nile and will consequently hamper flushing of the irrigation system. This is expected to further deteriorate the quality of surface water , which is currently in a critical state already; the water that currently reaches the sea is mostly saline and highly polluted (Stanley and Clemente, 2017). For example, the nitrate concentrations of the water inflow into the Manzala lagoon have increased by a factor 4.5 in the past 20-25 years, as an effect of the intensified agriculture and the reduced inflow of river water (Rasmussen et al., 2009). Given the increasing stress on the groundwater system, it is important to assess the status of the current and future freshwater volumes. Despite the large groundwater volume of the NDA, the amount of groundwater suitable for domestic, agricultural or industrial water supply is limited. A considerable fraction of the groundwater volume is saline (Kashef, 1983; Sefelnasr and Sherif, 2014) or even hypersaline (van Engelen et al., 2018), and unsuitable for most uses. Saline groundwater can be detrimental to Egypt's already critical food supply. For example, when increased irrigation caused the level of the brackish groundwater to rise in Tahrir, Cairo, wheat yields reduced by 41% within a four year period as soil salinity increased (Biswas, 1993).

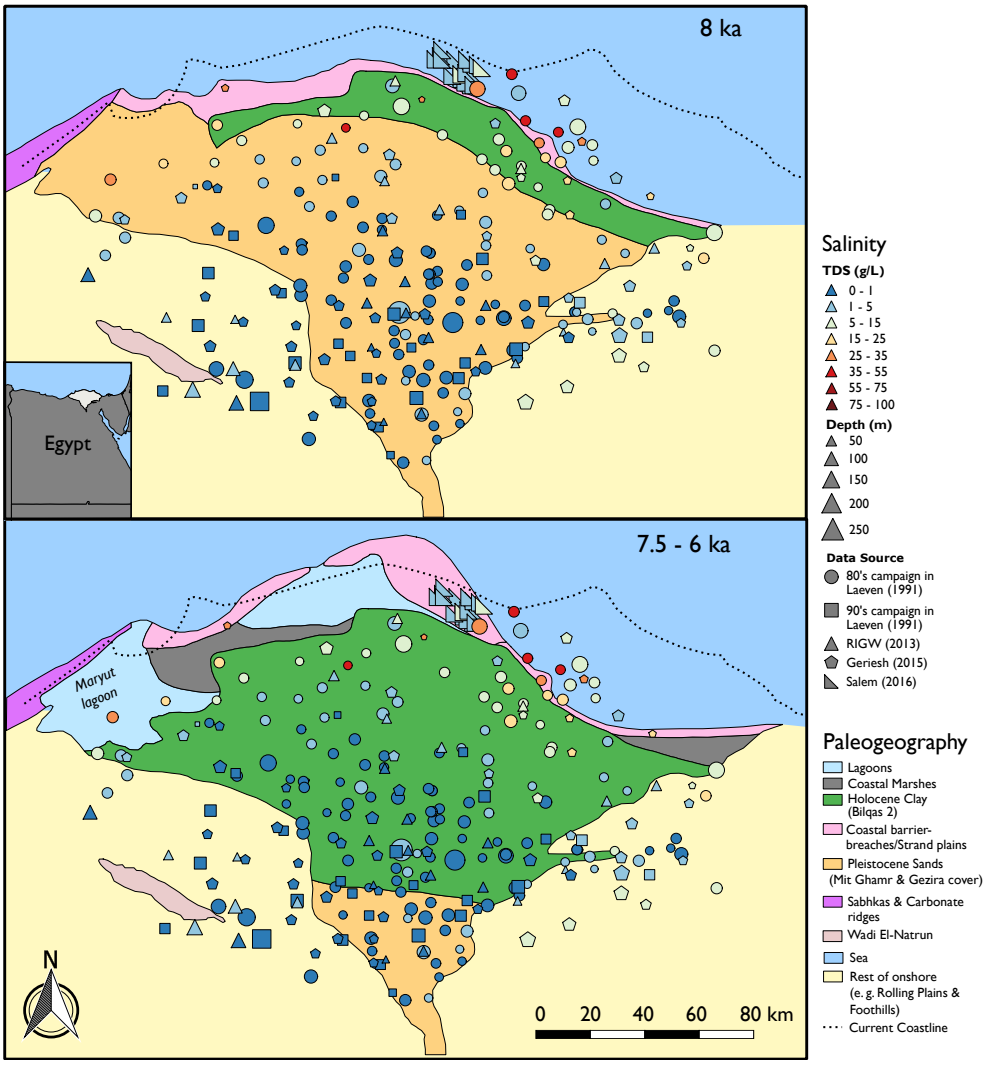

Figure 3.1: paleogeography and groundwater salinity measurements up to 250m depth of the Nile Delta. paleogeographical data from Pennington et al. (2017). The inset shows the location of the delta in Egypt.

3.2.2 *Hydrogeology*

The NDA is remarkably thick, reaching up to 1 km depth at the coast (Sestini, 1989). For reference, only 0.3% of the coastal aquifers in the world are estimated to exceed this thickness (Zamrsky et al., 2018). The NDA consists of the Late-Pliocene El Wastani formation and the Pleistocene Mit Ghamr formation. These both contain mainly coarse sands with a few clay intercalations (Sestini, 1989). It is capped by the Holocene Bilqas formation, which has recently been mapped extensively (Pennington et al., 2017). The Pliocene Kafr El Sheikh formation is generally assumed to be the hydrogeological base as it is 1.5 km thick and consists mainly of marine clays, though it is possible that there is compaction-driven salt transport through this layer (van Engelen et al., 2018). Hydrogeological research dealing with this area generally assumed that the connection between aquifer and sea is completely open (e. g. Kashef, 1983; Mabrouk et al., 2018; Sefelnasr and Sherif, 2014; Sherif et al., 1988), but there exists ample evidence against this assumption from both seismics (Abdel-Fattah, 2014; Abdel Aal et al., 2000; Samuel et al., 2003) as well as from the fact that offshore borelogs contain more clay than sands (Salem and El-Bayumy, 2016). These observations can be explained by the fact that the fraction of marine clays in deltas generally increases seawards (Nichols, 2009). These marine clays can even form large vertical clay barriers when deposited during aggradational or retrogradational phases (Nichols, 2009) with a major effect on the groundwater system (van Engelen et al., 2018).

3.2.3 *Groundwater salinity*

Figure 3.1 shows all groundwater Total Dissolved Solids (TDS) measurements above 250 m depth that we could find in literature (Geriesh et al., 2015; Laeven, 1991; Salem and El-Bayumy, 2016), combined with data of the Research Institute for Groundwater (RIGW) (Nofal et al., 2015). Other publications are not included as 1) these did not report measurement depths, 2) did not report measurement locations, or 3) only showed isohalines, from which the actual measurement locations are impossible to discern. The few available salinity measurements deeper than 250 m are not shown here as these are likely not influenced by the Holocene transgression (van Engelen et al., 2018). The depicted measurements highlight considerable spatial variation, especially in the brackish zone. This variability in measured salinity can be explained with 1) the different measurement depths, 2) different data sources, with different data quality and dates of their measurement campaigns, 3) heterogeneity in the hydraulic conductivity of the subsoil resulting in heterogeneous salt transport, and 4) heterogeneous evapoconcentration. The latter process is inferred from the observed salinities that exceed the salinity of sea water (35 g TDS L-1), which presumably are pockets of

evapoconcentrated Holocene groundwater (Diab et al., 1997). Despite the spatial variability in salinity, we observe a trend: the extent of the brackish zone seems to conform in the east to the coastline during the maximum transgression at 8 ka. Westwards, the extent of this zone can be explained with the location of the former Maryut lagoon, which had several periods where its salinities approached that of sea water (Flaux et al., 2013). It is important to note that our dataset is biased towards areas with low soil salinities, as measurements have been preferentially taken in the most productive agricultural areas, which are therefore of higher economic interest to monitor. A comparison of our dataset with soil salinity maps (Kubota et al., 2017) shows that in the coastal areas soil salinities are high, which are the areas where we have the least measurements. This bias is particularly evident from the data gathered by (Salem and El-Bayumy, 2016). These authors conducted research in the only coastal area with low soil salinities, which is an area that has predominantly consisted of coastal dunes from 7.5 ka until present (Sestini, 1989; Stanley and Warne, 1993), thus providing the hydrogeological circumstances for the development of a freshwater lens. The other, former dune areas (Figure 3.3) were either eroded naturally or removed by humans (El Banna, 2004; Malm and Esmailian, 2013; Stanley and Clemente, 2014) and have high soil salinities, presumably causing former freshwater lenses to salinize. Given this bias in our dataset towards fresh groundwater, the extent of the saline groundwater problem is likely underexpressed in figure 3.1.

3.3 METHODS

3.3.1 *Lithological Model*

A dataset of 159 borelogs was compiled using georeferenced data from different literature sources (Coleman et al., 1981; Nofal et al., 2016; Salem and El-Bayumy, 2016; Summerhayes et al., 1978). These were used to constrain a 3D lithological model using SKUA-GOCAD's implicit modelling engine (Paradigm, 2017). There are two main conceptual uncertainties in the resulting lithological model. The first pertains to the question of to what extent the continental slope is covered with low-permeable clayey sediments (section 3.2.2) and second whether the clay layers observed in the NDA are continuous, forming low permeable structures, or are disconnected with only a limited effect on regional groundwater flow. To account for these uncertainties, nine different lithological model scenarios were constructed (Figure 3.2), where we varied the height of the clayey sediments on the continental slope and the hydraulic conductivity of the onshore-reaching clay layers. The height of the clayey sediments determines how disconnected the deeper groundwater system is from the sea, and thus the ability of the system to preserve denser hypersaline groundwater in its aquifers

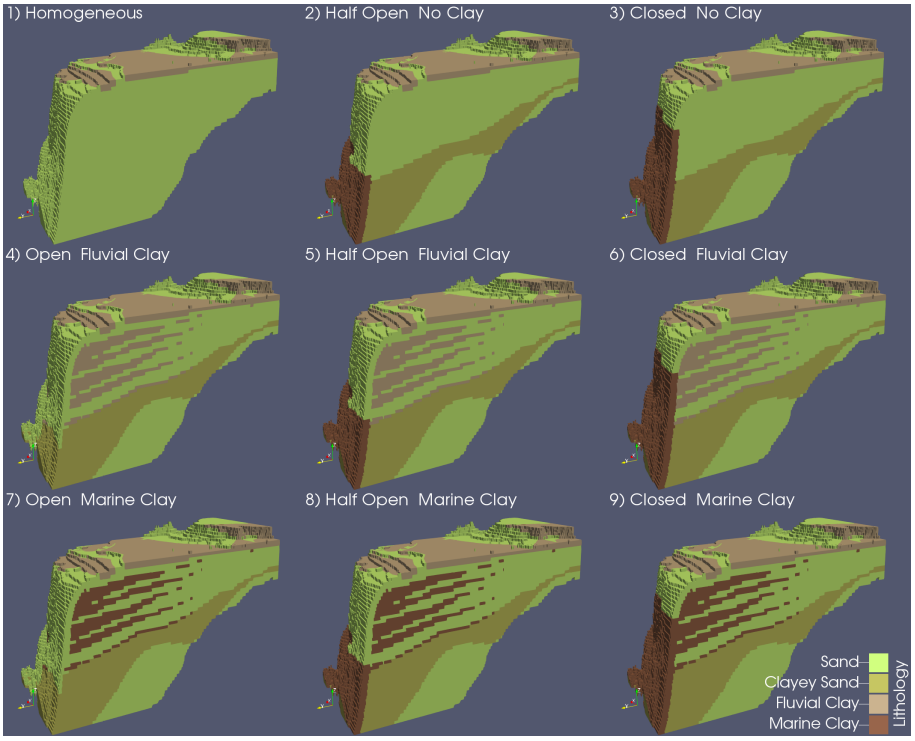

Figure 3.2: Snapshots of the lithological model scenarios that are used as input for the numerical variable-density groundwater flow model. The eastern half of the model is plotted here (see figure B.1 for the extent). The first word refers to the connection to the sea of the deeper part of the NDA, the second word to the assigned hydraulic conductivity of the onshore-reaching clay layers.

(van Engelen et al., 2018). The hydraulic conductivity of the onshore-reaching clay layers is varied to get a first-order approximation of the effect of clay layers on regional groundwater flow. We assigned a continuous hydraulic conductivity to these clay layers, based on three different lithologies (in order of decreasing hydraulic conductivity): sand, fluvial clay and marine clay (Table B.1). The rationale behind this is that small clay lenses have negligible effect on regional groundwater flow, thus are assigned a hydraulic conductivity of sand. Fluvial clay layers are assigned a hydraulic conductivity of the current confining Holocene clay layer, as this was deposited under fluvial conditions (Pennington et al., 2017). Marine clay layers present continuous layers of low conductivity with a big influence on the regional groundwater flow.

3.3.2 *Model code and computational resources*

We applied the newly developed iMOD-SEAWAT code (Verkaik et al., 2017) which is based on SEAWAT (Langevin et al., 2008), but supports distributed memory parallelization that allows for a significant reduction in computation times. The SEAWAT code is the industry standard for solving variable-density groundwater and coupled solute transport problems, therefore the reader is referred to its manuals for an extensive explanation (Guo and Langevin, 2002; Langevin et al., 2003; Langevin et al., 2008). The main improvement of the iMOD-SEAWAT code is that it replaces the original solver packages for variable-density groundwater flow and solute transport (respectively PCG and GCG) with the Parallel Krylov Solver package (PKS). The PKS linear solver is largely based on the unstructured PCGU-solver for MODFLOW-USG (Panday et al., 2013) and solves the global linear system of equations with the additive Schwarz parallel preconditioner (Dolean et al., 2015; Smith et al., 1996) using the Message Passing Interface (The MPI Forum, 1993) to exchange data between subdomains, where each subdomain is assigned its own private memory on a computational node. The variable-density flow problem and the solute transport problem are solved in parallel using respectively the additive Schwarz preconditioned Conjugate Gradient and BiConjugate Gradient Stabilize linear accelerators (Barrett et al., 2006; Golub and Van Loan, 1996). Simulations were conducted on the Dutch national computational cluster Cartesius (Surfsara, 2014), using Intel Xeon E5-2690 v3 processors. With this new code the model scenarios had a wall clock time ranging from 44 hours to 108 hours on 48 cores, depending on model complexity.

3.3.3 *Boundary conditions*

3.3.3.1 *Stress periods*

The paleohydrogeological reconstruction consisted of several consecutive stress periods (Figure 3.3), following Delsman et al. (2014), in which boundary conditions were kept constant. Each stress period was assigned a paleogeographic map (Pennington et al., 2017; Stanley and Warne, 1993) that defines the location of five geographical classes, namely sea, lagoon, sabkha, river, and dune/beach. Each was associated with boundary conditions that are explained more extensively in the sections "Surface Water", "Dunes and beaches", and "Extractions"; a summary of their data sources can be found in table 3.1. The lithological classes “clay” and “sand” indicate where the Holocene confining clay layer was respectively located and absent in each stress period. Firstly, stress periods 1 and 2 spanned the Late-Pleistocene, when sea-levels were low and therefore the coastline was located 70 km further to the North and the hydraulic gradient was high. The area consisted of an alluvial plain

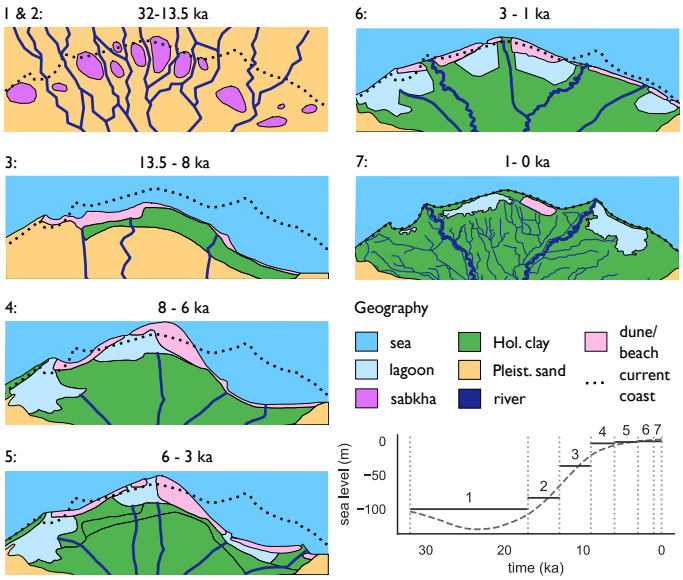

Figure 3.3: Stress periods with simplified paleogeography used as boundary conditions. Figures modified after Pennington et al. (2017) and Stanley and Warne (1993). The panels focus on the area around the present-day coastline (see figure B.1 for the extent), where the upper boundary conditions varied the most. The actual model domain extended beyond the extents of these panels. In the bottom right: the median eustatic sea-level curve (Spratt and Lisiecki, 2016) and the selected sea level for each stress period.

with braided rivers. In between these rivers, sabkha (salt flat) deposits were found in local depressions, which stayed fixed in location (Stanley and Warne, 1993). Next, stress period 3 represented the marine transgression, which was a period of rapid sea-level rise at the start of the Holocene. In stress period 4 the delta started prograding in the west and centre, and lagoons were formed. Of particular interest is the large extent of the Maryut lagoon in the west, filling up what is now known as the Maryut depression (Warne and Stanley, 1993). In stress period 5, progradation started in the east, leading to the symmetrical shape of the delta in stress period 6. This progradation was caused by the decreased hydraulic gradient that led to finer sediments being deposited, which were subsequently transported eastwards in accordance with the flow direction of sea currents. During stress period 7, humans converted most river branches to a system of irrigation channels, leaving only the Rosetta and Damietta river branches to persist.

Table 3.1: References to data used for spatially and/or time-varying input to the model.

Data	Temporal	Spatially	Reference	Remarks
Late Pleistocene sea-level (Eustatic)	yes	no	Spratt and Lisiecki 2016	
Holocene sea-level (Mediterranean Sea)	yes	no	Sivan et al. 2001	No detailed sea-levels for the Holocene exist for the Nile Delta, the closest data is from the Levant (Pennington, 2017)
paleosalinities lagoons	yes	no	Flaux et al. 2013	Data for Maryut lagoon, taken as representative for other lagoons
paleogeography	yes	yes	Pennington et al. 2017; Stanley and Warne 1993	paleogeography determines the spatial-temporal occurrence of the sea, dunes, rivers, and lagoons
Bathymetry	no	yes	GEBCO 2014	
DEM	no	yes	NASA 2014	
Groundwater extraction wells	yes	yes	Nofal et al. 2018	
Geological borelogs	no	yes	Nofal et al. 2018	

3.3.3.2 *Surface waters*

The surface water systems (the sea, rivers, and lagoons), were incorporated as a Robin boundary condition (Jazayeri and Werner, 2019), requiring a specified head, salinity, and bed resistance, the latter being the resistance exerted by the bed sediments. Of these three inputs, the least is known about the bed resistance. A 100 day resistance was used for all surface water systems (Table B.1), which is a common value for models of the Rhine-Meuse Delta (De Lange et al., 2014; Timmerman and Hemker, 1993). In Appendix B.2 we discuss the effects of this assumption in more detail. Sea boundary cells were placed on the edge of the coastal shelf and slope, following the present-day bathymetry (GEBCO, 2014) up to the paleocoastline. This coastline was specified, when possible, with paleogeographic maps (Figure 3.3), which meant that for the Late-Pleistocene (stress periods 1 and 2) we had to resort to using the paleo sea-level and the present-day bathymetry to approximate the coastline. We specified the head using paleo sea-level curves. No specific sea-level curves are available for the Nile Delta (Pennington et al., 2017). Hence we resorted to eustatic sea-levels for the Pleistocene (Spratt and Lisiecki, 2016) and a more local curve for the Holocene (Sivan et al., 2001), as this was the best information available. The minimum sea-level was fixed at -100 m, as below that achieving numerical convergence was cumbersome. This only slightly affected results as land surface inundation at these sea-levels was nearly equal due to the steep coastal slope. The salinity of the sea was set at a constant 35 g TDS L-1. Of the total of seven stress periods, the last four have lagoons, since lagoons started to form from 7.5 ka. The lagoon stage was set such that it was in hydrostatic equilibrium with the sea. Lagoonal paleo-salinities were estimated from the published strontium isotope ratios from the Maryut lagoon (Flaux et al., 2013) for each stress period. To be specific, the salinities assigned to stress periods 3 to 7 are respectively: 18, 9, 4.5, 2.5 g TDS L-1. The decreasing trend in salinities is partly the result of a progressively humid climate and increased human influence (Flaux et al., 2013) and partly the result of averaging over our stress periods. From 4 ka to 3 ka there was an arid period with high salinities (18 g TDS L-1), but since we based our stress periods on the available paleogeographic maps, this spike is dampened by the preceding 2 ka period of brackish conditions (5 g TDS L-1).

River stages were specified by creating linear profiles from the apex to the coastline. The location of the delta apex and its river stage were fixed through time at the present-day conditions. This is a simplification, as in reality the apex' location varied through time. For instance, the delta apex was located up to 65 km south of its current location somewhere in the last 6 ka (Bunbury, 2013), but due to the lack of data on apex migration for the rest of the modelled time domain we chose this simplification. Since the coastline is irregular in shape and the location of rivers was not fixed through time, river stages were determined

in the following manner: firstly, lines were drawn from the apex to points at the coastline for each raster cell at the coastline. Along these lines, river stages declined linearly to the paleo sea-level at the coastline. Secondly, these profiles were subsequently interpolated to a surface using Inverse Distance Weighting. Finally, the paleo river branches were clipped out of this surface. Rivers were assigned a salinity of 0 g TDS L-1, since the Nile Delta is not tide dominated (Galloway, 1975), meaning that saline water intrusion in river branches is limited.

3.3.3.3 *Dunes and beaches*

No recharge estimates of infiltrated rainfall for the dune and beach areas were available, so these areas were assigned a fixed recharge of 200 mm a-1, equal to the present-day average precipitation near Alexandria (WMO, 2006) and the current recharge along the Levant coast (Yechieli et al., 2010). Despite being higher than present-day recharge, it is considered reasonable, as the climate was predominantly wetter throughout the Holocene than at present (Geirnaert and Laeven, 1992). This recharge allowed for the formation of freshwater lenses underneath dunes and beaches, which were observed in the area during ancient times (Post et al., 2018).

3.3.3.4 *Extractions*

Groundwater extractions mainly occur in the South-West. This area, near Wadi El Natrun, was appointed a reclamation area by the Egyptian Government in 1990 and since then has seen a rapid increase in extraction rates (King and Salem, 2012; Switzman et al., 2015). This was implemented in the numerical model by including extraction wells (locations and rates) that were in the RIGW database (Nofal et al., 2018) for the last 30 years of the simulation (Figure B.2).

3.3.3.5 *Hypersaline groundwater provenances*

Below 400 m depth, hypersaline groundwater (HGw) has been observed in the NDA. (van Engelen et al., 2018) investigated potential origins of this hypersaline groundwater and identified two possible sources that are included in this model. Firstly, the Late-Pleistocene sabkhas could have been sources of the hypersaline groundwater. Therefore, we set the concentrations of these areas at 120 g TDS L-1 for certain scenarios that are specified further in the next section, so that hypersaline groundwater could be formed in these areas. We refer to these as scenarios where HGw originates from the "top". Secondly, another potential source of hypersaline groundwater could be seepage expulsed from the low-permeable Kafr El Sheikh formation due its compaction. This seepage flux was included in the model as

fixed fluxes at the bottom. The magnitude and salt concentration of these fluxes were set at 3E-06 m d^{-1} and 120 g TDS L-1 (van Engelen et al., 2018). These scenarios are referred to as those where HGw originates from the "bottom".

3.3.3.6 *Initial salinity distributions*

Initial 3D salinity distributions were set with a dynamic spin-up time for 160 ka using Late-Pleistocene boundary conditions. Although the 160 ka period exceeds a glaciation cycle, we observed that no significant changes in salinity concentrations occurred after 4 ka for the homogeneous and 80 ka for the heterogeneous cases, which is well within the range of a glaciation cycle. For the majority of the model scenarios we started the spin-up with a completely fresh NDA, except for the model scenarios receiving HGw from the bottom, where the output of a simulation from previous research (model "NDA-c" in 2) was used to set the initial conditions. This was a simulation of the effect of 2.5 Ma of compaction-induced upward flow solute transport through the Kafr El Sheikh formation into the aquifer under interglacial conditions (low hydraulic gradient).

3.3.4 *Model scenarios*

van Engelen et al. (2018) identified two sensitive inputs for hydrogeological models in predicting the distribution of hypersaline groundwater, which are the geological model and the source of hypersaline groundwater. Even though there are 18 possible combinations between the nine lithological model scenarios and the two HGw provenances (top and bot), only 13 were calculated. Based on previous findings in (van Engelen et al., 2018), three combinations could be excluded, as these would not produce the observed salinity distributions. These were the combinations with an upward HGw flux originating from the bottom and with a completely open sea boundary, which lead to all HGw to be immediately drained into the sea resulting in only a very small volume of HGw in the NDA. The other two excluded scenarios are those with a closed sea boundary, horizontal clay layers (fluvial or marine), and HGw coming from the top. The free-convective plumes in these scenarios created entrapped volumes of fresh groundwater in between clay layers. Pressures in these zones increased fast during sea-level rise, which, in combination with the heterogeneity, made it impossible to achieve numerical convergence for these two model scenarios, despite our best efforts.

As an addition to the paleohydrogeological reconstruction, we formulated for each geology-HGw provenance combination, an equivalent steady-state model which used only the present day hydrological forcings until its salinity distribution reached a steady state, comparable to previous 3D models made for the area (Mabrouk et al., 2018; Sefelnasr and

Table 3.2: Letters that are used to create model scenario codes.

Feature	Scenario member	Letter
Sea connection {sea}	Open	O
	Half-Open	H
	Closed	C
Horizontal clay layer {clayer}	No clay	N
	Fluvial clay	F
	Marine clay	M
HGw provenance {prov}	Top	T
	Bot	B
Temporal change {temp}	paleo	P
	Steady	S

Sherif, 2014). This resulted in 26 scenarios in total. To distinguish different model scenarios, we introduced a coding system. For each feature, the corresponding letters in table 3.2 are converted to a code as follows: sea-clayer-prov-temp. For example, the paleohydrogeological reconstruction (temp: P) of an aquifer with a half-open sea connection (sea: H), fluvial horizontal clay layers (clayer: F), and HGw seeping in from the bottom (prov: B) gets the following code: H-F-B-P. Its equivalent steady-state model is attributed the code H-F-B-S. Furthermore, all model scenarios that share the same feature are noted as "feature-model scenarios", e.g. "T-model scenarios" means all model scenarios where HGw originates from the top, i.e. the Pleistocene sabkhas. The scenarios with a "Homogeneous" lithological model (Figure 3.2) get the scenario codes "O-N".

3.3.5 *Model evaluation*

We compared our modelled salinity distributions to available TDS measurements (n=293), of which the majority is shown in figure 3.1. Comparing measurements with model salinities at the point location can be deceiving as sharp transition zones often occur in salinity distributions (Sanford and Pope, 2010). Therefore, we assessed our model's ability to reproduce measured salinity patterns as follows. First, TDS measurements were binned into classes as shown in figure 3.1, similar to what is common in the validation of hydrogeophysical products (e. g. Delsman et al., 2018). Second, isosurfaces were determined in our model

output for all bin edges with the Marching Cubes algorithm (van der Walt et al., 2014). If these classes did not correspond at the measurement location, the minimum displacement (Λ) to the observed class in the model output was determined by calculating the minimum Euclidean distance in 3D:

$$\Lambda = \min \left| \sqrt{\sum_{i=1}^{3} (o_i - \boldsymbol{l_i})^2} \, , \, \sqrt{\sum_{i=1}^{3} (o_i - \boldsymbol{u_i})^2} \right| \tag{3.1}$$

where o_i is the location of the observation in dimension i and $\boldsymbol{l_i}$ and $\boldsymbol{u_i}$ the locations of the isosurface vertices in dimension i for respectively the lower and upper bin edge (Figure B.3). All locations were normalized to a range of [0,1] since the model domain was a rectangular cuboid, in other words not a perfect cube, and thus unequal in size across each dimension. To assess the validity of the steady-state assumption, we checked for all equivalent steady-state models the time they reached a steady state. This time was determined by calculating the derivative of the freshwater volume over time. If this did not change more than 0.0001% of the total volume, we considered the model to have reached a steady state.

3.3.6 *Comparison paleohydrogeological reconstruction with its equivalent steady-state model*

The paleohydrogeological reconstruction was compared with its equivalent steady-state model in two manners. Firstly, we calculated:

$$\Delta \boldsymbol{C} = \boldsymbol{C}_p - \boldsymbol{C}_s \tag{3.2}$$

where $\boldsymbol{C}$ is the 3D salinity matrix at the last timestep, and p and s respectively are the paleohydrogeological and steady-state model scenarios. For locations where $\Delta \boldsymbol{C} > 0$, the paleohydrogeologocial reconstruction is saltier than its steady-state equivalent and vice versa. Secondly, we calculated isohalines for a set of TDS values (3, 10, 20, 30 g L-1) for both model scenarios and assessed at the distance between these isohalines in the y-dimension (North-South). As our coastline was irregular, these distances varied in the x-dimension (West-East), therefore the median (Md) was calculated across this dimension as a conservative measure of isosurface separation (ω), which for a given depth and concentration is defined as:

$$\omega = \mathrm{Md} \left| \boldsymbol{y}_{p,x} - \boldsymbol{y}_{s,x} \right|_x \tag{3.3}$$

where $\boldsymbol{y}$ are the isohaline locations in the y-dimension, and p and s respectively are the paleohydrogeological and steady-state model scenarios.

3.4 RESULTS

Five scenarios were selected that showed the best match with the observations. These are called the "acceptable" scenarios. We start with discussing the results of these five selected scenarios through space (3.4.1) and time (section 3.4.2), before discussing their selection criteria (section 3.4.3).

3.4.1 *Current spatial TDS distribution of acceptable model scenarios*

The acceptable model scenarios show different salinity distributions (Figure 3.4), despite similar model performance (Figure 3.6). The model scenarios H-F-T-P, H-N-T-P, and C-N-T-P, which have no or fluvial clay layers, have freshwater distributions very similar to the O-N-T-P model scenario. In the model scenarios with marine clay layers (M), however, fresh groundwater is preserved in between low-permeable clay layers, especially in the centre. Regardless of the differences between scenarios, in all realizations the fresh-salt interface roughly follows the coastline, except in the west where there is far extending salt water intrusion visible towards Wadi El Natrun (Figure 3.1). Next to this depression, (former) lagoons are visible as shallow brackish zones and (former) dune areas are visible as freshwater lenses.

3.4.2 *Salt sources over time*

Figure 3.5 shows the provenance of the different groundwater types as fraction of the total modelling domain. In all four T-model scenarios, the model domain starts initially mainly fresh, dominated by infiltrated Pleistocene river water. This water is then replaced by hypersaline groundwater. As sea-level rises, this hypersaline groundwater is in turn replaced with sea water. The C-M-B-P model scenario takes a slightly different course, as the model is in steady state during stress period 1, dominated by river water. As sea-level rises and the hydraulic gradient decreases, the hypersaline groundwater and infiltrated sea water volumes increase at the expense of river water volumes. Regardless of differences amongst model scenarios, the total volume of sea groundwater is lower than the total volume of hypersaline groundwater and river water in all model scenarios. The total amount of dune water remains small for all five model scenarios over the entire modelled time.

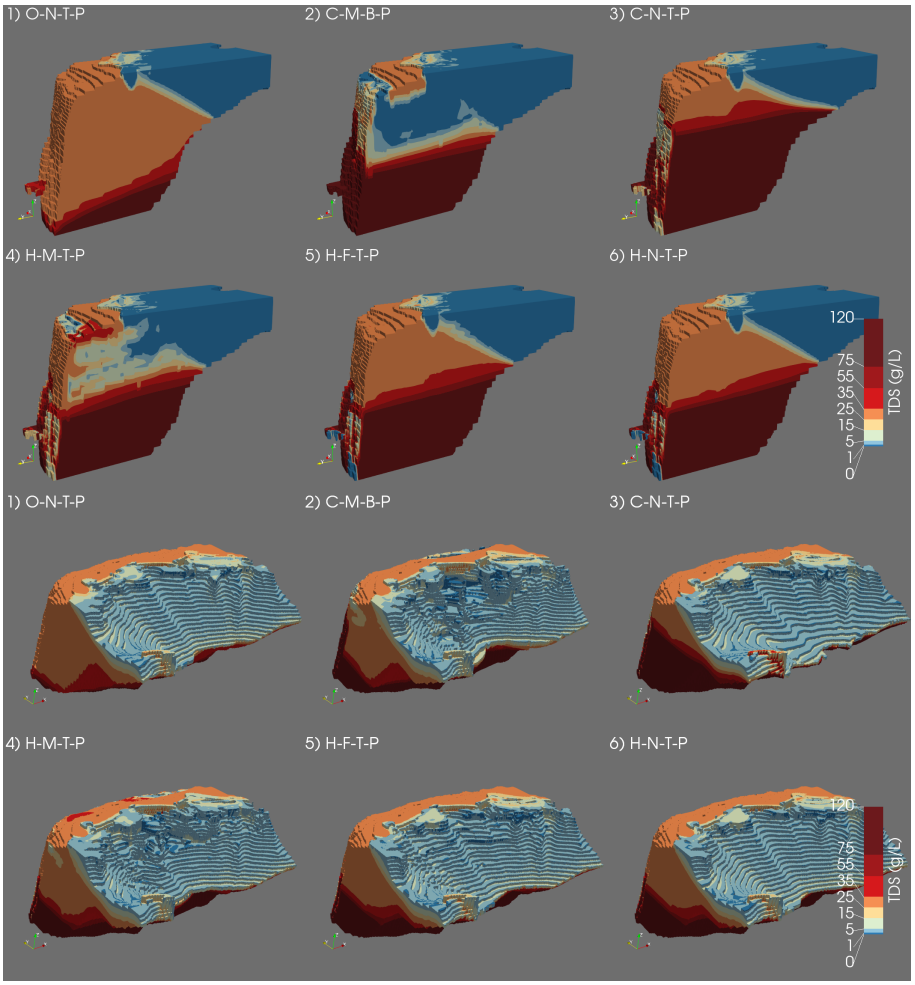

Figure 3.4: Salinity distributions of the five selected model scenarios after the validation; the results of the homogeneous model (viz. O-N-T-P) are also added as a first plot for reference. Note that the results are stretched in the z direction by a factor 150. In the top six plots the salinity distribution is sliced in half over the model domain and the camera is pointed in the south-easterly direction. In the bottom six plots the full delta is visible, but the fresh groundwater is made fully transparent. The camera is pointed downwards in the north-easterly direction.

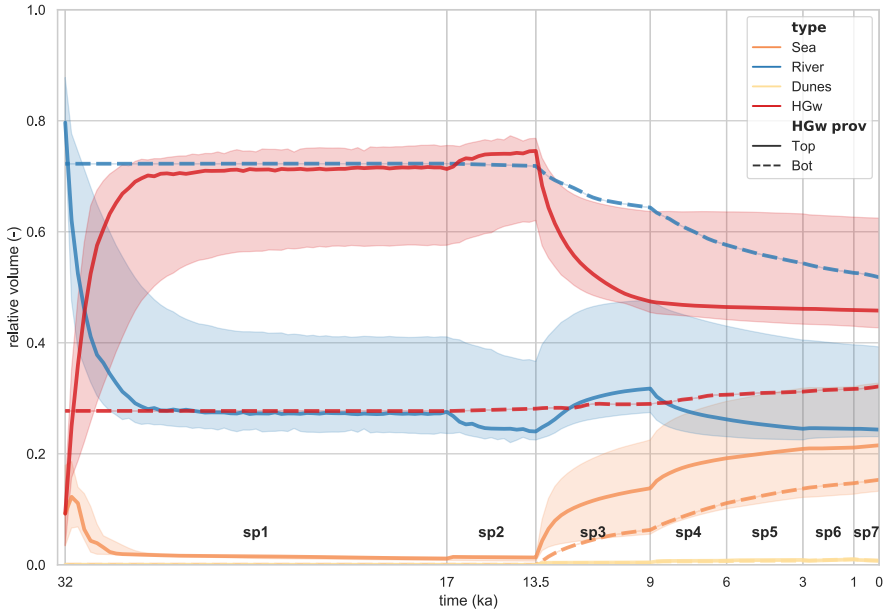

Figure 3.5: Groundwater provenance of different water types as a fraction of the total modelling domain for the five acceptable model scenarios. The dashed lines represent the C-M-B-P model. The shaded area indicates the range of the acceptable T-model scenarios (C-N-T-P, H-N-T-P, H-F-T-P, H-M-T-P), the thick line their median. Stress period numbers are indicated in bold, preceded by "sp".

3.4.3 *Model evaluation*

Figure 3.6 shows the evaluation results for all paleohydrogeological reconstructions. Note that the four classes above 5 g TDS L-1 in figure 3.1 were grouped into two classes: "saline" (5–35 g TDS L-1) and "hypersaline" (35–100 g TDS L-1), as the number of TDS measurements was low for these classes. All model scenarios matched the location of fresh groundwater correctly ($\mathcal{A} = 0$) at most the observation points. However, their accuracy worsens with increasing salinity. Despite having sometimes quite different salinity distributions (Figure 3.4), the majority of the model scenarios predict the location of the brackish and saline zone with the same error. More striking differences are observed in the hypersaline zone, where we observe a division around $\mathcal{A} = 0.07$ into two groups. There are the scenarios with $\mathrm{Md}|\mathcal{A}| < 0.07$, that predict the location of the HGw with a similar error as the location of saline groundwater. We call these scenarios "acceptable". Specifically, these are the following five model scenarios: C-M-B-P, C-N-T-P, H-M-T-P, H-F-T-P, H-N-T-P. The other scenarios perform considerably worse in predicting the location of the HGw. All equivalent steady-state scenarios required at least several thousands of years to reach a steady state (Table 3.3) from an initial Pleistocene steady state. Most notable are the B-scenarios, where the hypersaline groundwater caused the system to respond very slowly, over tens of thousands of years, thus exceeding the duration of the Holocene. The shortest scenarios were the N-T scenarios, as they did not include HGw and, compared to the scenarios with clay, the salt water experienced less resistance during its flow upwards from its initial Pleistocene state to the Holocene steady state.

Table 3.3: Time to reach steady-state for all steady-state scenarios.

Code	Time (ka)
C-F-B-S	35.0
C-M-B-S	90.5
C-N-B-S	23.5
C-N-T-S	22.5
O-N-T-S	5.5
O-F-T-S	10.5
O-M-T-S	10.0
H-F-B-S	37.5
H-F-T-S	7.5
H-M-B-S	44.5
H-M-T-S	10.0
H-N-B-S	19.5
H-N-T-S	5.5

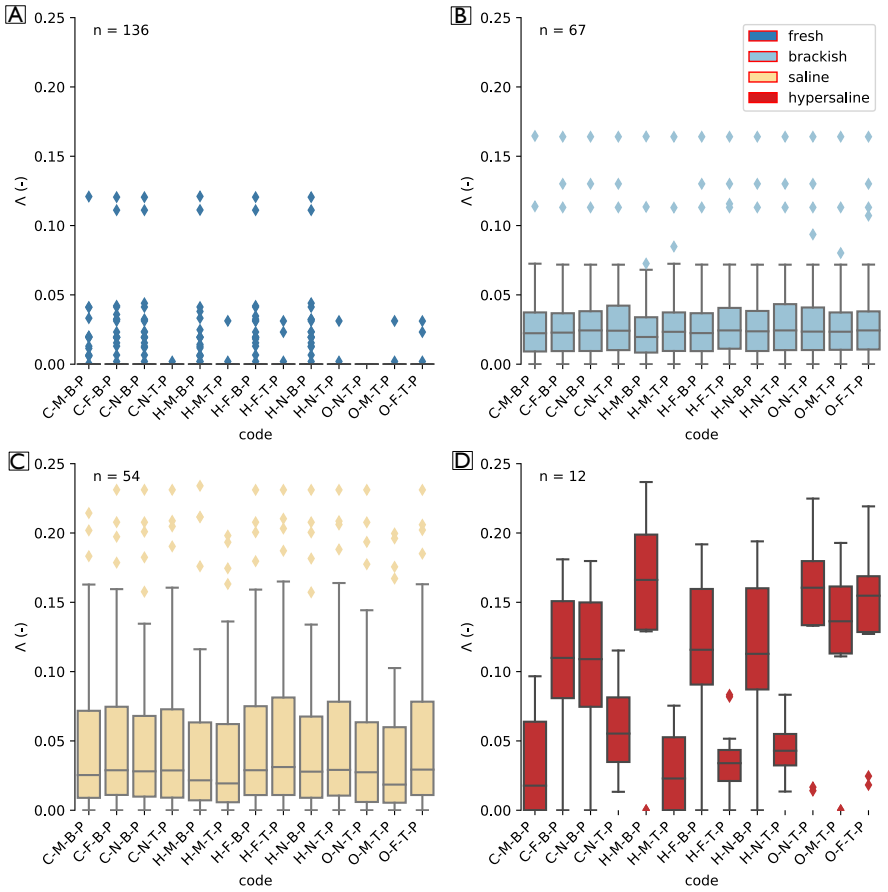

Figure 3.6: Goodness of fit boxplots for all paleohydrogeological reconstructions, binned in to four salinity classes. The higher the value of Λ, the worse the fit. Codes indicate model scenarios (Table 3.2). TDS values are binned in the classes [0, 1], [1, 5], [5, 35], [35, 100] g TDS L-1 for respectively "fresh", "brackish", "saline", "hypersaline", these are respectively plotted in panels A, B, C, D. "n" indicates the amount of observations available in the TDS bin to evaluate model results with. Diamonds indicate outliers, defined as values separated from the first or third quartile at 1.5 times the interquartile range. When no box is plotted for a scenario, 75% of the measurements equal zero, which consequently causes the interquartile range to be zero, rendering every non-zero value an outlier.

3.4.4 *Freshwater volume dynamics and sensitivity analysis*

Figure 3.7a shows that freshwater resources have declined strongly throughout the Late-Pleistocene and Holocene. In case of the T-model scenarios, first by free convection of hypersaline groundwater in stress period 1, next, for all model scenarios, by sea-level rise (stress period 2) and from 13.5 ka by the marine transgression. The total FGw volumes drop considerably with a factor ranging from 2 (C-M-B-P) up to 5 (C-N-T-P). There is also considerable variability amongst acceptable model scenario results, with the C-M-B-P having 74% more FGw than C-N-T-P. A peculiar observation for the model scenarios C-N-T-P, H-N-T-P, and H-F-T-P is that during the marine transgression (stress period 3) the total FGw volume recovers after a quick drop. This is caused by the disappearance of the sabkhas, stopping inflow of HGw, whereas outflow of HGw continues, allowing the total FGw volume to recover (see video supplement). The sensitivity analysis (Figure 3.7b) shows a clear influence of horizontal clay layers. For the M-model scenarios, more FGw is maintained in the transient model scenarios than in the steady-state model scenarios. In contrast, the opposite is visible for the N-model scenarios: FGw volumes are lower in the transient simulations than in their steady-state counterparts. In the model scenarios with marine clay layers there are still considerable fresh groundwater resources available below 300 m depth and in one case even offshore [C-M-B-P] (Table 3.4). This table shows that these parts of the model are the most uncertain as well, since disregarding potential deep and offshore fresh groundwater volumes decreases the range from 1133 to 478 km^3.

Table 3.4: End-state FGw volumes for acceptable model scenarios.

Code	Total fresh groundwater (km3)	Fresh groundwater <300 m (km3)	Fresh groundwater <300 m and onshore (km3)
H-M-T-P	1974	1853	1829
C-M-B-P	2659	2325	1989
C-N-T-P	1526	1512	1511
H-N-T-P	1728	1642	1641
H-F-T-P	1765	1670	1668

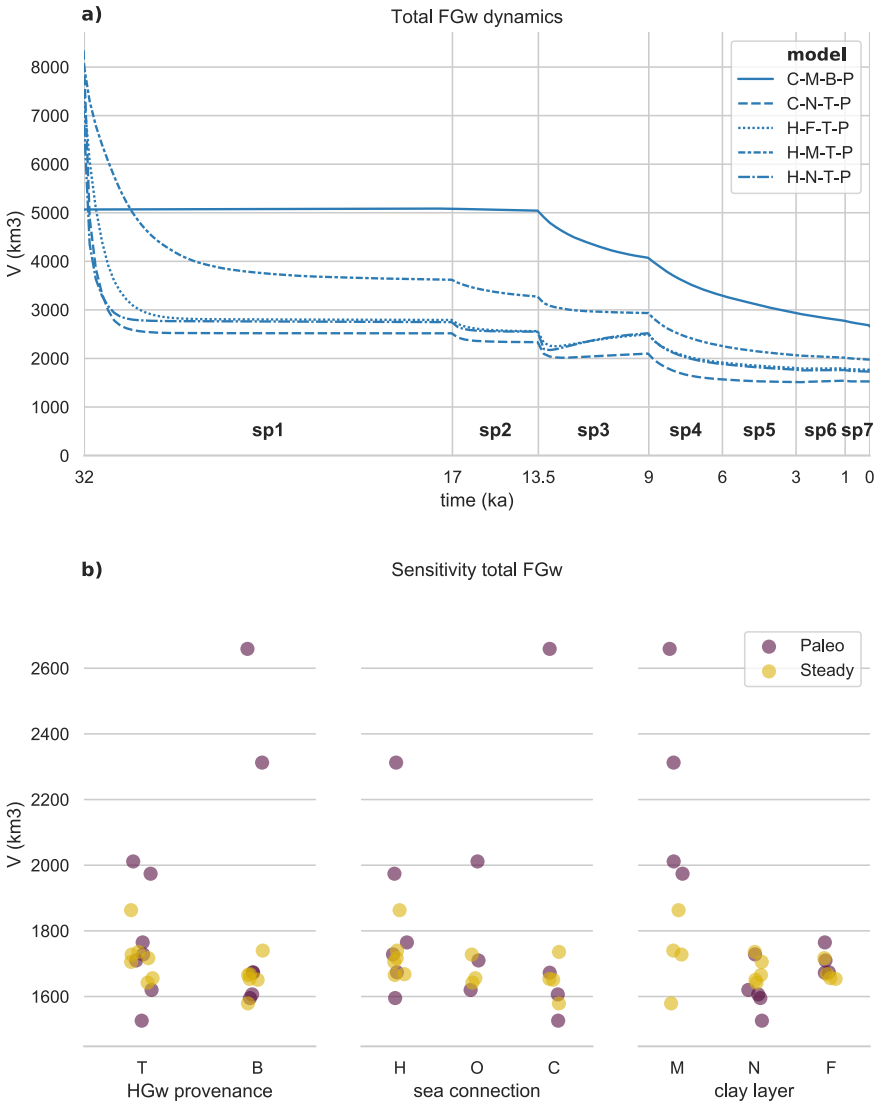

Figure 3.7: (a) the development of the total FGw volume through time for the five acceptable model scenarios. Stress period numbers are indicated in bold with "sp". (b) End state total FGw volumes of all model scenarios, grouped for different inputs. Colours of the dots indicate a steady state or paleohydrogeological reconstruction result. Dots are jittered to better show overlapping dots.

3.4.5 *Fresh-salt distribution: the paleohydrogeological reconstruction against its equivalent steady-state*

$\Delta \boldsymbol{C}$ (equation 3.2) is generally negative in the marine clay (M) comparisons (snapshots 2 and 4 in figure 3.8), as the low permeable clays block vertical intrusion during the marine transgression, concurrent with previous research (Kooi et al., 2000; Post et al., 2013). In the no clay (N) comparison (snapshots 1, 3, and 6 in figure 3.8) however, we observe something different: the shallow groundwater (< 200 m depth) is saltier, whereas the toe of the wedge of the steady-state equivalents lays further land inward. This pattern is most clearly visible in the homogeneous model (figure 3.8, plot 1) and is obscured more as heterogeneity increases. In the C-N-T scenario, the paleohydrogeological reconstruction is more saline nearly everywhere, as there is a larger volume of hypersaline groundwater that is influencing the toe of the seawater wedge (see also figure 3.4, snapshot 3). In all comparisons, (former) lagoons are visible (Figures 3.3 and 3.8). In the west, the former Maryut lagoon is clearly visible in all model scenarios as a red zone, stretching all the way towards the Wadi El Natrun depression. The central and eastern lagoons, however, are coloured blue. At these areas, the paleo-hydraulic gradients were the steepest as the lagoons lay more land inward up till 0.2 ka (Stanley and Warne, 1993), resulting in a quicker freshening of the groundwater at these locations. Figure 3.9 shows the isosurface separation ω for the model scenarios where the previous described pattern was visible. An S-shaped trend in ω is visible with depth, where there is a maximum isosurface separation at around -130 m and minimum at around -350 m depth. The latter is not visible in C-N-T as the hypersaline groundwater influences the fresh-salt interface. This trend means that for these four model scenarios, using a steady-state model results in an underestimation of the inland extent of the salt water wedge above -250 m depth and overestimation of the inland extent of the "toe" of the wedge. The median of this over- and underestimation of the seawater wedge top and toe ranges up to 10 km. The isosurface separation increases with concentration, because the denser surface has to rotate further to reach a steady state.

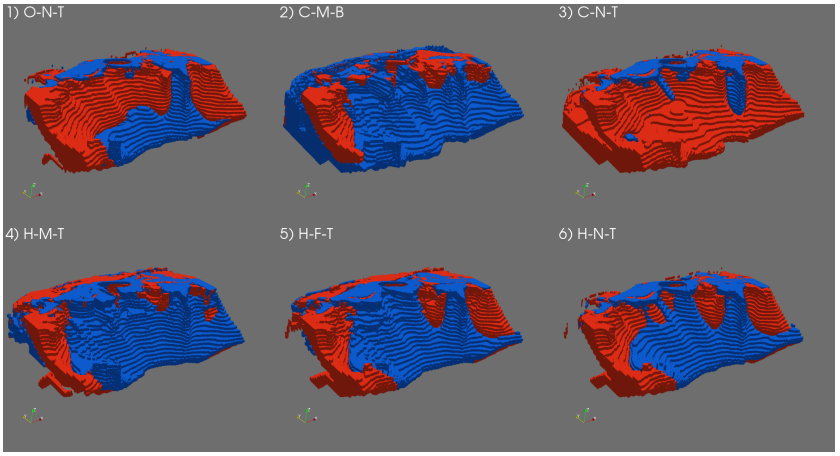

Figure 3.8: Comparison between the paleohydrogeological reconstructions and the steady-state model scenarios. Red colours indicate that $\boldsymbol{\Delta C} > 1$, meaning that the paleohydrogeological reconstruction is saltier than its steady-state equivalent. Vice versa for blue, where $\boldsymbol{\Delta C} < -1$. All values in between -1 and 1 are made transparent to focus purely on major differences. Groundwater below 450 m depth is not plotted, as the present-day fresh-salt interface was not located below these depths. Camera angle is the same as in the six bottom plots of figure 3.4

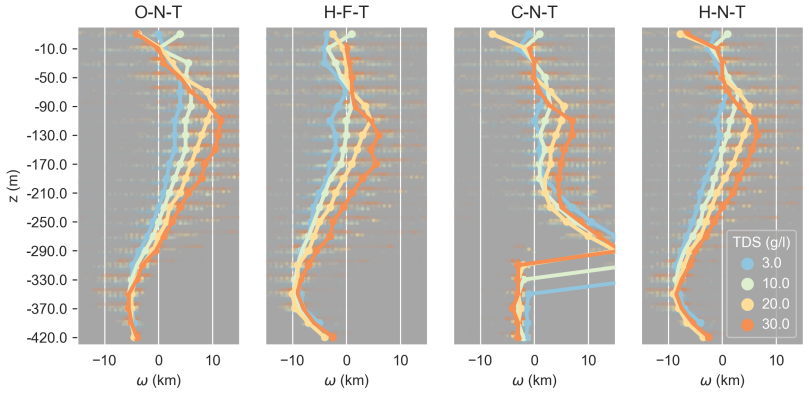

Figure 3.9: Isosurface separation ω with depth for different TDS values and selected model scenarios. The line indicates the median isosurface separation, the near transparent dots all data points. Positive ω means the isohaline of the paleohydrogeological reconstruction is located more land inwards than its' steady-state equivalent and vice versa.

3.5 DISCUSSION

The efforts of conducting 3D paleohydrogeological reconstructions were rewarded with new insights. According to our models, a strong reduction in FGw volume occurred in the NDA during the last 32 ka. As sea-level rose, FGw volumes were reduced with a factor ranging from 2 to 5 (Figure 3.7). Just as in the Netherlands (Delsman et al., 2014) and the Mekong (Van Pham et al., 2019), the system did not reach a steady state in the last 9 ka. Our simplest equivalent steady-state scenarios required at least 5.5 ka to reach a steady state (Table 3.3), a period in which already considerable changes occurred to the boundary conditions (Figure 3.3). This increased to tens of thousands of years for the more complex models. Using a steady-state approach with current boundary conditions can therefore not result in a reasonable estimate of the current fresh-salt groundwater distribution for such a complex, large-scale system. Moreover, the variance in FGw volumes of the paleohydrogeological reconstructions was larger than that of the steady-state model scenarios. This implies that conducting sensitivity and uncertainty analyses on steady-state model scenarios, can lead to grave underestimations of the uncertainty. Michael et al. (2016) showed with steady-state models that strong, well connected heterogeneities can lead to chaotic salinity distributions, showing a high spatial variability that we also observe in our most heterogenous cases (Figure 3.4). This variability further increases when paleohydrogeology is accounted for (Figure 3.7b), because there is less time for mixing to smoothen strong concentration gradients. Furthermore, we have shown that it is physically possible that the influences of the Holocene marine transgression can be still observed in the delta; either as pre-Holocene freshwater trapped in between clay layers in the northern part of the NDA, concurrent with earlier research (Kooi et al., 2000), or as a steeper fresh-salt interface than would be expected a priori from an exploratory steady-state model. The latter has to the authors' knowledge never been shown before in this detail. The implications of this steeper interface are that using the steady-state approach can lead to an underestimation of the amount of salt groundwater above roughly 250 m depth and an overestimation of the toe length of the interface (Figure 3.6). Likewise, this non-steady, steep interface could explain the observed freshening of the shallow NDA as observed in hydrogeochemical studies (Barrocu and Dahab, 2010; Geriesh et al., 2015), since only the zone above 250 m depth has been sampled. This is the zone that we expect to slowly freshen from our comparison between paleohydrogeological and steady-state models (Figure 3.9). It was however difficult to compare the observed freshening with model results directly, since the time scale over which this observed freshening has developed is often unknown (Stuyfzand, 2008). In our model simulations, freshening has continued for the last 3000 years (Figure B.4). Our simulations also show that it is indeed possible that the NDA was predominantly freshened with surface water (Figure 3.5), as hypothesized earlier by Geirnaert and Laeven (1992).

Deltas with abundant low permeable clay layers are expected to possess larger quantities of deep fresh groundwater than would be approximated with steady-state scenarios. Examples of such deltas are the Chao Praya Delta, Thailand (Yamanaka et al., 2011), Red River Delta, Vietnam (Larsen et al., 2017), and the Pearl Delta, China (Wang and Jiao, 2012). In deltaic groundwater systems consisting of mainly coarse material, a steady-state approximation may underestimate the slope of the fresh-salt interface. Examples of these deltaic areas are the Niger Delta, Nigeria (Summerhayes et al., 1978), and the Tokar Delta, Sudan (Elkrail and Obied, 2013). Note that the Holocene transgression in the above-mentioned Asian deltas reached more land inward than it did in the Nile Delta (Sinsakul, 2000; Tanabe et al., 2006; Zong et al., 2009), thus their salt groundwater distributions are expected to strongly deviate even more from steady-state approximations than in the research case in this study.

A wide range of model scenarios lead to acceptable results. This is mainly attributed to the limited availability of salinity observations in the saline zone, which is the area where the results of the acceptable scenarios differed the most. Although the number of observations may look adequate on a 2D map, it is still by far insufficient in 3D. Similar conclusions were drawn by Sanford and Pope (2010) for the Eastern Shore of Virginia (USA), an area with a similar observation density. Though it is generally assumed for the sake of simplicity that the northern part of the delta is completely saline, here we show that there might also be large, overlooked quantities of onshore and offshore fresh groundwater. Our model-based FGw volume estimates are on the large side. For instance, Mabrouk et al. (2018) estimated a total amount of 1290 km3 and Sefelnasr and Sherif (2014) 883 km3. We stress that those authors disregarded the 80 km of coastal shelf offshore and used a lower porosity value. Reducing the effective porosity from our 25% to their 17%, reduces our estimated FGw volume with 32%; disregarding the increased groundwater flow velocities this would result in, which in turn would slightly increase the extent of the FGw zone.

Of all groundwater types, hypersaline groundwater in the NDA is the main contributor to total salt mass (Figure 3.5). Apparent from the model evaluation is that the only acceptable model where HGw originates from the bottom has a strongly compartimentalized bottom of the aquifer, which requires a closed off continental slope and extending, low-permeable horizontal clay layers. When HGw originates from the top, a closed off bottom of the coastal slope is also necessary to preserve the observed amount of hypersaline groundwater since the last glacial period. This implies that regardless of HGw provenance, the interaction at the aquifer-sea connection needs to be very limited at the lower half of the aquifer to explain the observed salinities, as otherwise all HGw would have flowed out to the sea under the steep Late-Pleistocene (32 – 13.5 ka) hydraulic gradients. We can therefore limit the amount of potential combinations between lithology and HGw provenance that were posed in

van Engelen et al. (2018), as the current study also incorporated a steep glacial hydraulic gradient, whereas van Engelen et al. (2018) kept a constant low (interglacial) hydraulic gradient. The Wadi El Natrun depression might have started attracting, and eventually draining sea water from the Maryut lagoon as sea-level rose above the depression height. The amount of field evidence of this actually occurring is not overwhelming, but there are some observations in support of this model outcome (Ibrahim Hussein et al., 2017). Nevertheless, it is concerning that the area with the most far reaching seawater intrusion in our model scenarios, is also the area with the most intense groundwater pumping. Even though the 30 years of groundwater extraction in our model scenarios did not seem to show a large influence on seawater intrusion, this influence can increase in the coming century (Mabrouk et al., 2018). In addition, the large cell sizes of our model can also be the cause of the lack of visible quick responses to groundwater pumping, as large model cells tend to negate local saltwater upconing effects around wells (Pauw et al., 2015). It should also be kept in mind that for future hydrogeochemical analyses of the Wadi El Natrun area the former Maryut lagoon used to extend a lot more land inward towards this depression than currently, and that the composition of the water in this lagoon fluctuated strongly over time (Flaux et al., 2013).

Despite our efforts at increasing the realism of our model scenarios, some processes were only incorporated in a very simplistic manner. The most prominently simplified process in this arid area is salinization due to evapoconcentration and redissolution of precipitated salts. Though this does not currently seem to influence groundwater salinities, it is hypothesized to have been of influence in the past (Diab et al., 1997; Geirnaert and Laeven, 1992). In our T-scenarios, the Pleistocene sabkhas were assigned a fixed concentration (120 g TDS L^{-1}), meaning that free convection here was unconstrained by available salt and water mass. Our T-scenario results indeed show a very rapid change in the first 5 ka (Figures 3.5 and 3.7), after which they reach equilibrium conditions until the next stress period. This may seem very rapid, but experiments with smaller scale models which fully accounted for salt precipitation and dissolution, evapoconcentration, variable-density groundwater flow and the unsaturated zone, showed that higher salinities (> 200 g TDS L^{-1}) are possible under evaporation rates similar to those in the Nile Delta (Shen et al., 2018; Zhang et al., 2015). Given that the Late-Pleistocene sabkhas did not migrate (Stanley and Warne, 1993), we deem our T-model scenarios to be conservative. Likewise, rock salt dissolution is thought to influence salinities around the borders of the delta (Ibrahim Hussein et al., 2017). Either of these processes, evapoconcentration or rock salt dissolution, can explain the saline observations in the South-East (Figure 3.1), which our model cannot. In addition, for a proper physical representation of free convection, a finer grid is required. A coarse horizontal cell size results in a delay in the onset of free convection, while a coarse vertical cell size results in an onset

of free convection even for situations that are expected to be stable (Kooi et al., 2000). van Engelen et al. (2018) investigated the errors caused by coarse model cells for the Nile Delta and found that especially the crude horizontal grid size had an influence (Appendix A.4). They found that this resulted in similar downward fluxes, but a delay in the onset of free convection. This effect, however, was negligible after 50 years and thus dwarfed by the timescale used for our stress periods. The coarse vertical grid size was not an issue, since the marine transgression occurred over sand with a high hydraulic conductivity, meaning there is a highly unstable situation and free convection has to occur. We thus think that the errors made in modelling free convection will not impact our conclusions. Furthermore, the paleo river stages we assigned to the delta were modelled as simply as possible, namely a linear river stage profile from a static apex to coast. As mentioned in section 3.3.3, this apex was in reality not static but has moved over 60 km upstream (Bunbury, 2013), which, when taken into account, would result in a lower hydraulic gradient in our model. A detailed river stage reconstruction was outside the scope of this paper. Regardless, this uncertainty in the hydraulic gradient is small compared to the big changes in the hydraulic gradient that occurred at the start of the Holocene, so we think this simplification does not impact our conclusions.

Future research for this area would greatly benefit from an enhanced geological model, especially of the lithology of the delta shelf and slope. A lot of measurements were conducted for the petroleum industry (Sestini, 1989), but most of this data is still inaccessible for external researchers. Furthermore, the available publications on offshore geology are written mainly for the petroleum industry, focusing on the area >2.5 km depth, rendering them unsuitable for hydrogeological research of the NDA. Therefore, we think research for this area would benefit from a re-analysis of the available data with a hydrogeological perspective. In addition, a larger salinity dataset, especially in the saline zone would help validating groundwater models that are used more frequently in management decisions, e.g. Nofal et al. (2016).

3.6 CONCLUSIONS

A 3D variable-density groundwater flow and coupled salt transport model was used for a paleohydrogeological reconstruction of the salinity distribution of the Nile Delta Aquifer. It was found that large timescales are involved, and models required at least 5.5 ka to reach equilibrium. None of the evaluated paleohydrogeological scenarios reached a steady state over the last 9 ka, meaning that the transient boundary conditions during the Holocene must have had an influence on current groundwater salinity. We therefore conclude that steady-state models are not likely to result in realistic FGw distributions in the NDA and

comparable deltaic areas. Our results also show that the occurrence of past marine transgressions constitute a valid hypothesis explaining the occurrence of the extensive saline zone land inward. Nevertheless, the estimated FGw volumes were subject to considerable uncertainty, due to the lack of field data in this saline zone. Regardless, the paleohydrogeological reconstruction provided several insights. Firstly, during the Late-Pleistocene the total FGw volumes declined strongly, with estimates ranging from a factor 2 to 5. Secondly, ignoring past boundary conditions leads to an underestimation of FGw uncertainty resulting from a lack of knowledge on geological schematizations and HGw provenances. Thirdly, the differences between the fresh-salt distribution of the paleohydrogeological reconstruction and the steady-state scenarios varied, depending on the geology. In case of low permeable clay layers, the paleohydrogeological reconstruction resulted in considerable volumes of fresh groundwater stored underneath these clay layers. However, with more permeable or no clay layers, the fresh-salt interface was steeper than in the steady-state equivalents. Given the insights gained in our paleohydrogeological reconstruction, we think that further research into the past of coastal groundwater systems from a groundwater mechanical perspective will improve our understanding of these systems in both their past and present-day state.

3.7 ACKNOWLEDGEMENTS

Firstly, we would like to thank Benjamin Pennington for kindly providing the paleogeographical data and answering our questions on paleogeography. Secondly, we would like to thank Leanne Morgan and one anonymous reviewer for their comments, which significantly enhanced the quality of this paper. Thirdly, we would like to thank Gijs Janssen for his support in developing the iMOD-SEAWAT code. Fourthly, we would like to thank Huite Bootsma and Martijn Visser for their help with handling model output. Finally, we would like to thank Edwin Sutanudjaja for his tips on running jobs on Cartesius. Supplementary videos show the development of the groundwater fresh-salinity distribution through time for the five acceptable model scenarios. These can be found under the following DOI: `10.5281/zenodo.2628427`. Model input files can be found under the following DOI: `10.5281/zenodo.3461667`. Scripts and software to reproduce the figures are available in this repository: `https://github.com/JoerivanEngelen/Nile_Delta_post` with the DOI: `10.5281/zenodo.3461788`. This work is part of the research programme The New Delta, which is financed by the Netherlands Organisation for Scientific Research (NWO). Additionally, this work is partly financed by NWO and the Ministry of Infrastructure and Water Management under TTW Perspectives Program Water Nexus. This work was carried out on the Dutch national e-infrastructure with the support of SURF Cooperative, on a NWO Pilot Project Grant.

4

FACTORS DETERMINING THE NATURAL FRESH-SALT GROUNDWATER DISTRIBUTION IN DELTAS

ABSTRACT

A majority of river deltas are densely populated areas with intensive agriculture. The increased shortage of fresh surface water that results from rising demands are expected to lead to increased groundwater pumping, which leads to sea water intrusion. To correctly project the future of fresh groundwater resources in deltas, knowing the current fresh-salt groundwater distribution is a prerequisite. However, uncertainties about these distributions and their drivers are large. To understand these uncertainties, we conducted a global sensitivity analysis of a complex three-dimensional variable-density groundwater model of a synthetic delta, simulating the effect of the last glacial low stand and the subsequent marine transgression. The analysis is unique in its wide range of geometries, hydrogeological parameterizations and boundary conditions analyzed, making it representative for a large number of deltas worldwide. We find that the aquifer hydraulic conductivity is the most uncertain input and has a strong non-monotonous effect on the total salt mass onshore. The calculated fresh-salt groundwater distributions were classified into five classes and compared to real-world case studies. We find that salinity inversions occur in deltaic systems with high representative system anisotropies as a remnant of a marine transgression. These salinity inversions were observed in half of the real-world cases, indicating that their fresh-salt groundwater distributions are not in a dynamic equilibrium. We conclude that it is very likely that past marine transgressions are still reflected in the current fresh-salt groundwater distributions in deltas. This makes paleo-groundwater modeling a prerequisite for effective simulation of present-day groundwater salinity distributions in these systems.

Based on: van Engelen, J., Bierkens, M.F.P., Delsman, J.R., Oude Essink, G.H.P. (-) Factors determining the natural fresh-salt groundwater distribution in deltas; Under Review in: *Water Resources Research*

4.1 INTRODUCTION

River deltas are of high socio-economic value, since they are often densely-populated areas with high agricultural productivity (Neumann et al., 2015; Seto, 2011). The combination of growing population, increasingly intensive agriculture, and, in some areas, increased likelihood of droughts is expected to lead to fresh water shortages in surface water systems (Bucx et al., 2010). These stresses in turn will instigate more groundwater pumping, which leads to sea water intrusion and the upconing of saline groundwater (Michael et al., 2017; Werner et al., 2013). Despite that salinization poses a big problem to many large deltas (Rahman et al., 2019), the volume of fresh groundwater resources in many deltas is unknown, especially in the deeper parts of the groundwater system. While advances have been made in monitoring, especially with the onset of large-scale airborne electromagnetic (AEM) studies (King et al., 2018), 3D variable-density groundwater modeling still remains the only method to estimate a complete 3D fresh-salt groundwater distribution for large-scale groundwater systems (Faneca Sànchez et al., 2012). These models also have the added benefit of studying the effects of past and future stresses on groundwater systems (Meyer et al., 2019; Oude Essink et al., 2010). Model results, however, are often uncertain due to the joint effects of uncertainty about the, often heterogeneous, hydraulic conductivity (Enemark et al., 2019), scarce validation data (Sanford and Pope, 2010), and uncertainty about past transient boundary conditions (van Engelen et al., 2018). The first two of these problems are common in hydrogeology (Domenico and Schwartz, 1990), but the latter problem deserves extra explanation. The fact that large-scale groundwater systems often have long residence times is well known (Jasechko et al., 2017; Sturchio et al., 2004). This also means that solute transport in these systems is influenced by paleo-boundary conditions (Kooi et al., 2000; Meisler et al., 1984), which can lead to at first glance surprising observations. For instance, brackish and saline groundwater zones that occur far inland in multiple deltas are correlated to past marine transgressions (Larsen et al., 2017). Likewise, offshore fresh groundwater, which is observed globally, is linked to glacial low stands (Post et al., 2013). Though constraining these paleo-boundary conditions is possible with the help of paleogeographical maps, seawater curves, and paleo-salinities (Delsman et al., 2014; van Engelen et al., 2019; Meyer et al., 2019), this information is rarely available over the whole time span of the model. This hampers the use of models to explain the origin of saline groundwater (van Engelen et al., 2018), which can be highly variable (Stuyfzand and Stuurman, 2006). Next to the previously mentioned contemporary sea water intrusion and marine transgressions, saline intrusion in rivers (Ayers et al., 2016; Faye et al., 2005), seepage of deep brines (Griffioen et al., 2016; Hanor, 1994), and evapoconcentration (Fass et al., 2007; Geirnaert and Laeven, 1992; Han et al., 2011) can increase groundwater salinity. Up to now, insights into the drivers of the current fresh-salt groundwater distribution in the world's deltas are fragmented and incomplete, as it is

based on a limited number of modeled case studies and hydrogeochemical measurement campaigns; a systematic investigation is still lacking.

Sensitivity analyses are crucial to systematically investigate the effects of inputs and their influence on output uncertainty, thereby enhancing system understanding (Saltelli et al., 2004). We use "inputs" as an encompassing term for both model parameters (e.g. hydraulic conductivity) and boundary conditions (e.g. location shoreline), following the sensitivity analysis literature (Saltelli et al., 2004). There are plenty of studies that conducted a sensitivity analysis to investigate the effects of individual inputs on the fresh-salt groundwater distribution. A thorough overview of these studies is presented by Werner et al. (2013), to which we add a few examples not mentioned in that paper. These examples all applied 2D models, unless specified differently. Abarca et al. (2007) studied the effect of an aquifer slope parallel to the coast on the steady-state fresh-salt groundwater distribution with a 3D groundwater model, and found that this geometry can create quasi-horizontal circulation cells, to which the salt water wedge was more sensitive than the aquifer thickness or mechanical dispersion. Walther et al. (2017) investigated the effect of the slope of the sea-side boundary and found that this slope reduced the penetration length of the steady-state salt water wedge. In addition, this input had an increasing effect with increasing dispersivity and fresh water inflow, thus also showing input interaction. Ketabchi et al. (2016) used an inventive and exhaustive multi-model literature comparison to show that models with a fixed head boundary inland (head-controlled system) experienced more sea water intrusion due to sea level rise than those with a fixed flux inland (flux-controlled system). Moreover, they showed that the fresh-salt groundwater distribution is very sensitive to land surface inundation with sea water, especially in thick aquifers. Zamrsky et al. (2018) showed that the structure of the geology had a larger influence on the fresh-salt groundwater distribution than aquifer thickness. Rathore et al. (2018) found that in confined, stratified aquifers, under a constant transmissivity, the elevation of aquitards had a stronger influence on the shape of the salt water wedge than the ratio of the aquifer and aquitard hydraulic conductivity. Though these focused studies are very insightful, often the conducted sensitivity analyses are local, i.e. inputs are varied one-at-a-time around one location in the input hyperspace. This in contrast to global sensitivity analyses, which aim to explore input sensitivity across the complete input hyperspace. Local sensitivity analyses may provide a distorted view of input sensitivities as they completely miss inputs that interact or have non-linear effects on model output (Saltelli and Annoni, 2010). For example, Ebeling et al. (2019) conducted a global sensitivity analysis on a model that simulated the effect of hydraulic barriers to remediate sea water intrusion in an unconfined aquifer and concluded that the sensitivity of one input depended on the configuration of other inputs. Similar conclusions were drawn by Xu et al. (2018) for a variable-density groundwater model of a coastal karstic aquifer.

The above literature review showed that in order to fully understand which factors determine the onshore and offshore fresh-salt groundwater distributions in deltas, a sufficiently complex groundwater model is needed that is forced with paleo-boundary conditions and subject to a global sensitivity analysis. In this study we use a variable-density groundwater flow model to conduct a global sensitivity analysis of the fresh-salt groundwater distribution on a synthetic delta aquifer with a realistic heterogenous but deterministic geology and complex paleo-boundary conditions. The analysis is unique in its wide range of geometries, hydrogeological parameterizations and boundary conditions analyzed, making it representative for a large number of deltas worldwide. We focus on the natural fresh-salt groundwater distribution, since the development of the current fresh-salt groundwater distribution over long timescales is understudied, whereas plenty of research has been conducted on anthropogenic influence (Werner et al., 2013).

The remaining part of this chapter is set up as follows. Section 4.2 describes the parameterization of the synthetic fan shaped delta aquifer, in particular its geometry and hydrogeology, as well as the initial and boundary conditions used in the density-dependent paleo-groundwater model. These inputs are based on a number of real-world case studies of existing deltas. The sensitivity analysis setup is described next, as well as how results are analyzed. Section 4.3 provides the results of the sensitivity analysis and compares the fresh-salt groundwater distributions with the real-world cases studied. These results and limitations to our study are further discussed in section 4.4 followed by conclusions in section 4.5.

4.2 MATERIALS AND METHODS

We conducted a global sensitivity analysis on a model of 45 ka of variable-density groundwater flow in a synthetic, fan-shaped delta. A literature review was conducted to provide appropriate concepts and input ranges for the geometry, lithology, hydrogeology, and boundary conditions of the model (section 4.2.6). Consequently, the effect of each input on the fresh-salt distribution was analyzed based on four metrics (section 4.2.7). Furthermore, we classified the fresh-salt distributions into different types, linked these to inputs and compared these to fresh-salt distributions found in the literature.

4.2.1 *Parameterizing geometry*

The geometry of the synthetic delta aquifer was created by first specifying a geometry in polar coordinates (r, φ) (Figure 4.1a & 4.1c) and transforming this to a cartesian coordinate

system (x,y) (Figure 4.1b), creating a fan-shaped delta (Figure 4.1d). The reference depth was set to the present-day median eustatic sea-level. The length of the model domain L was fixed at 200 km, a representative size for major deltas; deltas with similar sizes are the Red River Delta (Vietnam), Chao Praya (Thailand), Rhine-Meuse (Netherlands), Nile (Egypt), and the Saloum (Senegal). l_a specifies the relative length of the onshore part. The inputs α, β, and γ respectively specified the slope of the onshore part, the coastal shelf and coastal slope. Finally, H_a and H_b respectively specified the depth of the aquifer at the apex and coast. The hydrogeological base was created as a half-ellipsoid across the φz-plane (Figure 4.1c), increasing in depth towards the coast (Figure 4.1a). For additional information, see section C.1. This half-ellipsoid shape is observed in for example the Yangtze Delta (Shi et al., 2012), the Pearl Delta (Zong et al., 2012) and the Red River delta (Winkel et al., 2011). This geometry was consequently horizontally discretized into cells of 1 km by 1 km (cf. van Engelen et al., 2018; Van Pham et al., 2019). Since H_b varied widely, we did not fix the vertical discretization, but instead discretized the vertical into 100 cells to keep the load balance for each simulation roughly similar. This resulted in a vertical resolution ranging from 1 m to 20 m (cf. van Engelen et al., 2018).

4.2.2 *Hydrogeology*

The lithology was created in a deterministic manner, where we specified a Holocene confining layer and a set of N_{aqt} aquitards. The relative thickness of these layers was set with f_{aqt}, which is fraction of the sediment column that is aquitard (see section C.1). The aquitards were created laterally continuous up to the apex, whereas the Holocene confining layer was not. This allowed for onshore recharge zones near the delta edges, similar to the infiltration zones near the edges of the Nile Delta (Pennington et al., 2017) and the Chao Praya delta (Sanford and Buapeng, 1996). The extent of the confining layer was set by l_{conf} (Figure 4.1f), which specified how far up to the apex the layer reached.

A horizontal hydraulic conductivity was assigned to the aquifers ($K_{h,\,aqf}$) and a vertical hydraulic conductivity to the aquitards and confining layer ($K_{v,aqt}$). These were subsequently converted to respectively a $K_{v,\,aqf}$ and a $K_{h,aqt}$ with a formation anisotropy (K_h/K_v). This approach was chosen to unite the input distributions (section 4.2.6) with the values found in the literature study (Figure 4.3). In the literature only a $K_{h,\,aqf}$ and a $K_{v,aqt}$ were usually provided, adhering to the main flow directions (Domenico and Schwartz, 1990).

Paleochannels were added as straight lines of 1 km width, a comparable width to paleochannels found in the Rhine-Meuse delta (van Asselen et al., 2017) and the West Bengal

delta (Samadder et al., 2011). In the field, these channels can form either high conductive zones when filled up with fluvial sediments (Mulligan et al., 2007) or low conductive zones when filled up with marine sediments (Larsen et al., 2017). In this study, we focus on the paleochannels' ability to incise through aquitards and as such forming preferential flow paths with $f_{K,pal}$, which is a factor that governs the hydraulic conductivity of the paleochannels. The closer $f_{K,pal}$ is to 1, the more the hydraulic conductivity of the paleochannel tends to that of the aquifers. The horizontal distance between two vertically consecutive preferential flow paths can affect vertical flow (Post and Simmons, 2010) and is therefore incorporated as s_{pal}.

To increase the physical plausibility of the generated lithology, erosion was modeled by removing all aquitards that were located above any of the surface water profiles occurring from the last glacial low stand until present (Figure 4.2c). Furthermore, the confining layer is deposited after the Holocene transgression has reached its maximum extent (t_{tra}), which is comparable to how this confining layer was deposited in most deltas (Fielding et al., 2006; Pennington et al., 2017; Stanley and Warne, 1994; Tanabe et al., 2006).

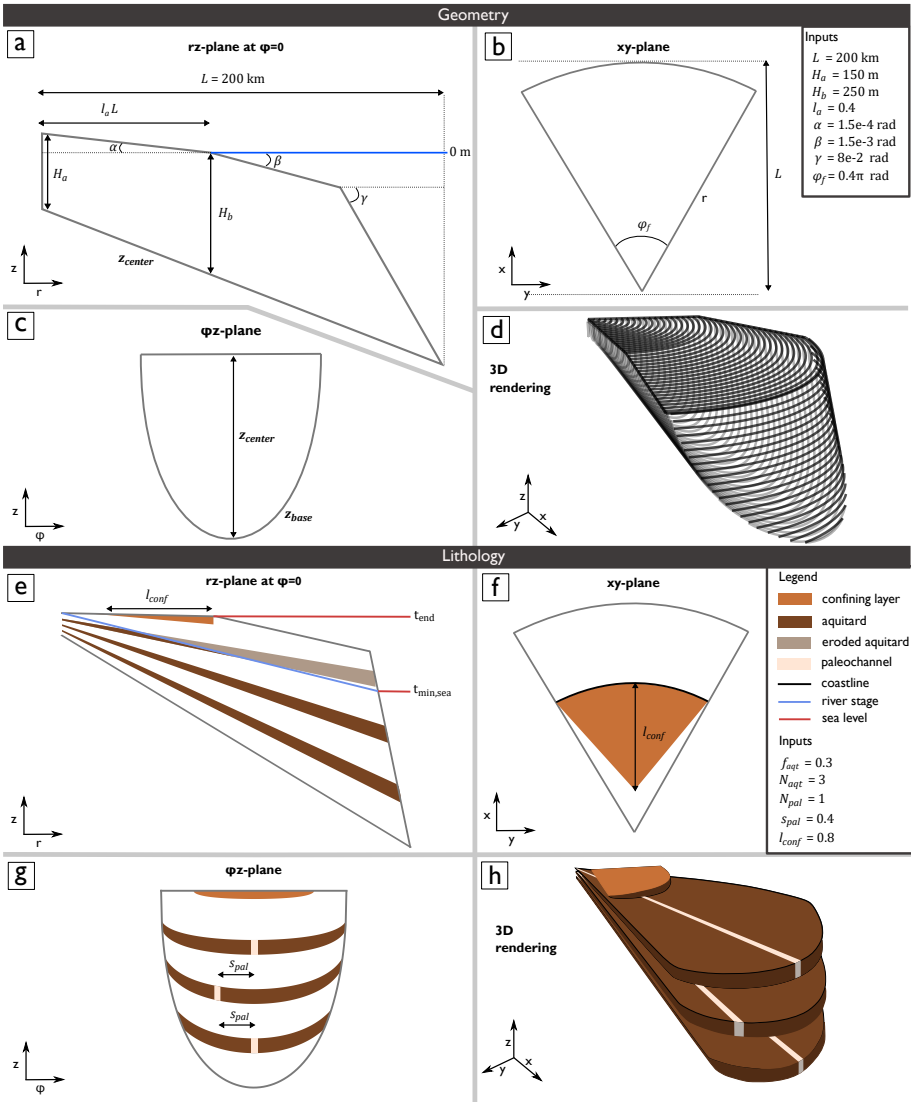

Figure 4.1: Visualization of the delta geometry and lithology across three planes. $r\varphi$ and xy respectively are the polar and cartesian coordinate systems. (a) The rz-plane, on the left-hand side is the delta apex and on the right-hand side the coast. The blue line indicates the reference depth. (b) The xy-plane, at the bottom is the delta apex, at the top is the sea. (c) The φz-plane, note the half-ellipse shaped bottom. (d) A rendering of the resulting geometry. The black lines visualize the top of the geometry, the gray lines the hydrogeological base. (e) Lithology across the rz-plane. The aquitard is eroded where it is intersected by the river stage during the glacial lowstand (at $t_{min,sea}$) (f) Lithology across the xy-plane, viewing the top confining layer. (g) Lithology across the φz-plane, note the paleochannels that form conducts through the aquitards. (h) 3D rendering of the aquitards and confining layer.

4.2.3 *Boundary conditions*

4.2.3.1 *Offshore*

The sea was incorporated as a Robin boundary condition (Jazayeri and Werner, 2019). We used the median eustatic sea level curve of the last 45 ka (Spratt and Lisiecki, 2016) to set the heads at the sea boundary. To simulate variable-density groundwater flow and coupled salt transport, we use iMOD-SEAWAT (see section 4.2.8). This code requires heads to be constant throughout stress periods, thus we calculated the mean sea level over each stress period. Stress periods were refined during the Holocene (the last 11 ka, see figure 4.2a), since this is the main period of interest where the marine transgression occurred. We use a coarser temporal discretization for the Late-Pleistocene as otherwise the amount of input data would get too large. The conductance between sea and aquifers and the salinity of the sea were kept constant through time at 1e5 m^2/d. This is on the high side compared to groundwater models that simulate the present-day Netherlands (De Lange et al., 2014), where values of 1e4 m^2/d are more common. However, we found that lower conductances (1e4 m^2/d) hampered free-convection during the marine transgression in simulations with lower $K_{h,\,aqf}$ values, despite Rayleigh number exceeding critical values (>40). The higher conductance is a reasonable assumption, since fine-grained sediments, which lower the conductance, started to be deposited relatively recently, during delta progradation (Stanley and Warne, 1994).

Sea cells were placed at the top active cells beyond the coastline. We use the point where sea level equals the topography, $r_{sea=top}$, to determine the location of the coastline during the Late-Pleistocene. This method, however, does not result in a marine transgression during the Holocene as the median sea-level never reaches sea-levels above 0 m. In reality, a lot of deltas experienced a marine transgression at the start of the Holocene, after which the delta progradation started as sea level rise decelerated (Stanley and Warne, 1994). To incorporate this without having to change the delta geometry, we therefore introduced l_{tra} (Text C.1), which is the relative length of the onshore part at $t_0 (t = 0\ ka)$ that is covered with sea water at the moment of maximum marine transgression t_{tra}. t_{tra} varied in reality between 8500 and 6500 ka (Stanley and Warne, 1994).

4.2.3.2 *Onshore*

Onshore surface waters were also incorporated as a Robin boundary condition (Jazayeri and Werner, 2019). Stages were assigned by drawing linear profiles from the delta apex to the contemporary coastline, following van Engelen et al. (2019). This boundary condition was assigned to all onshore cells with depths closest to the onshore surface water stage, so

that a fan of, lower conductive, surface water was created. Hereafter, a number of N_{riv} lines were drawn, each representing a large river branch. The conductance of onshore surface waters on these lines was multiplied with a factor, f_{chan}, to simulate the higher surface-groundwater interaction that occurs near large river branches (Sefelnasr and Sherif, 2014). The conductance was kept constant through time. Saline water intrusion in surface waters was incorporated by introducing a surface water saline intrusion length, l_{surf}, that specifies the extent of saline water intrusion at t_{end}. A linear salinity profile was drawn from r_{coast} to l_{surf}, as a first-order approximation of the more S-shaped or exponential salinity profiles (Figure C.2) observed in reality (Savenije, 2012). The intrusion length was corrected each stress period for the large changes in river gradient that occurred over time (section C.2), by substituting the Chezy formula (Chow et al., 1988) into Savenije's formula for the salinity intrusion length (Savenije, 2012).

A natural groundwater recharge flux of infiltrated rainfall (R) was assigned as a Neumann boundary condition at the upper active cells onshore, of which the magnitude was fixed throughout time. In reality, the natural groundwater recharge was very dynamic over the last 45 ka, as soil properties and climate varied strongly through this period (Gossel et al., 2010). The constant recharge was a first-order approximation of the model sensitivity to natural groundwater recharge. Adding more complex recharge functions would introduce more inputs, which would increase the amount of simulations required for the global sensitivity analysis (section 4.2.5).

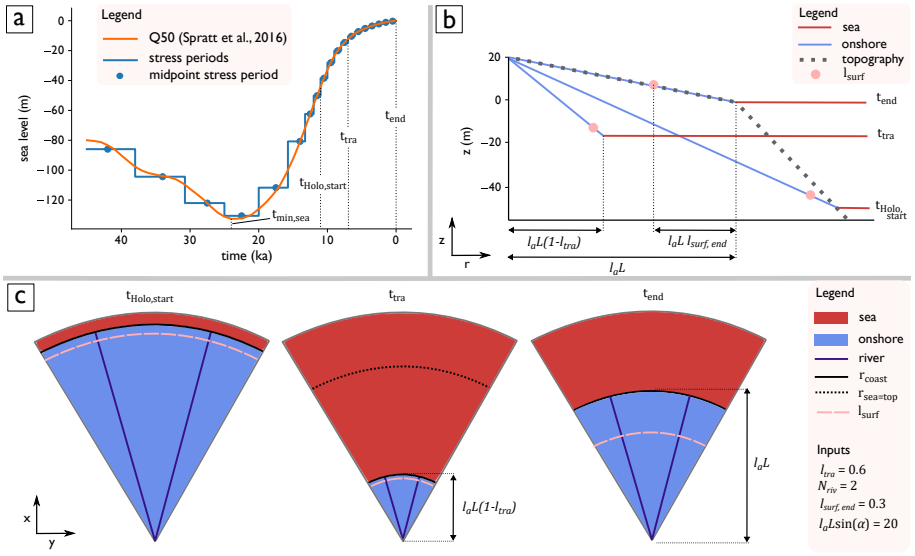

Figure 4.2: Description of the boundary conditions. (a) Eustatic sea level curve. In orange the median data of (Spratt and Lisiecki, 2016), in blue how we discretized this curve into constant stress periods. The vertical dotted lines indicate the sea-levels at the glacial lowstand ($t_{min,sea}$), at the start of the Holocene ($t_{Holo,\,start}$), at the maximum extent of the marine transgression (t_{tra}), and at 0 ka (t_{end}). (b) Location of the boundary conditions over the zr-plane. On the right-hand side the time each line belongs to. Note that the boundary conditions do not necessarily follow the (present-day) topography, because rivers can incise during lowstands and deltas prograded only after t_{tra}, which caused the present-day topography. (c) Location of the onshore and the offshore through time, respectively at the start the Holocene (t_{start}), at the maximum extent of the marine transgression (t_{tra}), and at 0 ka (t_{end}) over the xy-plane.

4.2.4 *Initial conditions*

As initial salinity, we set all groundwater below the minimum sea level (-130 m) as saline. In this way, we accounted for older saline groundwater that might be present in deeper aquifers (van Engelen et al., 2018; Hanor, 1994). We traced this old saline groundwater with a separate tracer. The initial heads were set equal to the heads of the surface water systems during the first stress period, corrected for salinity such that the freshwater heads (Post et al., 2007) were vertically constant.

4.2.5 *Sensitivity Analysis*

In total, our global sensitivity analysis covered 23 inputs. Since the wall clock time of individual simulations ranged up to 7 days on a computational node with 24 cores a sampling scheme was chosen that sufficiently explored the input hyperspace whilst keeping the required amount of simulations to a minimum. One of the few methods capable of this is Morris' method (Morris, 1991), which therefore is a commonly used sampling scheme in hydrology (e. g. Cloke et al., 2008; Herman et al., 2013; Song et al., 2015; Xu et al., 2018). Morris' method works as follows. First, all input distributions are transformed to a uniform unit distribution, ranging from 0 to 1. Next, the resulting unit hyperspace is discretized into N_{lev} levels. In this study we set N_{lev} to 4, which is a common value (Morris, 1991). Consequently, from a random starting point in this discretized hyperspace, one input at a time is varied consecutively. This results in a trajectory of length $N_{inp} + 1$, where N_{inp} is the number of inputs. An N_{traj} number of trajectories is created so that the effect of changing one input at a time is evaluated multiple times for each input. In other words, the effect of each input can be assessed in different areas of the input hyperspace. The trick is to create a set of trajectories that covers the input hyperspace the best, for which multiple algorithms have been developed (Campolongo et al., 2007; Khare et al., 2015; Ruano et al., 2012). In this research we use the algorithm of Khare et al. (2015) to create $N_{traj} = 10$ trajectories. The effect of each input is expressed as the elementary effect, which is the gradient of the change in model response (section 4.2.7) over the change in input (section 4.2.6). Since for each input N_{traj} elementary effects are calculated, a mean (μ) and standard deviation (σ) of the elementary effects can be calculated. The value μ serves as an estimate of the general sensitivity of the model to an input, σ as a proxy for the amount of non-linearity and/or interaction the input has. The higher the value of σ, the less likely a local sensitivity analysis is going to lead to an accurate assessment of the sensitivity of this input. Following Campolongo et al. (2007), we use the mean of the absolute elementary effects (μ^*) to correct

for non-monotonous effects that otherwise cancel each other out. This also allows us to calculate a measure of non-monotonicity, ε, for each input:

$$\varepsilon = \frac{\text{abs}\,|\mu|}{\mu^*} \tag{4.1}$$

An close to one means the elementary effect of the input is very monotonous, meaning the sign of the model response to a change in the input is always equal, regardless of the configuration of other inputs. Conversely, an close to zero means it is very non-monotonous.

4.2.6 *Input distributions*

A literature study was conducted to determine realistic input ranges. Table 4.1 lists the input distributions that were reported and varied in the sensitivity analysis. The inputs that were kept constant can be found in table C.1. For four inputs, complete overviews were already available from which a realistic input range could be inferred directly, namely the hydraulic gradient (α) (Syvitski and Saito, 2007), the contemporary salinity intrusion length ($l_{surf,\,end}$) (Savenije, 2012), longitudinal dispersivity (a_l) (Zech et al., 2015), and time of maximum transgression (t_{tra}) (Stanley and Warne, 1994). For the other inputs, mainly those dealing with the subsurface, we compiled a database of real-world case studies for different deltas (Figure 4.3). The lithological inputs (f_{aqt}, l_{conf}, N_{aqt}, N_{pal}) and groundwater system depths (H_a,H_b) were determined from reported geological cross-sections; l_{tra} and N_{chan} from paleogeographical maps; and the remaining geometrical inputs (l_a, β) by drawing profiles through the General Bathymetric Chart of the Oceans (GEBCO, 2014). The literature sources usually provided a separate range of hydrogeological inputs ($K_{h,\,aqf}$, $K_{v,aqt}$, K_h/K_v, R) in each delta. The reported range either represented spatial variability of the input (zoning), variable lithology, different model scenarios, or had an unspecified cause. Two studies did not report $K_{v,aqt}$, but instead very high effective anisotropies (10,000) (Bonsor et al., 2017; Cao et al., 2016) for the entire groundwater system. In these cases, we used those anisotropies to calculate $K_{v,aqt}$. The data of our literature review is included in the code package that accompanies this paper (van Engelen, 2020a).

Table 4.1: List of the chosen input distributions for the global sensitivity analysis.

Symbol	Description	Distribution	Range	Unit	Source
		Geometry			
l_a	Length of the onshore relative to the total length	uniform	0.1 – 0.8	-	GEBCO 2014
f_H	Ratio sediment thickness at the apex over that at the coastline (H_a/H_b)	uniform	0.0 – 0.8	-	Data review
H_b	Sediment thickness at the coastline	loguniform	70 – 1000	-	Data review
α	Angle onshore topography	loguniform	1e-5 – 1e-3	rad	Syvitski and Saito 2007
β	Angle coastal shelf	loguniform	1e-4 – 4e-3	rad	GEBCO 2014
φ_f	Angle sector across the xy-plane.	uniform	$\frac{1}{8}\pi - \frac{1}{2}\pi$	rad	Assumed
		Lithology			
f_{aqt}	Fraction aquitard of the sediment column	uniform	0.1 – 0.8	-	Data review
l_{conf}	Extent of the confining layer relative to the total onshore length	uniform	0.0 – 1.0	-	Data review
N_{aqt}	Number of aquitards	uniform	0 – 6	-	Data review
N_{pal}	Number of paleo channels per aquitard	uniform	1 – 4	-	Data review
s_{pal}	Relative paleochannel displacement	uniform	0 – 1	-	Data review
		Hydrogeology			
$K_{b,\,aqf}$	Horizontal hydraulic conductivity aquifer	loguniform	1e-1 – 2e2	m/d	Data review
$K_{v,\,aqt}$	Vertical hydraulic conductivity aquitard	loguniform	1e-6 – 1e-1	m/d	Data review
$f_{K,\,pal}$	Factor governing horizontal hydraulic conductivity paleo channel.	uniform	0 – 1	-	Assumed
K_h/K_v	Anisotropy of single formation, assumed equal for aquifers & aquitards.	loguniform	1 – 100	-	Data review
R	Recharge	uniform	0 – 3e-3	m/d	Data review
		Surface water			
N_{chan}	Number of river channels	uniform	1 - 7	-	Data review
f_{chan}	Factor with which river channel resistance is reduced compared to surrounding surface water	loguniform	1 - 10	-	Assumed
l_{sal}	salinity intrusion length in surface water at t = 0 ka relative to the onshore length.	uniform	0 – 1	-	Savenije 2012
l_{tra}	Length of maximum transgression relative to the onshore length	uniform	0 - 1	-	Data review
t_{tra}	Time of maximum trangression	uniform	9 – 6	ka	Stanley and Warne 1994
		Solute transport			
n_e	Effective porosity, assumed constant throughout domain	uniform	0.1 – 0.4	-	Data review
α_l	Longitudinal dispersivity	loguniform	0.25 - 10	m	Zech et al. 2015

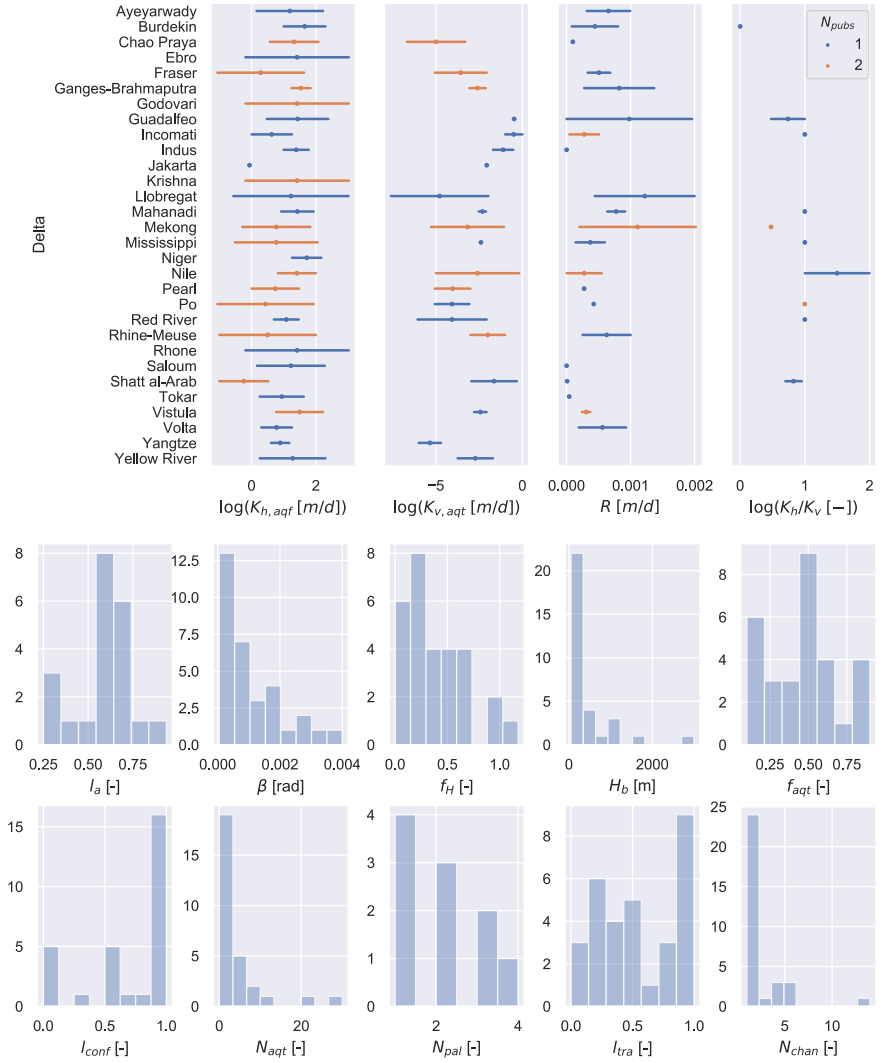

Figure 4.3: Distribution of inputs as found in the literature (previous compilations and additional real-world case studies, see Section 4.2.6). Inputs for which the input ranges are reported are plotted on top. Histograms at the bottom present the distribution of inputs for which no range was reported per delta.

4.2.7 *Sensitivity Metrics*

We computed sensitivity metrics to four outputs of interest, which we all evaluated at 0 ka. We work with relative volumes and masses as otherwise the sensitivity to geometrical inputs would dominate. First,

$$FW_{off} = \frac{V_{f,\ off}}{V_{off}} \tag{4.2}$$

where FW_{off} is the relative volume of brackish (<10 g TDS/l c.f. Post et al., 2013) groundwater offshore (-), $V_{f,\ off}$ is the absolute volume of brackish groundwater offshore (m3), and V_{off} are total volume of offshore groundwater (m3). Secondly,

$$S_{on} = \frac{M_{s,\ on}}{M_{w,\ on}} \tag{4.3}$$

$$S'_{on} = \frac{\partial S_{on}}{\partial t} \tag{4.4}$$

where S_{on} is the relative onshore salt mass (-), $M_{s,\ on}$ is the absolute onshore salt mass (kg), and $M_{w,\ on}$ is the absolute onshore water mass (kg), and S'_{on} is the time derivative of S_{on}. Thirdly,

$$S_{init} = \frac{M_{s,\ init}}{M_s} \tag{4.5}$$

where S_{init} is the relative mass of initial salt (-), $M_{s,\ init}$ is the absolute mass of initial salt (kg), and M_s is the absolute total salt mass (kg).

In addition, we visually classified the end-state (0 ka) fresh-salt groundwater distributions of each simulation into 5 different typologies, modified after the salinity distributions of the "modes of transgression" in Kooi et al. (2000): 1) the dispersive type, which has wide mixing zones (mode 1 in Kooi et al. (2000)), 2) the free convective type, where fingers are visible (mode 2 and 4 in Kooi et al. (2000)), 3) a mix of the previous two types, 4) a sharp interface between fresh and saline groundwater, and 5) the inverted type (mode 3 in Kooi et al. (2000)), where salt water is overlaying fresher water. We consequently compared these to published fresh-salt groundwater distributions of real-world case studies that we classified in the same way.

4.2.8 *Code description and computational resources*

We used iMOD-SEAWAT (Verkaik et al., 2017) to solve the combined variable-density groundwater flow and solute transport equations. This code is based on SEAWAT (Langevin et al., 2008), but supports distributed memory parallelization for a significant reduction in computation times. The SEAWAT code is the industry standard for solving variable-density groundwater and coupled solute transport problems. Therefore, the reader is referred to its' manuals for an extensive explanation (Guo and Langevin, 2002; Langevin et al., 2003; Langevin et al., 2008). All scripts to build, run, and post-process models are released as a Python package (van Engelen, 2020a), which heavily utilized the iMOD-Python library (Visser and Bootsma, 2019). The global sensitivity analysis required 240 simulations. These were conducted on the Dutch national computational cluster Cartesius (Surfsara, 2014) on computational nodes with Intel Xeon E5-2690 v3 processors, each node hosting 24 CPU cores. The wall clock time of individual simulations varied strongly, ranging from 3 hours to 7 days.

4.3 RESULTS

The main results of the global sensitivity study are given in figure 4.4, which shows that the onshore salinity mass S_{on} is strongly controlled by the hydraulic conductivity of the aquifers $K_{h,\,aqf}$ (Figure 4.4a). This is a very non-monotonous input for this variable (Figure4.4e), meaning that an increase in $K_{h,\,aqf}$ can both increase and decrease the amount of salt water onshore, depending on the other inputs. More specifically, a high $K_{h,\,aqf}$ both favors vertical intrusion of saltwater during the marine transgression (converted via the anisotropy) as well as subsequently flushing infiltrated salt during a marine regression and flushing of initial salt over the complete time domain (Figure C.1). Another, equally sensitive input is H_b, that largely determines the system thickness. A deeper system allows for relatively more salt onshore, since the salt water wedge can reach further inland as well as that the freshwater zone is relatively smaller with depth in a deep system in comparison to a shallow system. Furthermore, deeper systems have a higher capacity of preserving old salt. Next to these two dominant inputs, S_{on} is controlled to a lesser degree by the relative onshore length (l_a), the hydraulic gradient (α), and the extent of the marine transgression (l_{tra}). l_a might be a surprising input to see here, since we normalize over the total onshore mass to calculate S_{on}. However, the brackish zone stays equal in size with a larger l_a and hence decreases in relative size with increasing l_a. The fact that S_{on} is more sensitive to H_b than l_{tra}, implies that the amount of salt onshore S_{on} is controlled more strongly by the amount of initial salt retained than the amount of salt infiltrated during the Holocene transgression.

The offshore brackish water (FW_{off}) is dominantly controlled by three inputs: $K_{h,\,aqf}$, the vertical conductivity of the aquitards $K_{v,\,aqt}$, and porosity n. FW_{off} in our models was mainly the result of Pleistocene fresh water being preserved in the aquifers, instead of submarine groundwater discharge, which is the reason why this metric is mainly controlled by inputs that largely determine the velocity of the flow. Higher velocities result in a quicker replacement of fresh water with salt water.

Looking at the system dynamics, both $S\prime_{on}$ and the relative mass of initial salt S_{init} are predominantly controlled by $K_{h,\,aqf}$ and H_h. The remaining sensitive inputs are different though, the short-term change in onshore salt mass $S\prime_{on}$ is additionally controlled by the hydraulic gradient α and extent of the marine transgression l_{tra}, whereas S_{init} is additionally controlled by inputs that control the total clay resistance (N_{aqt}, $K_{v,\,aqt}$,f_{aqt}) and l_a. This means that, though S_{on} is controlled strongly by the amount of initial salt retained by resistant layers, the current freshening or salinizing is controlled more strongly by the hydraulic gradient and the extent of the marine transgression.

The swarmplot in figure 4.5 plots $K_{h,\,aqf}$ against the vertical resistance of the top sediments up to and including the first aquitard at the coastline (r_s [d]). To calculate this, we summed the resistance of one aquifer and one aquitard, disregarding the resistance of the confining layer because this is deposited only after the Holocene transgression:

$$r_s = H_h \left(\frac{f_{aqt}}{N_{aqt} K_{v,\,aqt}} + \frac{\left(1 - f_{aqt}\right) K_h / K_v}{N_{aqt} + 1} \right) \tag{4.6}$$

Despite noise due to different boundary conditions for different simulations, patterns are visible. At lower hydraulic conductivities the system has a high probability of still being in a chaotic free-convective state. In some of these cases, the initial saline water in the aquifer was still preserved as a wide brackish zone, leading to the mixed type. With increasing $K_{h,\,aqf}$, a transition is visible towards an increased probability of a sharp interface. At high $K_{h,\,aqf}$ and r_s, meaning very high anisotropies of large-scale representative conductivities $K_{h,\,rep}/K_{v,\,rep}$, salinity inversions can occur.

Table 4.2 presents the results of a literature study where we classified all reported salinity distributions we could find for various deltas (a subset of the real-world case studies given in figure 4.3). Only types 1 (with wide mixing zones) and 5 (salinity inversion) are found in the reported field studies. If reported, we include the hypothesized source of the salt, and in one case we added a hypothesis ourselves. Namely, the Holocene transgression extended 150

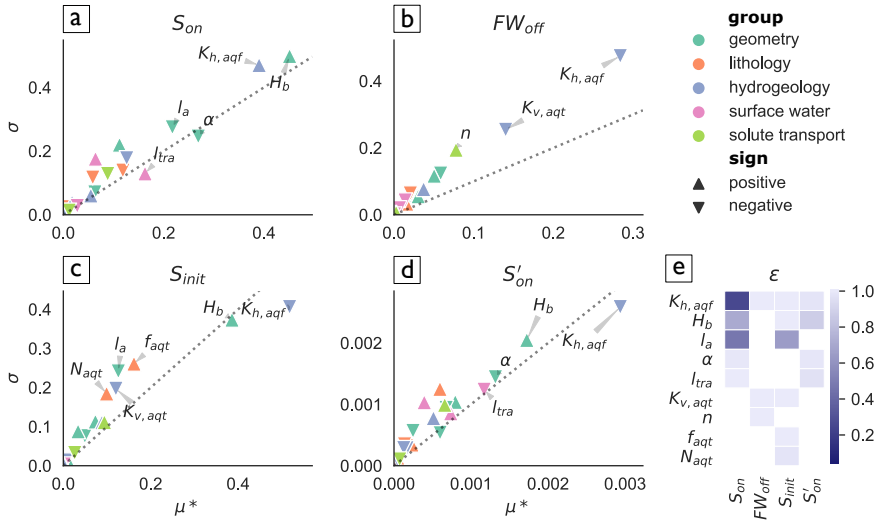

Figure 4.4: Scatter plots of the mean absolute elementary effect (μ^*) against its' standard deviation (σ) of each input for the four metrics (S_{on}, FW_{off}, S_{init}, S'_{on}). Each input is represented by a triangle, the orientation of which indicates whether the input has a positive effect on the metric or not. The colors indicate the group the inputs belong to in table 4.1. The dotted line represents where $\mu^* = \sigma$; inputs located above this line have a strong non-linear effect or are strongly interacting. The labeled inputs are the most sensitive. (e) The monotonicity heatmap (ε) for all the labeled inputs per output: the closer this value is to 1, the more monotonous the response of a metric to a change in an input.

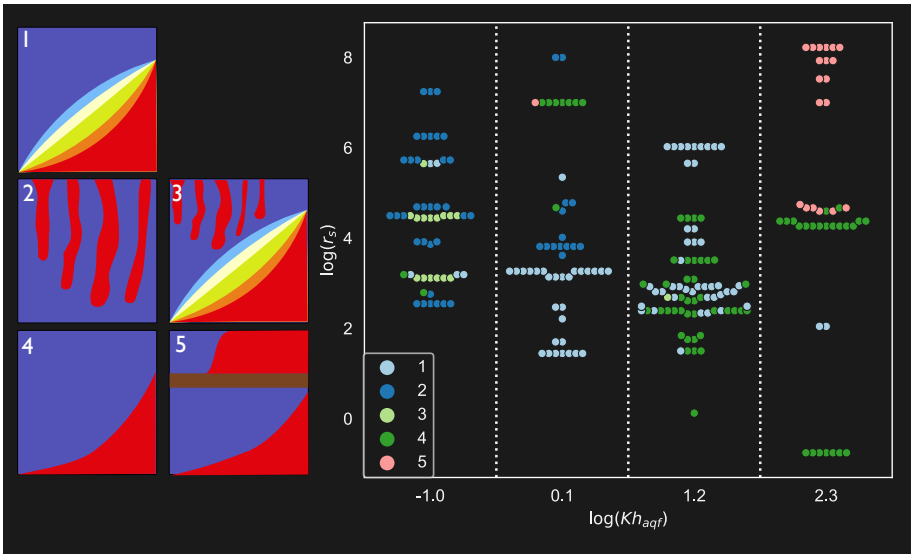

Figure 4.5: Swarmplot of the fresh-saline types. The numbers in the legend point to a fresh-saline type (section 4.2.7), of which sketches can be found on the left-hand side. On the x-axis the logarithm of the horizontal aquifer hydraulic conductivity, on the y-axis the resistance up to and including the first aquitard r_s (equation 4.6). Note that the x-axis is categorical, since we discretized the input hyperspace.

km landwards in the Yellow River delta (Saito et al., 2001), which causes a similar salinity inversion in the neighboring southern coastal aquifers of the Laizhou Bay (Han et al., 2011). There are two cases of clear contemporary salt water intrusion. Firstly, groundwater pumping in the 70 m thick deeper aquifer of the Llobregat delta led to increased salinities (Iribar et al., 1997). In the Rhine-Meuse delta, peat excavation in the polders caused land surface levels below sea-level, which consequently led to the polders draining (old marine) sea water (Delsman et al., 2014). In most cases, there were often relict salts of past transgressions present in the brackish and saline waters. Comparing the reported ranges of $K_{h,\,aqf}$ and values we estimated for r_s for the respective deltas to the trend observed in figure 4.5, we find that these comply with each other.

Table 4.2: Classification of reported fresh-salt water distributions for various deltas across the world. Salt sources in cursive are hypothesized by us, in roman as hypothesized by the referenced authors.$K_{h,\,aqf}$ and r_s are respectively retrieved and calculated from our data literature review.

Delta	Country	Type	$K_{h,\,aqf}$ [m/d]	r_s [d]	Source salt onshore	Reference
Ganges-Brahmaputra	Bangladesh & India	5	20 - 70	5e4 - 4e5	(Paleo)-salinity intrusion in rivers & aquaculture & marine transgression	Naus et al. 2019; Sarker et al. 2018
Incomati	Mozambique	1	1 - 18	5e1 - 5e3	Marine transgression	Nogueira et al. 2019
Kelehantan	Malaysia	5	NaN	NaN	Marine transgression	Samsudin et al. 2008
Llobregat	Spain	1	1 - 1000	4e3 - 1e9	Holocene transgression (in aquitards) & Contemporary sea water intrusion (deep aquifer)	Iribar et al. 1997; Manzano et al. 2001
Mahanadi (South)	India	1	8 - 85	7e3 - 2e4	Unknown	Radhakrishna 2001
Mahanadi (North)	India	5	8 - 85	7e3 - 2e4	Unknown	Radhakrishna 2001
Mekong	Vietnam	5	1 - 67.5	3e2 - 5e6	Holocene transgression	Van Pham et al. 2019
Nile	Egypt	1	7 - 100	2e2 - 1e7	Holocene transgression & evapoconcentration & rock salt dissolution	van Engelen et al. 2019; Geirnaert and Laeven 1992
Red River	Vietnam	5	5 - 30	5e3 - 5e7	Holocene transgression	Larsen et al. 2017
Rhine-Meuse	The Netherlands	1	0.1 - 100	1e2 - 9e3	Holocene transgression & contemporary sea water intrusion	Delsman et al. 2014
Rhone	France	1	NaN	NaN	Holocene transgression	de Montety et al. 2008
Saloum	Senegal	1	1 - 190	6e1 - 1e6	Salinity intrusion in rivers	Faye et al. 2005
Vistula	Poland	1	9 - 168	7e3 - 4e4	Pre-Holocene transgression	Kozerski 1983
Yellow River	China	5	2 - 200	6e2 - 7e4	*Holocene transgression*	Cao et al. 2016

4.4 DISCUSSION

The combination of a model with a large time domain and the global nature of our sensitivity analysis led to new insights. Firstly, all the sensitivity metrics were very sensitive to hydraulic conductivity of the aquifers $K_{h,\,aqf}$ (Figure 4.3), which also had a very non-monotonous effect on the onshore salt mass S_{on}, because $K_{h,\,aqf}$ both enhanced infiltration of salt water during the marine transgression as well as flushing of salt water from the system. This shows that care should be taken conducting a local sensitivity analysis on $K_{h,\,aqf}$ for transient models, as its effect on the total onshore salt mass at present depends on the configuration of other inputs. In sensitivity analyses with a more fixed geometry, the thickness of the groundwater system H_h will be a more constrained input than $K_{h,\,aqf}$, which means that $K_{h,\,aqf}$ only increases in relative importance in these experiments.

In addition, from the abundance of type 5 salinity distributions (Figure 4.5), we conclude that a high $K_{h,\,aqf}$ alone does not necessarily imply that the fresh-salt groundwater distribution is currently in a dynamic equilibrium. Moreover, as recently shown by van Engelen et al. (2019) (using a regional groundwater model with $K_{h,\,aqf}$ = 75 m/d), even relatively sharp fresh-salt groundwater distributions (type 4) can be still be affected by past conditions. In fact, the past occurrence of Holocene transgression in this case led to a steeper fresh-salt interface compared to the interface of an equivalent steady-state model. Furthermore, we found that different timescales are influenced differently by inputs. We can infer this from a comparison between S_{init} and S'_{on}. S_{init} is a measure of the long-term system dynamics (40 ka), whereas S'_{on} is a measure of the shorter-term dynamics (3 ka) (Figure 4.3): The long-term groundwater memory is predominantly controlled by clay resistance, whereas the shorter-term memory by the hydraulic gradient and the extent of the Holocene transgression. This has implications for groundwater dating studies in similar systems, as the long-term groundwater memory operates within the time scale of ^{14}C groundwater dating (2 ka – 40 ka) and the shorter-term approaches the timescale of that of ^{39}Ar (50 a – 1000 a) (Suckow, 2014).

Comparing the inferred typologies in figure 4.5 to field cases provides a sense of the plausibility of the input configurations. Three of the five typologies are not observed in the real-world case studies analyzed.

Firstly, sharp interfaces (type 4) are not observed, since all reviewed cases reported wide brackish zones. In the models with sharp interfaces, the transient boundary conditions and simple heterogeneities of our approach did not produce brackish zones. This means either that the reviewed deltas did not have a high effective aquifer conductivity $K_{h,\,aqf}$,

or that despite our best efforts, some important processes were not incorporated in this computational experiment. For instance, Michael et al. (2016) showed that stochastically generated hydraulic conductivity fields can create wide brackish zones, even with steady-state boundary conditions. Alternatively, kinetic mass transfer models, which are able to reproduce the tailing of a passing solute plume, also create wider brackish zones under transient conditions (Lu et al., 2009). We incorporated neither of these two approaches in our model setup, as constraining data was considered too scarce for this experiment. Generating stochastic hydraulic conductivity fields would require realistic parameters on spatial variation of conductivities or small-scale lithological variation for a wide range of deltas, which are not readily available. Also, the computational efforts needed to analyze the sensitivity to these parameters (a global sensitivity analysis, now with Monte Carlo sampling) would be at least an order of magnitude larger than the current study and is a topic for future research. Furthermore, estimates of the additional parameters required for kinematic mass transfer models are very limited (Sanford et al., 2017). Secondly, free convection (type 2 and 3) events are not observed in the field on a large scale, only as short-lived events on smaller scales (Andersen et al., 2007; Van Dam et al., 2009; Stevens et al., 2009). We are not aware of any reported large-scale, free-convective systems on a delta scale, which raises doubts on the realism of an aquifer with a representative conductivity $K_{v,\,aqf}$ between 0.001 – 0.1 m/d. Instead, chaotic salinity patterns are now often ascribed to heterogeneity in lithology and salt sources (e. g. Delsman et al., 2014; van Engelen et al., 2019; Michael et al., 2016; Naus et al., 2019). Given that many deltas have experienced a Holocene transgression (Larsen et al., 2017), the lack of free convection distribution in real-world cases provides an additional constraint on $K_{v,\,aqf}$ and thus indirectly on $K_{h,\,aqf}$. Because nearly all the simulations with $K_{h,\,aqf} = 0.1$ m/d were classified as the free-convective type, we deem it unlikely that deltaic aquifers would have a representative hydraulic conductivity on a regional scale that approaches this value. In contrast, the case-studies analyzed suggest that a high resistance up to and including the first aquitard r_s and high $K_{h,\,aqf}$, in other words a high representative anisotropy ($K_{h,\,rep}/K_{v,\,rep}$), results in a high probability of retaining an overtopping (type 5). For instance, the Quaternary aquifer underlying the Yellow River Delta has a high representative anisotropy and shows a brackish zone overlying fresh water (Cao et al., 2016). Similarly, high values of ($K_{h,\,rep}/K_{v,\,rep}$) were required to reproduce the observed salinity inversion in the Red River Delta (Larsen et al., 2017). The strongly heterogeneous Ganges-Brahmaputra delta also has a very high $K_{h,\,rep}/K_{v,\,rep}$ (Michael and Voss, 2009) and an observed salinity inversion at 200 m depth (Sarker et al., 2018).

Three salt sources were included our model: pre-Holocene salt water, Holocene sea water, and saline water by intrusion in rivers. The model results turned out to be very sensitive to the total amount of salt present initially, which we infer from the fact that S_{on} was very

sensitive to H_b. With increasing system thickness, there was an increasing amount of initial salt still present and longer travel times for sea water circulation. Despite that this old salt water can occupy large fractions of larger deltaic groundwater systems, its origins and flow paths are often underexplored in case studies and thus uncertain (van Engelen et al., 2018; Griffioen et al., 2016; Han et al., 2011). The fact that S_{on} was more sensitive to the extent of the marine transgression l_{tra} than the saline intrusion length in rivers $l_{surf,\,end}$ implies that the amount of salt water intruded via rivers was usually less in our modeled groundwater systems than the amount of Holocene sea water, despite that the Holocene transgression occurred only temporarily. This is a result of both the salinity and the hydraulic gradient of the river systems that stimulate flushing with fresher water, contrary to the constant sea level and salinity of the sea. The relatively small effect of salt water originating from rivers is also observed in case studies, as a local phenomenon constrained to areas in proximity to (paleo)-channels in the upper 50 m of the groundwater system (Ayers et al., 2016; Faye et al., 2005; Naus et al., 2019).

Despite our best efforts, there are limitations to this study. Even though we conducted an exhaustive literature study to attain realistic input distributions, this could not prevent some unrealistic input combinations for two reasons. First, as mentioned earlier in the discussion, delta aquifers with a regional-scale representative hydraulic conductivity of 0.1 m/d presumably do not exist, as this would result in large-scale, free-convective systems that are still present, which are not observed in the field. This means that the range of our $K_{h,\,aqf}$ input distribution is too large, meaning that the sensitivity to this input may be overestimated. Secondly, we disregarded anthropogenic effects. One case where clear large-scale anthropogenic influence on the fresh-salt groundwater distribution is the heavily engineered Rhine-Meuse delta (Delsman et al., 2014), mainly because of the land reclamation projects that cause large upward head gradients from 1850 AD up to now. Table 4.2, however, shows that humans did not influence the large-scale fresh-salt groundwater distribution for most deltas (yet). If human influence is observed, it is in the shallow aquifers (e.g. Ganges-Brahmaputra). A rigorous study where the human impacts on the fresh-salt groundwater distribution are quantified in deltaic systems is a topic for further study. In addition, our classification is based on visual interpretation, introducing subjectivity. A possible solution to this problem is presented by Werner (2016), who created a classification of fresh-salt groundwater distributions based on analytical solutions. However, this framework is not (yet) suitable for classifying the complex outputs produced by our 3D models.

4.5 CONCLUSION

We conducted a unique global-sensitivity analysis of a model with complex boundary conditions over geological time scales. The analysis is unique in its wide range of geometries, hydrogeological parameterizations and boundary conditions analyzed, making it representative for a large number of deltas worldwide. Model results, in particular onshore saline and its gradient, proved to be highly sensitive to the aquifer hydraulic conductivity ($K_{h,\,aqf}$) and thickness of groundwater system (H_h), and to a lesser degree to the hydraulic gradient (α) and the extent of the Holocene transgression (l_{tra}). We showed a non-monotonous sensitivity to $K_{h,\,aqf}$ on the total salt mass onshore, indicating interactions between the various model inputs. Furthermore, by classifying the model groundwater salinity distributions and comparing these with distributions of real-world cases, we showed that in at least half of these cases, the groundwater salinity distribution is not in a dynamic equilibrium. This is most likely caused by a combination of past marine transgressions and high effective anisotropies. We conclude that it is very likely that past marine transgressions are still reflected in the current fresh-salt groundwater distributions in deltas. This makes paleo-groundwater modeling a prerequisite for effective simulation of current groundwater salinity distributions in these systems.

ACKNOWLEDGEMENTS, SAMPLES, AND DATA

We like to thank Perry de Louw for his helpful suggestions for our model setup. This research has been supported by the Nederlandse Organisatie voor Wetenschappelijk Onderzoek (NWO) under the New Delta program (grant no. 869.15.013). This work was carried out on the Dutch national e-infrastructure with the support of the SURF Cooperative, on a NWO Pilot Project Grant. The authors declare that they have no conflict of interest. 3D renderings of all 240 model results can be found online under the following DOI (van Engelen, 2020b): `https://doi.org/10.5281/zenodo.3653876`. The code and data to reproduce the models and figures can be found under the following DOI (van Engelen, 2020a): `https://doi.org/10.5281/zenodo.3653734`.

5

SUSTAINABILITY OF FRESH GROUNDWATER RESOURCES IN 15 MAJOR DELTAS AROUND THE WORLD

ABSTRACT

Growth of the population, urbanization and intensification of irrigated agriculture in the world's river deltas boost the demand for fresh water resources, with extensive groundwater extraction as a result. This, in turn, leads to sea water intrusion and salt water upconing, which poses a threat to near-future water and food security. Managing fresh groundwater resources in deltas requires accurate knowledge about the current status of their fresh groundwater resources. However, this knowledge is scarcely present, especially for larger depths. Here, we use three-dimensional variable-density groundwater model simulations over the last 125 ka to estimate fresh groundwater resources for 15 major deltas around the world. We estimate current volumes of onshore fresh groundwater resources for individual deltas to vary between 10^{10}m^3 and 10^{12}m^3. The variability of our estimations of offshore fresh groundwater resources is considerably larger but they are generally much smaller. Based on current groundwater extraction rates, we estimate the time until in-situ fresh groundwater resources are completely exhausted (ignoring local-scale problems), partly leading to groundwater level decline and mostly replacement with river water or saline groundwater. Results show that four deltas risk complete exhaustion of fresh groundwater resources in 200 years, of which three suffer from saline surface water which means their groundwater resources will progressively salinize. With a fourfold increase in extraction rates, nine deltas risk a complete exhaustion within 200 years, of which seven suffer from saline surface water. We stress that the groundwater of these seven deltas should be carefully managed, since the progressive depletion of fresh groundwater resources in these deltas will hamper their ability to resist periods of water scarcity.

Based on: van Engelen, J., Oude Essink, G.H.P. , Bierkens, M.F.P. (-) Sustainability of fresh groundwater resources in 15 major deltas around the world; *In preparation*

5.1 INTRODUCTION

River deltas are economic hotspots that are commonly densely populated and harbor lands with high agricultural productivity (Neumann et al., 2015; Seto, 2011). Their growing population in combination with urbanization and intensification of irrigated agriculture are a cause for rising fresh water shortages (Bucx et al., 2010), which encourages increased groundwater extractions. These, in turn, lead to sea water intrusion and salt water upconing (Michael et al., 2017; Werner et al., 2013). Currently, salinization is already affecting many large deltas (Rahman et al., 2019), leading to significant agricultural yield loss (Biswas, 1993), which in turn decreases regional food security and creates new socio-economic challenges such as migration (Giosan et al., 2014) and changing farming practices (Smajgl et al., 2015). Moreover, a relatively high chloride content (> 500 mg Cl/L) in drinking water is associated with serious health risks (Khan et al., 2014; Talukder et al., 2017).

Managing fresh groundwater resources in deltas requires accurate knowledge about the current status of their fresh groundwater resources. This knowledge, however, is very limited, especially for larger depths, which is a result of a lack of measurements. Obtaining better insight into fresh groundwater resources in the world's deltas will help pinpointing vulnerable areas and is an important missing factor to add to the delta inter-comparison projects, of which numerous have been conducted in the last decade (e.g. Bucx et al., 2010; Van Driel et al., 2015; Syvitski et al., 2009; Tessler et al., 2015; Wolters and Kuenzer, 2015).

Here, we use three-dimensional variable-density groundwater model simulations over the last 125 ka to estimate fresh groundwater volumes for 15 major deltas around the world. We compared these volumes to estimates of current groundwater extraction rates for each delta, to acquire a sense of the deltas' vulnerability to groundwater extraction on a delta-scale. The selected deltas vary strongly in size, climatic zone, and human activity, but face similar challenges. For example, the deep, densely populated Ganges-Brahmaputra delta (Bangladesh and India) dwarfs the shallow, sparsely populated Saloum delta (Senegal) in scale and population, but both have saline surface water and are therefore strongly relying on groundwater for drinking water and irrigation (Ayers et al., 2016; Faye et al., 2005).

5.2 METHODS

5.2.1 *Model description*

To estimate the current volumes of fresh groundwater in 15 major deltas, we used three-dimensional variable-density groundwater models ("paleohydrogeologic models" in short) which we integrated over the last 125 ka, encompassing a full glacial cycle. We applied the paleohydrogeologic models to a number of synthetic deltas with a simplified geometry and lithology. These models are similar in makeup (size, form and hydrogeology) as the considered actual deltas, whereby the parameters with the largest uncertainty and impact on fresh groundwater resources (aquifer horizontal conductivity and aquitard vertical conductivity) were varied to account for uncertainty (explained in full detail in chapter 4; van Engelen et al., under review). Each model was forced with a combination of the eustatic sea level curve (Spratt and Lisiecki, 2016) and a Holocene transgression (van Engelen, 2020a) to simulate the fresh-salt groundwater distribution and in this way recreate the groundwater salinity distribution representative for today (Figure 5.1). The major change made to the model in chapter 4 is that we simulate the last 125 ka, instead of the last 40 ka, and start initially completely saline. This initially saline groundwater is traced with a separate tracer in the solute transport component of the model, to get a sense of the memory of the groundwater system.

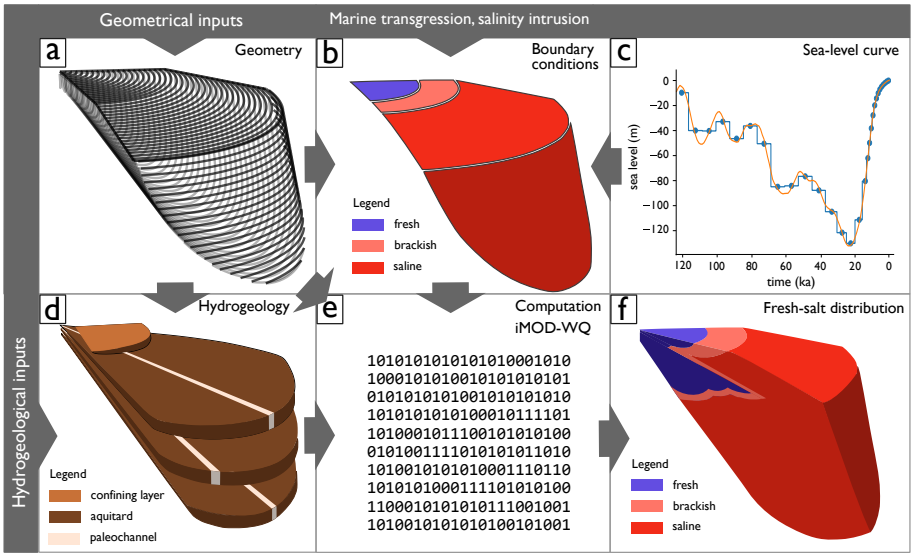

Figure 5.1: Overview of the paleohydrogeologic modelling process, in which the grey arrows indicate dataflow. A set of geometrical inputs is used to create a geometry (a). This geometry is then combined with a set of hydrogeological inputs to create a hydrogeological schematization (d). The geometry is combined with a discretized sea-level curve (c) and with data on the extent of the salinity intrusion in the surface water system and marine transgression to create boundary conditions (b). The geometry, hydrogeology, and boundary conditions are consequently used to compute a fresh-salt groundwater distribution with the computer code iMOD-WQ (e). This results in a fresh-salt groundwater distribution (f), which is halved in panel f for the sake of a clear visualization.

5.2.2 *Input data and parameterization*

Our idealized models required a set of 21 inputs to create a geometry, lithology, hydrogeology, and boundary conditions. We conducted a literature study to obtain representative inputs for 30 deltas (chapter 4), of which the values for the 15 deltas simulated in this paper can be found in table 5.1 and the literature sources can be found in table 5.2. Due to budget constraints on the computational cluster, we could not compute more paleohydrogeologic reconstructions. The lateral geometry, the topography, and bathymetry were specified with global datasets (GEBCO, 2014; Kulp and Strauss, 2019; Syvitski and Saito, 2007). Groundwater system thicknesses were, if available, retrieved from case studies, or, if not, from the global aquifer system thickness estimation dataset (Zamrsky et al., 2018). The lithological inputs were retrieved purely from local studies (Table 5.2), as no global dataset of groundwater system interiors exist. No lithological data could be found for the Tokar delta (Sudan), so here we used the median value of each lithological input across all deltas in our dataset. The boundary condition inputs (salinity intrusion length and marine transgression) were also retrieved from local studies, except for the cases where no data could be found for the salinity intrusion length in the surface water system (The Tokar, Kelantan, and Burdekin delta). A comparison with a global dataset of the tidal factor and tidal intrusion length (Nienhuis et al., 2020) confirmed that saline water intrusion is presumably not occurring in these deltas and could be set to zero. For the hydrogeologic inputs, input ranges were usually provided in the local studies. Based on a previous global sensitivity analysis (see chapter 4), we varied the inputs that created the most output uncertainty, namely the horizontal hydraulic conductivity in the aquifers ($K_{h,\,aqf}$) and the vertical hydraulic conductivity of the aquitard ($K_{v,\,aqt}$). If no input range was available for $K_{h,\,aqf}$ in a delta, a data range was taken from a global permeability dataset (Huscroft et al., 2018), which provided a wide range that varied roughly three orders of magnitude. If no input range could be found for $K_{v,\,aqt}$ in a delta, an input range was created by taking the logarithmic mean of the minimum and maximum values for $K_{v,\,aqt}$ across all deltas. The other hydrogeologic inputs were averaged across their reported range, which were the porosity, infiltration recharge, and the formation anisotropy. If data was missing for one of these four inputs for a delta, the median value of all deltas was assigned. We discretized the input range of $K_{h,\,aqf}$ and $K_{h,\,aqt}$ in three levels (minimum, logarithmic mean and maximum), and conducted a full factorial analysis for each delta. This resulted in 9 simulations per delta. Finally, extraction rates were obtained from the PCR-GLOBWB output, which calculates groundwater extraction based on water demand and available surface water resources (Sutanudjaja et al., 2018).

Table 5.1: The inputs for all 15 deltas, based on a literature study (see table 5.2). For an explanation of the symbols, see figure 5.2. Inputs in cursive were values filled with the median value across 30 deltas.

Symbol	L_a	L_b	α	β	H_a	H_b	φ_f	N_{aqt}	f_aqt	l_conf
Delta	[km]	[km]	[rad]	[rad]	[m]	[m]	[πrad]	[-]	[-]	[-]
Burdekin	32	130	5.0e-4	6.7e-4	10	100	0.6	2	0.6	1
Chao Praya	164	200	3.0e-5	1.3e-4	300	600	0.18	7	0.5	1
Ganges-Brahmaputra	335	200	9.0e-5	5.0e-4	250	500	0.31	50	0.75	1
Kelantan	35	200	2.5e-4	2.0e-4	50	250	0.29	2	0.2	1
Mekong	232	200	3.0e-5	4.3e-4	250	500	0.32	8	0.4	1
Mississippi	197	180	2.0e-5	1.5e-3	600	1000	0.33	30	0.5	1
Nile	175	46	9.0e-5	2.0e-3	200	1000	0.33	4	0.4	1
Pearl	106	200	2.9e-5	1.0e-3	15	50	0.16	1	0.9	1
Po	56	200	4.0e-5	4.0e-4	300	1000	0.41	10	0.5	0
Red River	136	200	5.0e-5	3.5e-4	40	150	0.26	1	0.3	1
Rhine-Meuse	131	200	7.5e-5	1.7e-4	180	280	0.28	3	0.1	1
Saloum	73	32	4.2e-5	2.6e-3	80	80	0.18	1	0.1	0
Tokar	45	73	1.1e-3	4.0e-3	50	250	0.36	*2*	*0.5*	0.3
Yangtze	215	200	6.0e-5	3.0e-4	50	250	0.24	4	0.5	1
Yellow River	181	200	1.0e-3	1.5e-4	30	300	0.26	5	0.2	0.6

Symbol	N_{pal}	s_{pal}	$K_{h,aqf}$	$K_{v,aqt}$	n	l_{tra}	t_{tra}	N_{chan}	l_{sal}	R
Delta	[-]	[-]	[m/d]	[m/d]	[-]	[-]	[ka]	[-]	[-]	[m/d]
Burdekin	*2*	*0.6*	10.0 - 200.0	*7.8e-6 - 1.5e-1*	0.3	1	10	2	0	2.55e-4
Chao Praya	*2*	*0.6*	3.7 - 120.0	2.1e-7 - 5.0e-4	*0.3*	0.7	6	1	0.36	9.78e-5
Ganges-Brahmaputra	30	*0.6*	17.3 - 69.1	8.6e-4 - 7.8e-3	*0.3*	0.1	7	4	0.55	6.13e-4
Kelantan	2	*0.6*	8.6e-4 - 8.64	*7.8e-6 - 1.5e-1*	*0.3*	0.25	6	1	0	2.90e-4
Mekong	*2*	*0.6*	0.518 - 67.5	5.2e-6 - 8.6e-2	0.3	1	8	4	0.18	6.36e-4
Mississippi	*2*	*0.6*	0.3 - 114.0	4.0e-3 - 4.0e-2	0.3	1	8	1	0	2.90e-4
Nile	*2*	*0.6*	6.6 - 100.0	1.0e-5 - 6.6e-1	0.3	0.15	8	2	0	0.0
Pearl	2	0.6	1.0 - 30.0	8.6e-6 - 1.0e-3	*0.3*	0.8	6.8	5	0.34	2.74e-4
Po	2	0.6	0.0864 - 86.4	8.6e-6 - 8.6e-4	0.3	0.43	6	1	0	4.24e-4
Red River	2	0.6	4.92 - 29.4	8.6e-7 - 8.6e-3	0.2	0.8	9	3	0.08	2.90e-4
Rhine-Meuse	4	0.2	0.1 - 100.0	1.0e-3 - 1.0e-1	0.3	0.2	7.5	2	0.27	5.00e-4
Saloum	*2*	*0.6*	1.47 - 190.0	*7.8e-6 - 1.5e-1*	*0.3*	0.9	4.5	2	1.67	0.0
Tokar	*2*	*0.6*	1.79 - 42.2	*7.8e-6 - 1.5e-1*	0.3	0.75	6	1	0	4.11e-5
Yangtze	*2*	*0.6*	4.0 - 15.0	1.0e-6 - 2.0e-5	*0.3*	1	7	1	0.12	2.90e-4
Yellow River	*2*	*0.6*	1.8 - 200.0	1.8e-4 - 2.0e-2	0.3	0.2	6	1	0	2.90e-4

Table 5.2: Literature used to obtain the inputs in table 5.1.

Delta	Geometry	Lithology	Hydrogeology	Boundary conditions
Burdekin	Fass et al. 2007; Mcmahon et al. 2000	Mcmahon et al. 2000	Mcmahon et al. 2000; Narayan et al. 2007	Fielding et al. 2006; Nienhuis et al. 2020
Chao Praya	Sanford and Buapeng 1996; Yamanaka et al. 2011	Sanford and Buapeng 1996; Yamanaka et al. 2011	Giao et al. 1998; Das Gupta 1985	Savenije 2012; Sinsakul 2000
Ganges-Brahmaptura	Bonsor et al. 2017	Bonsor et al. 2017; Michael and Voss 2009	Michael and Voss 2009	Goodbred and Kuehl 2000; Shamsudduha and Uddin 2007
Kelantan	Sefie et al. 2018	Samsudin et al. 2008; Samsudin et al. 1997	Huscroft et al. 2018	Nienhuis et al. 2020; Tilmans 1991
Mekong	Minderhoud et al. 2017; Van Pham et al. 2019	Minderhoud et al. 2017; Van Pham et al. 2019	Minderhoud et al. 2017; Van Pham et al. 2019	Nguyen and Savenije 2006; Tamura et al. 2009
Mississippi	Griffith 2003	Griffith 2003	Griffith 2003; Thompson et al. 2007	Coleman et al. 1998; Nienhuis et al. 2020
Nile	Sestini 1989	van Engelen et al. 2019	van Engelen et al. 2019; Kashef 1983	Nienhuis et al. 2020; Pennington et al. 2017; Stanley and Warne 1993
Pearl	Wang and Jiao 2012; Zong et al. 2012	Wang and Jiao 2012; Zong et al. 2012	Kwong and Jiao 2016; Yang et al. 2013	Zhang et al. 2013; Zong et al. 2009
Po	Teatini et al. 2011	Colombani et al. 2017; Teatini et al. 2011	Colombani et al. 2016; Teatini et al. 2011	Amorosi and Colalongo 2005; Nienhuis et al. 2020
Red River	Larsen et al. 2017; Winkel et al. 2011	Larsen et al. 2017; Winkel et al. 2011	Larsen et al. 2017	Ca et al. 1994; Tanabe et al. 2006
Rhine-Meuse	DINOLOKET	DINOLOKET	De Lange et al. 2014; Oude Essink et al. 2010	de Haas et al. 2018; Peelen 1970
Saloum	Faye et al. 2005	Faye et al. 2005	Faye et al. 2005	Ausseil-Badie et al. 1991; Nienhuis et al. 2020
Tokar	Zamrsky et al. 2018	No Data	Hussein 1982	Nienhuis et al. 2020
Yangtze	Shi et al. 2012; Xue et al. 2008	Shi et al. 2012; Xue et al. 2008	Chen et al. 2014	Saito et al. 2001; Wu and Zhu 2010
Yellow River	Han et al. 2011	Han et al. 2011	Cao et al. 2016	Saito et al. 2001

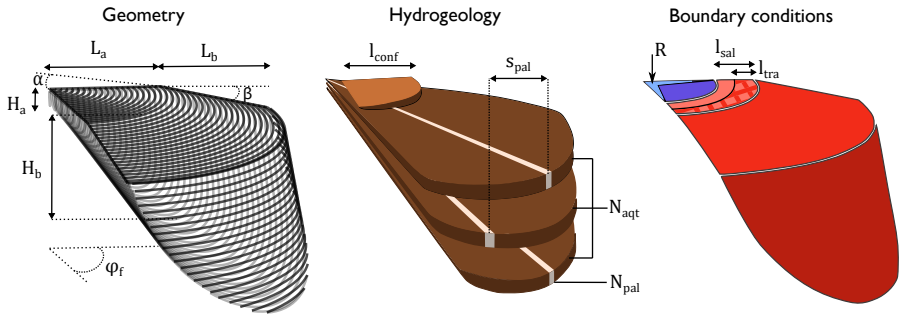

Figure 5.2: Visual description of symbols used for inputs, for their values see table 5.1. For further explanation, the reader is referred to chapter 4

5.2.3 *Metrics*

Our simulations result in current fresh-salt groundwater distributions for 15 of the major deltas in the world under natural conditions. Note therefore that the effects of groundwater extractions over the last decades that is prominent in many of these deltas is not included. To characterize the volumes of fresh groundwater and compare between deltas we use the following metrics. Firstly, $V_{fw,on}$ and $V_{fw,off}$ which are respectively the total onshore and offshore volumes of fresh groundwater in the delta. Secondly, S_{init} is the mass fraction of initial salt (initial condition of the paleohydrogeologic model 125 ka ago) still present in the model domain over the total salt mass. Finally, t_d is the exhaustion time, which is the time until the onshore fresh groundwater is exhausted, when taking only the (unpolluted) diffuse recharge of infiltrated rainfall into account. This is calculated as $t_d = \frac{V_{fw,on}}{(Q-R)}$, where Q is the total groundwater extraction flux (based PCR-GLOBWB) of the delta and R is the diffuse groundwater flux in the delta. When R exceeds Q, t_d is set to infinite. The rationale behind t_d is that it relates to the volume of "clean" fresh groundwater that can be pumped. After this time, this volume is exhausted and a) partly taken out of storage leading to head decline; b) mostly replaced by (often brackish or polluted) river water from concentrated recharge or by saline water from below. The definition of t_d does therefore not account for enhanced recharge from rivers (Bredehoeft, 2002). Moreover, t_d does not include local-scale problems due to overpumping, such as saline groundwater upconing. Instead, the underlying assumption is that whenever a groundwater well salinizes, a new one is immediately created to pump in a region with fresh groundwater. To therefore be on the safe side, we consider deltas with a logarithmic mean t_d of less than 200 years at high

risk. Deltas that cross the 200-year threshold only after increasing Q 4 times are appointed a medium risk.

5.2.4 *Validation*

Validating our fresh groundwater volume estimations is challenging as data is limited. To utilize the available data as much as possible, two approaches were taken. First, we compared our volume estimates to a three-dimensional distribution inferred from observations (Rhine-Meuse: Delsman et al. 2020; Mekong: Gunnink et al. 2020) or estimated fresh groundwater volumes of a more detailed regional model (Nile: van Engelen et al. 2019). Secondly, as a form of indirect validation we used reported depth distributions of local well data to infer if our fresh-salt distribution approached reality sufficiently with the following simple decision scheme. For each x, y location in the model, wells are dug until an aquifer is found that contains no salt in the vertical direction, up to a limit of 300 m. That is, if the upper aquifer is saline, the well filter will be placed in the first aquifer that is fresh below it, where we have used 20 m under its' confining layer, as suggested in Wittmeyer et al. (1996). In this way well distributions are created with depth that can be compared to the local data (van Engelen et al., 2019; De Lange et al., 2014; Minderhoud et al., 2017).

5.3 RESULTS

5.3.1 *Groundwater well depths as indirect validation*

Figure 5.3 shows a comparison between the observed and simulated depth distributions of groundwater wells. In the Nile Delta, groundwater is mainly extracted at 50 m depth, whereas our simulated distributions seem to avoid this depth. We attribute these differences to our simplification of the confining layer. In reality, the thickness of this layer increases from a few meters at the apex to nearly 100 m near the coast with strong lateral variation (Pennington et al., 2017). In our model, the thickness increases linearly from apex to coast, without any variation. Furthermore, the poor quality of the surface water (Rasmussen et al., 2009) is a reason to deepen wells that is not accounted for in our approach. For the Mekong delta, there are two simulations that replicate the observed well depth distributions, namely the simulations that have low conductive aquitards and high conductive aquifers allowing the existence of a salinity inversion (van Engelen et al., under review). The other simulations all simulate fresh groundwater in the upper aquifer, which is not observed in the field (Minderhoud et al., 2017). For the Rhine-Meuse delta, the models with a low aquifer hydraulic conductivity seem to reproduce the observed well depth distribution the

Table 5.3: A comparison between the daily total extracted groundwater in the regional datasets and in PCR-GLOBWB. The "factor" column states the division between these two datasets.

Delta	Regional Dataset (m3/d)	PCR-GLOBWB (m3/d)	Factor (-)
Mekong	2.4e6	2.2e6	1.1
Nile	7.2e6	1.8e6	4.0
Rhine-Meuse	3.2e6	7.7e6	0.41

best. These simulations capture the low number of wells at 10 m depth and the peak in wells at 30 m depth. The tail of the depth distribution is not captured, likely due to the simplifications in our lithological model. We also checked the total extracted fluxes in the available extraction data to the simulated PCR-GLOBWB data, shown in table 5.3. This table shows that considerable differences can exist. The total extraction rates in the Mekong are simulated quite well by PCR-GLOBWB but are underestimated in the Nile delta and overestimated in the Rhine-Meuse delta.

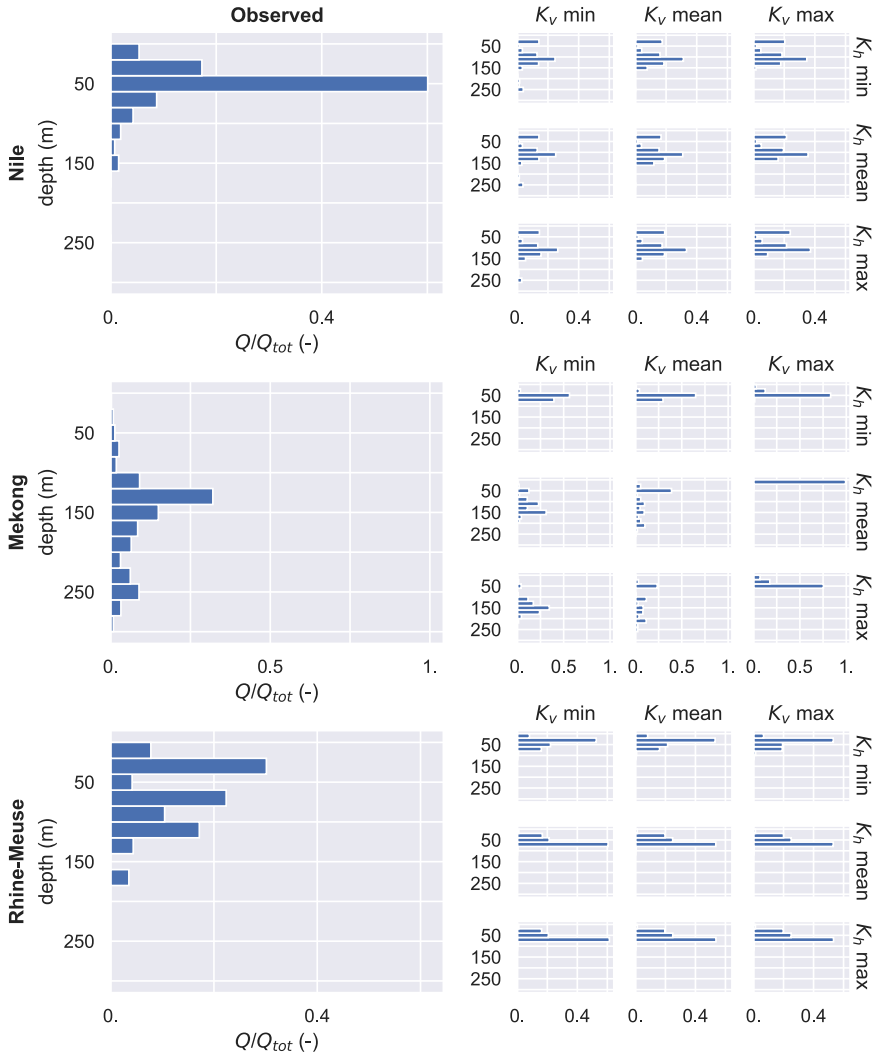

Figure 5.3: Comparison between observed and simulated well extraction distributions with depth for the Nile, Mekong, and Rhine-Meuse delta. In each panel, the vertical axis represents the depth, and the horizontal axis the normalized extraction flux. The larger panels on the left-hand side of the figure are the observed distributions (van Engelen et al., 2019; De Lange et al., 2014; Minderhoud et al., 2017), the smaller matrix of panels on the right-hand side represent the 9 simulations. For each panel matrix, the columns indicate the vertical hydraulic conductivity value for the aquitards ($K_{v,\,aqt}$) and the rows the horizontal hydraulic conductivity of the aquifers ($K_{h,\,aqf}$).

5.3.2 *End-state fresh-salt distributions*

Figure 5.4 shows example end-state fresh-salt distributions for 15 deltas. The wide variability in geometry is visible. For example, the groundwater system of the Pearl delta (nr. 8 in figure 5.4) is significantly shallower than the thick Po delta (nr. 9 in figure 5.4). It also shows that in some simulations, for example the Kelantan (nr.4), a vast amount of fresh groundwater is located offshore underneath clay layers, indicating the system is not in equilibrium. Several fresh-salt typologies that were found in 4 are also shown in figure 5.4. For example, the inverted type in the Kelantan (nr. 4), the sharp interface type in the Rhine-Meuse (nr. 11), and the free convective type in the Mississippi (nr. 6). The latter delta has a lot of clay layers and paleochannels, following the conceptual model of (Griffith, 2003), causing fingers of salt water to persist in the deep groundwater system after the Holocene transgression.

5.3.3 *Fresh groundwater volumes through time*

Figure 5.5 presents the time series of the total volume of fresh groundwater onshore ($V_{fw,\,on}$) over 125 ka. Fresh groundwater volumes increase throughout the Pleistocene, after which they rapidly decline during the marine transgression that marks the start of the Holocene. In some small deltas, namely the Burdekin and the Tokar, a full recovery from this transgression to the Pleistocene fresh groundwater volume is simulated as the delta prograded, but in most cases $V_{fw,on}$ does not recover. In the very thick groundwater systems (Ganges-Brahmaputra, Po, Nile, and Mekong), it seems that V_{fw} has not reached its potential maximum value in one glacial cycle. Thus, for these systems V_{fw} is a conservative estimation, because of our salt initial condition. In most cases, the range in estimated V_{fw} values is mainly caused by the uncertainty in the horizontal hydraulic conductivity of the aquifers, with the Nile delta as exception where the properties of the aquitards are much more uncertain (van Engelen et al., 2019).

5.3.4 *End-state metrics*

Figure 5.6 presents the end-state metrics for the 15 deltas. Most deltas have an onshore fresh groundwater volume ($V_{fw,\,on}$) ranging from 10^{10} to 10^{12}m^3, with the main exception being the Saloum delta in Senegal which has a very shallow groundwater system. In all cases where there is data to validate $V_{fw,\,on}$ estimations, The Mekong delta, the Rhine-Meuse delta and Nile delta, our simulations are on the conservative side. The variance in $V_{fw,\,on}$ estimations is small compared to the variance in the offshore fresh groundwater volumes ($V_{fw,\,off}$), which is stronger controlled by free-convection. Furthermore, the logarithmic

means of these offshore volumes are usually at least an order of magnitude smaller than their onshore counterparts, except for the Burdekin and Kelantan delta. This is because the offshore domain of these two deltas is a lot larger than its onshore counterpart. It can also be seen that the residence times of salt in many deltas presumably exceeds that of a glaciation cycle, as S_{init} often has a value higher than 0%. Finally, we observe that four of the simulated deltas has an expected exhaustion time (t_d) that is shorter than 200 years. The deltas with low extraction rates in the PCR-GLOBWB data (Tokar) or a high recharge (Mississippi, Po, Kelantan, Burdekin) have a large exhaustion time. Multiplying extractions by a factor four causes 8 of the deltas to have a t_d shorter than 200 years. The exhaustion time t_d of the Saloum delta varies strongly because of its low extraction rate and $V_{fw,\,on}$ that is (close to) zero.

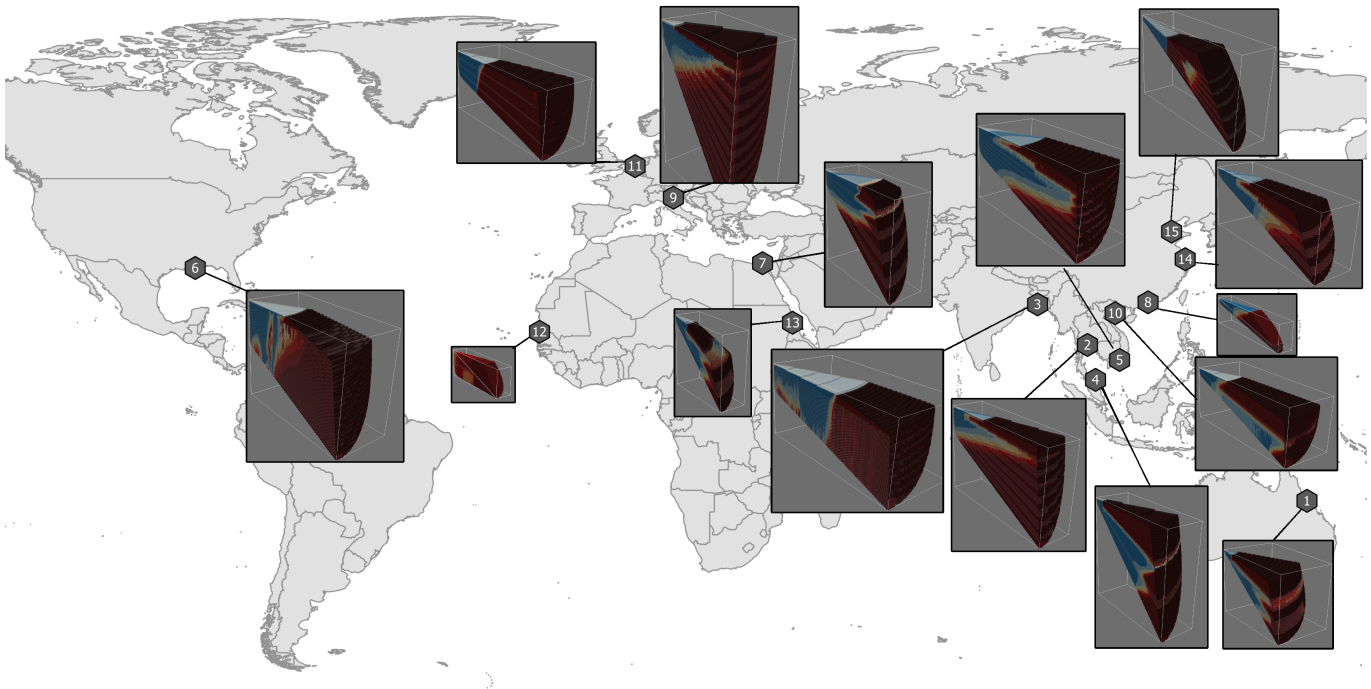

Figure 5.4: Example fresh-salt distributions for the 15 studied deltas, results are halved for a better visual representation. Note that for each delta 9 distributions were calculated in our full factorial analysis, of which only 1 manually selected result is shown in this figure. The light grey, fan-shaped surface on top of the delta shows the present-day onshore part of the model domain, the dark red surface on top the offshore part. The numbers refer to the entries in table 4, where the names of the deltas can be found. In the 3D renderings the vertical axis is stretched by a factor $4000 * \sqrt{z}$.

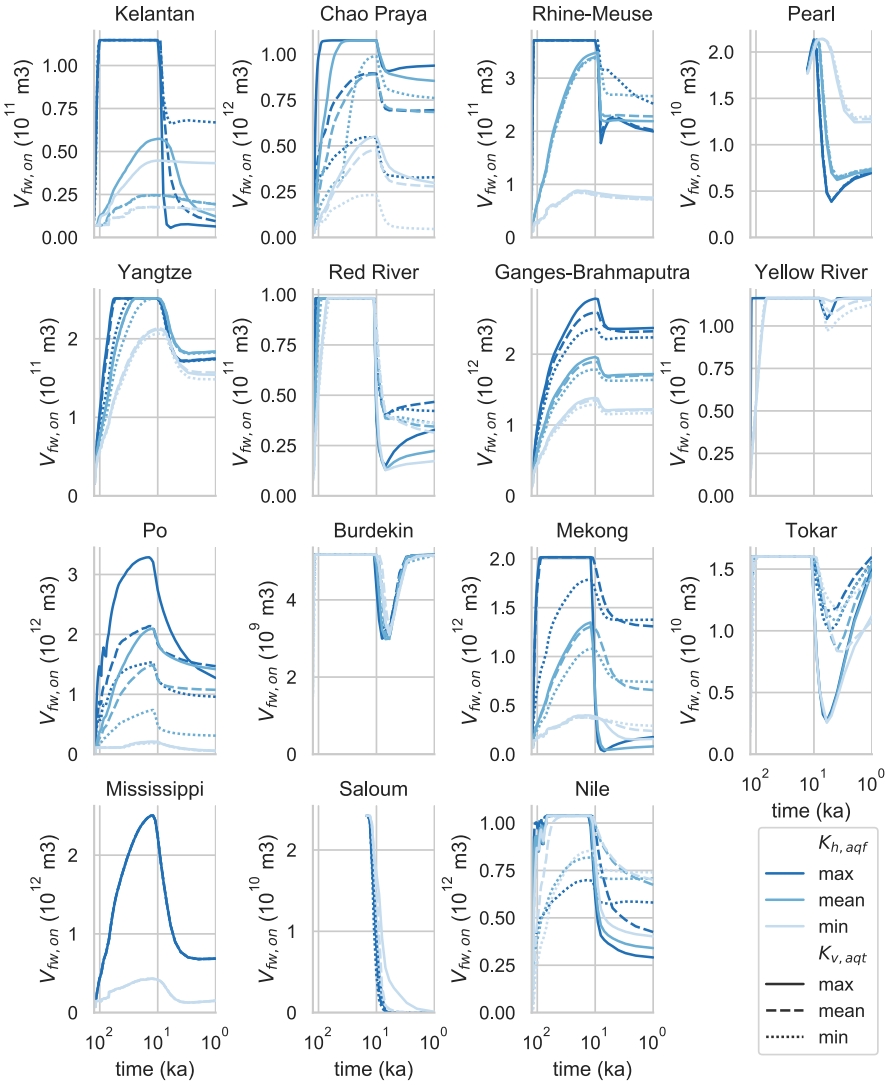

Figure 5.5: Onshore fresh groundwater volumes through time, 10 ka marks the start of the Holocene. Note that the horizontal axis is plotted on a logarithmic scale. The colors of the lines indicate the value for $K_{h,\,aqf}$, their linestyle the value for $K_{v,\,aqt}$. The Saloum and Pearl delta are very thin groundwater systems (<80 m to the hydrogeological base), thus these start at the onset of the Holocene (11.5 ka) from a completely fresh state.

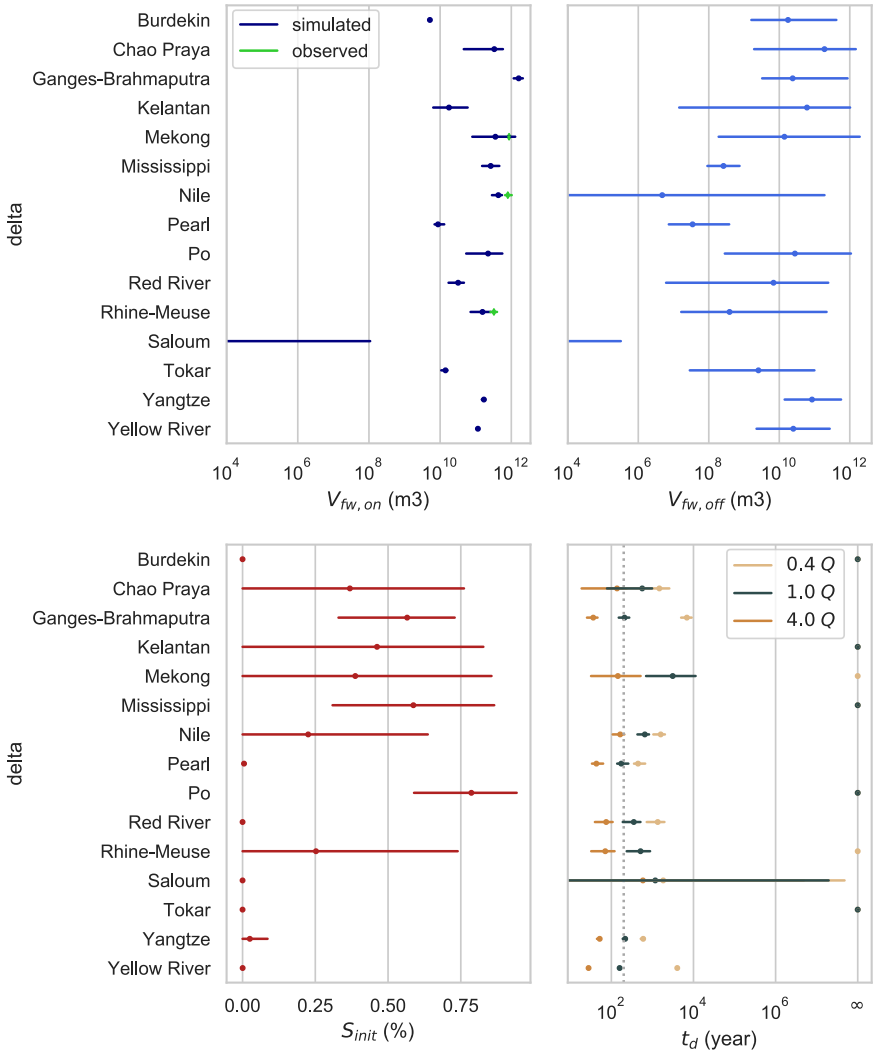

Figure 5.6: End state results for four metrics. The line indicates the range of the 9 simulations conducted for each delta, the dot the logmean for $V_{fw,\,on}$, $V_{fw,\,off}$ (the total onshore and offshore volumes of fresh groundwater in the delta), and t_d (the groundwater exhaustion time) and the mean for S_{init} (mass fraction of initial salt still present in the model domain over the total salt mass). The orange color in t_d indicate the effect of increasing the extraction rates with a factor four, the light brown color decreasing these rates with a factor 2.5. The dotted line presents $t_d = 200$ year. An infinite t_d implies that the diffuse recharge exceeds the extraction rate.

Table 5.4: Reasons for groundwater extraction for 15 deltas. The id column refers to the symbol number in figures 3 and 6.

Delta	id	Reasons to extract groundwater		References
		Problems with water quantity	Problems with water quality surface water	
Burdekin	1	Surface water scarcity (dry season)	-	Davis et al. 2014
Chao Praya	2	-	Bacteria, Nutrients, Turbidity	Simachaya et al. 2000
Ganges-Brahmaputra	3	Surface water scarcity (dry season)	Nutrients, Salinity	Ayers et al. 2016; Shamsudduha et al. 2011
Kelantan	4	-	Turbidity (sediments)	Sefie et al. 2018
Mekong	5	-	Salinity, Nutrients	Minderhoud et al. 2017
Mississippi	6	-	Salinity, Temperature (Energy plants)	LGWRC 2012; LPHI and AAE 2016
Nile	7	-	Salinity, Nutrients	El-Agha et al. 2017
Pearl	8	-	Salinity, Nutrients	Lu et al. 2009; Shi and Jiao 2014
Po	9	-	Salinity	Colombani et al. 2016; Giambastiani et al. 2013
Red River	10	-	Nutrients, Salinity	Ca et al. 1994; Hoang et al. 2018
Rhine-Meuse	11	Surface water scarcity	Nutrients, Pesticides	Oude Essink et al. 2010; Pellenbarg 1997
Saloum	12	-	Salinity	Faye et al. 2005
Tokar	13	Surface water scarcity	Salinity	Elkrail and Obied 2013
Yangtze	14	-	Nutrients, Salinity	Dai et al. 2011; Shi et al. 2012
Yellow River	15	-	Nutrients	Chen et al. 2007; Fan et al. 2012

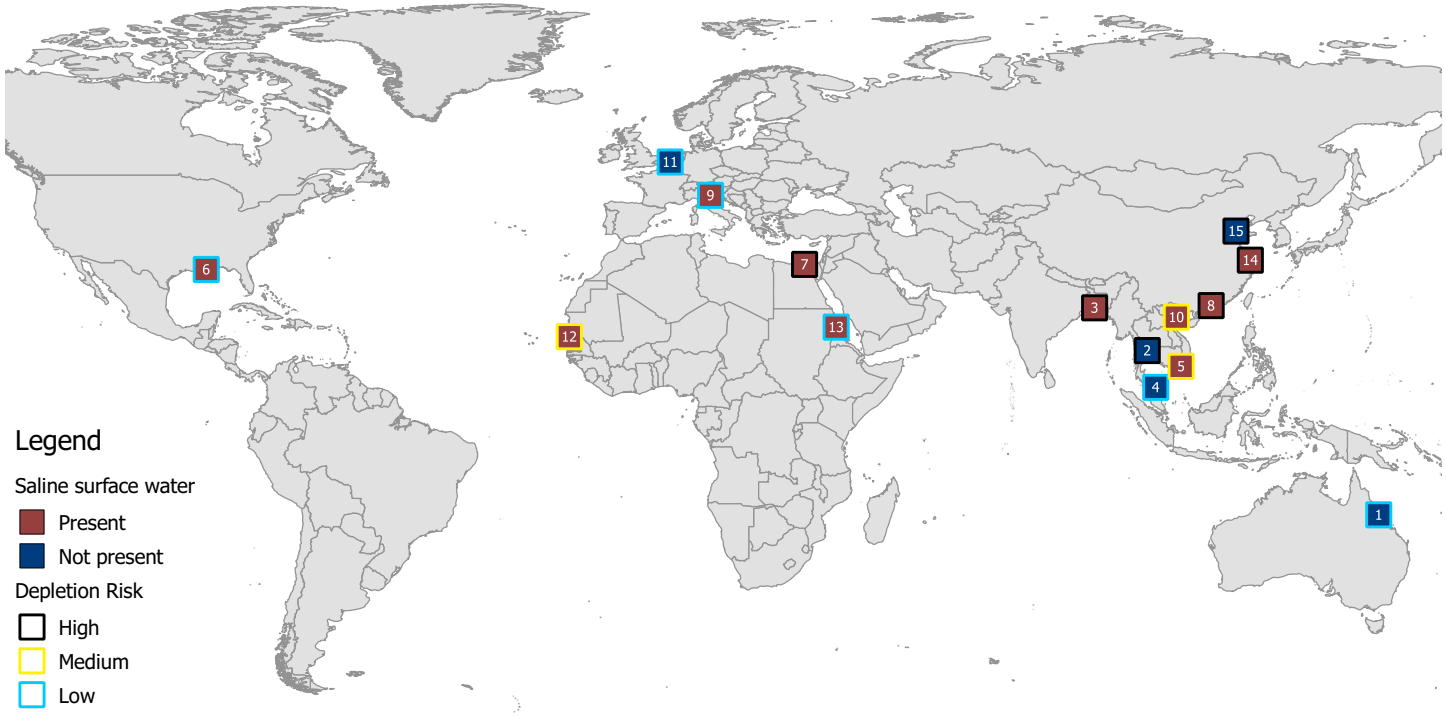

Figure 5.7: Map showing the depletion risk and whether there are issues with saline surface water for 15 deltas. The numbers in the boxes refer to id numbers in table 5.4.

5.4 DISCUSSION & CONCLUSION

We have conducted paleohydrogeologic reconstructions for 15 deltas across the world, varying widely in geometry, lithology, and boundary conditions. The results show that fresh groundwater resources of these areas have experienced large changes over time, especially at the start of the Holocene, when the eustatic sea level increased rapidly. The fresh groundwater resources of two simulated smaller deltas, namely the Burdekin and Tokar, experience a complete recovery to Pleistocene freshwater volumes after the Holocene transgression. In the field, traces of the past marine transgressions are still found in these deltas (Elkrail and Obied, 2013; Fass et al., 2007), thus the fresh groundwater volumes in these small deltas are presumably overestimated. A possible explanation for this is that a single porosity model, as used in this chapter, is not able to capture the tailing of a passing salt front. A dual-porosity model manages to capture this phenomenon (Lu et al., 2009), which would result in a slower flushing of salt water after the Holocene transgression. For the larger deltas, however, our simulations possibly underestimate the available onshore fresh groundwater resources ($V_{fw,on}$), as shown by the Nile and Rhine-Meuse delta in figure 5.6. Nearly all deltas possess onshore fresh groundwater volumes that range between 10^{10} to 10^{12}m^3 and offshore fresh groundwater volumes that are presumably one to two orders of magnitude smaller. Comparing these volumes to present-day recharge of infiltrated rainfall and extraction rates shows that four deltas have a fresh groundwater exhaustion time t_d of less than 200 years and are likely at risk, another five might be at risk with increasing extractions, and six deltas have a low risk since they receive ample recharge or have little groundwater extractions.

Table 5.4 provides, based on literature, the reasons why groundwater is used rather than surface water in the deltas considered. We observe that groundwater is extracted for water quality reasons in most deltas, the Burdekin being the only exception. The most common issues with surface water are surface water salinity, caused by either tidal differences or evapoconcentration, and nutrients, often caused by over fertilization or human waste effluents. Ten deltas experience saline surface water, and eight deltas experience an abundance of nutrients in their surface water. In only five deltas, groundwater was extracted for quantitative reasons because of surface water scarcity. We have mapped whether deltas have saline surface water and their exhaustion risk ($t_d < 200$) years in figure 5.7. Note that the Nile and Rhine-Meuse were appointed respectively a high and low risk, instead of a medium risk, as we corrected their extraction rates with the available field data, and thus respectively used 4.0 Q and 0.4 Q for these deltas (Table 5.3). There are four deltas that have both a high fresh groundwater exhaustion risk and surface water salinity issues, namely the Ganges-Brahmaputra, the Nile, the Pearl, and the Yangtze delta. The Mekong and Red River delta, and possibly the Saloum

delta, currently possess ample fresh groundwater resources, but are seriously under pressure with increasing extractions.

The definition of t_d does not account for enhanced recharge from rivers (Bredehoeft, 2002), which is likely the main source of groundwater recharge in case of intensive pumping in deltaic areas. We have deliberately left this term out of the sustainability measure t_d, because the usefulness of riverine recharge for freshwater supply is questionable since groundwater is usually extracted in deltas because of an insufficient surface water quality (Table 5.4). Riverine recharge contaminated with pollutants that break down or are adsorbed to sediments might be good enough for extraction immediately or after treatment. An example of this is the Rhine water that is first treated and then used to artificially recharge drinking water resources in the Netherlands (Stuyfzand, 1997). However, when surface water is saline, riverine recharge will progressively salinize groundwater resources, gradually rendering these resources unusable. This is the case for 10 out of the studied 15 deltas (Table 5.4 and Figure 5.7), so for these at least t_d is a useful metric. A combination of a low t_d and saline recharge leads to progressively saline groundwater resources on a human timescale, which means the delta's capacity to withstand periods of water scarcity decreases. This combination exists in four deltas (Ganges-Brahmaputra, Nile, Pearl, and Yangtze), and arises in three more deltas with increased extraction rates (Mekong, Red River, and Saloum) (Figure 5.7).

Some further remarks should be made on t_d. A t_d of 200 years does not mean that the fresh groundwater volumes are completely safeguarded for 200 years. Before t_d is reached, deltas already face more local-scale problems from groundwater extraction, such as enhanced sea water intrusion (Michael et al., 2017) and saline groundwater upconing (Pauw et al., 2015; Werner et al., 2013). In the latter case, pumping results in a rise of saline groundwater (Jakovovic et al., 2016) and furthermore the induced vertical groundwater velocities will increase mechanical dispersion and cause mixing of fresh and saline groundwater (Zhou et al., 2005). This increases the salinity of the pumped groundwater becoming saline, making it unusable. Underneath abandoned wells, a thick brackish zone could persists for tens of years, significantly hindering the restart of these wells (Zhou et al., 2005). An example of these local-scale problems can be found in the Rhine-Meuse delta, where issues with saline groundwater do exist near the coast despite it having a low risk in figure 5.7 (Delsman et al., 2018). Moreover, since extraction rates are expected to increase in most areas, t_d will decrease, as can be seen for a fourfold increase in extraction rates in figure 5.6. Reducing extractions, on the other hand, can increase t_d by an order of magnitude. The fourfold increase of Q in figure 5.6 may seem large, but mind that similar increases are expected for deltas with a booming population, such as the Nile Delta (Mabrouk et al., 2018). In addition, PCR-GLOBWB underestimated total extraction rates in the Nile Delta by a factor four. PCR-GLOBWB's

water allocation scheme has a tendency to underestimate extraction rates in deltas, as the current version of the model does not incorporate the effects of water quality (Sutanudjaja et al., 2018). Since in terms of water quantity, ample surface water is usually available in most river deltas, groundwater is extracted mainly because of an insufficient surface water quality (Table 5.4). On the other hand, the higher extraction rates of PCR-GLOBWB in the Rhine-Meuse delta are presumably caused by the fact that our model area does not include the ice-pushed sandy moraines. Many extractions in the Netherlands are located in these moraines, because of its good water quality (De Lange et al., 2014; Stuyfzand and Stuurman, 2006). The uncertainty in Q had a stronger effect on t_d than the uncertainty in $V_{fw,on}$. The latter uncertainty was considerably smaller, which is also shown in the two cases where we had validation data for $V_{fw,on}$ (Nile and Rhine-Meuse).

Finally, we would like to stress that for 9 out of 15 simulated deltas (Figures 5.5 and 5.6), fresh groundwater volumes were formed over very long timescales. The fact that mankind currently already has the capacity to deplete the fresh groundwater volumes for six of these (Nile, Pearl, Yangtze, Yellow River, Rhine-Meuse, and Ganges-Brahmaputra), undoing thousands of years of natural development within three human generations, is concerning. The fresh groundwater resources should be carefully managed in the deltas that have poor quality surface water, as replacing good quality groundwater with poor quality surface water reduces the delta's defenses from (future) water scarcity. Reducing groundwater extractions can pay off, as halving the total extracted groundwater often increases t_d by an order of magnitude (Figure 5.6).

ACKNOWLEDGEMENTS

We thank Jaap Nienhuis for helping with the estimation of tidal factors and tidal intrusion length. Furthermore, we thank Philip Minderhoud and Liduin Burgering for providing the well extraction data of the Mekong and Rhine-Meuse delta respectively. In addition, we thank Joost Delsman for providing the salinity data of the Rhine-Meuse delta. All scripts to pre-process, process, and post-process the data are released as a package that can be found under following URL: `https://github.com/JoerivanEngelen/delta_aquifer`. This work was carried out on the Dutch national e-infrastructure with the support of the SURF Cooperative, on an NWO Pilot Project Grant. This research has been supported by the Nederlandse Organisatie voor Wetenschappelijk Onderzoek under the New Delta programme (grant no. 869.15.013).

6 SYNTHESIS

6.1 INTRODUCTION

The main objective of this thesis is to assess the status and drivers of the current fresh-salt groundwater distributions in major deltas of the world. Various aspects of this objective are discussed in chapters 2 to 5. In this synthesis the research questions will be answered that are posed in the introduction. Furthermore, the effect of marine transgressions on groundwater salinity will be elaborated on and recommendations for further research will be provided.

6.2 RESEARCH QUESTIONS

What processes influence groundwater salinity in deltas at large depths?

Groundwater salinity at large depth is not necessarily controlled by the classical coastal sea water wedge, because its occurrence alone cannot explain the hypersaline groundwater that is observed at large depths in several deltas. There are cases where its origins are thought to be from lower strata as well as from upper strata. In the Mississippi delta it is thought to have originated from the dissolution of salt domes, brought upwards by thermal convection (Hanor and Mercer, 2011). In the Rhine-Meuse delta, hypersaline water observed below the hydrogeological base and transport is thought mainly to be controlled by diffusion (Griffioen et al., 2016). It is however thought not to have affected salinities in the active shallower groundwater system to a large degree (Delsman et al., 2014). Evapoconcentrated hypersaline groundwater has been found both in the Burdekin and near the Yellow River delta (Fass et al., 2007; Han et al., 2011). In the Burdekin, this groundwater has sunk to the bottom of the groundwater system; in the Yellow River delta, it is still located in the upper strata.

Hypersaline groundwater has been observed in the Nile Delta as well and was investigated in more detail in chapter 2. Here, it is concluded that the hypersaline groundwater was either the result of Pleistocene free convective systems that were the effect of evapoconcentration, or of compaction-induced upward transport of salt, provided that there is the right

coastal boundary condition at larger depth. An open connection between aquifer and sea causes hypersaline groundwater to be drained towards the sea and falsifies the hypothesis of compaction-induced upward salt transport. A closed coastal boundary, on the other hand, favors the preservation of both fresh and hypersaline groundwater. These deep pockets of fresh groundwater are deemed the most likely with a limited aquifer-sea connection and the hypersaline groundwater originating from free-convective systems. Age-dating of hypersaline groundwater would provide more insight to its origins and indirectly provide information on the aquifer-sea connection. It was however impossible to arrive at a definitive conclusion on its' origins, since quite some potential causes exist (Hanor, 1994) and it is hard to test them with the scarce available data. Data is often scarce in many deltas and this data paucity is only exacerbated at large depths. Groundwater ages, environmental tracers, and groundwater temperature measurements will presumably shed new light on the origins of deep hypersaline groundwater in deltas.

Figure 6.1 illustrates the depth to the presumed aquiclude of 32 deltas across the world, as estimated from the extensive literature review in chapter 5. A thicker sediment thickness implies faster sedimentation rates (Syvitski et al., 2003), which means that is more likely that these areas experienced compaction-induced upward seepage of saline groundwaters as well (Neuzil, 2003). Very likely to have experienced this are the deltas of the rivers Ayeyarwady, Ganges-Brahmaputra, Niger, Mississippi, Nile, and the Po (black symbols in figure 6.1). Whether traces of this old groundwater are still observable in the delta's lower aquifers very likely depends on the connection of the lower aquifers to the sea.

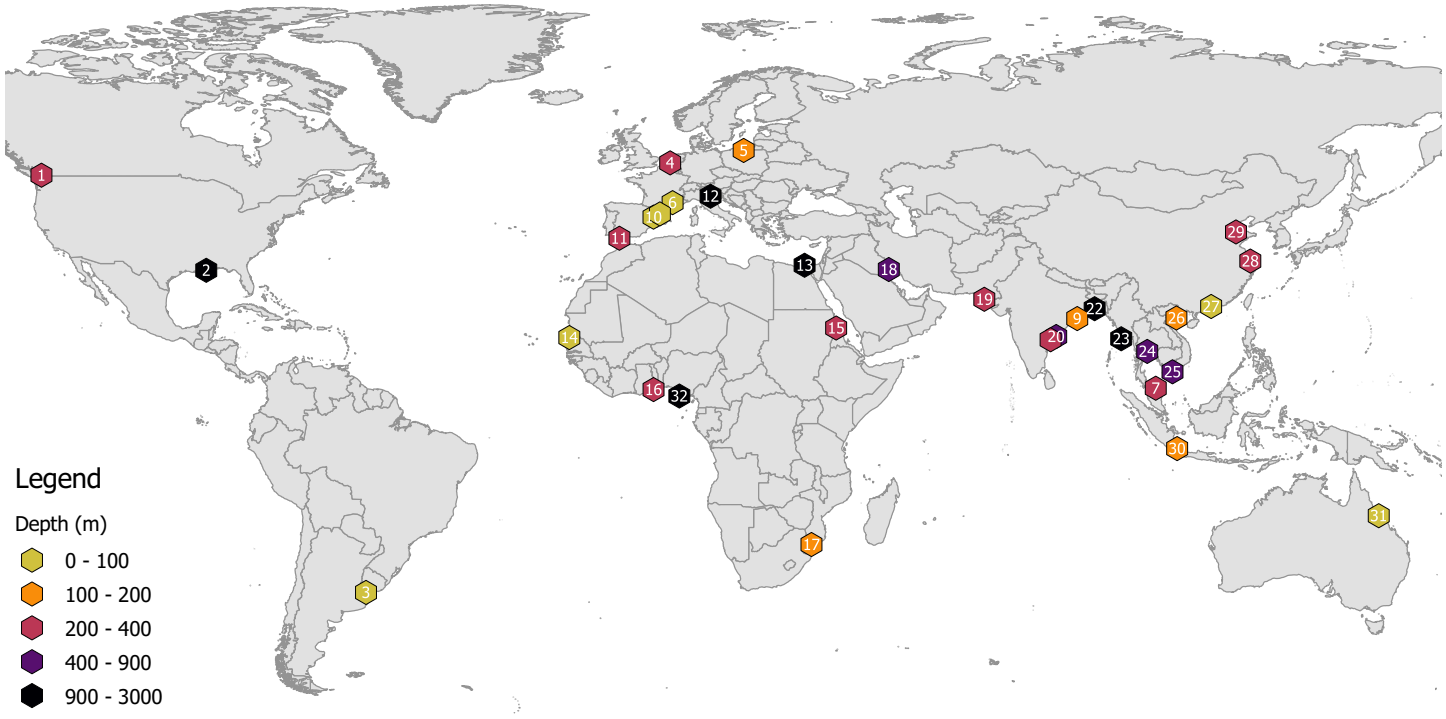

Figure 6.1: Depth to aquiclude (m) for 32 major deltas across the world. The numbers refer to the entry in table 6.1. The thicker deltas are the result of higher subsidence rates and may contain hypersaline groundwater at depth. The estimated depths are taken from a literature study described in chapter 5.

How did the fresh groundwater volumes evolve over time?

Long timescales are involved in the evolution of the fresh-salt distribution in deltas. Chapter 3 shows that reaching a steady-state fresh-salt distribution for the large Nile delta aquifer requires model simulations exceeding at least 5.5 ka, which is already a timeframe during which large differences occurred in its boundary conditions (Pennington et al., 2017). This condition also applies to other deltas (Delsman et al., 2014; Larsen et al., 2017; Van Pham et al., 2019; Sanford and Buapeng, 1996), because the Holocene transgression occurred between 8.5 and 6.5 ka in most deltas on the world areas of the world (Stanley and Warne, 1994), which means around 5.5 ka the deltas were still prograding and their shorelines were located more landwards than at present.

The general evolution of the fresh-salt groundwater reserves is shown in both Chapter 3 and 5 and is illustrated in figure 6.2. During the Pleistocene lowstand (Figure 6.2a) fresh groundwater volumes increased through time due to the larger hydraulic gradient and because part of the continental shelf was exposed to natural fresh groundwater recharge. At the onset of the Holocene these volumes started to rapidly and strongly decline due to rising sea-levels, especially in the areas with an extensive Holocene transgression (Figure 6.2b). For example, the fresh groundwater volumes were either halved or quartered in the Nile Delta during this period of the Holocene. After the transgression reached its maximum extent, the fresh groundwater volumes partly recovered due to subsequent delta progradation, but not to their level during the Glacial Maximum (Figure 6.2c). More recently, humans started to influence the fresh-salt groundwater distribution (Figure 6.2d), this will be discussed more in section 6.4.2.

There are several processes that further reduced fresh groundwater resources which are specific to certain deltas. For example, there are land reclamation projects that cause drainage levels below mean sea-level in the Rhine-Meuse and Po deltas, which lead to autonomous salt water intrusion and seepage of saline groundwater (Figure 6.2d) (Delsman et al., 2014; Giambastiani et al., 2007; De Louw et al., 2011). In addition, in deltas with an arid climate, evapoconcentration can create an extra influx of salt water. This is observed in the Indus delta (Naseem et al., 2018) and likely in the Nile delta as well (Chapter 3).

What are the current fresh groundwater volumes in deltas and will they be depleted?

Nearly all the researched deltas were estimated to possess onshore fresh groundwater volumes that ranged between 10^{10} and $10^{12} m^3$, the only exception being the Saloum delta which

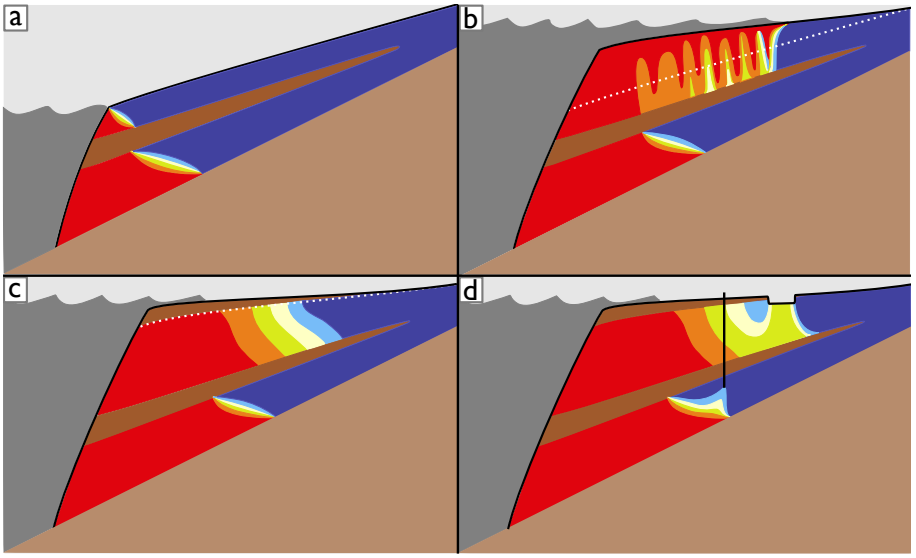

Figure 6.2: Illustration of the general evolution of the fresh-salt groundwater distribution in a deltaic groundwater system. The blue, yellow, and red colors indicate the salinity from low to high respectively. The aquitards are colored brown and the bottom aquiclude is light brown. The white dotted line indicates the surface level of the previous panel. The sedimentation model is adopted from Anderson et al. (2019). Panel "a" portrays the situation during the Pleistocene, panel "b" during the Holocene transgression (8.5-6.5 ka), panel "c" the natural fresh-salt distribution after the Holocene regression (3 ka), and panel "d" during the Anthropocene (0.1 ka). The latter panel shows the effect of groundwater extraction and land reclamation projects.

was estimated to have considerably less fresh groundwater. The variability in offshore fresh groundwater volumes was considerably larger, with estimates usually ranging from 10^7 to $10^{12} m^3$.

Several deltas face serious challenges under the current groundwater extraction rates. For instance, the Ganges-Brahmaputra, Nile, Pearl, and Yangtze deltas are projected to suffer from serious exhaustion of their fresh groundwater resources in the coming century. Without any adaptive or mitigative strategies/measures, their groundwater resources will gradually deteriorate due to saline riverine recharge and saline groundwater upconing. With increasing extraction rates, the Saloum, Mekong, and Red River delta can be added to the list of deltas of which the fresh groundwater reserves are under serious stress.

6.3 GROUNDWATER AFFECTED BY MARINE TRANSGRESSIONS

It is necessary to elaborate further on the effect of marine transgressions on groundwater salinity, since the traces they have left behind cause present-day fresh water availability issues. The effect of the Holocene transgression was not very pronounced in the sensitivity analysis performed in Chapter 4, which is because the metrics in this chapter did not punish salinity in the upper aquifers. As mentioned earlier, provided that the groundwater system has strong effective anisotropies, only the upper aquifers salinize during a marine transgression. This is troublesome, as saline upper aquifers lead to poor quality water being extracted with hand pumps (Khan et al., 2014) and saline soils in seepage areas (e.g. in the Yellow River delta, Fan et al., 2012). These saline soils also occur when an extra influx of water causes the water table of saline groundwater to rise leading to saltier water in the capillary zone. This happened near Cairo in the Nile Delta apex after the construction of a large irrigation system enhanced recharge (Biswas, 1993).

In many deltas across the globe, inland zones of saline groundwater have been hypothesized or proven to be caused by a marine transgression (Figure 6.3 and table 6.1), making this a global phenomenon. This can be easily explained with the long timescales that are involved in the establishment of the fresh-salt groundwater distribution (Chapters 3 and 5), and the fact that nearly all deltas have experienced a marine transgression sometime between 8.5 ka to 6.5 ka (Stanley and Warne, 1994). The only exception to this is the Incomati delta, which did not experience a Holocene transgression but endured several Pleistocene transgressions (Salman and Abdula, 1995), of which traces still can be found in its groundwater salinity today (Nogueira et al., 2019).

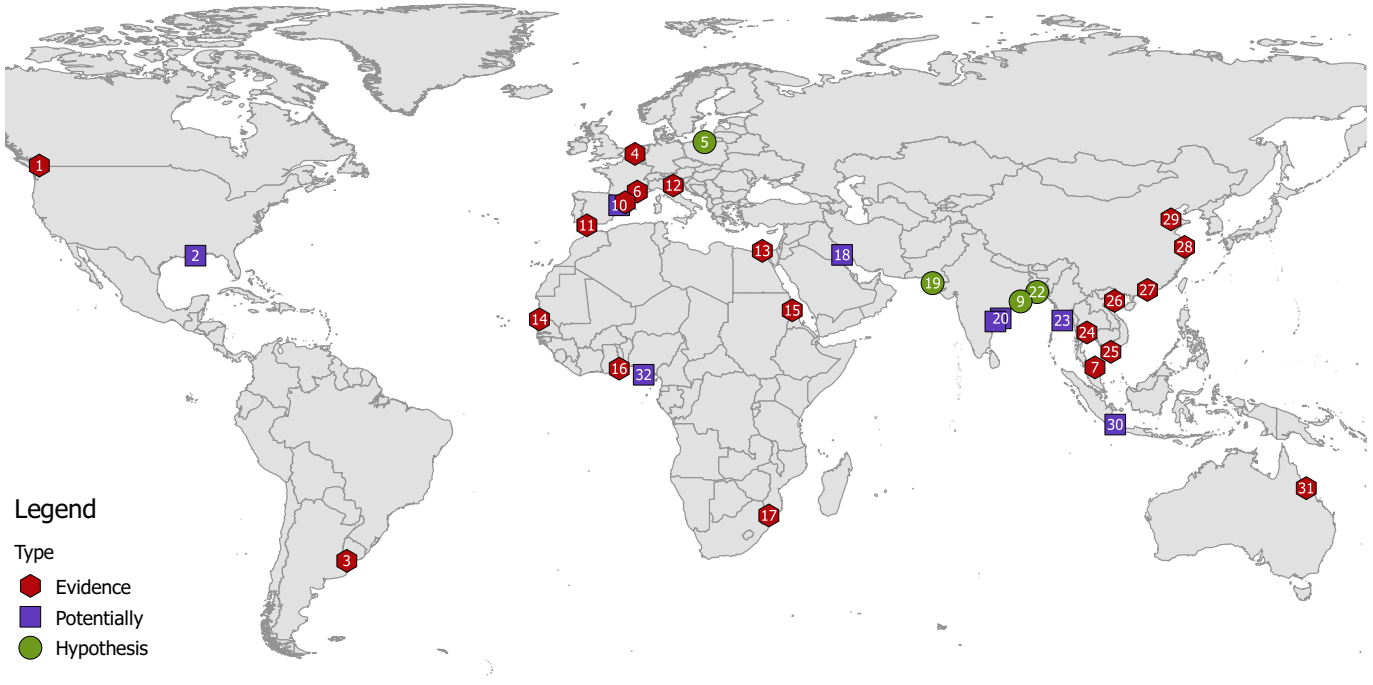

Figure 6.3: Groundwater in 32 deltas (possibly) affected by marine transgressions. "Evidence" means that based on several proxies a marine transgression has been shown to be likely concluded in the case study in table 6.1. "Hypothesis" means a marine transgression is used in the case study in table 6.1 to explain anomalously landward salinities. “Potentially” means a large fraction of the contemporary delta was covered with seawater during the Holocene transgression, which might still be reflected in groundwater salinities. The numbers refer to the entry number in table 6.1.

6.4 RECOMMENDATIONS FOR FURTHER RESEARCH

For further research into the status of the fresh groundwater reserves in deltas, a few challenges remain:

6.4.1 *The effects of heterogeneity*

Deltaic heterogeneity in this thesis was simplified into a set deterministic aquifers and aquitards, the latter possibly permeated with idealized paleochannels. Additional smaller-scale effects of heterogeneity on solute transport were accounted for in the mechanical dispersion. This is a simplified approach and there are multiple opportunities for further research on heterogeneity. In fact, the debate on how to incorporate more advanced models of heterogeneity into regional groundwater models is still ongoing (Fogg and Zhang, 2016; Pool et al., 2015), a question that becomes even more complex if heterogeneity is to be included in solute transport models (Guo et al., 2019). More realistic hydraulic conductivity fields can be generated with stochastic methods. An example of this is the research of Michael et al. (2016), who used a lot of well logs of the Ganges-Brahmaputra delta to constrain multiple two-dimensional stochastic realizations of hydraulic conductivities, with which they conducted variable-density groundwater flow simulations. They found that in their heterogenous models the seawater wedge was located far more offshore than in equivalent homogeneous models. However, Houben and Post (2017) mentioned that the exact opposite is visible in three-dimensional stochastic models (Kerrou and Renard, 2010), since the flow can deviate parallel to the coastline when encountering resistance. The mentioned studies (Houben and Post, 2017; Kerrou and Renard, 2010; Michael et al., 2016) all looked at the fresh-salt distribution under steady-state conditions. Therefore, understanding the effects of heterogeneous hydraulic conductivity fields under the strong sea-level changes during a glacial cycle is an interesting topic for further research. Creating stochastic realizations of hydraulic conductivity usually requires a lot of geological data, which is only available in a few deltas (Michael et al., 2016; Stafleu et al., 2011). A less data-intensive alternative to constrain stochastic models is to use sediment transport models to generate realistic grain-size distributions and couple these to hydraulic conductivities (Anderson et al., 2019). For solute transport, multiple models are available that capture the tailing of a passing concentration front better than the Gaussian mechanical dispersion model (Guo et al., 2019). Under transient boundary conditions, these models lead to wider brackish zones (Lu et al., 2009), since salt is retained longer in the pores, which hampers the flushing of saline groundwater that has been infiltrated during a marine transgression. This means that

the effects of a transgression on groundwater salinity will be stronger with advanced solute transport models; the size of this difference could be a topic for further research.

6.4.2 *Human impacts and future climate change*

A lot of attention in this thesis went to the paleohydrogeological reconstructions while human impacts on the fresh-salt groundwater distribution are only studied briefly, namely in chapters 3 and 5. In chapter 3 no strong influence was observed of 30 years of pumping on groundwater salinities in the Nile delta aquifer, presumably because the vast volumes of fresh groundwater in relation to the summed extraction rates over time, it is a slow-responding system, and a large grid size was used (Pauw et al., 2015). Larger effects were observed for a 100 year period of pumping in the Nile Delta in a different study (Mabrouk et al., 2018). In Chapter 5, fresh groundwater volumes were compared to present extraction rates, but no actual modelling of these extractions was conducted. An interesting topic for further research would be to find the moment at which mankind starts to have a stronger influence on the fresh-salt groundwater distribution than the natural processes of the past, for several deltas. There will likely be strong differences between deltas, since humans have modified deltas in different ways on different timescales. For example, the Rhine-Meuse delta has been engineered for over 500 years and has suffered from saline seepage caused by lake reclamation projects for over hunderds of years (Delsman et al., 2014). This in contrast to the Saloum delta, which had its' first hand pumps installed 30 years ago and where up to now little human influence on groundwater is observed (Dieng et al., 2017).

6.4.3 *Incorporating the risk of groundwater salinization into delta intercomparison projects*

Several delta intercomparison projects have been conducted (e.g. Bucx et al., 2010; Van Driel et al., 2015; Syvitski et al., 2009; Tessler et al., 2015) that mostly mapped out threats at the surface (e.g. flooding, deterioration of wetland ecology, overpopulation). These projects help prioritizing international efforts at delta improvement. However, the subsurface has been grossly overlooked in these projects, except for land subsidence due to overpumping, presumably because subsurface data is scarce. However, since potable and irrigable fresh groundwater reserves are key in creating resilient deltas, incorporating a metric for groundwater vulnerability is a necessity. The time to groundwater exhaustion proposed in chapter 5 could be a starting point, but next to the threat of groundwater salinization, this metric should also consider other major threats to deltaic groundwater quality, such as the arsenic that endangers deltas in South and South-East Asia (Brunt et al., 2004; Erban et al., 2013; Michael and Voss, 2008)

Table 6.1: Literature review of deltas with evidence for saline groundwater affected by marine transgressions. This table builds upon the initial table published in Larsen et al. (2017)

Nr	Delta	Country	Type	Proxies	Reference
1	Fraser	Canada	Evidence	ions	Simpson and Hutcheon 1995
2	Mississippi	United States	Potentially	-	Stanton et al. 2017
3	Rio de la Plata	Argentina	Evidence	ions	Santucci et al. 2016
4	Rhine-Meuse	The Netherlands	Evidence	ions, isotopes, groundwater ages, modelling, paleogeography	Delsman et al. 2014
5	Vistula	Poland	Hypothesis	paleogeography	Kozerski 1983
6	Rhone	France	Evidence	ions, groundwater ages	de Montety et al. 2008
7	Kelantan	Malaysia	Evidence	geophysics, ions	Samsudin et al. 2008; Sefie et al. 2018
8	Llobregat	Spain	Evidence	ions, isotopes	Manzano et al. 2001
9	Mahanadi	India	Hypothesis	ions, (saline inversion)	Behera et al. 2019
10	Ebro	Spain	Potentially	paleogeography	Edmunds 2001
11	Doñana	Spain	Evidence	ions, isotopes, noble gas	Manzano et al. 2001
12	Po	Italy	Evidence	ions	Colombani et al. 2017
13	Nile	Egypt	Evidence	ions, isotopes, paleogeography, modelling	van Engelen et al. 2019; Geirnaert and Laeven 1992; Geriesh et al. 2015
14	Saloum	Senegal	Evidence	ions (major and minor), isotopes, paleogeography	Ausseil-Badie et al. 1991; Faye et al. 2005
15	Tokar	Sudan	Evidence	ions	Elkrail and Obied 2013
16	Volta	Ghana	Evidence	isotopes, modelling	Akouvi et al. 2008
17	Incomati	Mozambique	Evidence	ions, isotopes	Nogueira et al. 2019
18	Shatt al-Arab	Iraq	Potentially	paleogeography	Cooke 1985
19	Indus	Pakistan	Hypothesis	ions	Naseem et al. 2018
20	Godovari	India	Potentially	paleogeography	Prabaharan et al. 2018
21	Krishna	India	Potentially	paleogeography	Prabaharan et al. 2018
22	Ganges-Brahmaputra	Bangladesh	Evidence	ions, isotopes	Naus et al. 2019; Sarker et al. 2018
23	Ayeyarwady	Myanmar	Potentially	paleogeography	Giosan et al. 2018
24	Chao Phraya	Thailand	Hypothesis	ions, isotopes	Stoecker et al. 2013; Yamanaka et al. 2011
25	Mekong	Vietnam	Evidence	geophysics, modelling, groundwater ages, ions	Bording et al. 2017; Van Pham et al. 2019; Tran et al. 2019
26	Red River	Vietnam	Evidence	geophysics, modelling, isotopes	Larsen et al. 2017; Tran et al. 2012
27	Pearl	China	Evidence	ions, groundwater ages	Wang and Jiao 2012
28	Yangtze	China	Evidence	stratigraphy, ions	Chen et al. 1997
29	Yellow River	China	Evidence	isotopes, ions, groundwater ages	Han et al. 2011
30	Ciliwung	Indonesia	Potentially	paleogeography	Dirks et al. 1989; Hehanussa 1980; Kooy et al. 2016
31	Burdekin	Australia	Evidence	ions, isotopes, groundwater ages	Fass et al. 2007
32	Niger	Nigeria	Potentially	paleogeography	Allen 1964; Anthony 1995

APPENDIX

APPENDIX TO CHAPTER 2

A.1 SUPPLEMENTARY RESULTS

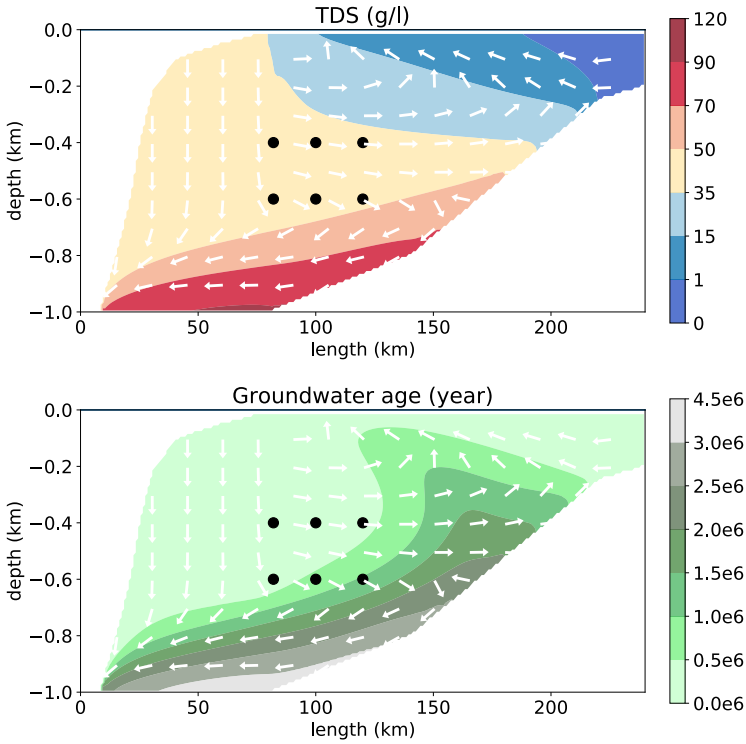

Figure A.1: Salinities (TDS) and groundwater ages after 2.5 million years in the open case NDA-c model without clay layers. The black dots represent the approximate location where observations are taken; the white arrows indicate the direction of the groundwater flow. Note that the cross-section is stretched in the vertical direction by a factor 100.

A.2 ONSET OF CONVECTION DURING THE PLEISTOCENE AND HOLOCENE

We assess the onset of free convection under two conditions applicable to (semi-)arid deltas: during an inundation and during a dry stand. For values, sources and definitions of symbols used in this analysis, the reader is referred to table A.1. The onset of free convection underneath a dry salt lake is determined by the destabilizing buoyancy force and the stabilizing upward flux caused by evapotranspiration (Zimmermann et al., 2006). Wooding et al. (1997) derived a dimensionless number for the (theoretical) onset of free convection underneath a dry salt lake, with impermeable boundaries at the bottom and sides:

$$R_\partial = \frac{(\rho_m - \rho_a) K_v n_e}{\rho_a ET} \tag{A.1}$$

Where ρ_m and ρ_a are the salinity of the salt lake and surrounding water (kg/m^3), respectively, K_v is the vertical hydraulic conductivity (m/d), n_e is the effective porosity (-), and ET the evapotranspiration rate (m/d). It was found, with both lab and numerical experiments, that for R_∂ values above 10, free convection is expected (Wooding et al., 1997). For flooded conditions the onset of free convection can be assessed by the Rayleigh number (Nield and Bejan, 2013):

$$Ra_c = \frac{(\rho_m - \rho_a) K_v H}{\rho_a D} \tag{A.2}$$

Where H is the thickness of the aquifer (m). And D is the dispersion tensor (m^2/d), here taken as the scalar effective diffusion constant D_c^* (since we assume initially stagnant water). With a fixed head on top (due to an inundation), the critical value for Ra_c = 27.10 (Nield, 1968). Important underlying assumptions of both these dimensionless numbers are a) a homogeneous hydraulic conductivity, b) a linear upward trend in concentration, and c) initially stagnant water. We, therefore, want to stress that the values of these numbers only allow for a qualitative interpretation, as, under field conditions, free convection can still occur below these critical numbers due to heterogeneities, non-linear trends in concentration and changing boundary conditions (Simmons et al., 2001).

For $K_v = K_{v,\,clay}$, R_∂ = 0.19 and Ra_c = 3600; and for $K_v = K_{v,\,sand}$, R_∂ = 470 and Ra_c = 8.6e^7. We interpret these values as follows: during the Pleistocene, amidst a salt inversion, free convection endured little resistance and definitely developed. During the Holocene, buoyancy forces endured increasing resistance from the deposited clay. Free convection

Table A.1: Limits of parameters chosen in Rayleigh and Wooding number analysis (equations A.1 and A.2). We are purposely inconsistent with units as this allows for better comparison with the literature.

Parameter	Description	Value	Unit
$K_{h,\,sand}$	Horizontal hydraulic conductivity sand. Compaction case and free convection case	10 [75]	m/d
$K_{h,\,clay}$	Horizontal hydraulic conductivity horizontal clay layer.	5e-4	m/d
$\frac{K_h}{K_v}$	Anisotropy	10	-
$\alpha_l, \alpha_t, \alpha_v$	Longitudinal, transversal and vertical dispersion length	10, 1, 0.1	m
n_e	Effective porosity	0.10	-
$\frac{\partial z_b}{\partial t}$	Sedimentation rate	3.9e-4 [0]	m/year
$\frac{\Delta h_{riv}}{\Delta x}$	River gradient	3.125e-2 [9.375e-2]	m/km
S_f	Specific storage in terms of fresh water head	1e-5	1/m
$\frac{\partial \rho}{\partial C}$	Slope linear equation of state	0.71	(kg/m3)/(g/l).

likely still occurred with inundations during and after dry periods, where respectively evapoconcentration and dissolution of salts might have occurred, but unlikely occurred on a large scale during periods without any inundations.

A.3 A COMPARISON BETWEEN COMPACTION IN SEAWAT AND AN ANALYTICAL SOLUTION

Here, we compare numerical results of overpressure to the analytical solution of (Bredehoeft and Hanshaw, 1968), who wrote the original solution of (Gibson, 1958) in terms of excess head instead of excess pressure. They define excess head as:

$$h\prime = h - h_s \tag{A.3}$$

Where h is head, h_s is the steady state component of head if there would be no compaction, and $h\prime$ is the excess head generated by compaction. The latter component can be

transient. Assuming a constant density of incompressible water and homogeneous hydraulic conductivity and by ignoring compression in the spatial derivatives, the one dimensional equation that describes the excess head in sediments is:

$$K\frac{\partial^2 h'}{\partial z^2} = S_s\left[\frac{\partial h\prime}{\partial t} - \frac{\rho\prime}{\rho_w}\frac{\partial l}{\partial t}\right] \tag{A.4}$$

with:

$$\rho\prime = \rho_b - \rho_w \tag{A.5}$$

Where K is the hydraulic conductivity, z is the height above the impermeable base, S_s is the specific storage, t is time, ρ_b is the bulk density of the sediments, ρ_w is the density of fresh water, and l is the sediment thickness. Gibson considered the following problem: sediment is deposited at a constant rate on top of an impermeable base. This base is taken as the reference datum. The sediment deposition causes the upward boundary, where $h\prime = 0$, to move upwards at constant rate. The initial thickness of the aquifer is zero. The equation that describes excess head with time and depth is then:

$$\begin{aligned} h\prime = \quad & \frac{l\rho\prime}{\rho_w} - \frac{l\rho\prime}{\rho_w}\left(\frac{\pi Kt}{S_s l^2}\right)^{-\frac{1}{2}} \exp\left[-\left(\frac{z}{l}\right)^2 \frac{S_s l^2}{4Kt}\right] \cdot \\ & \int_0^\infty \xi\prime \tanh\left(\frac{\xi\prime S_s l^2}{2Kt}\right) \cosh\left[\left(\frac{z}{l}\right)\frac{\xi\prime S_s l^2}{2Kt}\right] \exp\left(-\frac{\xi\prime^2 S_s l^2}{4Kt}\right) \mathrm{d}\xi\prime \end{aligned} \tag{A.6}$$

For a derivation see Bredehoeft and Hanshaw (1968) and Gibson (1958). If we assume $h_s = 0$, then $h\prime = h$ and we can calculate the amount of overpressure generated with SEAWAT. This requires two boundary conditions to be set in SEAWAT: An upward moving top boundary and a volumetric source term, which equals the strain rate. The first is implemented similar as how we approached the Pleistocene sedimentation in the NDA-c model: By stacking Cauchy boundary cells and deactivating them upwards through time. The latter is implemented as how we modelled the effects of compaction on groundwater flow in the KES model, by adding source terms to every cell in the domain injecting a fixed flux, equalling the strain rate, in this case:

$$q_s = S_s\left[\frac{\rho\prime}{\rho_w}\frac{\partial l}{\partial t}\right] \tag{A.7}$$

Equation A.7 is very similar to equation 2.15 in the main text. For the reader familiar with SEAWAT, we used the GHB and the WEL package respectively.

In figure A.2 we recreated figure 6 in Bredehoeft and Hanshaw (1968). It shows an excellent fit between the numerical model and analytical solution. We conclude that using SEAWAT in combination with our modifications is appropriate to model groundwater problems on a geological timescale, as one can solve a moving boundary problem and incorporate the effects of compaction with SEAWAT.

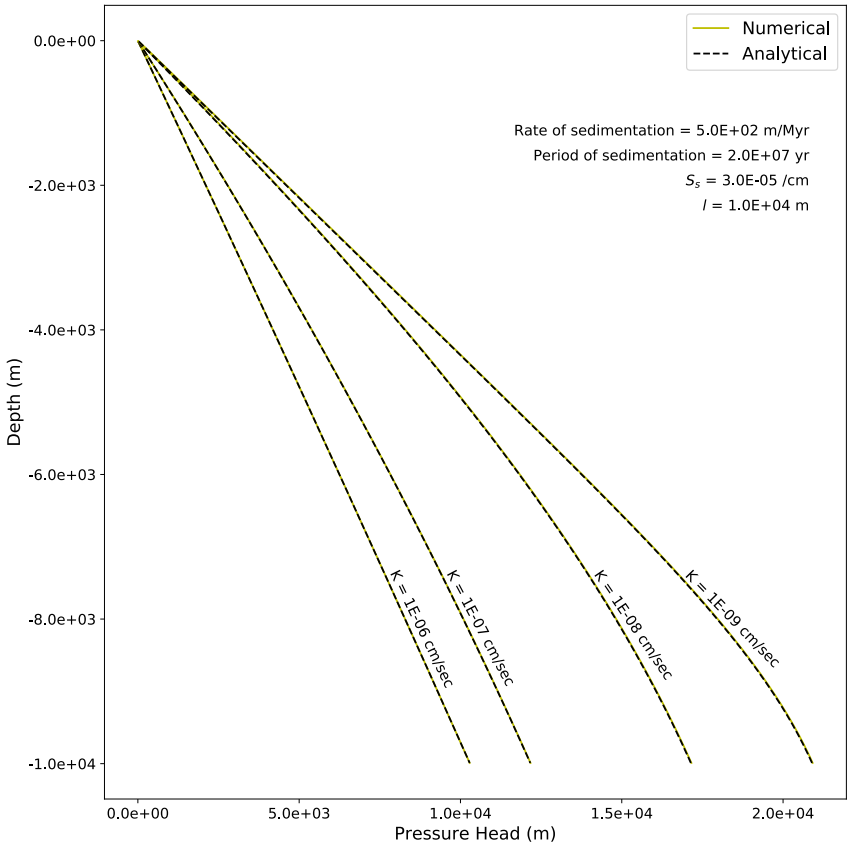

Figure A.2: Recreation of figure 6 in Bredehoeft and Hanshaw (1968), including our numerical results, showing an excellent fit.

A.4 EFFECTS OF CELL DISCRETIZATION

A grid convergence test was conducted for both the KES model as the NDA-c model. Cell discretization was decreased or increased in both dimensions, one at a time. As the KES model provides the basal boundary condition for the NDA-c model, we ensured that the models had the same cell size in each simulation. Thus hypothetical numerical errors of the KES model are also reflected in the TDS distribution of the NDA-c model. Figure A.3 shows a comparison of the TDS contours of the NDA-c model. The contours for the finer discretization are sufficiently similar to the base case. The coarser grid sizes tend to underestimate the height of the 70 g/l contour; we ascribe this to numerical dispersion. We conclude that the cell size is sufficient and if it were not, it would not affect our conclusions in this paper, since the 70 g/l contour would only be higher.

For the NDA-f model, a different approach was taken, to assess the effect of a wider range of Δx, since this dimension had the coarsest resolution (1 km). We modeled a simple 800 m thick sandbox with a hypersaline lake on top. This allowed us to stretch the domain as much as necessary in the horizontal direction. The chosen parameters for this model are the same as in table 2.3. The amount of cells was kept at 100 in the horizontal direction. Ξ is the normalized fluid mass increase, which is calculated by dividing the increase in fluid mass across the top boundary by the maximum mass storage increase:

$$\Xi = \frac{\int\int \frac{Q}{\Delta x}\rho \, \mathrm{d}x\mathrm{d}t}{V_{tot}\left((\rho_{max}-\rho_0)n + \frac{1}{2}S_f\frac{\rho_{max}-\rho_0}{\rho_0}z_{max}\rho_{max}\right)} \tag{A.8}$$

where Q is the volumetric flux through a boundary cell (m^2/d), V_{tot} is the total volume of the model domain (m^2), ρ_{max} is the concentration at the top boundary which was set at 1078 kg/m^3, ρ_0 was the initial density of the groundwater in the domain (1000 kg/m^3), S_f is the specific storage in terms of fresh water head (d^{-1}), z_{max} the depth of the domain (m), and n the porosity (-). For the test with Δx, Δz was kept at 10 m; in testing Δz, Δx was kept at 10 m. As the density at the top boundary of the model was perturbed randomly, 10 simulations were started for each discretization, of which the minimum, maximum and mean of Ξ are plotted. It can be seen in figure A.4 that there is some spread in Ξ, which is caused both by integration errors and differences between realizations. Furthermore a larger Δx causes a delay in the onset of free convection and causes a slower downward movement of fingers. However, all errors are unimportant on timescales larger than 100 years, and thus also on our timescales of interest, which is over 1000 years.

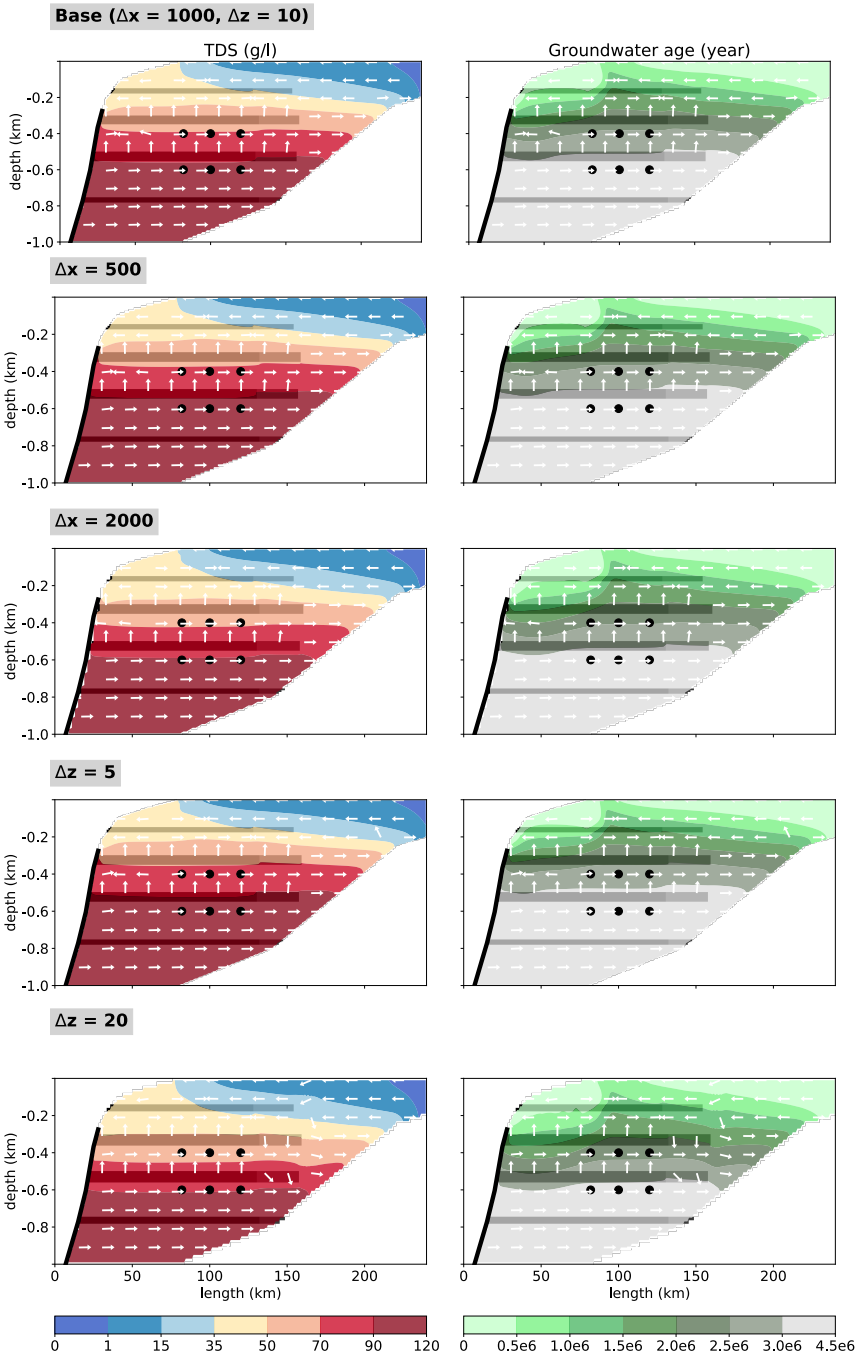

Figure A.3: Grid convergence test of the NDA-c model. The white arrows now represent velocities instead of fluxes, as in figure 2.5. The grey box shows the grid cell size deviations from the base case.

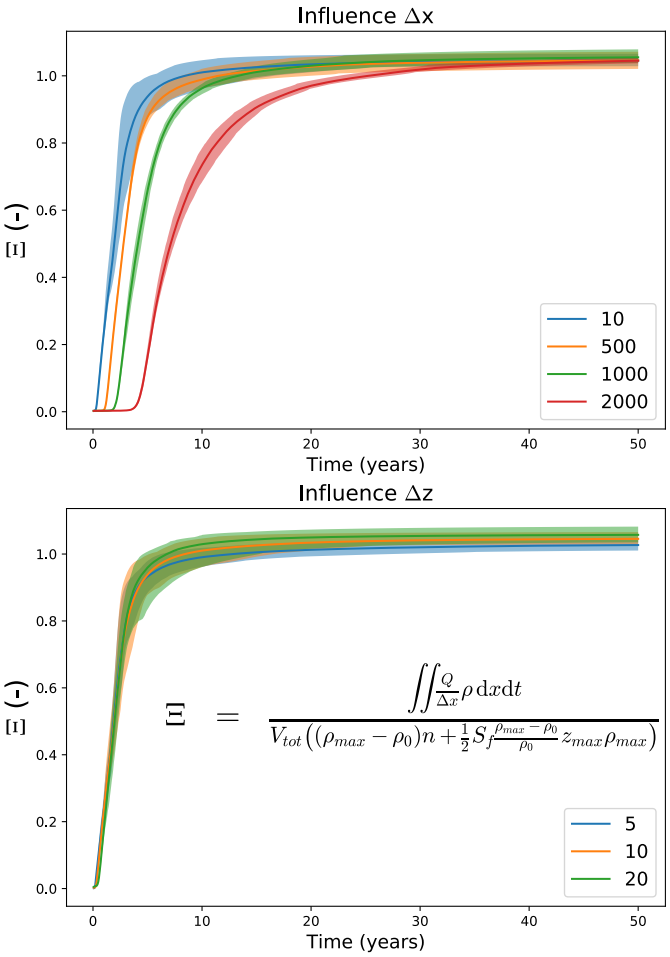

Figure A.4: Results of the test of the errors that are introduced in the free convection model by the large grid size.

B

APPENDIX TO CHAPTER 3

B.1 ADDITIONAL FIGURES & TABLES

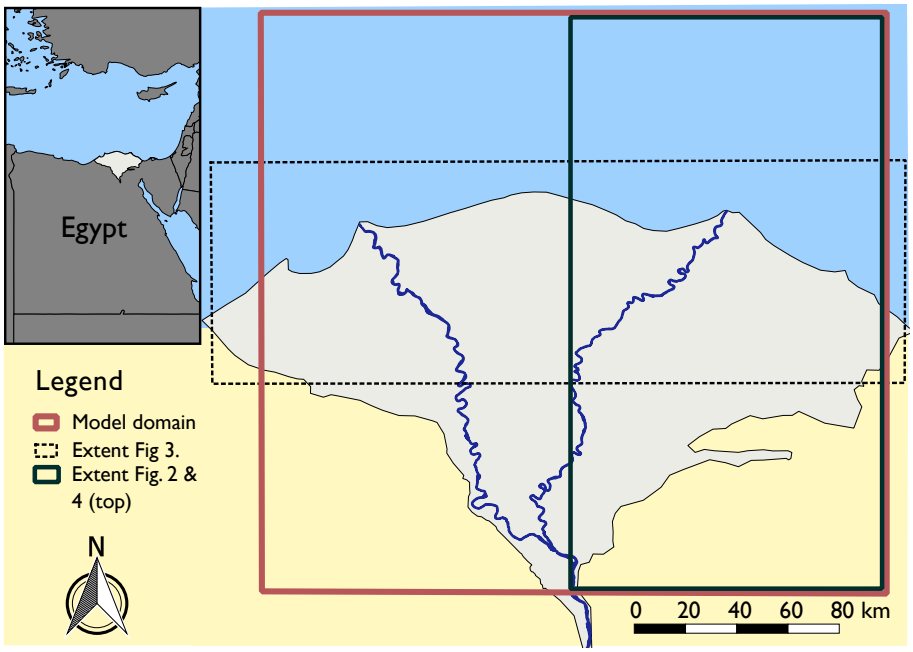

Figure B.1: Overview of the Nile Delta with boxes indicating the model domain and the extents of several figures. The main Nile river branches are plotted as a geographical reference. The red rectangle shows the extent of our model domain, the dark green box the plotted area in figure 3.2 and the top half of figure 3.4, and the dotted box the plotted area in figure 3.3. The inset on the upper left corner shows the location of the Nile Delta in Egypt.

Table B.1: Parameters fixed throughout simulation.

Parameter	Value	Unit	Reference	Remarks
Effective porosity	0.25	-	Mabrouk et al. 2018	
Longitudinal dispersivity	2	m	Oude Essink et al. 2010	Value for Rhine Meuse Delta, a similar system
Transverse dispersivity	0.2	m	Gelhar et al. 1992	Reference used for anisotropy between transverse and longitudinal dispersivity
Vertical dispersivity	0.02	m	Gelhar et al. 1992	Reference used for anisotropy between vertical and longitudinal dispersivity
Molecular diffusion coefficient	$8.64e^{-5}$	m^2 d-1	-	
Horizontal hydraulic conductivity Holocene fluvial clay	0.2	m d-1	Gallichand et al. 1992	Average value taken here
Horizontal hydraulic conductivity Quaternary sands	75	m d-1	Barrocu and Dahab 2010; Laeven 1991; Mabrouk et al. 2013	
Horizontal hydraulic conductivity Quaternary marine clays	$1e^{-4}$	m d-1	Domenico and Schwartz 1990)	Upper limit taken here, as these values stem from lab scale measurements and we model on a large scale.
Horizontal hydraulic conductivity Quaternary clayey sands	75	m d-1	Farid 1980	Author states that kh clayey sands is close to kh of sands
Anisotropy	10 (100 for Holo clay)	-	Farid 1980	
Resistance surface water beds	100	d	De Lange et al. 2014; Timmerman and Hemker 1993	Value for Rhine Meuse Delta, a similar system
River stage apex delta	15	m	NASA 2014	
Salinity sea (TDS)	35	g L-1	-	
Salinity sabkha (TDS)	120	g L-1	van Engelen et al. 2018	Based on previous model in reference
Salinity inflow from hydrogeological base (TDS)	120	g L-1	van Engelen et al. 2018	Based on previous model in reference
Flux from hydrogeological base	$3e^{-6}$	m d-1	van Engelen et al. 2018	Based on previous model in reference
Recharge in dunes	$5.5e^{-4}$	m d-1	WMO 2006	Precipitation near Alexandria

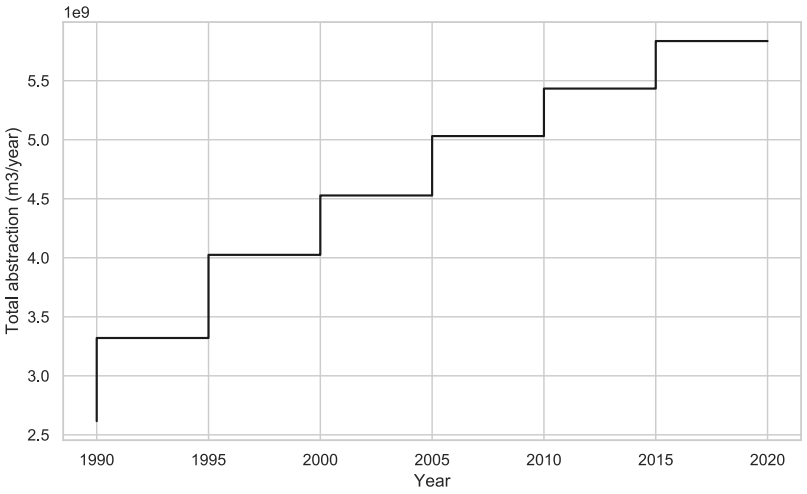

Figure B.2: Total annual abstraction used as model input for the last 30 years of the simulation. This period has stress periods of 5 years.

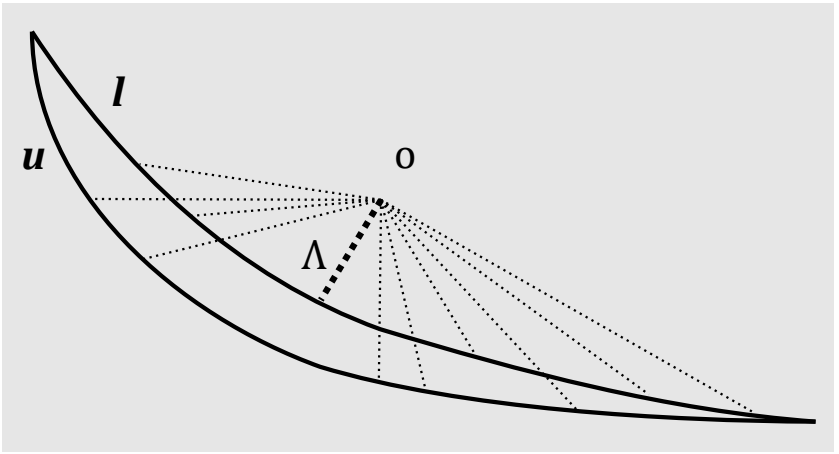

Figure B.3: Sketch of how Λ is determined with equation 3.1 for a 2-dimensional example. The circle represents the location of the observation. $\boldsymbol{l}$ and $\boldsymbol{u}$, the isosurfaces of the lower and upper bound, respectively. The thick dotted line represents the minimum Eucledian distance to an isosurface bound, Λ. The thinner dotted lines some other Euclidian distances.

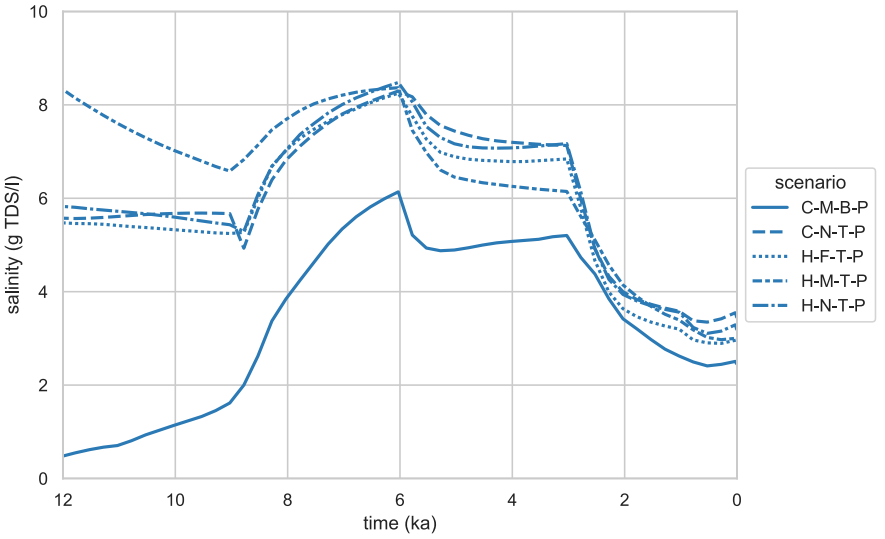

Figure B.4: Mean modeled salinity during the Holocene. The dash type indicates the scenario. Salinities were sampled in the model domain at 40 locations where a freshening was observed in the field and averaged.

B.2 SENSITIVITY ANALYSIS OF THE RESISTANCE OF THE BOUNDARIES

To assess the effects of our assumption of the boundary resistance, we ran two alternative versions of the "H-N-T-P" scenario with a different resistance (Fig. B.5). This scenario was chosen as it presumably is the "acceptable" scenario that would be affected the most by the resistance value, as it has no horizontal clay layers that resist changes in boundary conditions and the sea boundary has the most open connection with the sea. We multiplied the resistance with a factor 0.5 and 2. Lowering the resistance more than with a factor 0.5 lead to numerical convergence issues. Fig. B1 shows that throughout the Pleistocene the resistance influences the groundwater types, as the lower resistance allows more river water to be replaced with hypersaline groundwater. The groundwater types of the different models quickly converge, however, through the Holocene. We therefore think that the choice of boundary resistance has limited effect on our results and conclusions, despite that we only varied the resistance to a limited extent in this sensitivity analysis.

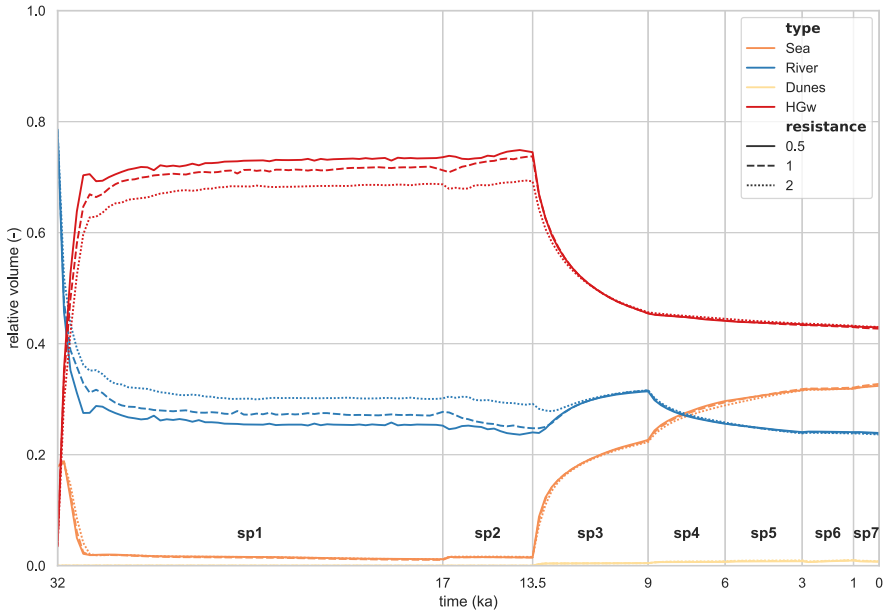

Figure B.5: Groundwater origins for scenario "H-N-T-P" with three resistances. The colour indicates the groundwater type, the linestyle the value the original resistance is multiplied with. Stress period numbers are indicated in bold with "sp".

C

APPENDIX TO CHAPTER 4

C.1 ADDITIONAL EXPLANATION TO MODEL GEOMETRY, LITHOLOGY, AND BOUNDARY CONDITIONS

The geometry of the synthetic delta aquifer was created by specifying a set of inputs over three planes. Two of these planes (Fig. 4.1a & 4.1c) were in polar coordinates (r, φ) and the third plane (Fig. 4.1b) was consequently used to convert these to a cartesian coordinate system (x, y). First, the geometry was determined along the rz-plane (Fig. 4.1a), a cross-section from delta apex to the coast through the delta center. By connecting the depth specified at the apex (H_a) and at the coast (H_b) the hydrogeological base at $\varphi = 0$, $\boldsymbol{z_{center}}$, was drawn and extrapolated until it intersected the top of the aquifer at the coastal slope. Furthermore, we specified the shape along the xy-plane by creating a sector ("pizza slice") with angle φ_f (Fig. 4.1b). To complete the geometry of the hydrogeological base, the depth across the φz-plane $\boldsymbol{z_{base}}$ was calculated as a half-ellipse (Fig. 4.1c) by inserting $\boldsymbol{z_{center}}$ as z in:

$$z_{ellipse}\left(\varphi, z\right) = \frac{z}{\varphi_f}\sqrt{\varphi_f^2 - \varphi^2} \tag{C.1}$$

For the lithology of the delta, we distinguished between the Holocene confining clay layer and the other pre-Holocene aquitards. A set of N_{aqt} aquitards was created that had the following thickness d_{clay}:

$$d_{clay} = \frac{f_{aqt} * \boldsymbol{z_{center}}}{N_{aqt} + 1} \tag{C.2}$$

where f_{aqt} is fraction of the sediment column that is aquitard. These N_{aqt} aquitards curved downward across the φz-plane (Fig. 4.1g) and dip downward in the coastal direction of the rz-plane (Fig. 4.1e), by calculating:

$$z_{clay,i} = \frac{i}{N_{aqt} + 1} \cdot \frac{\boldsymbol{z_{center}} + \boldsymbol{z_{base}}}{2} \tag{C.3}$$

with $i = 1 \ldots N_{aqt}$

This confining layer had one additional input, l_{conf} that set its onshore extent (Fig. 4.1f). Beyond this point, the confining layer had zero thickness. The thickness of the confining layer was consequently calculated by calculating the thickness at the coast with equation 2, and linearly interpolating this with respect to l_{conf}.

The location of the coast was specified as follows. We call the location and moment of maximum transgression respectively r_{tra} and t_{tra} (Fig. 4.2c). To arrive at a smooth transition from the point where sea level equals the topography $r_{sea=top}$ to r_{tra}, we introduce the following equations:

$$r_{coast} = l_a L \, (1 - l_{tra}) \tag{C.4}$$

where l_a is the relative length of the onshore, L the total length of the onshore, which we set to 200 km, l_{tra} the relative length of onshore covered with sea water at t_{tra}, and w as a weighting factor which is defined as:

$$w = \begin{cases} 0, & t < t_{start} \\ \frac{t - t_{start}}{t_{tra} - t_{start}}, & t_{start} > t >= t_{tra} \\ \frac{t - t_{tra}}{t_{end} - t_{tra}}, & t_{tra} < t < t_{end} \end{cases} \tag{C.5}$$

with t_{start} as the start of the Holocene and t_{end} as the present day ($t = 0$ ka).

Table C.1: Fixed inputs in the global sensitivity analysis

Symbol	Description	Value	Unit	Reference
		Morris		
N_{lev}	Number of levels	4	-	Morris 1991
N_{traj}	Number of trajectories	10	-	Khare et al. 2015
N_{inp}	Number of inputs	23	-	4.1
		Geometry		
γ	Angle coastal slope	2.5e-2	rad	GEBCO 2014
L	Absolute total extent delta	200	km	Section 2.1 main article
		Hydrogeology		
S_s	Specific storage	6.3e-5	1/d	Mean value of data review
		Surface water		
rs_{surf}	Resistance surface waters	10	d	Assumed
C_f	Concentration fresh water.	0	g TDS/l	Assumed
C_s	Concentration sea water.	35	g TDS/l	Millero 2010
		Solute transport		
α_t/α_l	Ratio of transversal over longitudinal dispersion length	1e-1	-	Gelhar et al. 1992
α_v/α_l	Ratio of vertical over longitudinal dispersion length	1e-2	-	Gelhar et al. 1992
D_m	Molecular diffusion coefficient	8.64e-5	m2/d	Guo and Langevin 2002
$\partial\rho/\partial C$	Linear density conversion slope	0.7143		Kohfahl et al. 2015

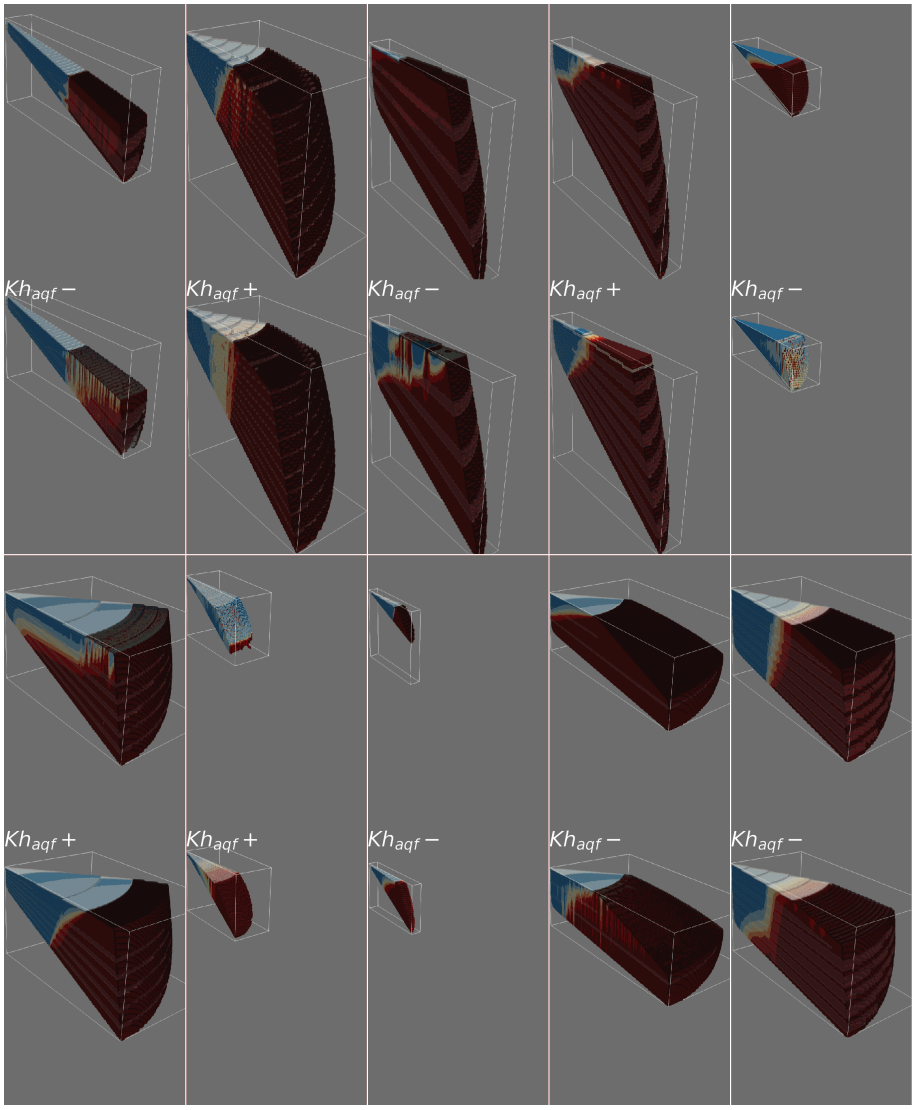

Figure C.1: Effects of changes of $K_{h,\,aqf}$ on the fresh-salt distribution for ten trajectories. The bottom figure in each panel presents the effect of change in $K_{h,\,aqf}$. The sign designates if $K_{h,\,aqf}$ is increased (+) or decreased (-). The colors indicate the salinity: red is saline, yellow is brackish, and blue is fresh. A lighter shade of color indicates a clay layer. Note that the vertical of each distribution with the following is stretched by a factor $4000\Delta z$, since the system thickness varied logarithmically.

C.2 SUPPORT FOR CHOICE LINEAR SALINITY PROFILE ONSHORE SURFACE WATERS AND ITS CORRECTION FACTOR BASED ON RIVER GRADIENTS

To reduce the amount of inputs in our global sensitivity analysis, a simple linear model was fitted to Savenije (2012, 's model), based on l_{surf}. Figure C.1 shows that the fit of this simplification to the original model is in most cases satisfactory, from which we conclude that the linear salinity profile is sufficient to observe the effect of salinity intrusion on the groundwater salinity. We correct the salinity intrusion length l_{surf} for each stress period to incorporate the effect of the large changes in river gradient as follows. Firstly, a river gradient correction factor f_i is defined.

$$\frac{i}{i_{end}} = \frac{f_i}{f_{i,\,end}} \tag{C.6}$$

Where i is the river gradient at any moment in time, i_{end} is the river gradient at 0 ka (which is equal to the topography (α) in our model setup), and $f_{i,\,end} = 1$, the correction factor for the last timestep. The reason why we explicitly define this last factor is shown hereafter in equation C.12. The Chezy formula is defined as (eq 2.5.5 in Chow et al., 1988):

$$Q_{f,\,riv} = A_{riv} C \sqrt{R_{riv} i} \tag{C.7}$$

Where $Q_{f,\,riv}$ is the fresh water flow of the river, C is the Chezy constant, R_{riv} the hydraulic radius and A_{riv} the cross-sectional area. Savenije's equation for the salinity intrusion length in estuaries l_{surf} is (eq. 5.48 in Savenije, 2012):

$$l_{surf} = l_{con} \ln\left(\frac{1}{\delta} + 1\right) \tag{C.8}$$

Where l_{con} is the cross-sectional convergence length and δ is the tidal dispersion reduction rate (eq. 5.47 in Savenije, 2012):

$$\delta = B\, l_{con}\, Q_{f,\,riv}\, D_{mouth}\, A_{mouth} \tag{C.9}$$

Where B is the van der Burgh coefficient, and D_{mouth} and A_{mouth} respectively are the longitudinal tidal dispersion and the cross-sectional surface area at the estuary mouth. $Q_{f,\,riv}$ is governed by the climate and is assumed constant, so the higher velocities due to an increase

in i would lead to a decrease in A_{riv}, which we assume to be proportional to the decrease in A_{mouth} this would also result in, leading to:

$$\frac{\frac{1}{A_{mouth}}}{\frac{1}{A_{mouth,\,end}}} = \frac{\sqrt{f_i}}{\sqrt{f_{i,\,end}}} \tag{C.10}$$

Subsequently assuming only A_{mouth} is not constant over time in eq C.9, we can substitute equation C.10 into equation C.9, yielding:

$$\frac{\partial}{\partial_{end}} = \frac{f_i}{f_{i,\,end}} \tag{C.11}$$

Which can then be consequently used to correct l_{surf} by substituting C.11 into C.8 (as a reminder $f_{i,\,end} = 1$):

$$\frac{l_{surf}}{l_{surf,\,end}} = \frac{\ln\left(\frac{1}{\sqrt{f_i}}\right)}{\ln\left(\frac{1}{\sqrt{f_{i,\;end}}}\right)} = \frac{\ln\left(\frac{1}{\sqrt{f_i}}\right)}{\ln(2)} \tag{C.12}$$

Since $f_{i,\,end} = 1$ and $i_{end} = \alpha$ in our model setup, we can substitute eq. C.6 into C.12, yielding the intrusion length correction factor f_l:

$$f_l = \frac{l_{surf}}{l_{surf,\,end}} = \frac{\ln\left(\frac{1}{\sqrt{\frac{i}{\alpha}}}\right) + 1}{\ln(2)} \tag{C.13}$$

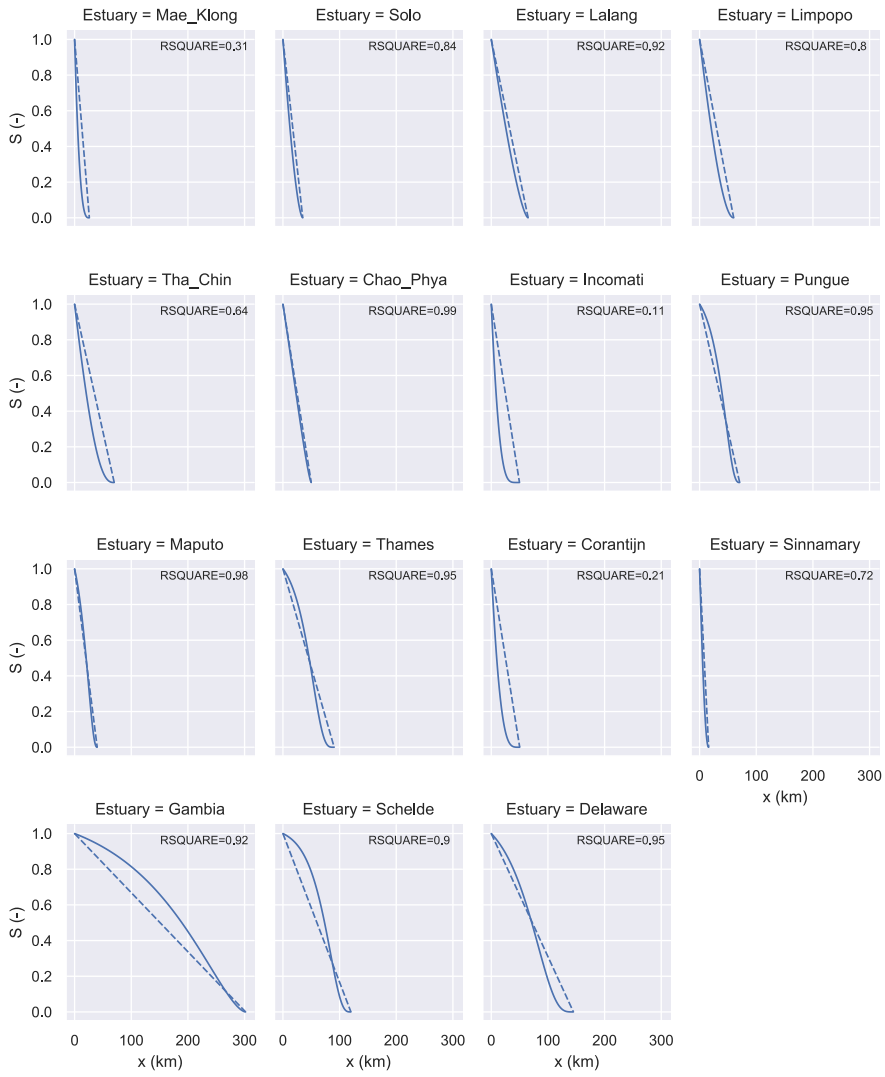

Figure C.2: Fits of a linear model to the more advanced salinity intrusion models of Savenije (2012). x is the length landwards, S is the relative salinity. $S = 1$ is sea salinity, $S = 0$ is fresh water salinity. Inputs for all estuaries are from the mentioned source.

BIBLIOGRAPHY

Abarca, Elena, Jesús Carrera, Xavier Sánchez-Vila, and Clifford I. Voss (2007). "Quasi-horizontal circulation cells in 3D seawater intrusion." In: *Journal of Hydrology* 339.3-4, pp. 118–129. DOI: 10.1016/j.jhydrol.2007.02.017.

Abd-Allah, Ali M A, Mohamed H. Abdel Aal, and Ahmad Ghandour (2012). "Structural characteristics and tectonic evolution of the northwestern margin of the Nile Delta, Egypt." In: *Journal of African Earth Sciences* 68.June, pp. 82–95. DOI: 10.1016/j.jafrearsci.2012.02.006.

Abdel Aal, A., A. El Barkooky, M. Gerrits, H. Meyer, M. Schwander, and H. Zaki (2000). "Tectonic evolution of the Eastern Mediterranean Basin and its significance for hydrocarbon prospectivity in the ultradeepwater of the Nile Delta." In: *The Leading Edge* 19.10, p. 1086. DOI: 10.1190/1.1438485.

Abdel-Fattah, M. I. (2014). "Petrophysical characteristics of the messinian abu madi formation in the baltim east and north fields, offshore Nile delta, Egypt." In: *Journal of Petroleum Geology* 37.2, pp. 183–195. DOI: 10.1111/jpg.12577.

Aeschbach-Hertig, Werner (2014). "Radiokrypton dating finally takes off." In: *Proceedings of the National Academy of Sciences of the United States of America* 111.19, pp. 6856–6857. DOI: 10.1073/pnas.1405830111.

El-Agha, Doaa Ezzat, Alvar Closas, and François Molle (2017). "Below the radar: the boom of groundwater use in the central part of the Nile Delta in Egypt." In: *Hydrogeology Journal* 25, pp. 1621–1631. DOI: 10.1007/s10040-017-1570-8.

Akouvi, Ari, Martial Dray, Sophie Violette, Ghislain de Marsily, and Gian Maria Zuppi (2008). "The sedimentary coastal basin of Togo: Example of a multilayered aquifer still influenced by a palaeo-seawater intrusion." In: *Hydrogeology Journal* 16.3, pp. 419–436. DOI: 10.1007/s10040-007-0246-1.

Allen, J. R.L. (1964). "Sedimentation in the Modern Delta of the River Niger, West Africa." In: *Developments in Sedimentology* 1.C, pp. 26–34. DOI: 10.1016/S0070-4571(08)70463-1.

Amorosi, Alessandro and Maria Luisa Colalongo (2005). "The Linkage between Alluvial and Coeval Nearshore Marine Successions: Evidence from the Late Quaternary Record of the PO River Plain, Italy." In: *Fluvial Sedimentology VII*, pp. 255–275. DOI: 10.1002/9781444304350.ch15.

Andersen, M.S., R. Jakobsen, V. Nyvang, F.D. Christensen, P. Engesgaard, and D. Postma (2007). "Density-driven seawater plumes in a shallow aquifer caused by a flooding

event - Field observations, consequences for geochemical reactions and potentials for remediation schemes." In: *GQ07: Securing Groundwater Quality in Urban and Industrial Environments (Proc. 6th International Groundwater Quality Conference held in Fremantle, Western Australia, 2–7 December 2007)*. 324, pp. 2–7.

Anderson, Aspen M., Diana M. Allen, and Jeremy G. Venditti (2019). "Influence of heterogeneity in the preservation of subsurface saline paleowater in coastal deltas." In: *Agu Fall Meeting 2019*. San Fransisco.

Anthony, E. J. (1995). "Beach-ridge development and sediment supply: examples from West Africa." In: *Marine Geology* 129.1, pp. 175–186. DOI: 10.1016/j.ocecoaman.2017.11.008.

Ausseil-Badie, Josiane, J. Paul Barusseau, Cyr Descamps, E. H. Salif Diop, P. Giresse, and Mieczyslaw Pazdur (1991). "Holocene Deltaic Sequence in the Saloum Estuary, Senegal." In: *Quaternary Research* 36.PP0012, pp. 178–194. DOI: 10.1016/0033-5894(91)90024-Y.

Ayers, John C., Steven Goodbred, Gregory George, David Fry, Laura Benneyworth, George Hornberger, Kushal Roy, Md Rezaul Karim, and Farjana Akter (2016). "Sources of salinity and arsenic in groundwater in southwest Bangladesh." In: *Geochemical Transactions* 17.1, pp. 1–22. DOI: 10.1186/s12932-016-0036-6.

Bakker, M., V. Post, C. D. Langevin, J. D. Hughes, J. T. White, J. J. Starn, and M. N. Fienen (2016). "Scripting MODFLOW Model Development Using Python and FloPy." In: *Groundwater*. DOI: 10.1111/gwat.12413.

Barrett, Richard et al. (2006). "Templates for the Solution of Linear Systems: Building Blocks for Iterative Methods." In: *Mathematics of Computation* 64.211, p. 1349. DOI: 10.2307/2153507.

Barrocu, Giovanni and Kamal Dahab (2010). "Changing climate and saltwater intrusion in the Nile Delta , Egypt." In: *Groundwater Response to a changing Climate*. Ed. by Taniguchi Makato and Ian Holman. Boca Raton, Florida: Taylor & Francis. Chap. 2, pp. 11–25.

Bear, Jacob (1972). *Dynamics of Fluids in Porous Media*. Dover 1988. New York: Dover Publications INC., p. 764.

Beaton, C.F., D.K. Edwards, and E.U. Schlunder (1987). "Chapter 5.3.3." In: *Heat Exchanger Design Handbook*. Ed. by E.U. Schlunder. Chap. 5.3.3. DOI: 10.1615/AtoZ.s.steam_tables.

Becker, R H and M Sultan (2009). "Land subsidence in the Nile Delta: inferences from radar interferometry RID A-9120-2010." In: *Holocene* 19.6, pp. 949–954. DOI: 10.1177/0959683609336558.

Behera, A. K., G. J. Chakrapani, S. Kumar, and N. Rai (2019). "Identification of seawater intrusion signatures through geochemical evolution of groundwater: a case study based

on coastal region of the Mahanadi delta, Bay of Bengal, India." In: *Natural Hazards* 97.3, pp. 1209–1230. DOI: 10.1007/s11069-019-03700-6.

Bense, V. F., T. Gleeson, S. E. Loveless, O. Bour, and J. Scibek (2013). "Fault zone hydrogeology." In: *Earth-Science Reviews* 127, pp. 171–192. DOI: 10.1016/j.earscirev.2013.09.008.

Biswas, Asit K (1993). "Land Resources for Sustainable Agricultural Development in Egypt." In: *Ambio* 22.8, pp. 556–560.

Bonsor, H. C. et al. (2017). "Hydrogeological typologies of the Indo-Gangetic basin alluvial aquifer, South Asia." In: *Hydrogeology Journal* 25.5, pp. 1377–1406. DOI: 10.1007/s10040-017-1550-z.

Bording, T., Anders V. Christiansen, E. Auken, J. Gunnink, and Gualbert H.P. Oude Essink (2017). "Groundbased TEM Survey in the Subsiding Mekong Delta." In: *23rd European Meeting of Environmental and Engineering Geophysics*. September, pp. 2015–2018.

Bredehoeft, J. D. and B. B. Hanshaw (1968). "On the maintenance of anomalous fluid pressures: I. Thick Sedimentary Sequences." In: *Bulletin of the Geological Society of America* 79.9, pp. 1107–1122. DOI: 10.1130/0016-7606(1968)79[1107:OTMOAF]2.0.CO;2.

Bredehoeft, J.D. (2002). *The Water Budget Myth Revisited: Why Hydrogeologists Model*. DOI: 10.1111/j.1745-6584.2002.tb02511.x.

Brunt, R, L Vasak, and Jasper Griffioen (2004). *Arsenic in groundwater: Probability of occurrence of excessive concentration on global scale*. Tech. rep. April. Utrecht: International groundwater resources assessment centre, p. 9.

Bucx, Tom, Marcel Marchand, Bart Makaske, and Cees van de Guchte (2010). *Comparative assessment of the vulnerability and resilience of 10 deltas - synthesis report.* Tech. rep. Delft-Wageningen: Delta Alliance International, p. 178.

Bunbury, Judith (2013). "Geomorphological development of the Memphite floodplain over the past 6,000 years." In: *Studia Quaternaria* 30.2, pp. 61–67. DOI: 10.2478/squa-2013-0005.

Ca, Vu Thanh, Suphat Vongvisessomjai, and Takashi Asaeda (1994). "Study on Salinity Intrusion in the Red River Delta." In: *Environmental Systems Research* 22.8, pp. 213–218. DOI: 10.2208/proer1988.22.213.

Campolongo, Francesca, Jessica Cariboni, and Andrea Saltelli (2007). "An effective screening design for sensitivity analysis of large models." In: *Environmental Modelling and Software* 22.10, pp. 1509–1518. DOI: 10.1016/j.envsoft.2006.10.004.

Cao, Guoliang, Dongmei Han, Matthew J. Currell, and Chunmiao Zheng (2016). "Revised conceptualization of the North China Basin groundwater flow system: Groundwater age, heat and flow simulations." In: *Journal of Asian Earth Sciences* 127, pp. 119–136. DOI: 10.1016/j.jseaes.2016.05.025.

Celoria, Francis (1966). "Delta as a geographical concept in Greek Literature." In: *Isis: A journal of the History of Science Society* 57.3, pp. 385–388. DOI: 10.1086/350146.

Chen, Jianyao, Makoto Taniguchi, Guanqun Liu, Kunihide Miyaoka, Shin Ichi Onodera, Tomochika Tokunaga, and Yoshihiro Fukushima (2007). "Nitrate pollution of groundwater in the Yellow River delta, China." In: *Hydrogeology Journal* 15.8, pp. 1605–1614. DOI: 10.1007/s10040-007-0196-7.

Chen, Xing Xian, Zu Jiang Luo, and Shi Ling Zhou (2014). "Influences of soil hydraulic and mechanical parameters on land subsidence and ground fissures caused by groundwater exploitation." In: *Journal of Hydrodynamics* 26.1, pp. 155–164. DOI: 10.1016/S1001-6058(14)60018-4.

Chen, Zhongyuan, Zhenglou Chen, and Weigou Zhang (1997). "Quaternary Stratigraphy and Trace-Element Indices of the Yangtze Delta, Eastern China, with Special Reference to Marine Transgressions." In: *Quaternary Research* 47.2, pp. 181–191. DOI: 10.1006/qres.1996.1878.

Chow, Ven Te, David R. Maidment, and Larry W. Mays (1988). "Applied Hydrology." In: *McGraw-Hill series in water resources and environmental engineering*. Ed. by B. J. Clark and John Morriss. Internatio. Vol. 1. 1. Singapore: McGraw - Hill Book Co. Chap. 2.5, p. 512.

Cloke, H.L., F. Pappenberger, and J.P. Renaud (2008). "Multi-Method Global Sensitivity Analysis (MMGSA) for modelling floodplain hydrological processes." In: *Hydrological Processes* 22, pp. 1660–1674.

Coleman, J. M., H. H. Roberts, S. P. Murray, and M. Salama (1981). "Morphology and dynamic sedimentology of the eastern nile delta shelf." In: *Developments in Sedimentology* 32.C, pp. 301–326. DOI: 10.1016/S0070-4571(08)70304-2.

Coleman, James M, Harry H Roberts, and Gregory W Stone (1998). "Mississippi River Delta : an Overview." In: *Journal of Coastal Research* 14.3, pp. 698–716.

Colombani, N., E. Cuoco, and M. Mastrocicco (2017). "Origin and pattern of salinization in the Holocene aquifer of the southern Po Delta (NE Italy)." In: *Journal of Geochemical Exploration* 175, pp. 130–137. DOI: 10.1016/j.gexplo.2017.01.011.

Colombani, N., A. Osti, G. Volta, and M. Mastrocicco (2016). "Impact of Climate Change on Salinization of Coastal Water Resources." In: *Water Resources Management* 30.7, pp. 2483–2496. DOI: 10.1007/s11269-016-1292-z.

Cooke, Gary A (1985). "Reconstruction of the Mesopotamian coastline in the Holocene." In: *Geological Society of America Abstracts* 2.1, pp. 15–28.

Dai, Zhijun, Ao Chu, Marcel Stive, Xiaoling Zhang, and Hong Yan (2011). "Unusual salinity conditions in the Yangtze Estuary in 2006: Impacts of an extreme drought or of the three gorges dam?" In: *Ambio* 40.5, pp. 496–505. DOI: 10.1007/s13280-011-0148-2.

Das Gupta, A. (1985). "Simulated salt-water movement in the Nakhon Luang Aquifer, Bangkok, Thailand." In: *Ground Water* 23.4.

Davis, A.M., S.E. Lewis, D.S. O'Brien, Z.T. Bainbridge, C. Bentley, J.F. Mueller, and J.E. Brodie (2014). "Water resource development and high value coastal wetlands on the Lower Burdekin Floodplain, Australia." In: *Water resource development and high value coastal wetlands on the Lower Burdekin Floodplain, Australia. Estuaries of Australia in 2050 and beyond*. Ed. by Eric Wolanski. June. Dordrecht: Springer. Chap. 13, pp. 223–245. DOI: https://doi.org/10.1007/978-94-007-7019-5_13.

De Lange, Willem J. et al. (2014). "An operational, multi-scale, multi-model system for consensus-based, integrated water management and policy analysis: The Netherlands Hydrological Instrument." In: *Environmental Modelling and Software* 59, pp. 98–108. DOI: 10.1016/j.envsoft.2014.05.009.

De Louw, P. G B, S. Eeman, B. Siemon, B. R. Voortman, J. Gunnink, E. S. Van Baaren, and G. H P Oude Essink (2011). "Shallow rainwater lenses in deltaic areas with saline seepage." In: *Hydrology and Earth System Sciences* 15.12, pp. 3659–3678. DOI: 10.5194/hess-15-3659-2011.

De Haas, T., H. J. Pierik, A. J.F. van der Spek, K. M. Cohen, B. van Maanen, and M. G. Kleinhans (2018). "Holocene evolution of tidal systems in The Netherlands: Effects of rivers, coastal boundary conditions, eco-engineering species, inherited relief and human interference." In: *Earth-Science Reviews* 177, pp. 139–163. DOI: 10.1016/j.earscirev.2017.10.006.

Delsman, J. R., K. R M Hu-A-Ng, P. C. Vos, P. G B De Louw, G. H P Oude Essink, P. J. Stuyfzand, and M. F P Bierkens (2014). "Paleo-modeling of coastal saltwater intrusion during the Holocene: An application to the Netherlands." In: *Hydrology and Earth System Sciences* 18.10, pp. 3891–3905. DOI: 10.5194/hess-18-3891-2014.

Delsman, Joost et al. (2018). "Large-scale, probabilistic salinity mapping using airborne electromagnetics for groundwater management in Zeeland, the Netherlands." In: *Environmental Research Letters* 13, pp. 1–12. DOI: 10.1088/1748-9326/aad19e.

Delsman, Joost R., Gualbert H.P. Oude Essink, Sebastian Huizer, Huite Bootsma, Tobias Mulder, Pieter Zitman, and Betsy Romero Verastegui (2020). *Actualisatie zout in het NHI - Toolbox NHI zoet-zout modellering en landelijk model*. Tech. rep. July. Utrecht: Deltares, p. 55. DOI: 10.13140/RG.2.2.17077.09447.

De Montety, V., O. Radakovitch, C. Vallet-Coulomb, B. Blavoux, and Y Travi (2008). "Geochemical Evolution and timescale of Seawater Intrusion in a Confined Coastal Aquifer: Case of the Rhone Delta." In: *13th IWRA World Water Congress 2008 Montpellier 1-4 Sept*. DOI: 10.1016/j.gca.2004.07.023.

Dermody, B. J., R. P. H. van Beek, E. Meeks, K. Klein Goldewijk, W. Scheidel, Y. van der Velde, M. F. P. Bierkens, M. J. Wassen, and S. C. Dekker (2014). "A virtual water network

of the Roman world." In: *Hydrology and Earth System Sciences* 18.12, pp. 5025–5040. DOI: 10.5194/hess-18-5025-2014.

Diab, M. Sh, K. A Dahab, and M. A El-Fakharany (1997). "Impact of the Paleohydrogeological conditions on the groundwater quality in the Northern Part of the Nile Delta, Egypt." In: *Egyptian Journal of Geology* 41.2B, pp. 779–796.

Diab, M. Sh and M. F. Saleh (1982). "The hydrogeochemistry of the Pleistocene aquifer in the Nile Delta area, Egypt." In: *Environment International* 7.3, pp. 221–230. DOI: 10.1016/0160-4120(82)90109-X.

Dieng, Ndeye Maguette, Philippe Orban, Joel Otten, Christine Stumpp, Serigne Faye, and Alain Dassargues (2017). "Temporal changes in groundwater quality of the Saloum coastal aquifer." In: *Journal of Hydrology: Regional Studies* 9, pp. 163–182. DOI: 10.1016/j.ejrh.2016.12.082.

Dirks, F. J. H., D. Rismianto, and G. J. De Wit (1989). "Groundwater in Bekasi District, West Java, Indonesia." In: *Natuurwetenschappelijk Tijdschrift.* 70.1/4, pp. 47–55.

Dolean, Victorita, Pierre Jolivet, and Frédéric Nataf (2015). *An Introduction to Domain Decomposition Methods : algorithms , theory and parallel implementation*. Tech. rep. Paris: Laboratoire Jacques-Louis Lions, Inria Paris-Rocquencourt, INSMI, p. 289.

Domenico, P.A. and F. W. Schwartz (1990). *Physical and Chemical Hydrogeology*. First edit. Toronto: John Wiley & Sons, p. 822.

Ebeling, Pia, Falk Händel, and Marc Walther (2019). "Potential of mixed hydraulic barriers to remediate seawater intrusion." In: *Science of The Total Environment* 693, p. 133478. DOI: 10.1016/j.scitotenv.2019.07.284.

Edmunds, W. M. (2001). "Palaeowaters in European coastal aquifers – the goals and main conclusions of the PALAEAUX project." In: *Geological Society, London, Special Publications* 189.1, pp. 1–16. DOI: 10.1144/GSL.SP.2001.189.01.02.

El Banna, Mahmoud M. (2004). "Nature and human impact on Nile Delta coastal sand dunes, Egypt." In: *Environmental Geology* 45.5, pp. 690–695. DOI: 10.1007/s00254-003-0922-y.

Elkrail, Adil Balla and Bashir A. Obied (2013). "Hydrochemical characterization and groundwater quality in Delta Tokar alluvial plain, Red Sea coast-Sudan." In: *Arabian Journal of Geosciences* 6.8, pp. 3133–3138. DOI: 10.1007/s12517-012-0594-6.

Ellis, Erle C. and Navin Ramankutty (2008). "Putting people in the map: Anthropogenic biomes of the world." In: *Frontiers in Ecology and the Environment* 6.8, pp. 439–447. DOI: 10.1890/070062.

Enemark, Trine, Luk J.M. Peeters, Dirk Mallants, and Okke Batelaan (2019). "Hydrogeological conceptual model building and testing: A review." In: *Journal of Hydrology* 569.November 2018, pp. 310–329. DOI: 10.1016/j.jhydrol.2018.12.007.

Eppelbaum, Lev, Izzy Kutasov, and Arkady Pilchin (2014). "Thermal Properties of Rocks and Density of Fluids." In: *Applied Geothermics*. 1st ed. Springer-Verlag Berlin Heidelberg. Chap. 2, pp. 99–149. DOI: 10.1007/978-3-642-34023-9.

Erban, Laura E, Steven M Gorelick, Howard a Zebker, and Scott Fendorf (2013). "Release of arsenic to deep groundwater in the Mekong Delta, Vietnam, linked to pumping-induced land subsidence." In: *Proceedings of the National Academy of Sciences of the United States of America* 110.34, pp. 13751–6. DOI: 10.1073/pnas.1300503110.

Fan, X., B. Pedroli, G. Liu, Q. Liu, H. Liu, and L. Shu (2012). "Soil salinity development in the yellow river delta in relation to groundwater dynamics." In: *Land Degradation and Development* 23.2, pp. 175–189. DOI: 10.1002/ldr.1071.

Faneca Sànchez, M., J. L. Gunnink, E. S. van Baaren, G. H. P. Oude Essink, B. Siemon, E. Auken, W. Elderhorst, and P. G. B. de Louw (2012). "Modelling climate change effects on a Dutch coastal groundwater system using airborne electromagnetic measurements." In: *Hydrology and Earth System Sciences* 16.12, pp. 4499–4516. DOI: 10.5194/hess-16-4499-2012.

FAO (2005). *Irrigation in Africa in figures: AQUASTAT survey*. Tech. rep. Rome: FAO, p. 89.

Farid, M. (1980). "Nile Delta Groundwater Study." MSc thesis. Cairo University. DOI: 10.1017/CBO9781107415324.004. arXiv: arXiv:1011.1669v3.

Farouk, Sherif, Abdelmohsen Ziko, Shehtta A. Eweda, and Ali E. Said (2014). "Subsurface Miocene sequence stratigraphic framework in the Nile Delta, Egypt." In: *Journal of African Earth Sciences* 91, pp. 89–109. DOI: 10.1016/j.jafrearsci.2013.12.010.

Fass, T., P. G. Cook, T. Stieglitz, and A. L. Herczeg (2007). "Development of saline ground water through transpiration of sea water." In: *Ground Water* 45.6, pp. 703–710. DOI: 10.1111/j.1745-6584.2007.00344.x.

Faye, Serigne, Piotr Maloszewski, Willibald Stichler, Peter Trimborn, Seynabou Cisse Faye, and Cheikh Beaye Gaye (2005). "Groundwater salinization in the Saloum (Senegal) delta aquifer: Minor elements and isotopic indicators." In: *Science of the Total Environment* 343.1-3, pp. 243–259. DOI: 10.1016/j.scitotenv.2004.10.001.

Fell, Christopher J.D and H. Peter Hutchison (1971). "Diffusion Coefficients for Sodium and Potassium Chlorides in Water." In: *Journal of Chemical and Engineering Data* 16.4, pp. 427–429. DOI: 10.1021/je60051a005.

Fielding, C. R., J. D. Trueman, and J. Alexander (2006). "Holocene Depositional History of the Burdekin River Delta of Northeastern Australia: A Model for a Low-Accommodation, Highstand Delta." In: *Journal of Sedimentary Research* 76.3, pp. 411–428. DOI: 10.2110/jsr.2006.032.

Flaux, Clément, Christelle Claude, Nick Marriner, and Christophe Morhange (2013). "A 7500-year strontium isotope record from the northwestern Nile delta (Maryut lagoon, Egypt)." In: *Quaternary Science Reviews* 78.August, pp. 22–33. DOI: 10.1016/j.quascirev.2013.06.018.

Fogg, Graham E. and Yong Zhang (2016). "Debates—Stochastic subsurface hydrology from theory to practice: A geologic perspective." In: *Water Resources Research* 52, pp. 9235–9245. DOI: 10.1002/2016WR019699.Received.

Gallichand, J., D. Marcotte, S. O. Prasher, and R. S. Broughton (1992). "Optimal sampling density of hydraulic conductivity for subsurface drainage in the Nile delta." In: *Agricultural Water Management* 20.4, pp. 299–312. DOI: 10.1016/0378-3774(92)90004-G.

Galloway, W D (1975). "Process Framework for describing the morphologic and stratigraphic evolution of deltaic depositional systems." In: *Deltas: Models for Exploration*. Ed. by M.L. Broussard. 1st ed. Houston: Houston Geological Society. Chap. 1, pp. 86–98.

Garven, Grant (1995). "Continental-Scale Groundwater Flow and Geologic Processes." In: *Annual Review of Earth and Planetary Sciences* 23, pp. 89–117.

Gat, J R and Y Levy (1978). "Isotope hydrology of inland sabkhas in the Bardawil area, Sinai." In: *Limnology and Oceanography* 23.5, pp. 841–850. DOI: 10.4319/lo.1978.23.5.0841.

GEBCO (2014). *GEBCO Dataset*.

Geirnaert, W. and M. P. Laeven (1992). "Composition and history of ground water in the western Nile Delta." In: *Journal of Hydrology* 138.1-2, pp. 169–189. DOI: 10.1016/0022-1694(92)90163-P.

Gelhar, Lynn W., Claire Welty, and Kenneth R. Rehfeldt (1992). "A Critical Review of Data on Field-Scale Dispersion in Aquifers." In: *Water Resources Research* 28.7, pp. 1955–1974. DOI: 10.1029/92WR00607.

Geriesh, Mohamed H., Klaus-Dieter Balke, Ahmed E. El-Rayes, and Basma M. Mansour (2015). "Implications of climate change on the groundwater flow regime and geochemistry of the Nile Delta, Egypt." In: *Journal of Coastal Conservation* 19.4, pp. 589–608. DOI: 10.1007/s11852-015-0409-5.

Giambastiani, B. M.S., N. Colombani, M. Mastrocicco, and M. D. Fidelibus (2013). "Characterization of the lowland coastal aquifer of comacchio (ferrara, italy): Hydrology, hydrochemistry and evolution of the system." In: *Journal of Hydrology* 501, pp. 35–44. DOI: 10.1016/j.jhydrol.2013.07.037.

Giambastiani, Beatrice M.S., Marco Antonellini, Gualbert H.P. Oude Essink, and Roelof J. Stuurman (2007). "Saltwater intrusion in the unconfined coastal aquifer of Ravenna (Italy): A numerical model." In: *Journal of Hydrology* 340.1-2, pp. 91–104. DOI: 10.1016/j.jhydrol.2007.04.001.

Giao, P. H., N. Phien-Wej, and Y. Honjo (1998). "FEM quasi-3D modelling of responses to artificial recharge in the Bangkok multiaquifer system." In: *Environmental Modelling and Software* 14.2-3, pp. 141–151. DOI: 10.1016/S1364-8152(98)00065-6.

Gibson, R. E. (1958). "The Progress of Consolidation in a Clay Layer Increasing in Thickness with Time." In: *Géotechnique* 8.4, pp. 171–182. DOI: 10.1680/geot.1958.8.4.171.

Giosan, Liviu, James Syvitski, Stefan Constantinescu, and John Day (2014). "Climate change: Protect the world's deltas." In: *Nature* 516.729, pp. 31–33. DOI: 10.1038/516031a.

Giosan, Liviu et al. (2018). "On the Holocene evolution of the Ayeyawady megadelta." In: *Earth Surface Dynamics* 6.2, pp. 451–466. DOI: 10.5194/esurf-6-451-2018.

Golub, Gene and Charles F. Van Loan (1996). *Matrix Computations*. 3rd. London: The Johns Hobkins University Press.

Goodbred, S. L. and S. A. Kuehl (2000). "The significance of large sediment supply, active tectonism, and eustasy on margin sequence development: Late Quaternary stratigraphy and evolution of the Ganges-Brahmaputra delta." In: *Sedimentary Geology* 133.3-4, pp. 227–248. DOI: 10.1016/S0037-0738(00)00041-5.

Goode, Daniel J. (1996). "Direct simulation of groundwater age." In: *Water Resources Research* 32.2, pp. 289–296. DOI: 10.1029/95WR03401.

Gossel, Wolfgang, Ahmed Sefelnasr, and Peter Wycisk (2010). "Modelling of paleo-saltwater intrusion in the northern part of the Nubian Aquifer System, Northeast Africa." In: *Hydrogeology Journal* 18.6, pp. 1447–1463. DOI: 10.1007/s10040-010-0597-x.

Griffioen, Jasper, Hanneke Verweij, and Roelof Stuurman (2016). "The composition of groundwater in Palaeogene and older formations in the Netherlands. A synthesis." In: *Netherlands Journal of Geosciences* 95.3, pp. 349–372. DOI: 10.1017/njg.2016.19.

Griffith, Jason M. (2003). *Hydrogeologic Framework of Southeastern Louisiana*.

Gunnink, Jan L., Van Pham Hung, Gualbert H.P. Oude Essink, and Marc F.P. Bierkens (2020). "Geostatistical estimation of the 3D groundwater salinity distribution in the Mekong Delta, Vietnam." In: *HESSD*.

Guo, Weixing and Christian D. Langevin (2002). *User's Guide to SEAWAT: A computer program for simulation of three-dimensional variable-density ground-water flow*. Book 6. Tallahassee: USGS, chap A7.

Guo, Zhilin, Graham E. Fogg, and Christopher V. Henri (2019). "Upscaling of Regional Scale Transport Under Transient Conditions: Evaluation of the Multirate Mass Transfer Model." In: *Water Resources Research* 55.7, pp. 5301–5320. DOI: 10.1029/2019WR024953.

Han, Dongmei, Claus Kohfahl, Xianfang Song, Guoqiang Xiao, and Jilong Yang (2011). "Geochemical and isotopic evidence for palaeo-seawater intrusion into the south coast aquifer of Laizhou Bay, China." In: *Applied Geochemistry* 26.5, pp. 863–883. DOI: 10.1016/j.apgeochem.2011.02.007.

Hanor, J. S. and J. A. Mercer (2011). "Spatial Variations in the Salinity of Pore Waters in Northern Deep Water Gulf of Mexico Sediments: Implications for Pathways and Mechanisms of Solute Transport." In: *Geofluids* 10, pp. 83–93. DOI: 10.1002/9781444394900.ch7.

Hanor, Jeffrey S. (1994). "Physical and chemical controls on the composition of waters in sedimentary basins." In: *Marine and Petroleum Geology* 11.1, pp. 31–45. DOI: 10.1016/0264-8172(94)90007-8.

Hehanussa, P. E. (1980). "Appenndix 2: Excursion guide to the Cimanuk Delta complex, west Java." In: *Proceedings of the Jakarta workshop on coastal resources management*.

Herman, J. D., J. B. Kollat, P. M. Reed, and T. Wagener (2013). "Technical Note: Method of Morris effectively reduces the computational demands of global sensitivity analysis for distributed watershed models." In: *Hydrology and Earth System Sciences* 17.7, pp. 2893–2903. DOI: 10.5194/hess-17-2893-2013.

Higgins, Stephanie a. (2016). "Review: Advances in delta-subsidence research using satellite methods." In: *Hydrogeology Journal*, pp. 587–600. DOI: 10.1007/s10040-015-1330-6.

Hoang, Hang Thi Thu et al. (2018). "Impact of anthropogenic activities on water quality and plankton communities in the Day River (Red River Delta, Vietnam)." In: *Environmental Monitoring and Assessment* 190.2. DOI: 10.1007/s10661-017-6435-z.

Houben, Georg and Vincent E. A. Post (2017). "The first field-based descriptions of pumping-induced saltwater intrusion and upconing." In: *Hydrogeology Journal* 25.1, pp. 243–247. DOI: 10.1007/s10040-016-1476-x.

Huscroft, Jordan, Tom Gleeson, Jens Hartmann, and Janine Börker (2018). "Compiling and Mapping Global Permeability of the Unconsolidated and Consolidated Earth: GLobal HYdrogeology MaPS 2.0 (GLHYMPS 2.0)." In: *Geophysical Research Letters* 45.4, pp. 1897–1904. DOI: 10.1002/2017GL075860.

Hussein, Mohamed Tahir (1982). "Evaluation of groundwater resources in tokar delta, sudan." In: *Hydrological Sciences Journal* 27.2, pp. 139–145. DOI: 10.1080/02626668209491096.

Ibrahim Hussein, Hend Ahmed, Adam Ricka, Tomas Kuchovsky, and Maged Mostafa El Osta (2017). "Groundwater hydrochemistry and origin in the south-eastern part of Wadi El Natrun, Egypt." In: *Arabian Journal of Geosciences* 10.7, pp. 1–14. DOI: 10.1007/s12517-017-2960-x.

Iribar, V., J. Carrera, E. Custodio, and A. Medina (1997). "Inverse modelling of seawater intrusion in the Llobregat delta deep aquifer." In: *Journal of Hydrology* 198.1-4, pp. 226–244. DOI: 10.1016/S0022-1694(96)03290-8.

Jakovovic, Danica, Adrian D. Werner, Perry G.B. de Louw, Vincent E.A. Post, and Leanne K. Morgan (2016). "Saltwater upconing zone of influence." In: *Advances in Water Resources* 94, pp. 75–86. DOI: 10.1016/j.advwatres.2016.05.003.

Jasechko, Scott et al. (2017). "Global aquifers dominated by fossil groundwaters but wells vulnerable to modern contamination." In: *Nature Geoscience* 10.April, pp. 425–430. DOI: 10.1038/ngeo2943.

Jazayeri, Amir and Adrian D. Werner (2019). "Boundary condition nomenclature confusion in groundwater flow modelling." In: *Groundwater* 57.5, gwat.12893. DOI: 10.1111/gwat.12893.

Jones, Gareth D., Fiona F. Whitaker, Peter L. Smart, and Ward E. Sanford (2002). "Fate of reflux brines in carbonate platforms." In: *Geology* 30.4, pp. 371–374. DOI: 10.1130/0091-7613(2002)030<0371:FORBIC>2.0.CO.

Kang, Mary and Robert B Jackson (2016). "Salinity of deep groundwater in California : Water quantity , quality , and protection." In: *Proceedings of the National Academy of Sciences of the United States of America*, p. 6. DOI: 10.1073/pnas.1600400113.

Kashef, Abdel-Aziz I. (1983). "Salt-Water Intrusion in the Nile Delta." In: *Groundwater* 21.2, pp. 160–167. DOI: 10.1111/j.1745-6584.1983.tb00713.x.

Kerrou, Jaouher and Philippe Renard (2010). "A numerical analysis of dimensionality and heterogeneity effects on advective dispersive seawater intrusion processes." In: *Hydrogeology Journal* 18.1, pp. 55–72. DOI: 10.1007/s10040-009-0533-0.

Ketabchi, Hamed, Davood Mahmoodzadeh, Behzad Ataie-Ashtiani, and Craig T. Simmons (2016). "Sea-level rise impacts on seawater intrusion in coastal aquifers: Review and integration." In: *Journal of Hydrology* 535, pp. 235–255. DOI: 10.1016/j.jhydrol.2016.01.083.

Khan, Aneire Ehmar, Pauline Franka Denise Scheelbeek, Asma Begum Shilpi, Queenie Chan, Sontosh Kumar Mojumder, Atiq Rahman, Andy Haines, and Paolo Vineis (2014). "Salinity in Drinking Water and the Risk of (Pre)Eclampsia and Gestational Hypertension in Coastal Bangladesh: A Case-Control Study." In: *PLoS ONE* 9.9, e108715. DOI: 10.1371/journal.pone.0108715.

Khare, Y. P., R. Muñoz-Carpena, R. W. Rooney, and C. J. Martinez (2015). "A multi-criteria trajectory-based parameter sampling strategy for the screening method of elementary effects." In: *Environmental Modelling and Software* 64, pp. 230–239. DOI: 10.1016/j.envsoft.2014.11.013.

King, Caroline and Boshra Salem (2012). "A socio-ecological investigation of options to manage groundwater degradation in the western desert, Egypt." In: *Ambio* 41.5, pp. 490–503. DOI: 10.1007/s13280-012-0255-8.

King, Jude, Gualbert Oude Essink, Marios Karaolis, Bernhard Siemon, and Marc F.P. Bierkens (2018). "Quantifying Geophysical Inversion Uncertainty Using Airborne Frequency Domain Electromagnetic Data—Applied at the Province of Zeeland, the Netherlands." In: *Water Resources Research* October. DOI: 10.1029/2018WR023165.

Kirschbaum, M A, C J Schenk, R Charpentier, T R Klett, M E Brownfield, J K Pitman, T A Cook, and M E Tennyson (2010). "Assessment of Undiscovered Oil and Gas Resources of the Nile Delta Basin Province, Eastern Mediterranean." In: *USGS Fact Sheet* 3027, pp. 1–4.

Kohfahl, C., V. E A Post, E. Hamann, H. Prommer, and C. T. Simmons (2015). "Validity and slopes of the linear equation of state for natural brines in salt lake systems." In: *Journal of Hydrology* 523, pp. 190–195. DOI: 10.1016/j.jhydrol.2015.01.054.

Kooi, H. and J. Groen (2001). "Offshore continuation of coastal groundwater systems; predictions using sharp-interface approximations and variable-density flow modelling." In: *Journal of Hydrology* 246.1-4, pp. 19–35. DOI: 10.1016/S0022-1694(01)00354-7.

Kooi, H. and J. Groen (2003). "Geological processes and the management of groundwater resources in coastal areas." In: *Geologie en Mijnbouw/Netherlands Journal of Geosciences* 82.1, pp. 31–40. DOI: 10.1017/S0016774600022770.

Kooi, H., J. Groen, and A. Leijnse (2000). "Modes of seawater intrusion during transgressions." In: *Water Resources Research* 36.12, pp. 3581–3589. DOI: 10.1029/2000WR900243.

Kooy, Michelle, Carolin Tina Walter, and Indrawan Prabaharyaka (2016). "Inclusive development of urban water services in Jakarta: The role of groundwater." In: *Habitat International* March 2017. DOI: 10.1016/j.habitatint.2016.10.006.

Kozerski, B (1983). "PROBLEMS OF THE SALT WATER ORIGIN IN THE VISTULA DELTA AQUIFERS." In: *Proceedings of the 8th Salt Water Intrusion Meeting, Bari, Italy*, pp. 325–334.

Kubota, A, B Zayed, H Fujimaki, T Higashi, S Yoshida, M M A Mahmoud, Y Kitamura, and W H Abou El Hassan (2017). "Chapter 7: Water and salt movement in Soils of the Nile Delta." In: *Irrigated Agriculture in Egypt*. Ed. by Masayoshi Satoh and Samir Aboulroos. 1st ed. Switzerland: Springer International Publishing, pp. 153–186. DOI: 10.1007/978-3-319-30216-4.

Kulp, Scott A. and Benjamin H. Strauss (2019). "New elevation data triple estimates of global vulnerability to sea-level rise and coastal flooding." In: *Nature Communications* 10.1. DOI: 10.1038/s41467-019-12808-z.

Kwong, Hiu Tung and Jiu Jimmy Jiao (2016). "Hydrochemical reactions and origin of offshore relatively fresh pore water from core samples in Hong Kong." In: *Journal of Hydrology* 537, pp. 283–296. DOI: 10.1016/j.jhydrol.2016.03.050.

Laeven, M.P. (1991). *Hydrogeological Study of the Nile Delta and Adjacent Desert Areas Egypt with emphasis on hydrochemistry and isotope hydrology*. Tech. rep. January 1991. Amsterdam: Amsterdam Free University, pp. 1–70.

Langevin, C D, W B Shoemaker, and W Guo (2003). *MODFLOW-2000, the U.S. Gelogical Survey Modular Ground-Water Model-Documentation of the SEAWAT-2000 version*

with the Variable-Density Flow Process (VDF) and the Integrated MT3DMS Transport Process (IMT). Tech. rep., p. 43.

Langevin, Christian D., Daniel T. Thorne Jr., Alyssa M. Dausman, Michael C. Sukop, and Weixing Guo (2008). "SEAWAT Version 4: A Computer Program for Simulation of Multi-Species Solute and Heat Transport." In: *U.S. Geological Survey Techniques and Methods Book 6*. Ed. by Dirk Kempthorne and Mark D. Myers. Reston, Virginia: USGS. Chap. A22, p. 39.

Larsen, Flemming, Long Vu Tran, Hoan Van Hoang, Luu Thi Tran, Anders Vest Christiansen, and Nhan Quy Pham (2017). "Groundwater salinity influenced by Holocene seawater trapped in incised valleys in the Red River delta plain." In: *Nature Geoscience* 10.May, pp. 376–382. DOI: 10.1038/ngeo2938.

Levy, Yitzhak (1977). "The origin and evolution of brine in coastal sabkhas, Northern Sinai." In: *Journal of Sedimentary Petrology* 47.1.

LGWRC (2012). *Managing Louisiana's Groundwater Resources*. Tech. rep. Baton Rouge: Louisiana Ground Water Resources Commission Commission, p. 116.

Lindsay, J. F., D. W. Holliday, and A. G. Hulbert (1991). *Sequence stratigraphy and the evolution of the Ganges-Brahmaputra delta complex*.

Lopez, D.L. and L. Smith (1995). "Fluid flow in fault zones: Analysis of the interplay of convective circulation and topographically driven groundwater flow." In: *Water Resouces Research* 31.6, pp. 1489–1503.

Loucks, Daniel P. (2019). "Developed river deltas: Are they sustainable?" In: *Environmental Research Letters* 14.11. DOI: 10.1088/1748-9326/ab4165.

LPHI and AAE (2016). *Groundwater for power plants: A big risk to New Orleans East*. Tech. rep. New Orleans, Louisiana: Lousiana Public Health Institute, p. 15.

Lu, Chunhui, Peter K. Kitanidis, and Jian Luo (2009). "Effects of kinetic mass transfer and transient flow conditions on widening mixing zones in coastal aquifers." In: *Water Resources Research* 45.12, pp. 1–17. DOI: 10.1029/2008WR007643.

Maas, C (1987). "Het vóórkomen van zout grondwater in Nederland." In: *H2O* 22.7, pp. 214–219.

Mabrouk, M. B., A. Jonoski, D. Solomatine, and S. Uhlenbrook (2013). "A review of seawater intrusion in the Nile Delta groundwater system – the basis for assessing impacts due to climate changes and water resources development." In: *Hydrology and Earth System Sciences Discussions* 10.8, pp. 10873–10911. DOI: 10.5194/hessd-10-10873-2013.

Mabrouk, Marmar, Andreja Jonoski, Gualbert H.P. Oude Essink, and Stefan Uhlenbrook (2018). "Impacts of sea level rise and increasing fresh water demand on sustainable groundwater management." In: *Water* 10.1690, pp. 1–14. DOI: 10.3390/w10111690.

Maczyńska, Agnieszka (2014). *Studies in African Archaeology vol 13: The Nile Delta as a centre of cultural interactions between Upper Egypt and the Southern Levant in the 4th*

millennium BC. Ed. by Agnieszka Maczyńska. 1st. Poznan: Poznan Archaeological Museum and authors, p. 318.

Malm, Andreas and Shora Esmailian (2013). "Ways In and Out of Vulnerability to Climate Change: Abandoning the Mubarak Project in the Northern Nile Delta, Egypt." In: *Antipode* 45.2, pp. 474–492. DOI: 10.1111/j.1467-8330.2012.01007.x.

Manzano, M, E Custodio, H Loosli, M C Cabrera, X Riera, and J Custodio (2001). "Palaeowater in coastal aquifers of Spain." In: *Geological Society, London, Special Publications* 189.1, pp. 107–138. DOI: 10.1144/gsl.sp.2001.189.01.08.

Mcmahon, Gerard A, N Jerome Arunakumaren, and Kiran Bajracharya (2000). "Hydrogeological Conceptualisation of the Burdekin River Delta." In: *Proceedings f the 3rd international Hydrology and Water Resources Symposium of the Institution of Engineers, Perth, Western Australia, Australia*. January 2000.

Meisler, H, P. P Leahy, and L. L Knobel (1984). "Effect of Eustatic Sea-Level Changes on Saltwater-Freshwater in the Northern Atlantic Coastal Plain." In: *USGS Water Supply Paper: 2255*. Ed. by William P. Clark and Dallas L. Peck. Alexandria, Virginia: U.S. Geological Survey, p. 28.

Meyer, Rena, Peter Engesgaard, and Torben O. Sonnenborg (2019). "Origin and Dynamics of Saltwater Intrusion in a Regional Aquifer: Combining 3-D Saltwater Modeling With Geophysical and Geochemical Data." In: *Water Resources Research* 55.3, pp. 1792–1813. DOI: 10.1029/2018WR023624.

Michael, Holly A, Vincent E.A. Post, Alicia M. Wilson, and Adrian D. Werner (2017). "Science, society, and the coastal groundwater squeeze." In: *Water Resources Research* April. DOI: 10.1002/2017WR020851.

Michael, Holly A., Kaileigh C. Scott, Mohammad Koneshloo, Xuan Yu, Mahfuzur R. Khan, and Katie Li (2016). "Geologic influence on groundwater salinity drives large seawater circulation through the continental shelf." In: *Geophysical Research Letters* 43.20, pp. 10, 782–10, 791. DOI: 10.1002/2016GL070863.

Michael, Holly A. and Clifford I. Voss (2008). "Evaluation of the sustainability of deep groundwater as an arsenic-safe resource in the Bengal Basin." In: *Proceedings of the National Academy of Sciences of the United States of America* 105.25, pp. 8531–8536. DOI: 10.1073/pnas.0710477105.

Michael, Holly A. and Clifford I. Voss (2009). "Estimation of regional-scale groundwater flow properties in the Bengal Basin of India and Bangladesh." In: *Hydrogeology Journal* 17.6, pp. 1329–1346. DOI: 10.1007/s10040-009-0443-1.

Millero, F.J. (2010). "History of the equation of state of seawater." In: *Oceanography* 23.3, pp. 18–33. DOI: 10.5670/oceanog.2010.21..

Minderhoud, P. S. J., G. Erkens, V.H. Pham, V.T. Bui, L. Erban, H. Kooi, and E. Stouthamer (2017). "Impacts of 25 years of groundwater extraction on subsidence in the Mekong

delta, Vietnam." In: *Environmental Research Letters* 12.6, p. 64006. DOI: doi.org/10.1088/1748-9326/aa7146.

Morris, Max D (1991). "Factorial Sampling Plans for Preliminary Computational Experiments." In: *Technometrics* 33.2, pp. 161–174. DOI: 10.2307/1269043.

Mulligan, Ann E., Rob L. Evans, and Dan Lizarralde (2007). "The role of paleochannels in groundwater/seawater exchange." In: *Journal of Hydrology* 335.3-4, pp. 313–329. DOI: 10.1016/j.jhydrol.2006.11.025. arXiv: arXiv:1011.1669v3.

Narayan, Kumar A., Carsten Schleeberger, and Keith L. Bristow (2007). "Modelling seawater intrusion in the Burdekin Delta Irrigation Area, North Queensland, Australia." In: *Agricultural Water Management* 89.3, pp. 217–228. DOI: 10.1016/j.agwat.2007.01.008.

NASA (2014). *Shuttle Radar Topography Mission*. Pasadena, California.

Naseem, Sadaf, Viqar Husain, and Shella Bano (2018). "Origin of Salinity and Other Constituents in Indus Deltaic Plain Groundwater, Thatta District, Pakistan." In: *Journal of Coastal Research* 344.4, pp. 883–891. DOI: 10.2112/jcoastres-d-17-00052.1.

Nashaat, M (1998). "Abnormally high formation pressure and seal impacts on hydrocarbon accumulations in the Nile Delta and North Sinai basins, Egypt." In: *Abnormal pressures in hydrocarbon environments. AAPG. Memoir no. 70* 70, pp. 161–180.

Naus, Floris Loys, Paul Schot, Koos Groen, Kazi Matin Ahmed, and Jasper Griffioen (2019). "Groundwater salinity variation in Upazila Assasuni (southwestern Bangladesh), as steered by surface clay layer thickness, relative elevation and present-day land use." In: *Hydrology and Earth System Sciences* 23.3, pp. 1431–1451. DOI: 10.5194/hess-23-1431-2019.

Neumann, Barbara, Athanasios T. Vafeidis, Juliane Zimmermann, and Robert J. Nicholls (2015). "Future coastal population growth and exposure to sea-level rise and coastal flooding - A global assessment." In: *PLoS ONE* 10.3. DOI: 10.1371/journal.pone.0118571.

Neuzil, C. E. (2003). "Hydromechanical coupling in geologic processes." In: *Hydrogeology Journal* 11.1, pp. 41–83. DOI: 10.1007/s10040-002-0230-8.

Nguyen, A D and H H G Savenije (2006). "Salt intrusion in multi-channel estuaries: a case study in the {Mekong} {Delta}, {Vietnam}." In: *Hess* 10, pp. 743–754. DOI: 10.5194/hessd-3-499-2006.

Nichols, Gary (2009). "Sequence Stratigraphy and Sea-level Changes." In: *Sedimentology And Stratigraphy*. Ed. by Gary Nichols. 2nd ed. Chichester: John Wiley & Sons. Chap. 23, pp. 349–380. DOI: 10.1016/B978-0-444-59425-9.00013-5.

Nield, D. A. (1968). "Onset of Thermohaline Convection in a Porous Medium." In: *Water Resources Research* 4.3, pp. 553–559. DOI: 10.1103/PhysRevLett.94.205502.

Nield, Donald A. and Adrian Bejan (2013). *Convection in porous media*. Fourth Edi. New York: Springer, pp. 1–778. DOI: 10.1007/978-1-4614-5541-7. arXiv: arXiv:1011.1669v3.

Nienhuis, Jaap H., Andrew D. Ashton, Douglas A. Edmonds, A.J.F. Hoitink, Albert J. Kettner, Joel C. Rowland, and Torbjorn E. Tornqvist (2020). "Global-scale human impact on delta morphology has led to net land area gain." In: *Nature* 1.January. DOI: 10.1038/s41586-019-1905-9.

Nofal, E.R., M.A. Amer, S.M. El-Didy, and M.F. Akram (2015). "Sea Water Intrusion in Nile Delta in Perspective of New Configuration of the Aquifer Heterogeneity Using the Recent Stratigraphy Data." In: *Journal of American Science* 11.6, pp. 567–570.

Nofal, E.R., H.F.A. Mostafa, W. van der Linden, and G.H.P. Oude Essink (2016). *Enhanced Water Resources Management Project Egypt, Technical Study 4: Groundwater Modelling, Nile Delta.* Tech. rep. August. Cairo: National Water Research Center (NWRC); Research Institute for Groundwater (RIGW); Deltares.

Nofal, Eman Ragab, Akram Mohamed Fekry, Mostafa Helmy Ahmed, and Mohamed Mostafa El-Kharakany (2018). "Groundwater: Extraction versus recharge; vulnerability assessment." In: *Water Science* 32.2018, pp. 287–300. DOI: 10.1016/j.wsj.2018.07.002.

Nogueira, G., T. Y. Stigter, Y. Zhou, F. Mussa, and D. Juizo (2019). "Understanding groundwater salinization mechanisms to secure freshwater resources in the water-scarce city of Maputo, Mozambique." In: *Science of the Total Environment* 661, pp. 723–736. DOI: 10.1016/j.scitotenv.2018.12.343.

Oude Essink, Gualbert H.P (2001). "Improving fresh groundwater supply—problems and solutions." In: *Ocean & Coastal Management* 44.5, pp. 429–449. DOI: 10.1016/S0964-5691(01)00057-6.

Oude Essink, Gualbert H.P., Esther S. Van Baaren, and Perry. G.B. De Louw (2010). "Effects of climate change on coastal groundwater systems: A modeling study in the Netherlands." In: *Water Resources Research* 46.10, pp. 1–16. DOI: 10.1029/2009WR008719.

Panday, Sorab, Christian D. Langevin, Richard G. Niswonger, Motomu Ibaraki, and Joseph D. Hughes (2013). "MODFLOW-USG Version 1: An Unstructured Grid Version of MODFLOW for Simulating Groundwater Flow and Tightly Coupled Processes Using a Control Volume Finite-Difference Formulation." In: *U.S. Geological Survey Techniques and Methods Book 6*. Reston, Vi. A. Chap. 45, p. 66.

Paradigm (2017). *SKUA-GOCAD*.

Park, Jungho, Craig M. Bethke, Thomas Torgersen, and Thomas M. Johnson (2002). "Transport modeling applied to the interpretation of groundwater 36 Cl age." In: *Water Resources Research* 38.5, pp. 1–15. DOI: 10.1029/2001WR000399.

Pauw, Pieter S., Sjoerd E A T M van der Zee, Anton Leijnse, and Gualbert H P Oude Essink (2015). "Saltwater Upconing Due to Cyclic Pumping by Horizontal Wells in Freshwater Lenses." In: *Groundwater* 54.4, pp. 521–531. DOI: 10.1111/gwat.12382.

Peelen, R. (1970). "Changes in salinity in the delta area of the rivers Rhine and Meuse resulting from the construction of a number of enclosing Dams." In: *Netherlands Journal of Sea Research* 5.1, pp. 1–19. DOI: 10.1016/0077-7579(70)90002-5.

Pellenbarg, N P (1997). "Groundwater Management in the Netherlands: Background and Legislation." In: *ILRA Workshop Groundwater Management*. March 1984, pp. 137–149.

Pennington, B T, Fraser Sturt, Penelope Wilson, Joanne Rowland, and Antony G Brown (2017). "The fluvial evolution of the Holocene Nile Delta." In: *Quaternary Science Reviews* 170, pp. 212–231. DOI: 10.1016/j.quascirev.2017.06.017.

Pennington, Benjamin T., Judith Bunbury, and Niels Hovius (2016). "Emergence of Civilization, Changes in Fluvio-Deltaic Style, and Nutrient Redistribution Forced by Holocene Sea-Level Rise." In: *Geoarchaeology* 31.3, pp. 194–210. DOI: 10.1002/gea.21539.

Person, M a and G Garven (1994). "A Sensitivity Study of the Driving Forces on Fluid Flow During Continental Rift Evolution." In: *Geological Society of America Bulletin* 106.April, pp. 461–475.

Pierre, Catherine; Germain; Bayon, Marie-Madeleine; Blanc-Valleron, Jean; Mascle, and Stephanie; Dupre (2014). "Authigenic carbonates related to active seepage of methane-rich hot brines at the Cheops mud volcano, Menes caldera (Nile deep-sea fan, eastern Mediterranean Sea) Catherine." In: *Geo-Marine Letters* 34.2, pp. 253–267.

Pool, M., J. Carrera, A. Alcolea, and E. M. Bocanegra (2015). "A comparison of deterministic and stochastic approaches for regional scale inverse modeling on the Mar del Plata aquifer." In: *Journal of Hydrology* 531, pp. 214–229. DOI: 10.1016/j.jhydrol.2015.09.064.

Post, Vincent E.A. (2004). "Groundwater salinization processes in the coastal area of the Netherlands due to transgressions during the Holocene." PhD thesis. Vrije Universiteit Amsterdam, p. 138.

Post, Vincent E.A., Georg J. Houben, and Joeri van Engelen (2018). "What is the Ghijben-Herzberg principle and who formulated it?" In: *Hydrogeology Journal* 26, pp. 1801–1807.

Post, Vincent E.A., Henk Kooi, and Craig T. Simmons (2007). "Using hydraulic head measurements in variable-density ground water flow analyses." In: *Ground Water* 45.6, pp. 664–671. DOI: 10.1111/j.1745-6584.2007.00339.x.

Post, Vincent E.A. and Craig T. Simmons (2010). "Free convective controls on sequestration of salts into low-permeability strata: insights from sand tank laboratory experiments and

numerical modelling." In: *Hydrogeology journal* 18.1, pp. 39–54. DOI: 10.âĂŃ1007/âĂŃs10040-009-0521-4.

Post, Vincent E.A., Alexander Vandenbohede, Adrian D. Werner, Maimun, and Michael D. Teubner (2013). "Groundwater ages in coastal aquifers." In: *Advances in Water Resources* 57, pp. I–II. DOI: 10.1016/j.advwatres.2013.03.011.

Prabaharan, S., C. Lakshumanan, and T. Subramani (2018). "Geomorphic Anomalies and Natural Resource of Krishna Godavari Basin Using Remote Sensing Techniques." In: *International Journal of Earth Sciences and Engineering* 11.01, pp. 35–40. DOI: 10.21276/ijee.2018.11.0106.

Prasad, Awadhesh and Craig T. Simmons (2005). "Using quantitative indicators to evaluate results from variable-density groundwater flow models." In: *Hydrogeology Journal* 13.5-6, pp. 905–914. DOI: 10.1007/s10040-004-0338-0.

Radhakrishna, I (2001). "Saline fresh water interface structure in Mahanadi delta region , Orissa, India." In: *Environmental Geology* 40.January.

Rahman, M. M. et al. (2019). "Salinization in large river deltas: Drivers, impacts and socio-hydrological feedbacks." In: *Water Security* 6.February, p. 100024. DOI: 10.1016/j.wasec.2019.100024.

Ranganathan, Vishnu and Jeffrey S. Hanor (1988). "Density-driven groundwater flow near salt domes." In: *Chemical Geology* 74.1-2, pp. 173–188. DOI: 10.1016/0009-2541(88)90152-0.

Rasmussen, E. Kock, O. Svenstrup Petersen, J. R. Thompson, R. J. Flower, and M. H. Ahmed (2009). "Hydrodynamic-ecological model analyses of the water quality of Lake Manzala nile delta, northern Egypt." In: *Hydrobiologia* 622.1, pp. 195–220. DOI: 10.1007/s10750-008-9683-7.

Rathore, Saubhagya Singh, Yue Zhao, Chunhui Lu, and Jian Luo (2018). "Defining the Effect of Stratification in Coastal Aquifers Using a New Parameter." In: *Water Resources Research* 54.9, pp. 5948–5957. DOI: 10.1029/2018WR023114.

Riad, S., E. M. Abdelrahman, E. Refai, and H. M. El-Ghalban (1989). "Geothermal studies in the Nile Delta, Egypt." In: *Journal of African Earth Sciences* 9.3-4, pp. 637–649. DOI: 10.1016/0899-5362(89)90048-1.

Rizzini, Antonio, Franco Vezzani, Vincenzo Cococcetta, and George Milad (1978). "Stratigraphy and sedimentation of a Neogene-Quaternary section in the Nile Delta area (A.R.E.)" In: *Marine Geology* 27.3-4, pp. 327–348. DOI: 10.1016/0025-3227(78)90038-5.

Ruano, M. V., J. Ribes, A. Seco, and J. Ferrer (2012). "An improved sampling strategy based on trajectory design for application of the Morris method to systems with many input factors." In: *Environmental Modelling and Software* 37, pp. 103–109. DOI: 10.1016/j.envsoft.2012.03.008.

Saito, Yoshiki, Zuosheng Yang, and Kazuaki Hori (2001). "The Huanghe Yellow River and Changjiang Yangtze River deltas: a review on their characteristics, evolution and sediment discharge during the Holocene." In: *Geomorphology* 41, pp. 219–231.

Salem, Zenhom E. and Dina A. El-Bayumy (2016). "Hydrogeological, petrophysical and hydrogeochemical characteristics of the groundwater aquifers east of Wadi El-Natrun, Egypt." In: *NRIAG Journal of Astronomy and Geophysics* 5.1, pp. 124–146. DOI: 10.1016/j.nrjag.2015.12.001.

Salman, G. and I. Abdula (1995). "Development of the Mozambique and Ruvuma sedimentary basins, offshore Mozambique." In: *Sedimentary Geology* 96.1-2, pp. 7–41. DOI: 10.1016/0037-0738(95)00125-R.

Saltelli, Andrea and Paola Annoni (2010). "How to avoid a perfunctory sensitivity analysis." In: *Environmental Modelling and Software* 25.12, pp. 1508–1517. DOI: 10.1016/j.envsoft.2010.04.012.

Saltelli, Andrea, Stefano Tarantola, Francesca Campolongo, and Marco Ratto (2004). *Sensitivity Analysis in Practice: A Guide to Assessing Scientific Models*. Ed. by Andrea Saltelli. 1st ed. Chichester, England: John Wiley & Sons, p. 219. DOI: 10.1002/0470870958.

Samadder, Ratan K., Sudhir Kumar, and Ravi P. Gupta (2011). "Paleochannels and their potential for artificial groundwater recharge in the western Ganga plains." In: *Journal of Hydrology* 400.1-2, pp. 154–164. DOI: 10.1016/j.jhydrol.2011.01.039.

Samsudin, A. R., A. Haryono, U. Hamzah, and A. G. Rafek (2008). "Salinity mapping of coastal groundwater aquifers using hydrogeochemical and geophysical methods: A case study from north Kelantan, Malaysia." In: *Environmental Geology* 55.8, pp. 1737–1743. DOI: 10.1007/s00254-007-1124-9.

Samsudin, Abdul Rahim, Umar Hamzah, and Ghani Rafek (1997). "Salinity study of coastal groundwater aquifers in north Kelantan , Malaysia." In: *Abbual Geological Conference '97*.

Samuel, Andy, Ben Kneller, Samir Raslan, Andy Sharp, and Cormac Parsons (2003). "Prolific deep marine slope channels of the Nile Delta, Egypt." In: *AAPG Bulletin* 87.4, pp. 541–560. DOI: 10.1306/1105021094.

Sanford, Ward E. and Somkid Buapeng (1996). "Assessment of a groundwater flow model of the bangkok basin, Thailand." In: *Hydrogeology Journal* 4.4.

Sanford, Ward E., L. Niel Plummer, Gerolamo Casile, Ed Busenberg, David L. Nelms, and Peter Schlosser (2017). "Using dual-domain advective-transport simulation to reconcile multiple-tracer ages and estimate dual-porosity transport parameters." In: *Water Resouces Research* 53, pp. 5002–5016. DOI: 10.1002/2016WR019469.

Sanford, Ward E. and Jason P. Pope (2010). "Current challenges using models to forecast seawater intrusion: lessons from the Eastern Shore of Virginia, USA." In: *Hydrogeology Journal* 18.1, pp. 73–93. DOI: 10.1007/s10040-009-0513-4.

Santucci, L., E. Carol, and E. Kruse (2016). "Identification of palaeo-seawater intrusion in groundwater using minor ions in a semi-confined aquifer of the Río de la Plata littoral (Argentina)." In: *Science of the Total Environment* 566-567, pp. 1640–1648. DOI: 10.1016/j.scitotenv.2016.06.066.

Sarker, Md Mizanur Rahman, Marc Van Camp, Mazeda Islam, Nasir Ahmed, and Kristine Walraevens (2018). "Hydrochemistry in coastal aquifer of southwest Bangladesh: origin of salinity." In: *Environmental Earth Sciences* 77.2, pp. 1–20. DOI: 10.1007/s12665-017-7196-2.

Savenije, H.H.G. (2012). *Salinity and tides in alluvial estuaries*, p. 163. DOI: http://dx.doi.org/10.1016/B978-044452107-1/50006-X.

Schreiber, B.C and Kenneth J. Hsu (1980). "Evaporites." In: *Developments in Petroleum Geology*. Chap. 3, p. 120.

Sefelnasr, Ahmed and Mohsen Sherif (2014). "Impacts of Seawater Rise on Seawater Intrusion in the Nile Delta Aquifer, Egypt." In: *Groundwater* 52.2, pp. 264–276. DOI: 10.1111/gwat.12058.

Sefie, Anuar, Ahmad Zaharin Aris, Mohammad Firuz Ramli, Tahoora Sheikhy Narany, Mohd Khairul Nizar Shamsuddin, Syaiful Bahren Saadudin, and Munirah Abdul Zali (2018). "Hydrogeochemistry and groundwater quality assessment of the multilayered aquifer in Lower Kelantan Basin, Kelantan, Malaysia." In: *Environmental Earth Sciences* 77.10, pp. 1–15. DOI: 10.1007/s12665-018-7561-9.

Sestini, G. (1989). "Nile Delta: a review of depositional environments and geological history." In: *Geological Society, London, Special Publications* 41.1, pp. 99–127. DOI: 10.1144/GSL.SP.1989.041.01.09.

Seto, Karen C. (2011). "Exploring the dynamics of migration to mega-delta cities in Asia and Africa: Contemporary drivers and future scenarios." In: *Global Environmental Change* 21.SUPPL. 1, S94–S107. DOI: 10.1016/j.gloenvcha.2011.08.005.

Shackelford, Charles D and David E Daniel (1991a). "Diffusion in Saturated Soil. I: Background." In: *Journal of Geotechnical Engineering* 117.3, pp. 467–484.

Shackelford, Charles D. and David E Daniel (1991b). "Diffusion in Saturated Soil. II: Results for Compacted Clay." In: *Journal of Geotechnical Engineering* 117.3, pp. 485–506. DOI: 10.1061/(ASCE)0733-9410(1991)117:3(485).

Shamsudduha, M. and Ashraf Uddin (2007). "Quaternary shoreline shifting and hydrogeologic influence on the distribution of groundwater arsenic in aquifers of the Bengal Basin." In: *Journal of Asian Earth Sciences* 31.2, pp. 177–194. DOI: 10.1016/j.jseaes.2007.07.001.

Shamsudduha, Mohammad, Richard G. Taylor, Kazi M. Ahmed, and Anwar Zahid (2011). "The impact of intensive groundwater abstraction on recharge to a shallow regional

aquifer system: Evidence from Bangladesh." In: *Hydrogeology Journal* 19.4, pp. 901–916. DOI: 10.1007/s10040-011-0723-4.

Sharp, J. M. and P. A. Domenico (1976). "Energy transport in thick sequences of compacting sediment." In: *Bulletin of the Geological Society of America* 87.3, pp. 390–400. DOI: 10.1130/0016-7606(1976)87<390:ETITSO>2.0.CO;2.

Shata, Abdou A. (1999). "Contribution to the hydrogeology of the Nile delta region - Egypt." In: *Deltas, Modern & Ancient*. Cairo, p. 19.

Shata, Abdou A. and K. Hefny (1995). *Strategies for planning and management of groundwater in the Nile Valley and Nile Delta in Egypt.* Tech. rep. Cairo: Strategic Research Program (SRP), NWRC-MPWWR.

Shen, Chengji, Chenming Zhang, Pei Xin, Jun Kong, and Ling Li (2018). "Salt Dynamics in Coastal Marshes: Formation of Hypersaline Zones." In: *Water Resources Research* 54.5, pp. 3259–3276. DOI: 10.1029/2017WR022021.

Sherif, Mohsen M., Vijay P. Singh, and Abdelwahab M. Amer (1988). "A two-dimensional finite element model for dispersion (2D-FED) in coastal aquifers." In: *Journal of Hydrology* 103.1-2, pp. 11–36. DOI: 10.1016/0022-1694(88)90003-0.

Shi, Lei and Jiu Jimmy Jiao (2014). "Seawater intrusion and coastal aquifer management in China: a review." In: *Environmental Earth Sciences* 72.8, pp. 2811–2819. DOI: 10.1007/s12665-014-3186-9.

Shi, Xiaoqing, Rui Fang, Jichun Wu, Hongxia Xu, Yuan Yuan Sun, and Jun Yu (2012). "Sustainable development and utilization of groundwater resources considering land subsidence in Suzhou, China." In: *Engineering Geology* 124.1, pp. 77–89. DOI: 10.1016/j.enggeo.2011.10.005.

Siemon, Bernhard, Anders Vest Christiansen, and Esben Auken (2009). "A review of helicopter-borne electromagnetic methods for groundwater exploration." In: *Near Surface Geophysics* 7.5-6, pp. 629–646. DOI: 10.3997/1873-0604.2009043.

Simachaya, Wijarn, Pimon Watanamahart, Vuttichai Kaewkrajang, and Akaluk Yenpiem (2000). "Water quality situation in the Chao Phraya Delta." In: *Proceedings of the international conference: The Chao Phraya Delta: Historical development, dynamics and challenges of Thailand's rice bowl* 662, pp. 1–21.

Simmons, Craig T., Thomas R. Fenstemaker, and John M. Sharp (2001). "Variable-density groundwater flow and solute transport in heterogeneous porous media: approaches, resolutions and future challenges." In: *Journal of Contaminant Hydrology* 52.1-4, pp. 245–275. DOI: 10.1016/S0169-7722(01)00160-7.

Simmons, Craig T., A. V. Kuznetsov, and D. A. Nield (2010). "Effect of strong heterogeneity on the onset of convection in a porous medium: Importance of spatial dimensionality and geologic controls." In: *Water Resources Research* 46.9, pp. 1–12. DOI: 10.1029/2009WR008606.

Simpson, Graham and Ian Hutcheon (1995). "Pore-Water Chemistry and Diagenesis of the Modern Fraser River Delta." In: *Journal of Sedimentary Research* Vol. 65A.4a, pp. 648–655. DOI: 10.1306/D426818A-2B26-11D7-8648000102C1865D.

Sinsakul, Sin (2000). "Late Quaternary geology of the Lower Central Plain, Thailand." In: *Journal of Asian Earth Sciences* 18.4, pp. 415–426. DOI: 10.1016/S1367-9120(99)00075-9.

Sivan, D., S. Wdowinski, K. Lambeck, E. Galili, and A. Raban (2001). "Holocene sea-level changes along the Mediterranean coast of Israel, based on archaeological observations and numerical model." In: *Palaeogeography, Palaeoclimatology, Palaeoecology* 167.1-2, pp. 101–117. DOI: 10.1016/S0031-0182(00)00234-0.

Smajgl, A., T. Q. Toan, D. K. Nhan, J. Ward, N. H. Trung, L. Q. Tri, V. P. D. Tri, and P. T. Vu (2015). "Responding to rising sea levels in the Mekong Delta." In: *Nature Climate Change* 5.2, pp. 167–174. DOI: 10.1038/nclimate2469.

Smith, B.F., P.E. Bjørstad, and W.D. Gropp (1996). *Domain Decomposition: Parallel Multilevel Methods for Elliptic Partial Differential Equations.* NY, USA: Cambridge University Press.

Song, Xiaomeng, Jianyun Zhang, Chesheng Zhan, Yunqing Xuan, Ming Ye, and Chonggang Xu (2015). "Global sensitivity analysis in hydrological modeling: Review of concepts, methods, theoretical framework, and applications." In: *Journal of Hydrology* 523.225, pp. 739–757. DOI: 10.1016/j.jhydrol.2015.02.013.

Spratt, Rachel M. and Lorraine E. Lisiecki (2016). "A Late Pleistocene sea level stack." In: *Climate of the Past* 12.4, pp. 1079–1092. DOI: 10.5194/cp-12-1079-2016.

Stafleu, Jan, Denise Maljers, and Jan Gunnink (2011). "3D modelling of the shallow subsurface of Zeeland , the Netherlands." In: *Dutch Journal of Geosciences* 90.4. DOI: 10.1017/S0016774600000597.

Stanley, Daniel J. (1997). "Mediterranean deltas: subsidence as a major control of relative sea-level rise." In: *Bulletin de l'Institut Océanographique Monaco, Science Series* 3, pp. 35–62.

Stanley, Daniel J. and Pablo L. Clemente (2017). "Increased land subsidence and sea-level rise are submerging Egypt's nile delta coastal margin." In: *GSA Today* 27.5, pp. 4–11. DOI: 10.1130/GSATG312A.1.

Stanley, Daniel J. and Andrew G Warne (1993). "Nile Delta: Recent Geological Evolution and Human Impact." In: *Science* 260.5108, pp. 628–634. DOI: 10.1126/science.260.5108.628.

Stanley, Daniel J. and Andrew G. Warne (1994). "Worldwide initiation of Holocene marine deltas by deceleration of sea-level rise." In: *Science* 265, pp. 228–231. DOI: 10.1126/science.265.5169.228.

Stanley, Jean-Daniel and Pablo L Clemente (2014). "Clay Distributions, Grain Sizes, Sediment Thicknesses, and Compaction Rates to Interpret Subsidence in Egypt's Northern Nile Delta." In: *Journal of Coastal Research* 30.1, pp. 88–101. DOI: 10.2112/JCOASTRES-D-13-00146.1.

Stanton, Jennifer S. et al. (2017). *Brackish Groundwater in the United States*, p. 185. DOI: 10.3133/pp1833.

Stevens, Joel D., John M. Sharp, Craig T. Simmons, and T. R. Fenstemaker (2009). "Evidence of free convection in groundwater: Field-based measurements beneath wind-tidal flats." In: *Journal of Hydrology* 375.3-4, pp. 394–409. DOI: 10.1016/j.jhydrol.2009.06.035.

Stoecker, Falko, Mukand S. Babel, Ashim Das Gupta, Aldrin A. Rivas, Mariele Evers, Futaba Kazama, and Takashi Nakamura (2013). "Hydrogeochemical and isotopic characterization of groundwater salinization in the Bangkok aquifer system, Thailand." In: *Environmental Earth Sciences* 68.3, pp. 749–763. DOI: 10.1007/s12665-012-1776-y.

Strack, O. D. L. (1989). *Groundwater Mechanics*. Portland, Oregon: Prentice Hall, p. 732.

Sturchio, N C et al. (2004). "One million year old groundwater in the Sahara revealed by krypton-81 and chlorine-36." In: *Geophysical Research Letters* 31.5, pp. 2–5. DOI: 10.1029/2003GL019234. arXiv: 0402092 [physics].

Stuyfzand, Pieter J. (2008). "Base exchange indices as indicators of salinization or freshening of (coastal) aquifers." In: *20th Salt Water Intrusion Meeting (June 23-27)*. 1941. Naples, Florida, USA, pp. 262–265.

Stuyfzand, Pieter J. and Roelof J. Stuurman (2006). "Origin , distribution and chemical mass balances of non-anthropogenic , brackish and (hyper) saline groundwaters in the Netherlands." In: pp. 151–164.

Suckow, Axel (2014). "The age of groundwater - Definitions, models and why we do not need this term." In: *Applied Geochemistry* 50.October, pp. 222–230. DOI: 10.1016/j.apgeochem.2014.04.016.

Summerhayes, Colin P., G. Sestini, R. Misdorp, and Nancy Marks (1978). "Nile Delta: Nature and Evolution of Continental Shelf Sediments." In: *Marine Geology* 27.3890, pp. 43–65.

Surfsara (2014). *Description of the Cartesius system*.

Sutanudjaja, Edwin H. et al. (2018). "PCR-GLOBWB 2: A 5 arcmin global hydrological and water resources model." In: *Geoscientific Model Development* 11.6, pp. 2429–2453. DOI: 10.5194/gmd-11-2429-2018.

Switzman, Harris, Paulin Coulibaly, and Zafar Adeel (2015). "Modeling the impacts of dryland agricultural reclamation on groundwater resources in Northern Egypt using

sparse data." In: *Journal of Hydrology* 520, pp. 420–438. DOI: 10.1016/j.jhydrol.2014.10.064.

Syvitski, James P M, Scott D. Peckham, Rachael Hilberman, and Thierry Mulder (2003). "Predicting the terrestrial flux of sediment to the global ocean: A planetary perspective." In: *Sedimentary Geology* 162.1-2, pp. 5–24. DOI: 10.1016/S0037-0738(03)00232-X.

Syvitski, James P. M. et al. (2009). "Sinking deltas due to human activities." In: *Nature Geoscience* 2.10, pp. 681–686. DOI: 10.1038/ngeo629.

Syvitski, James P.M. and Yoshiki Saito (2007). "Morphodynamics of deltas under the influence of humans." In: *Global and Planetary Change* 57.3-4, pp. 261–282. DOI: 10.1016/j.gloplacha.2006.12.001.

Szabo, Sylvia et al. (2016). "Population dynamics, delta vulnerability and environmental change: comparison of the Mekong, Ganges–Brahmaputra and Amazon delta regions." In: *Sustainability Science* 11.4, pp. 539–554. DOI: 10.1007/s11625-016-0372-6.

Talukder, Mohammad Radwanur Rahman, Shannon Rutherford, Cunrui Huang, Dung Phung, Mohammad Zahirul Islam, and Cordia Chu (2017). "Drinking water salinity and risk of hypertension: A systematic review and meta-analysis." In: *Archives of Environmental and Occupational Health* 72.3, pp. 126–138. DOI: 10.1080/19338244.2016.1175413.

Tamura, Toru, Yoshiki Saito, Sotham Sieng, Bunnarin Ben, Meng Kong, Im Sim, Sokuntheara Choup, and Fumio Akiba (2009). "Initiation of the Mekong River delta at 8 ka: evidence from the sedimentary succession in the Cambodian lowland." In: *Quaternary Science Reviews* 28.3-4, pp. 327–344. DOI: 10.1016/j.quascirev.2008.10.010.

Tanabe, Susumu, Yoshiki Saito, Quang Lan Vu, Till J.J. Hanebuth, Quang Lan Ngo, and Akihisa Kitamura (2006). "Holocene evolution of the Song Hong (Red River) delta system, northern Vietnam." In: *Sedimentary Geology* 187.1-2, pp. 29–61. DOI: 10.1016/j.sedgeo.2005.12.004.

Taniguchi, Makoto, William C. Burnett, Jaye E. Cable, and Jeffrey V. Turner (2002). "Investigation of submarine groundwater discharge." In: *Hydrological Processes* 16.11, pp. 2115–2129. DOI: 10.1002/hyp.1145.

Teatini, P., L. Tosi, A. Viezzoli, L. Baradello, M. Zecchin, and S. Silvestri (2011). "Understanding the hydrogeology of the Venice Lagoon subsurface with airborne electromagnetics." In: *Journal of Hydrology* 411.3-4, pp. 342–354. DOI: 10.1016/j.jhydrol.2011.10.017.

Tessler, Z.D., C.J. Vorosmarty, M. Grossberg, I. Gladkova, H. Aizenman, James P M Syvitski, and E. Foufala-Georgiou (2015). "Profiling risk and sustainability in coastal deltas of the world." In: *Science* 349.6248, pp. 638–643.

The MPI Forum (1993). "MPI: A Message Passing Interface." In:

Thomas, A. T., S. Reiche, M. Riedel, and C. Clauser (2019). "The fate of submarine fresh groundwater reservoirs at the New Jersey shelf, USA." In: *Hydrogeology Journal* 27.7, pp. 2673–2694. DOI: 10.1007/s10040-019-01997-y.

Thompson, Craig, Leslie Smith, and Roudrajit Maji (2007). "Hydrogeological modeling of submarine groundwater discharge on the continental shelf of Louisiana." In: *Journal of Geophysical Research: Oceans* 112.3, pp. 1–13. DOI: 10.1029/2006JC003557.

Tilman, David, Christian Balzer, Jason Hill, and Belinda L. Befort (2011). "Global food demand and the sustainable intensification of agriculture." In: *Proceedings of the National Academy of Sciences of the United States of America* 108.50, pp. 20260–20264. DOI: 10.1073/pnas.1116437108.

Tilmans, Wiel M.K. (1991). "Coast erosion management-The Kelantan case." In: *Ocean and Shoreline Management* 15.2, pp. 87–124. DOI: 10.1016/0951-8312(91)90026-X.

Timmerman, P H A and C J Hemker (1993). "Determination of the entry-resistance of the Lek and the vertical resistances of the floodplains and polders near Langerak (Alblasserwaard, NL) [article in Dutch]." In: *H2o* 26.1, pp. 2–7.

Tran, Dang An, Maki Tsujimura, Le Phu Vo, Van Tam Nguyen, Dwight Kambuku, and Thanh Duc Dang (2019). "Hydrogeochemical characteristics of a multi-layered coastal aquifer system in the Mekong Delta, Vietnam." In: *Environmental Geochemistry and Health* 9. DOI: 10.1007/s10653-019-00400-9.

Tran, Luu T., Flemming Larsen, Nhan Q. Pham, Anders V. Christiansen, Nghi Tran, Hung V. Vu, Long V. Tran, Hoan V. Hoang, and Klaus Hinsby (2012). "Origin and extent of fresh groundwater, salty paleowaters and recent saltwater intrusions in Red River flood plain aquifers, Vietnam." In: *Hydrogeology Journal* 20.7, pp. 1295–1313. DOI: 10.1007/s10040-012-0874-y.

Trevisan, O.V. and A Bejan (1990). "Combined Heat and Mass Transfer by Natural Convection in a Vertical Enclosure." In: *Advances in Heat Transfer* 20.1, pp. 315–352.

Van Dam, Remke L., Craig T. Simmons, David W. Hyndman, and Warren W. Wood (2009). "Natural free convection in porous media: First field documentation in groundwater." In: *Geophysical Research Letters* 36.11, pp. 1–5. DOI: 10.1029/2008GL036906.

Van der Walt, Stéfan, Johannes L. Schönberger, Juan Nunez-Iglesias, François Boulogne, Joshua D. Warner, Neil Yager, Emmanuelle Gouillart, and Tony Yu (2014). "scikit-image: image processing in Python." In: *PeerJ* 2, e453. DOI: 10.7717/peerj.453. arXiv: 1407.6245.

Van Driel, Wim et al. (2015). "Vulnerability Assessment of Deltas in Transboundary River Basins." In: *Delta Alliance contribution to the Transboundary Water Assessment Program, FSP River Basins Component. Delta Alliance Report* 9.

Van Pham, Hung, Frans C van Geer, Vuong Bui Tran, Wim Dubelaar, and Gualbert H.P. Oude Essink (2019). "Paleo-hydrogeological reconstruction of the fresh-saline

groundwater distribution in the Vietnamese Mekong Delta since the late Pleistocene." In: *Journal of Hydrology: Regional Studies* 23, pp. 1–22. DOI: https://doi.org/10.1016/j.ejrh.2019.100594.

Van Asselen, Sanneke, Kim M. Cohen, and Esther Stouthamer (2017). "The impact of avulsion on groundwater level and peat formation in delta floodbasins during the middle-Holocene transgression in the Rhine-Meuse delta, The Netherlands." In: *Holocene* 27.11, pp. 1694–1706. DOI: 10.1177/0959683617702224.

Van Engelen, Joeri (2020a). *delta_aquifer*. DOI: 10.5281/zenodo.3653734.

Van Engelen, Joeri (2020b). *Video supplement: Factors determining the natural fresh-salt groundwater distribution in deltas (Version v1)*.

Van Engelen, Joeri, Gualbert H.P. Oude Essink, Henk Kooi, and Marc F.P. Bierkens (2018). "On the origins of hypersaline groundwater in the Nile Delta aquifer." In: *Journal of Hydrology* 560, pp. 301–317. DOI: 10.1016/j.jhydrol.2018.03.029.

Van Engelen, Joeri, Jarno Verkaik, Jude King, Eman R. Nofal, Marc F. P. Bierkens, and Gualbert H. P. Oude Essink (2019). "A three-dimensional palaeohydrogeological reconstruction of the groundwater salinity distribution in the Nile Delta Aquifer." In: *Hydrology and Earth System Sciences* 23, pp. 5175–5198. DOI: 10.5194/hess-2019-151.

Vengosh, Avner, Gert J. De Lange, and Abraham Starinsky (1998). "Boron isotope and geochemical evidence for the origin of Urania and Bannock brines at the eastern Mediterranean: Effect of water-rock interactions." In: *Geochimica et Cosmochimica Acta* 62.19-20, pp. 3221–3228. DOI: 10.1016/S0016-7037(98)00236-1.

Vengosh, Avner, Arthur J Spivack, Yohanan Artzi, and Avner Ayalon (1999). "Geochemical and boron, strontium, and oxygen isotopic constraints on the origin of the salinity in groundwater from the Mediterranenan coast of Israel." In: *Water Resouces Research* 35.6, pp. 1877–1894.

Verkaik, Jarno, Joeri Van Engelen, Sebastian Huizer, and Gualbert H.P. Oude Essink (2017). "The New Parallel Krylov Solver for SEAWAT." In: *AGU Fall Meeting 2017 (11-15 Dec 2017)*. New Orleans, Louisiana.

Verweij, J M (1999). "Application of fluid flow systems analysis to reconstruct the post-Carboniferous hydrogeohistory of the onshore and offshore Netherlands." In: *Marine and Petroleum Geology* 16, pp. 561–579.

Visser, Martijn and Huite Bootsma (2019). *iMOD-Python: work with iMOD MODFLOW models in Python*. Utrecht.

Volker, A. (1961). "Source of Brackish ground water in Pleistocene formations beneath the Dutch Polderland." In: *Economic Geology* 56, pp. 1045–1057.

Voss, Clifford I. and Safaa M. Soliman (2013). "The transboundary non-renewable Nubian Aquifer System of Chad, Egypt, Libya and Sudan: classical groundwater questions

and parsimonious hydrogeologic analysis and modeling." In: *Hydrogeology Journal* 22.2, pp. 441–468. DOI: 10.1007/s10040-013-1039-3.

Voss, Clifford I. and Warren W. Wood (1993). "Synthesis of geochemical, isotopic and groundwater modeling analysis to explain regional flow in a coastal aquifer of southern Oahu, Hawaii." In: *Mathematical models and their applications to isotope studies in groundwater hydrology*. June. Vienna: IAEA, pp. 147–178.

Wada, Yoshihide, Ludovicus P H Van Beek, Frederiek C. Sperna Weiland, Benjamin F. Chao, Yun Hao Wu, and Marc F P Bierkens (2012). "Past and future contribution of global groundwater depletion to sea-level rise." In: *Geophysical Research Letters* 39.9, pp. 1–6. DOI: 10.1029/2012GL051230.

Walther, Marc, Thomas Graf, Olaf Kolditz, Rudolf Liedl, and Vincent Post (2017). "How significant is the slope of the sea-side boundary for modelling seawater intrusion in coastal aquifers?" In: *Journal of Hydrology* 551, pp. 648–659. DOI: 10.1016/j.jhydrol.2017.02.031.

Wang, Ya and Jiu Jimmy Jiao (2012). "Origin of groundwater salinity and hydrogeochemical processes in the confined Quaternary aquifer of the Pearl River Delta, China." In: *Journal of Hydrology* 438-439, pp. 112–124. DOI: 10.1016/j.jhydrol.2012.03.008.

Warne, Andrew G and Daniel Jean Stanley (1993). "Late Quaternary Evolution of the Northwest Nile Delta and Adjacent Coast in the Alexandria Region, Egypt." In: *Journal of Coastal Research* 9.1, pp. 26–64.

Way, A.G. (1955). *Caesar the Alexandrian war, African war, Spanish war.* Loeb Class. Cambridge: Harvard University Press, p. 402.

Werner, Adrian D. (2016). "On the classification of seawater intrusion." In: *Journal of Hydrology* 551, pp. 619–631. DOI: 10.1016/j.jhydrol.2016.12.012.

Werner, Adrian D., Mark Bakker, Vincent E A Post, Alexander Vandenbohede, Chunhui Lu, Behzad Ataie-Ashtiani, Craig T. Simmons, and D. A. Barry (2013). "Seawater intrusion processes, investigation and management: Recent advances and future challenges." In: *Advances in Water Resources* 51, pp. 3–26. DOI: 10.1016/j.advwatres.2012.03.004.

West, I. M., Y. A. Ali, and M. E. Hilmy (1979). "Primary gypsum nodules in a modern sabkha on the Mediterranean coast of Egypt." In: *Geology* 7.7, pp. 354–358. DOI: 10.1130/0091-7613(1979)7<354:PGNIAM>2.0.CO;2.

Winkel, Lenny H E, Thi Kim Trang Pham, Mai Lan Vi, Caroline Stengel, Manouchehr Amini, Thi Ha Nguyen, Hung Viet Pham, and Michael Berg (2011). "Arsenic pollution of groundwater in Vietnam exacerbated by deep aquifer exploitation for more than a century." In: *Proceedings of the National Academy of Sciences of the United States of America* 108.4, pp. 1246–1251. DOI: 10.1073/pnas.1011915108.

Wittmeyer, G.W., M.P. Miklas, R.V. Klar, D. Williams, and D. Balin (1996). *Use of groundwater in the arid and semi-arid Western United States: implications for Yucca Mountain area. Report NRC-02-93-005*. Tech. rep. August. San Antonio, Texas: Center for Nuclear Waste Regulatory Analyses, p. 52.

WMO (2006). *Weather Information for Alexandria*.

Wolters, Michel L. and Claudia Kuenzer (2015). "Vulnerability assessments of coastal river deltas - categorization and review." In: *Journal of Coastal Conservation* 19.3, pp. 345–368. DOI: 10.1007/s11852-015-0396-6.

Wooding, R. a., Scott W. Tyler, and Ian White (1997). "Convection in groundwater below an evaporating Salt Lake: 1. Onset of instability." In: *Water Resources Research* 33.6, p. 1219. DOI: 10.1029/96WR03534.

World Bank (2018). *Population, total*.

WRI (2008). *World Resources 2008 Data Tables*. Tech. rep. Washington D.C.: WRI, p. 30.

Wu, Hui and Jianrong Zhu (2010). "Advection scheme with 3rd high-order spatial interpolation at the middle temporal level and its application to saltwater intrusion in the Changjiang Estuary." In: *Ocean Modelling* 33.1-2, pp. 33–51. DOI: 10.1016/j.ocemod.2009.12.001.

Xu, Zexuan, Bill X. Hu, and Ming Ye (2018). "Numerical modeling and sensitivity analysis of seawater intrusion in a dual-permeability coastal karst aquifer with conduit networks." In: *Hydrology and Earth System Sciences* 22.1, pp. 221–239. DOI: 10.5194/hess-22-221-2018.

Xue, Yu Qun, Ji Chun Wu, Yun Zhang, Shu Jun Ye, Xiao Qing Shi, Zi Xin Wei, Qin Fen Li, and Jun Yu (2008). "Simulation of regional land subsidence in the southern Yangtze Delta." In: *Science in China, Series D: Earth Sciences* 51.6, pp. 808–825. DOI: 10.1007/s11430-008-0062-z.

Yamanaka, Tsutomu, Jun Shimada, Maki Tsujimura, Oranuj Lorphensri, Makoto Mikita, Atsushi Hagihara, and Shinichi Onodera (2011). "Tracing a confined groundwater flow system under the pressure of excessive groundwater use in the lower central plain, Thailand." In: *Hydrological Processes* 25.17, pp. 2654–2664. DOI: 10.1002/hyp.8007.

Yang, Jie, Thomas Graf, Maria Herold, and Thomas Ptak (2013). "Modelling the effects of tides and storm surges on coastal aquifers using a coupled surface-subsurface approach." In: *Journal of Contaminant Hydrology* 149, pp. 61–75. DOI: 10.1016/j.jconhyd.2013.03.002.

Yechieli, Y., E. Shalev, S. Wollman, Y. Kiro, and U. Kafri (2010). "Response of the Mediterranean and Dead Sea coastal aquifers to sea level variations." In: *Water Resources Research* 46.12, pp. 1–11. DOI: 10.1029/2009WR008708.

Yechieli, Yoseph, Uri Kafri, and Orit Sivan (2009). "The inter-relationship between coastal sub-aquifers and the Mediterranean Sea, deduced from radioactive isotopes analysis." In: *Hydrogeology Journal* 17.2, pp. 265–274. DOI: 10.1007/s10040-008-0329-7.

Zamrsky, Daniel, Maria E Karssenberg, Kim M Cohen, Marc F P Bierkens, H P Gualbert, and Oude Essink (2020). "Geological heterogeneity of coastal unconsolidated groundwater systems worldwide and its influence on offshore fresh groundwater occurrence." In: *Frontiers in Earth Science* 7.January, p. 339. DOI: 10.3389/feart.2019.00339.

Zamrsky, Daniel, Gualbert H.P. Oude Essink, and Marc F.P. Bierkens (2018). "Estimating the thickness of unconsolidated coastal aquifers along the global coastline." In: *Earth System Science Data* 10.3, pp. 1591–1603. DOI: 10.5194/essd-10-1591-2018.

Zech, Alraune, Sabine Attinger, Vladimir Cvetkovic, Gedeon Dagan, Peter Dietrich, Aldo Fiori, Y Rubin, and Georg Teutsch (2015). "Is unique scaling of aquifer macrodispersivity supported by field data?" In: *Water Resources Research* 51, pp. 7662–7679. DOI: 10.1002/2015WR017220.

Zhang, Chenming, Ling Li, and David Lockington (2015). "A physically based surface resistance model for evaporation from bare soils." In: *Water Resources Research* 51, pp. 1084–1111. DOI: 10.1002/2014WR015490.

Zhang, Wei, Haochuan Feng, Jinhai Zheng, A.J.F. Hoitink, M. van der Vegt, Yuliang Zhu, and Huijuan Cai (2013). "Numerical Simulation and Analysis of Saltwater Intrusion Lengths in the Pearl River Delta, China." In: *Journal of Coastal Research* 287.March, pp. 372–382. DOI: 10.2112/JCOASTRES-D-12-00068.1.

Zheng, Chunmiao (2010). *MT3DMS v5.3: Supplemental User's Guide*. Tech. rep. Tuscaloosa: University of Alabama, p. 51.

Zheng, Chunmiao and P Patrick Wang (1999). *A Modular Three-Dimensional Multispecies Transport Model*. Tech. rep. Tuscaloosa: University of Alabama, p. 239.

Zhou, Quanlin, Jacob Bear, and Jacob Bensabat (2005). "Saltwater upconing and decay beneath a well pumping above an interface zone." In: *Transport in Porous Media* 61.3, pp. 337–363. DOI: 10.1007/s11242-005-0261-4.

Zimmermann, S., P. Bauer, R. Held, W. Kinzelbach, and J. H. Walther (2006). "Salt transport on islands in the Okavango Delta: Numerical investigations." In: *Advances in Water Resources* 29.1, pp. 11–29. DOI: 10.1016/j.advwatres.2005.04.013.

Zong, Y., G. Huang, A. D. Switzer, F. Yu, and W. W.S. Yim (2009). "An evolutionary model for the Holocene formation of the Pearl River delta, China." In: *Holocene* 19.1, pp. 129–142. DOI: 10.1177/0959683608098957.

Zong, Yongqiang, Kangyou Huang, Fengling Yu, Zhuo Zheng, Adam Switzer, Guangqing Huang, Ning Wang, and Min Tang (2012). "The role of sea-level rise, monsoonal discharge and the palaeo-landscape in the early Holocene evolution of the Pearl River delta,

southern China." In: *Quaternary Science Reviews* 54, pp. 77–88. DOI: 10.1016/j.quascirev.2012.01.002.

ACKNOWLEDGMENTS

Ik heb erg genoten van mijn promotietraject, waarin ik veel geleerd heb en de kans heb gekregen om conferenties te bezoeken waar ik veel internationale collega's heb leren kennen. Het afronden van een promotietraject is echter ook een flinke uitdaging waarbij de steun vanuit mijn omgeving erg pretting was. Ik ben daarom meerdere mensen nog mijn dank verschuldigd. Sommige van deze mensen zijn het Nederlands niet machtig, dus een enkele keer schakel ik over naar het Engels in dit stuk.

Allereerst wil ik mijn promotors Marc en Gu bedanken voor de begeleiding, die beiden altijd wel een moment voor mij in hun drukke agenda's wisten te vinden. Ik heb altijd veel energie uit jullie enthousiasme gehaald. Marc wil ik verder bedanken voor het bewaken van de grote lijn, belangrijk voor een detailist als ik, en begeleiden in "how to sell your science". Gu bedank ik verder voor het meenemen van mij in de "zoet-zout" wereld en zijn rol als mentor die hij automatisch aannam. Jij coachte me zowel op professioneel vlak als op het gebied van "het leven" in het algemeen, wat ik erg waardeer!

Going to the office for four years to work on one single project takes self-discipline, but more important were the colleagues that made going there a lot more enjoyable. Therefore I would like to thank the guys and girl of "The Man Cave": Mo, Stormy Dan, Twinkels, Janice, Josi, Judas, and Fabi. The banter, beers, and memes we shared made the PhD life ten times better! Honorable mentions are also for Marcio and Ed, with whom I shared additional beers and interesting conversations. Yes, the PhD life strained the health, but luckily Jakob and Emmy introduced me to climbing and joined me on a lot of trips to the bouldergym, so thank you for the "gezelligheid" and for keeping me fit!

Verder wil ik mijn collega's bij Deltares bedanken voor hun hulp, gezelligheid, en hun interesse in mijn onderzoek, ik ben dan ook erg blij dat ik nu echt onderdeel van jullie team kan zijn. Gijs en Jarno wil ik nog bedanken voor hun ondersteuning bij de parallelle iMOD-SEAWAT code (nu onderdeel van iMOD-WQ). Wim en Jacco voor het stimuleren van mij om het onderzoek in te gaan. En last but not least Huite, in zijn ingewikkelde rol als beste vriend, huisgenoot, en collega, die hij met verve vervult.

Ook de Wageningen-connectie bleef belangrijk in mijn PhD, zowel op professioneel als privé vlak. Om te beginnen Paul Torfs die mij het "vaderlijk advies" (zijn woorden) gaf om toch het onderzoek in te gaan, zonder dit advies was ik waarschijnlijk niet snel aan een PhD begonnen. En buiten mijn werk had ik met Daan, Aljosha, en Bart, toch nog als Gruismachine een succesje meegepakt op het bevrijdingsfestival in het eerste jaar van mijn PhD; en sinds we zijn gestopt als band experimenteren wij nu nog vrolijk elektronisch

verder. Daarnaast nog de heren van de T-Tour: het zooitje ongeregeld waarmee ik ieder jaar op vakantie ben gegaan, onder andere naar de Donau delta! De sterke verhalen die in deze vakanties verzameld zijn, zullen voor eeuwig herhaald (en aangedikt) worden bij kampvuren/BBQ's.

Allerlaatst wil ik mijn vader, moeder, en broer bedanken voor hun onafgebroken steun en betrokkenheid, tijdens de hoogte- en dieptepunten die iedereen meemaakt in een vierjarig promotietraject.

SUMMARY

Deltas are often densely-populated hubs with intensive agriculture, because of their flat topography, their excellent location for ports, and their fertile soils. Though traditionally depending mainly on surface water to meet water demands, their ever-growing population and intensifying agriculture will increase groundwater extractions. These extractions will lead to salt water intrusion and upconing, reducing the deltas' precious fresh groundwater reserves. Despite the increasing importance of these reserves, little is known about the actual size of these fresh groundwater reserves and the important factors that control them. Hence the main objective of this thesis was to assess the status and drivers of the current fresh-salt distribution. To this end, I have formulated the following research questions:

1. *What processes influence groundwater salinity in deltas at large depths?* (Chapter 2)
2. *How did the fresh water volumes in deltas evolve over time?* (Chapter 3 & 5)
3. *What are the driving factors of the natural fresh-salt distribution?* (Chapter 4)
4. *What are the current fresh groundwater volumes in deltas and will they be depleted?* (Chapter 5)

Since data on deltaic groundwater resources is often scarce and long timescales were presumably involved in their establishment, I resorted to numerical models that simulated thousands of years of variable-density groundwater flow and coupled solute transport. At large depths, hypersaline groundwater was found in multiple deltas, of which the Nile delta was studied in detail in chapter 2. Here, I used a set of analytical and numerical models to study four hypotheses as to the origins of this hypersaline groundwater. It was concluded that the hypersaline groundwater originated either from Pleistocene free-convective systems that were formed underneath sabkhas (salt flats), or from compaction-induced seepage of hypersaline groundwater. The latter hypothesis especially is also of interest to several other deltas, as these have experienced the high sedimentation rates that cause compaction as well. Whether the old groundwater that has slowly seeped upwards is still present in the present-day, active groundwater system, depends on the connection to the sea. When there is an open connection, this water is flushed out of the system.

The evolution of fresh groundwater reserves was studied with three-dimensional variable-density groundwater flow models for both the Nile delta and an idealized generic delta,

driven by paleohydrological forcings. It was found that long timescales were involved. In general, this evolution was as follows, starting initially salt from the latest Pleistocene highstand (120 ka), the saline aquifers are flushed during the last Pleistocene lowstand until the start of the Holocene (11 ka). From then, sea-levels rise so rapidly that sedimentation cannot keep up with it, resulting in a marine transgression around 8.5 – 6.5 ka. During the Holocene, fresh groundwater reserves reduce strongly. For example, in some of the simulations of the Nile Delta, fresh groundwater reserves are even quartered. After the Holocene transgression had passed, fresh groundwater volumes started to replenish again, but usually not to their Pleistocene levels.

A global sensitivity analysis was conducted on a generic model of an idealized delta to assess the factors that determine the natural deltaic fresh-salt groundwater distribution. In total, 23 inputs of the model were included in the sensitivity analysis. It was found that the model was the most sensitive to the hydraulic conductivity of the aquifers, which are often also the most uncertain. This input both facilitates the flushing of aquifers during the Pleistocene, as well as infiltration of saline groundwater during the Holocene. The other input the model was strongly sensitive to, was the thickness of the groundwater system. To a lesser degree but still important were the hydraulic gradient and the extent of the Holocene transgression.

Fresh groundwater reserves were estimated using the generic, idealized model together with a set of representative inputs for each delta. Since the models were found to be particularly sensitive to hydraulic conductivity of the aquifers and aquitards and these usually are the most uncertain, a full factorial analysis was conducted for these two inputs. This resulted in nine simulations per delta. The onshore fresh groundwater volumes for most deltas fall somewhere in the range of $10^{10}m^3$ and $10^{12}m^3$. Offshore fresh groundwater volumes varied a lot more, usually ranging from 10^7 to 10^{12} m^3. With the current extraction rates there are deltas that face serious challenges; the Ganges-Brahmaputra, Nile, Pearl, and Yangtze delta face serious depletion of their fresh groundwater resources in the coming century. Without any measures, their fresh groundwater resources will be gradually replaced with saline riverine recharge. With increasing extraction rates, the Saloum, Mekong, and Red River delta can be added to this list of deltas under stress.

SAMENVATTING

Delta's zijn meestal dichtbevolkte gebieden met intensieve landbouw, vanwege hun vlakke topografie, hun uitstekende locatie voor havens, en hun vruchtbare gronden. Hoewel delta's traditioneel afhankelijk zijn van oppervlaktewater, stijgt hun grondwatergebruik door een groeiende bevolking en intensiever wordende landbouw. Dit grondwatergebruik leidt tot zoutwaterintrusie en opkegeling, met als gevolg een afname van kostbare zoetwatervoorraden. Ondanks het toenemende belang van deze voorraden, weet men weinig van hun daadwerkelijke omvang en welke factoren bepalend zijn voor deze omvang. Vandaar het hoofddoel van dit proefschrift is om de status en aandrijvers van de huidige zoet-zout verdeling in delta's te bepalen. Hiervoor heb ik de volgende hoofdvragen gedefinieerd:

1. *Welke processen zijn van invloed op het zoutgehalte van het grondwater in delta's op grote diepte?* (Hoofdstuk 2)
2. *Hoe zijn de zoetwatervolumes in delta's ontwikkeld door de tijd?* (Hoofdstuk 3 & 5)
3. *Wat zijn de drijvende krachten achter de natuurlijke zoet-zout verdeling in delta's?* (Hoofdstuk 4)
4. *Wat zijn de huidige grondwatervolumes in delta's en zullen deze uitgeput raken?* (Hoofdstuk 5)

Omdat data over grondwatervoorraden in delta's vaak schaars is en ze waarschijnlijk over een grote tijdschaal gevormd zijn, heb ik numerieke modellen gebruikt die duizenden jaren aan dichtheids-variable grondwaterstroming en gekoppeld stoftransport simuleren. Op grote dieptes is hypersalien grondwater gevonden in meerdere delta's, van welke ik de Nijl delta onderzocht heb in hoofdstuk 2. Hier heb ik een combinatie van analytische en numerieke modellen gebruikt om vier hypotheses naar de oorsprong van dit hypersaline grondwater te onderzoeken. De conclusie was dat hypersalien grondwater waarschijnlijk is ontstaan uit ofwel vrije-convectie systemen die gevormd werden onder sabkha's (zoutvlaktes), ofwel door compactie opgewekte kwel van hypersalien grondwater. Vooral die laatste hypothese is interessant voor verschillende andere delta's, aangezien deze ook de hoge sedimentatiesnelheden hebben ervaren die compactie veroorzaakten. Of dit langzaam opgekwelde grondwater ten heden dage nog steeds vindbaar is in het actieve grondwatersysteem, hangt af van de verbinding met de zee. Als het systeem in open verbinding met de zee is, is dit water weggespoeld uit het grondwatersysteem.

De ontwikkeling van zoetwatervoorraden in grondwater is gesimuleerd met driedensionale variabele-dichtheid grondwaterstromings modellen voor zowel de Nijl delta als eem geïdealiseerde, generieke delta, gedreven door een paleohydrologische forcering. Het bleek dat hierbij grote tijdschalen een rol speelden. Over het algemeen was deze ontwikkeling als volgt: Vanaf een initieel zout systeem na de laatste Pleistocene hoge zeestand (120 ka), werden de zoute aquifers langzaam schoongespoeld met zoet grondwater tot de start van het Holoceen (11 ka). Op dat moment begint de zeespiegel dusdanig snel te stijgen dat de sedimentatie van delta's het niet kan bijbenen, wat leidt tot een mariene transgressie ergens tussen 8.5 – 6.5 ka. Tijdens het Holoceen nemen de zoetwatervoorraden in het grondwater snel af. In de simulaties van de Nijl Delta, bijvoorbeeld, worden de zoete grondwatervoorraden gevierendeeld. Na deze Holocene trangressie beginnen de zoete grondwater voorraden weer langzaam toe te nemen, maar meestal niet tot hun Pleistocene formaat.

Een globable gevoeligheidsanalyse is ondernomen op een generiek model van een geïdealiseerde delta om de bepalende factoren voor de natuurlijke zoet-zoutverdeling te vinden. In totaal zijn er 23 invoervariabelen van het model inbegrepen in de gevoeligheidsanalyse. Het bleek dat het model het meest gevoelig was voor hydraulische doorlatendheid van de aquifers, welk meestal ook het meest onzeker is. Deze invoervariabele bevordert zowel het verzoeten van aquifers gedurende het Pleistoceen, als het infiltreren van zout grondwater tijdens het Holoceen. Nog een invoervariabele van belang was de dikte van het grondwatersysteem. Daaropvolgend, in iets lichtere mate, kwamen de gradiënt van de rivieren en de omvang van de Holocene transgressie.

Zoete grondwatervoorraden zijn ingeschat gebruikmakend van een generiek, geïdealiseerd model met een set van representatieve waardes voor de invoer van iedere delta. Omdat er werd bevonden dat de zoet-zout verdeling van de modellen voornamelijk afhankelijk was van de hydraulische doorlatendheid van de aquifers en aquitards, en deze meestal het meest onzeker zijn, is een volledige factoranalyse gedaan voor deze twee invoervariabelen. Dit resulteerde in negen simulaties per delta. De onshore zoete grondwatervoorraden varieerden meestal tussen $10^{10}m^3$ en $10^{12}m^3$. De offshore voorraden varieerden een stuk sterker, van $10^{7}m^3$ tot $10^{12}m^3$. Met de huidige onttrekkingen zijn er vier delta's die grote uitdagingen te wachten staan: de Ganges-Brahmaputra, de Nijl, de Parelrivier, en de Yangtze delta wacht een grote uitdaging de komende eeuw. Zonder maatregelen zullen deze delta's hun grondwatervoorraden langzaamaan zien verzilten. Met een toename in onttrekkingen kunnen ook de Saloum, de Mekong, en de Rode River delta aan deze lijst toegevoegd worden.

ABOUT THE AUTHOR

Joeri van Engelen was born on the 25th of January 1992 in the city of Delft. He attended high school at the Stedelijk Gymnasium Leiden in Leiden, where, next to learning dead languages, he developed an interest in geography. In 2010 he moved to Wageningen to follow a bachelor study appropriately named "Soil, Water, and Atmosphere". During his master's, also in Wageningen, he specialized in groundwater hydrology. His thesis concerned developing a geohydrological model of a floating fen, located in the nature reserve the "Nieuwkoopse Plassen". He did his internship at Deltares in Utrecht, where he conducted a sensitivity and uncertainty analysis for a regional groundwater model that simulated the effects of a channel deepening. It is during this internship that he discovered he liked conducting research. In 2016 he started his PhD in a joint project between Utrecht University and Deltares to study the fresh-salt groundwater distribution in major deltas, of which the findings are bundled in this thesis. Joeri currently works at Deltares as a medior researcher and advisor.

PUBLICATIONS

Scientific Publications

Post, Vincent E.A., Georg J. Houben, and Joeri van Engelen (2018). "What is the Ghijben-Herzberg principle and who formulated it?" In: *Hydrogeology Journal* 26, pp. 1801–1807.

Stofberg, Sija F., Joeri van Engelen, Jan Philip M. Witte, and Sjoerd E.A.T.M. van der Zee (2016). "Effects of root mat buoyancy and heterogeneity on floating fen hydrology." In: *Ecohydrology* 9.7, pp. 1222–1234. DOI: 10.1002/eco.1720.

Van Engelen, Joeri, Gualbert H.P. Oude Essink, Henk Kooi, and Marc F.P. Bierkens (2018). "On the origins of hypersaline groundwater in the Nile Delta aquifer." In: *Journal of Hydrology* 560, pp. 301–317. DOI: 10.1016/j.jhydrol.2018.03.029.

Van Engelen, Joeri, Jarno Verkaik, Jude King, Eman R. Nofal, Marc F. P. Bierkens, and Gualbert H. P. Oude Essink (2019). "A three-dimensional palaeohydrogeological reconstruction of the groundwater salinity distribution in the Nile Delta Aquifer." In:

Hydrology and Earth System Sciences 23, pp. 5175–5198. DOI: 10.5194/hess-2019-151.

Professional publications

De Louw, Perry G.B., Gualbert H.P. Oude Essink, Joost R. Delsman, Esther S. Van Baaren, Ilja America, and Joeri Van Engelen (2019). "Het langetermijngeheugen van de zoet-zoutverdeling." In: *Stromingen* 33.1, pp. 43–60.

Conference Proceedings

Van Engelen, Joeri, Marc F.P. Bierkens, and Gualbert H.P. Oude Essink (2018). "3D Paleohydrogeological modelling of the Nile Delta." In: *25th Salt Water Intrusion Meeting, 17-22 June 2018, Gdansk, Poland*, pp. 338–339.

Van Engelen, Joeri, Marc F.P. Bierkens, and Gualbert H.P. Oude Essink (2019). "Disentangling the driving processes of the fresh-salt groundwater distribution in deltas." In: *Agu Fall Meeting 2019*, H23L–2059.

Van Engelen, Joeri, Gualbert H.P. Oude Essink, and Marc F.P. Bierkens (2016). "Fresh groundwater reserves in 40 major deltas under global change." In: *24th Salt Water Intrusion Meeting and the 4th Asia-Pacific Coastal Aquifer Management Meeting, 4 –8 July 2016, Cairns, Australia*. Ed. by Adrian D. Werner. Cairns, pp. 7–8.

Van Engelen, Joeri, Gualbert H.P. Oude Essink, Henk Kooi, and Marc F.P. Bierkens (2017). "On the origins of hypersaline groundwater in the Nile Delta Aquifer." In: *EGU General Assembly Conference Abstracts 2017*.

Verkaik, Jarno, Sebastian Huizer, Joeri Van Engelen, Raju Ram, and Kees Vuik (2018). "Parallel Computing with SEAWAT." In: *25th Salt Water Intrusion Meeting*, p. 13040.